

OPTIMISATION OF THE ALUMINIUM COMPRESSOR IMPELLER MACHINING PROCESS

by

RATTANACHAI RATTANAKIT

A thesis submitted to
The University of Birmingham
for the degree of
Engineering Doctorate (EngD)

School of Metallurgy and Materials
College of Engineering and Physical Sciences
University of Birmingham
September 2012

UNIVERSITY OF
BIRMINGHAM

University of Birmingham Research Archive

e-theses repository

This unpublished thesis/dissertation is copyright of the author and/or third parties. The intellectual property rights of the author or third parties in respect of this work are as defined by The Copyright Designs and Patents Act 1988 or as modified by any successor legislation.

Any use made of information contained in this thesis/dissertation must be in accordance with that legislation and must be properly acknowledged. Further distribution or reproduction in any format is prohibited without the permission of the copyright holder.

SYNOPSIS

Four phases of experimental work were carried out on the machinability of Al-Si alloys following an extensive literature review. The review highlighted a number of studies focusing on hypereutectic alloys >13 wt% silicon. Adhered workpiece material, built-up edge on the tool and a high rate of tool wear were found to be the common machining issues. Cutting tool materials for aluminium alloys have progressed from the use of uncoated tungsten carbides (WC) to advanced diamond tools, including polycrystalline diamond (PCD) and chemical vapour deposition (CVD) diamond, as a means to improving workpiece quality and productivity.

The first experimental phase of the project involved an assessment and capability study of the Al-Si C355 compressor impeller machining processes within Doncasters Sterling. Component critical features related to bore/hole diameter, its surface roughness, cylindricity, squareness of the component back-face and nose. The overall equipment effectiveness (OEE) of the Index G200 machine tool was 80%, which was deemed acceptable for the duration of the machine capability assessment. Machine idle time (breakdown, job changeovers, etc.) was found to be the main factor undermining overall effectiveness. Scrap levels associated with machining (burrs, over/undersize, setting, tool breakage, etc.) equated to ~6%. The study also showed that capability indices, Cp (process capability index) and Cpk (minimum process capability index), were above the automotive industries required level of 1.66 and indicated that the machine tools used together with the standard fixtures and tooling were capable of producing parts to specification. This work was followed by production tooling trials and comparative tests involving alternative cutting tool materials including titanium nitride (TiN) and PCD products against existing standard uncoated carbide tooling (Phase 2). Capital cost per edge of the PCD tools was between 10 to 20 times higher than with the standard carbide. All the PCD tools tested met customer requirements with extensive tool life/lower operational cost per part compared with the standard carbide tools. In addition, a substantial ~60% reduction in the setup times was achieved with the PCD reamer, providing improved productivity. Uncharacteristically, the TiN coated tools showed poorer results in terms of thrust force, torque and workpiece surface roughness when compared against uncoated carbide tools. The latter were 27% cheaper in relation to operational costs than the coated tools.

Phase 3 research involved an evaluation of the effect of diamond-like carbon (DLC) coatings against uncoated carbide when blind-hole drilling (28mm deep) and reaming (25mm deep) ~300 holes and assessed tool life/wear, workpiece quality, hole surface roughness and integrity. The Graphit-iC™ coating demonstrated better cutting performance in both drilling and reaming operations with benefits including extensive tool life, ~40% and ~50% lower wear rate when drilling and reaming respectively, and reduced material adhesion/BUE. Surface integrity studies showed microhardness profiles of machined subsurfaces ranging from 141-189HK_{0.025} to a depth of ~75µm for the specimens evaluated. Workpieces machined using WC and Dymon-iC™ experienced pitting and tearing which was not seen with the Graphit-iC™ coating. Microstructural evaluation showed no significant evidence of plastic deformation or microcracks.

The final phase of the research (Phase 4) assessed the performance of CVD diamond coated and PCD tools against standard uncoated carbide when blind-hole drilling and reaming ~1680 holes in automotive aluminium C355. The diamond products showed significantly lower wear rate with little or no workpiece adhesion and BUE compared with uncoated carbide in both drilling and reaming experiments. The CVD diamond coating however produced lower hole diameter accuracy, with poor coating-to-substrate bonding leading to tool catastrophic failure at higher cutting speeds during drilling. In contrast, the brazed PCD tools produced consistent hole quality with surface roughness of maximum ~0.3µm Ra for both drilled and reamed holes. A hardened layer of up to 169.7HK_{0.025} (~10% above bulk hardness) and up to a depth of 75µm from the machined/hole surface was observed in the majority of drilled specimens machined with worn tools, whilst a ~17% increase in microhardness alteration was found in the reaming tests involving the CVD diamond at 96m/min cutting speed. Evaluation of cross-sectioned specimens revealed no surface/subsurface damage in all tests involving the standard carbide, the CVD diamond or the brazed PCD reamers. Minor pitting was observed in drilling tests using the uncoated WC tools, but this would be expected to be removed by a subsequent finishing/reaming operation, and no microstructural alterations were evident during the drilling and reaming trials.

ACKNOWLEDGEMENTS

First and foremost, I would like to thank Dr. Sein Leung Soo (Lecturer and Head of Machining Research Group) and Prof. David Keith Aspinwall in the School of Mechanical Engineering for their academic supervision and guidance over the course of this research. I would also like to thank Mrs. Elaine Aspinwall for helpful discussions on aspects of quality control and statistical experimental design given at various stages of the study.

My sincerest gratitude and appreciation are due to Mr. Brenden Haffner and Dr. Zhu Zhang (Doncasters Sterling), Mr. Dick Arnold (Mapal Ltd.), Mr. Neels Pretorius and Dr. Peter Harden (Element Six Ltd.) for their technical support as well as providing workpiece materials, tooling and funding for the work.

I am also indebted to Mr. Richard Fasham (formerly Senior Technical Engineer) and Mr. Andy Loat (Technical Engineer) in the School of Mechanical Engineering for their assistance with machine tool setup/operation and preparation of workpiece materials for experimental trials. I would like to thank my fellow students in the Machining Research Group for the many insightful discussions over the course of the work. Special thanks also go to the members of staff, machine shop and factory floor members at Doncasters Sterling for their valuable time, sharing of experience and support during production trials. Financial support from the Engineering and Physical Sciences Research Council (EPSRC) is also gratefully acknowledged.

Finally, I would like to express my love and appreciation to my family for their endless encouragement, patience and support throughout the duration of this project.

TABLE OF CONTENTS

Synopsis	i
Acknowledgements	iii
List of figures	xii
List of tables	xxiv
Nomenclature	xxvii
Chapter 1. Introduction	1
1.1 Background to the project.....	1
1.2 Company and project overview	1
1.3 Project collaborators	2
1.4 Specific aims and objectives	3
Chapter 2. Aluminium compressor impeller production and requirements at Doncasters	4
2.1 Introduction	4
2.2 Compressor impeller machining operations, design and varieties	5
2.3 Machine tools	8
2.4 Machine fixtures	9
2.5 Cutting tools and parameters	10
2.5.1 Operation 1 (1a and 1b): Rough turn back-face and outside diameter	11
2.5.2 Operation 2: Centre (spot) drill and chamfer.....	11
2.5.3 Operation 3: Core drill (blind-hole).....	12
2.5.4 Operation 4: Ream (blind-hole).....	13
2.5.5 Operation 5: Finish turn outside diameter and back-face.....	13

2.5.6 Operation 6: Part-off nose	14
2.5.7 Operation 7 (7a and 7b): Rough turn nose and blade	15
2.5.8 Operation 8 (8a and 8b): Finish turn nose and blade.....	15
2.5.9 Operation 9: Chamfer nose.....	16
2.6 Remarks on the current compressor aluminium impeller production at Doncasters Sterling.....	16
Chapter 3. Literature review	18
3.1 Machining of aluminium	18
3.1.1 Background.....	18
3.1.2 Machinability of aluminium alloys	19
3.1.2.1 Effects of silicon in aluminium	22
3.1.2.2 Tool life and wear.....	24
3.1.2.3 Drilling of aluminium alloys	26
3.1.2.4 Cutting forces associated with drilling operations	30
3.1.2.5 Reaming of aluminium alloys.....	31
3.2 Cutting tool materials for aluminium alloys.....	33
3.2.1 Cemented carbides.....	34
3.2.2 Polycrystalline diamond	35
3.2.2.1 Introduction	35
3.2.2.2 Properties and performance	36
3.2.3 Diamond and diamond-like carbon coated tools	39
3.2.3.1 Diamond coated tools	39
3.2.3.2 Diamond-like carbon coated tools.....	41

3.3 Workpiece quality.....	43
3.3.1 Hole dimensional accuracy.....	43
3.3.2 Cylindricity and out-of-roundness.....	43
3.3.3 Workpiece surface finish and integrity.....	46
3.3.3.1 Techniques for surface roughness and integrity measurement.....	52
3.4 Statistical process control	54
3.4.1 Introduction	54
3.4.2 Causes of quality variation	55
3.4.3 Types of control charts and design.....	55
3.4.4 Process capability analysis	56
Chapter 4. Experimental work.....	58
4.1 Workpiece materials	58
4.1.1 Industry based work	58
4.1.1.1 Aluminium compressor impellers for Phase 1 and Phase 2 trials	58
4.1.2 Laboratory based work	59
4.1.2.1 Aluminium blocks for Phase 3A tests	59
4.1.2.2 Aluminium blocks for Phase 3B experiments	61
4.1.2.3 Aluminium blocks for Phase 4 tests	62
4.2 Tool geometries, materials and coatings	64
4.2.1 Industry based work	66
4.2.1.1 Phase 1: Assessment and capability study of current compressor impeller machining processes	66
4.2.1.2 Phase 2: Production tooling trials and comparative work of Sterling standard tools against alternative cutting tool materials.....	67

4.2.2 Laboratory based work	70
4.2.2.1 Phase 3: Evaluation of diamond-like carbon coated tools when drilling and reaming aluminium alloys.....	70
4.2.2.2 Phase 4: Evaluation of diamond coated and PCD tools when drilling and reaming cast C355 aluminium alloy	71
4.3 Equipment.....	74
4.3.1 Machine tools and fixtures	74
4.3.2 Cutting fluid application.....	75
4.3.3 Tool wear evaluation	76
4.3.4 Force measurement.....	77
4.3.5 Workpiece feature geometrical accuracy measurement	78
4.3.6 Workpiece surface roughness and integrity assessment.....	80
4.4 Experimental design, procedures and test arrays.....	83
4.4.1 Industry based work	83
4.4.1.1 Phase 1: Assessment and capability study of current compressor impeller machining processes	83
4.4.1.2 Phase 2: Production tooling trials and comparative work of Sterling standard tools against alternative cutting tool materials.....	84
4.4.2 Laboratory based work	86
4.4.2.1 Phase 3A: Evaluation of diamond-like carbon coated tools when drilling cast C355 aluminium alloy.....	86
4.4.2.2 Phase 3B: Evaluation of diamond-like carbon coated tools when reaming 6082-T6 aluminium alloy	89
4.4.4.3 Phase 4: Evaluation of diamond coated and PCD tools when drilling and reaming cast C355 aluminium alloy	90

Chapter 5. Results and discussion	93
5.1 Industry based work	93
5.1.1 Phase 1: Assessment and capability study of current compressor impeller machining processes	93
5.1.1.1 Machine capacity, scrap level and production issues	93
5.1.1.2 Process capability study on Index G200 machining centre	94
5.1.1.3 Drilling and reaming process control charts.....	96
5.1.2 Phase 2: Production tooling trials and comparative work of Sterling standard tools against alternative cutting tool materials	96
5.1.2.1 Phase 2A: WC and PCD cutting inserts (Operation 1, rough turning/facing). 96	
5.1.2.2 Phase 2B: WC and TiN coated drills (Operation 3, blind-hole drilling).....	103
5.1.2.3 Phase 2C: WC and PCD reamers (Operation 4, blind-hole reaming)	106
5.2 Laboratory based work	107
5.2.1 Phase 3A: Evaluation of diamond-like carbon coated tools when drilling cast C355 aluminium alloy	107
5.2.1.1 Tool life/wear and workpiece material adhesion.....	107
5.2.1.2 Cutting forces	112
5.2.1.3 Workpiece quality.....	114
5.2.1.4 Workpiece surface roughness and integrity.....	116
5.2.1.5 Production tooling trial of Graphit-iC™ coated drills.....	121
5.2.2 Phase 3B: Evaluation of diamond-like carbon coated tools when reaming 6082-T6 aluminum alloy	123
5.2.2.1 Tool life/wear and workpiece material adhesion.....	123
5.2.2.2 Cutting forces	126

5.2.2.3 Workpiece quality.....	128
5.2.2.4 Workpiece surface roughness and integrity.....	129
5.2.3 Phase 4A: Evaluation of diamond coated and PCD tools when drilling cast C355 aluminium alloy	133
5.2.3.1 Tool life/wear and workpiece material adhesion.....	133
5.2.3.2 Cutting forces	138
5.2.3.3 Chip/swarf morphology analysis	140
5.2.3.3 Workpiece quality.....	144
5.2.3.4 Workpiece surface roughness and integrity.....	146
5.2.4 Phase 4B: Evaluation of diamond coated and PCD tools when reaming cast C355 aluminium alloy	152
5.2.4.1 Tool conditions and cutting force.....	152
5.2.4.2 Workpiece quality.....	156
5.2.4.3 Workpiece surface roughness and integrity.....	157
Chapter 6. Conclusions	164
6.1 Literature review.....	164
6.2 Experimental work	165
6.2.1 Industry based work	165
6.2.1.1 Phase 1: Assessment and capability study of current compressor impeller machining processes	165
6.2.1.2 Phase 2: Production tooling trials and comparative work of Sterling standard tools against alternative cutting tool materials.....	166
6.2.2 Laboratory based work	167
6.2.2.1 Phase 3A: Evaluation of diamond-like carbon coated tools when drilling cast C355 aluminium alloy.....	167

6.2.2.2 Phase 3B: Evaluation of diamond-like carbon coated tools when reaming 6082-T6 aluminium alloy	169
6.2.2.3 Phase 4A: Evaluation of diamond coated and PCD tools when drilling cast C355 aluminium alloy.....	169
6.2.2.4 Phase 4B: Evaluation of diamond coated and PCD tools when reaming cast C355 aluminium alloy.....	171
6.3 Summary and recommendations for machining operations of aluminium compressor impellers	171
6.3.1 Process capability study on Index G200 machining centre.....	171
6.3.2 Roughing turning/facing, Op1, of aluminium compressor impellers.....	172
6.3.3 Blind-hole drilling, Op3, of aluminium compressor impellers	172
6.3.4 Blind-hole reaming, Op4, of aluminium compressor impellers	173
Chapter 7. Recommendations for future work.....	175
References.....	176
Appendix A.....	189
Collaborators' contact details	189
Appendix B.....	190
Machine capacity study	190
Process capability study on Index G200	191
Appendix C.....	197
Phase 3A: Evaluation of diamond-like carbon coated tools when drilling cast C355 aluminium alloy.....	197
Appendix D.....	201
Phase 3B: Evaluation of diamond-like carbon coated tools when reaming 6082-T6 aluminium alloy	201

Appendix E	203
Phase 4A: Evaluation of diamond coated and PCD tools when drilling cast C355 aluminium alloy	203
Appendix F	206
Phase 4B: Evaluation of diamond coated and PCD tools when reaming cast C355 aluminium alloy	206
Appendix G	209
List of publications:	209

LIST OF FIGURES

Figure 1: Turbocharger (a) whole assembly and (b) cutaway	4
Figure 2: Compressor impellers (a) cast and (b) machined.....	4
Figure 3: Details of casting and machine defects (a) casting inclusion, (b) positive and (c) blowhole.....	5
Figure 4: Breakdown of impeller machining operations (a) Op1-6 and (b) Op7-9.....	6
Figure 5: Compressor impeller machining process flowchart.....	7
Figure 6: Index G200 CNC centre lathe.....	8
Figure 7: Schematic layout of Index G200 [4].....	8
Figure 8: View of the spindles and turrets on the Index G200.....	9
Figure 9: Main spindle workpiece holding (a) assembly and (b) collet and multi-pin unit for Operations 1 to 5	9
Figure 10: Counter spindle workpiece holding (a) assembly and (b) back stop unit and collet for Operations 6 to 9	10
Figure 11: Carbide roughing insert.....	11
Figure 12: Centre/spot drill.....	11
Figure 13: Core drill	12
Figure 14: Reamer	13
Figure 15: PCD finishing insert.....	13
Figure 16: Part-off insert	14
Figure 17: PCD roughing insert	15
Figure 18: Carbide finishing insert.....	15

Figure 19: Optical images of aluminium BUE on HSS drill cutting edges in (a) dry and (b) H ₂ O-MQL conditions and aluminium adhesion to HSS drill flutes in (c) dry and (d) H ₂ O-MQL conditions [24]	22
Figure 20: Mechanical properties of Al-Si alloys as function of silicon content [36]	23
Figure 21: SEM pictures of conditions of carbide K10 tools after machining (a) pure aluminium and (b) AlSi12 for 30seconds and chip morphology after machining (c) pure aluminium and (d) AlSi12 for 30seconds [40].....	24
Figure 22: Average tool flank wear for different cutting speeds and conditions when machining 6061 aluminium alloy. Feed rate $f = 0.15\text{mm/rev}$ and depth of cut $d = 1.0\text{mm}$ [45]	25
Figure 23: Wear curves (a) normal wear and (b) evolution of flank wear land VB_B at different cutting speeds [26].....	26
Figure 24: Typical formed chips (a) conical, (b) fan shaped, (c) chisel edge, (d) amorphous, (e) needle, f) impacted when drilling cast SAE 308 and 390 aluminium alloys [52]	27
Figure 25: Photos of material build up in drill flutes at speeds (a) 2500rev/min, (b) 5000rev/min, (c) 7500rev/min and (d) 10000rev/min [57]	28
Figure 26: Various types of drill wear [63]	30
Figure 27: Schematic diagram of a reamer [38]	32
Figure 28: Hardness and toughness of cutting tool materials [51]	33
Figure 29: Typical hot hardness characteristics of various tool materials [86].....	34
Figure 30: Polycrystalline diamond (a) blanks and (b) cutting insert [121].....	36
Figure 31: Tool wear for different polycrystalline diamond grades when machining Al-Si alloy (18%Si) [73]	38
Figure 32: Structure of different PCD grades [121]	38
Figure 33: Tool life performance of PCD against other cutting tool materials in the machining of hypereutectic Al-Si die casting alloy [115].....	39

Figure 34: Surface finish performance of Uncoated WC, Diamond coated WC and PCD on cutting aluminium alloy 6351 [129]	39
Figure 35: Assessment of roundness (a) ring gauge, (b) plug gauge, (c) minimum zone and (d) least squares [181]	44
Figure 36: Form deviation of (a) internal and (b) external roundness features [182]	45
Figure 37: Reference cylinders used for cylindricity analysis (a) minimum circumscribed, (b) maximum inscribed, (c) minimum zone and (d) least square [183, 184]	45
Figure 38: Variations in shape of cylindrical features (a) hourglass, (b) barrel, (c) bell-mouth, (d) banana and (e) taper [185]	46
Figure 39: Schematic surface features of a manufactured component [189]	47
Figure 40: Micrograph of AlSi9 machined surface [195]	49
Figure 41: Optical micrograph of Al-Si drilled workpiece subsurface [18]	49
Figure 42: Workpiece surface roughness and fatigue life as a function of cutting speed [198]	50
Figure 43: Variation of surface roughness with different cutting speeds and feeds for Al and Al/SiC [199]	51
Figure 44: SEM images of Al MMC machined surface showing (a) cracks, (b) pits, (c) micro cracks and (d) fracture/crushed SiC particle [33, 202]	51
Figure 45: Machined subsurface of Al MMC [202]	52
Figure 46: Schematic of typical surface roughness profile parameters [204]	53
Figure 47: Typical control chart	55
Figure 48: C355 aluminium compressor impellers in (a) cast and (b) machined condition for Phase 1 and 2 trials	59
Figure 49: Al workpiece blocks in (a) cast and (b) cast/machined form for Phase 3A tests...	60
Figure 50: Adapted mould for casting workpiece blocks	60
Figure 51: Machined aluminium 6082-T6 test pieces	61

Figure 52: Phase 4 workpiece preparation for (a) permanent cast iron die, (b) die assembly and (c) cast/machined aluminium blocks	63
Figure 53: Walter Titex A1167B uncoated carbide twist drill	64
Figure 54: Walter Titex A1167B cemented tungsten carbide drill geometry details, dimensions are in mm [219]	65
Figure 55: Mapal Beck RV3188 cemented tungsten carbide reamer	65
Figure 56: Mapal Beck RV3188 uncoated carbide reamer geometry details, dimensions are in mm [220]	65
Figure 57: Turning inserts (a) Kennametal CCGT09T308HP KC5410 TiB ₂ coated carbide for roughing and (b) Exactaform DCGT11T304 PCD for finishing.....	66
Figure 58: Turning inserts (a) Exactaform CCGT09T308 and (b) Kennametal DCGT11T304HP KC5410 TiB ₂ coated carbide.....	67
Figure 59: PCD roughing inserts (a) standard Mapal CCGW09T308 F01N 0AA and (b) Mapal with chip breaker geometry CCGT09T308F01N C2A	68
Figure 60: Guhring 611 TiN coated carbide drill	69
Figure 61: Mapal brazed Syndite CTB002 PCD reamer	69
Figure 62: Mapal brazed PCD CTB002 reamer geometry details [220]	69
Figure 63: Tools used in Phase 3A (a) uncoated WC, (b) Graphit-iC™ and (c) Dymon-iC™	70
Figure 64: Tools used in Phase 3B (a) uncoated WC, (b) Dymon-iC™ and (c) Graphit-iC™	71
Figure 65: Uncoated, CVD diamond coated carbide and PCD drills.....	72
Figure 66: Brazed Syndite CTB010 PCD drill.....	72
Figure 67: Geometry details of brazed PCD drill [220]	73
Figure 68: Uncoated, CVD diamond coated carbide and brazed PCD reamers.....	73
Figure 69: Geometry details of brazed PCD reamer [220].....	74
Figure 70: Workpiece and work holding unit used in Sterling.....	75

Figure 71: Matsuura FX-5 high speed machining centre	75
Figure 72: Cutting fluid arrangements on FX-5 (a) flood and (b) high pressure cutting fluid	76
Figure 73: High pressure through-tool cutting fluid arrangement on FX-5 for Phase 3B and 4B	76
Figure 74: Typical tool flank wear measurement setup for (a) round cutting tools and (b) inserts.....	77
Figure 75: Force measurement setup and equipment (a) Kistler turning dynamometer and (b) Kistler drilling/reaming dynamometer	78
Figure 76: Typical force calibration on the dynamometer	78
Figure 77: Hole diameter measurement equipment (a) Mahr air gauge unit and (b) mandrel with setting ring	79
Figure 78: Images of (a) MG squareness test unit and (b) Mitutoyo Surftest series SJ400	79
Figure 79: Images of (a) Taylor Hobson series 131 and (b) hole diameter measuring equipment.....	80
Figure 80: Illustration of (a) Taylor Hobson Talyrond series 300 and (b) hole assessment setup.....	80
Figure 81: Illustration of (a) Taylor Hobson Form Talysurf series 120L and (b) surface roughness setup.....	81
Figure 82: Typical cold resin mounted sample with schematic layout of drilled hole sectioning	81
Figure 83: Illustration of (a) Buehler grinder/polisher and (b) SiC paper and polishing cloths	82
Figure 84: Illustration of (a) Mitutoyo microhardness test unit and (b) Leica DMLM microscope	83
Figure 85: Compressor impeller critical quality features/dimensions.....	84
Figure 86: Surface roughness measurement setup for rough turning operation 1	85

Figure 87: Test setup for blind hole drilling trials.....	87
Figure 88: Force measurement setup.....	88
Figure 89: Typical measurement of workpiece microhardness.....	89
Figure 90: Typical reaming force with high pressure cutting fluid at 32m/min speed and 0.12mm/rev feed rate	90
Figure 91: Machine shop scrap analysis for year 2008 over weeks 11-21	93
Figure 92: Burr formation on impeller blades	97
Figure 93: Micrographs of (a) new and (b) worn Kennametal Type 1 WC insert	97
Figure 94: Micrographs of (a) new and (b) worn Mapal Type 3 PCD insert.....	98
Figure 95: Micrographs of (a) new and (b) worn Mapal Type 4 PCD insert.....	98
Figure 96: SEM image of failed Exactaform Type 2 PCD insert.....	99
Figure 97: Chips shapes produced by different inserts during rough turning operation	100
Figure 98: Cutting force during the first turning/facing stages: A-outside diameter, B-main back-face and C-back-face profile.....	100
Figure 99: Average maximum cutting forces (Fx) of inserts on roughing operation.....	101
Figure 100: Workpiece surface roughness by different cutting inserts	102
Figure 101: Micrographs of (a) new and (b) worn tungsten carbide Titex A1167B drill	103
Figure 102: Micrographs of (a) worn chisel edge and (b) worn drill flute.....	103
Figure 103: Micrographs of (a) new and (b) worn TiN coated carbide Guhring 611 drill ...	104
Figure 104: Micrographs of (a) worn chisel edge and (b) worn drill flute.....	104
Figure 105: Average maximum drilling thrust force by Titex and Guhring drills.....	104
Figure 106: Average maximum drilling torque by Titex and Guhring drills	105
Figure 107: Average workpiece surface roughness by Titex and Guhring drills.....	105
Figure 108: Schematic tool reground area on the PCD blank	106

Figure 109: End of test micrographs of uncoated carbide drills in (a) Test 1 and (b) Test 2	108
Figure 110: End of test micrographs of uncoated carbide drills in (a) Test 7 and (b) Test 8	108
Figure 111: End of test micrographs of Graphit-iC™ coated drills in (a) Test 3 and (b) Test 4	109
Figure 112: End of test micrographs of Graphit-iC™ coated drills in (a) Test 9 and (b) Test 10	109
Figure 113: End of test micrographs of Dymon-iC™ coated drills in (a) Test 5 and (b) Test 6	109
Figure 114: End of test micrographs of Dymon-iC™ coated drills in (a) Test 11 and (b) Test 12	110
Figure 115: Phase 3A – Drill wear curves under low pressure cutting fluid application	110
Figure 116: Phase 3A – Drill wear curves under high pressure cutting fluid application	112
Figure 117: Phase 3A – Drilling thrust force for all tests	112
Figure 118: Typical impurity/defect found within the work material	113
Figure 119: Phase 3A – Drilling torque of all tests	114
Figure 120: Phase 3A – Drilled hole diameter under low pressure/flood cutting fluid application	115
Figure 121: Phase 3A – Drilled hole diameter under high pressure cutting fluid application	115
Figure 122: Phase 3A – Drilled hole quality	116
Figure 123: Phase 3A – Drilled surface roughness (2mm from hole entry)	117
Figure 124: Phase 3A – Drilled surface roughness (23mm from hole entry)	118
Figure 125: Typical adhered material observed on cross-section of hole	118
Figure 126: Phase 3A – Microhardness of cross-sections of drilled hole 1 (12mm from entry)	119

Figure 127: Phase 3A – Microhardness of cross-sections of drilled hole 154 (12mm from entry)	119
Figure 128: Phase 3A – Microhardness of cross-sections of drilled hole 307 (12mm from entry)	120
Figure 129: Phase 3A – Microstructure of subsurface of drilled hole (12mm from entry)...	120
Figure 130: Phase 3A – Production trial hole cylindricity result by Graphit-iC™ (data produced on Talyrond series 131).....	121
Figure 131: Phase 3A – Breakage of Graphit-iC™ drills during production trial due to incorrect setup and casting material defects.....	122
Figure 132: Photograph of (a) defect in material casting and (b) X-ray image of broken drill	122
Figure 133: Phase 3B – Micrograph of tool wear and swarf build up at the end of test	123
Figure 134: Phase 3B – Wear curve of reamers	124
Figure 135: Phase 3B swarf entrapment of cutting tool/tool holder for low and high cutting speeds	125
Figure 136: Phase 3B – Reaming thrust force.....	127
Figure 137: Phase 3B – Reaming torque.....	127
Figure 138: Phase 3B – Reamed hole diameter.....	128
Figure 139: Phase 3B – Reamed hole quality	129
Figure 140: Phase 3B – Reamed surface roughness (2mm from hole entry)	130
Figure 141: Phase 3B – Reamed surface roughness (23mm from hole entry)	130
Figure 142: Phase 3B – Microhardness of cross-sections of reamed hole (12mm from entry, reaming speed 32m/min).....	131
Figure 143: Phase 3B – Microhardness of cross-sections of reamed hole (12mm from entry, reaming speed 96m/min)	132

Figure 144: Subsurface microstructure of reamed hole produced with uncoated coated carbide tool (12mm from entry)	132
Figure 145: Subsurface microstructure of reamed hole produced with Graphit-iC™ tool (12mm from entry)	133
Figure 146: Subsurface microstructure of reamed hole produced with Dymon-iC™ tool (12mm from entry)	133
Figure 147: Phase 4A –Micrographs of uncoated carbide drills in the worn condition in (a) Test 1 and (b) Test 2.....	134
Figure 148: Phase 4A – End of test micrographs for CVD diamond coated drills under (a) Test 3 and (b) Test 4.....	134
Figure 149: Phase 4A – End of test micrographs for PCD CTB010 drills under (a) Test 5 and (b) Test 6.....	135
Figure 150: Phase 4A – End of test micrographs for PCD CTM302 drills under (a) Test 7 and (b) Test 8.....	135
Figure 151: SEM image of worn CVD diamond coated drill in Test 4 (260m/min)	135
Figure 152: New/as-received condition of PCD drills used in (a) Test 5, (b) Test 6, (c) Test 7 and (d) Test 8.....	136
Figure 153: Phase 4A – Drill flank wear curves	137
Figure 154: Phase 4A – Drilling force.....	138
Figure 155: Phase 4A – Drilling torque.....	139
Figure 156: Phase 4A – Various chip forms/shapes produced when drilling C355 aluminium at different cutting speeds and tool materials	141
Figure 157: Chip formation produced by uncoated tungsten carbide drills under different cutting speeds in (a) Test 1 (130m/min) and (b) Test 2 (260m/min)	142
Figure 158: Chip formation produced by CVD diamond coated drills under different cutting speeds in (a) Test 3 (130m/min) and (b) Test 4 (260m/min)	142

Figure 159: Chip formation produced by PCD CTB010 drills under different cutting speeds in (a) Test 5 (130m/min) and (b) Test 6 (260m/min)	143
Figure 160: Chip formation produced by PCD CTM302 drills under different cutting speeds in (a) Test 7 (130m/min) and (b) Test 8 (260m/min)	143
Figure 161: Phase 4A – Drilled hole diameter	145
Figure 162: Phase 4A – Drilled hole quality	145
Figure 163: Typical form cylindricity with positive parallelism observed in Test 6 using CTB010 PCD at a cutting speed of 260m/min.....	146
Figure 164: Phase 4A – Drilled hole surface roughness (2mm from entry).....	147
Figure 165: Phase 4A – Drilled hole surface roughness (25mm from entry).....	147
Figure 166: Cross-sections of holes from (a) Test 1 – entry and (b) Test 6 – exit.....	148
Figure 167: Phase 4A –Microhardness of cross-sections of drilled hole (12mm from entry, drilling speed 130m/min)	149
Figure 168: Phase 4A –Microhardness of cross-sections of drilled hole (12mm from entry, drilling speed 260m/min)	149
Figure 169: Phase 4A – Subsurface microstructure of drilled hole produced with uncoated carbide tool – Test 1 (12mm from entry)	150
Figure 170: Phase 4A – Subsurface microstructure of drilled hole produced with uncoated carbide tool – Test 2 (12mm from entry)	150
Figure 171: Phase 4A – Subsurface microstructure of drilled hole produced with CVD diamond coated tool – Test 3 (12mm from entry)	150
Figure 172: Phase 4A – Subsurface microstructure of drilled hole produced with PCD CTB010 tool – Test 6 (12mm from entry)	151
Figure 173: Phase 4A – Subsurface microstructure of drilled hole produced with PCD CTM302 tool – Test 7 (12mm from entry)	151
Figure 174: Phase 4A – Subsurface microstructure of drilled hole produced with PCD CTM302 tool – Test 8 (12mm from entry)	151

Figure 175: Phase 4B – End of test micrographs for uncoated carbide reamers in (a) Test 1 and (b) Test 2.....	152
Figure 176: Phase 4B – End of test micrographs for CVD diamond reamers in (a) Test 3 and (b) Test 4.....	153
Figure 177: Phase 4B – End of test micrographs for PCD CTB002 reamers in (a) Test 5 and (b) Test 6.....	153
Figure 178: Phase 4B – End of test micrographs for PCD CTM302 reamers in (a) Test 7 and (b) Test 8	153
Figure 179: Phase 4B – Maximum reaming thrust force.....	154
Figure 180: Phase 4B – Maximum reaming torque.....	154
Figure 181: SEM images of new (a) uncoated and (b) CVD diamond coated reamers	155
Figure 182: Typical unstable thrust force and torque signal recorded in Test 4 and 7	155
Figure 183: Phase 4B – Reamed hole diameter.....	156
Figure 184: Phase 4B – Reamed hole geometric quality	157
Figure 185: Phase 4B – Reamed hole surface roughness (2mm from entry).....	158
Figure 186: Phase 4B – Reamed hole surface roughness (23mm from entry).....	158
Figure 187: Phase 4B – Microhardness of cross-sections of reamed hole (12mm from entry, reaming speed 32m/min).....	159
Figure 188: Phase 4B – Microhardness of cross-sections of reamed hole (12mm from entry, reaming speed 96m/min).....	160
Figure 189: Phase 4B – Subsurface microstructure of reamed hole produced with uncoated carbide tool – Test 1 (12mm from entry)	160
Figure 190: Phase 4B – Subsurface microstructure of reamed hole produced with uncoated carbide tool – Test 2 (12mm from entry)	161
Figure 191: Phase 4B – Subsurface microstructure of reamed hole produced with CVD diamond carbide tool – Test 3 (12mm from entry)	161

Figure 192: Phase 4B – Subsurface microstructure of reamed hole produced with CVD diamond carbide tool – Test 4 (12mm from entry)	161
Figure 193: Phase 4B – Subsurface microstructure of reamed hole produced with PCD CTB002 tool – Test 5 (12mm from entry)	162
Figure 194: Phase 4B – Subsurface microstructure of reamed hole produced with PCD CTB002 tool – Test 6 (12mm from entry)	162
Figure 195: Phase 4B – Subsurface microstructure of reamed hole produced with PCD CTM302 tool – Test 7 (12mm from entry)	162
Figure 196: Phase 4B – Subsurface microstructure of reamed hole produced with PCD CTM302 tool – Test 8 (12mm from entry)	163

LIST OF TABLES

Table 1: Product and process information for Operation 1	11
Table 2: Product and process information for Operation 2	12
Table 3: Product and process information for Operation 3	12
Table 4: Product and process information for Operation 4	13
Table 5: Product and process information for Operation 5	14
Table 6: Product and process information for Operation 6	14
Table 7: Product and process information for Operation 7	15
Table 8: Product and process information for Operation 8	16
Table 9: Product and process information for Operation 9	16
Table 10: Aluminium classifications [5, 6]	18
Table 11: Properties of cast C355 aluminium alloys [1, 9]	19
Table 12: Power and cutting force requirements in machining of different materials [10]	20
Table 13: Properties of WC-Co tool materials at room temperature [73]	35
Table 14: Physical properties of polycrystalline diamond [108, 126]	37
Table 15: List of surface alterations during material removal [188]	47
Table 16: Different levels of surface integrity data tests [191, 192]	48
Table 17: Recommended minimum values for process capability C_p [211]	57
Table 18: Mechanical and physical properties of cast C355 Al alloy [1]	59
Table 19: Heat treatment times and temperatures for C355 material used at Doncasters Sterling [1]	59
Table 20: Average mechanical properties of the cast C355 Al alloy made using the adapted plaster mould [1]	61

Table 21: Mechanical properties of commercial aluminium 6082-T6 alloy [1]	62
Table 22: Mechanical properties of the C355 alloy produced using the cast iron permanent die [1].....	63
Table 23: Tool details for hole machining operations [219, 220]	66
Table 24: Tool details of roughing and finishing indexable inserts used in Phase 1 [221, 222]	67
Table 25: Tool details for Mapal PCD roughing inserts used in Phase 2 [121, 220].....	68
Table 26: Details for alternative tools used for drilling and reaming operations in Phase 2 [121, 220, 223].....	70
Table 27: Details of tools and coatings used in Phase 3 [73, 224].....	71
Table 28: Details of drills used in Phase 4 [73, 121, 225].....	73
Table 29: Details of reamers used in Phase 4 [73, 121, 225]	74
Table 30: Buehler grinding and polishing procedure for Al alloy	82
Table 31: Component critical features and associated limits	84
Table 32: Test operating parameters	85
Table 33: Test matrix for Phase 2A rough facing	86
Table 34: Test matrix for Phase 2B drilling	86
Table 35: Test matrix for Phase 2C reaming.....	86
Table 36: Test matrix for Phase 3A.....	87
Table 37: Test matrix for Phase 3B.....	90
Table 38: Test matrix for Phase 4A.....	91
Table 39: Test matrix for Phase 4B.....	92
Table 40: Process capability indices/values based on compressor impeller critical quality features.....	95

Table 41: Operational cost of roughing inserts	102
Table 42: Operation cost of drills	106
Table 43: Operational cost of reamers.....	107
Table 44: Summary of Operation 1/rough turning/facing.....	172
Table 45: Summary of Operation 3/drilling	173
Table 46: Summary of Operation 4/reaming.....	174

NOMENCLATURE

%	:	Percentage
<	:	Less than
>	:	More than
°C	:	Degree Celsius
μ	:	Coefficient of friction
μm	:	Micrometre
aC	:	Amorphous carbon
Al	:	Aluminium
BUE	:	Built-up edge
C	:	Carbon
CL	:	Centre line
cm	:	Centimetre
CMM	:	Co-ordinate measuring machine
Co	:	Cobalt
COE	:	Coefficient of thermal expansion
Cp	:	Process capability index
Cpk	:	Minimum process capability index
CR	:	Critical quality feature
Cu	:	Copper
CVD	:	Chemical vapour deposition
D	:	diameter (mm)
DLC	:	Diamond-like carbon

EDM	:	Electrical discharge machining
EDX	:	Energy dispersive x-ray spectroscopy
Fe	:	Iron
GPa	:	Gigapascal
HB	:	Brinell hardness
HK	:	Knoop hardness
HRC	:	Rockwell hardness
HSS	:	High speed steel
HV	:	Vickers hardness
K	:	Kelvin
kg	:	Kilogram
LCL	:	Lower control limit
LSL	:	Lower specification limit
m	:	Metre
max.	:	Maximum
MeC	:	Metal containing carbon
Mg	:	Magnesium
min	:	Minute
mm	:	Millimetre
Mn	:	Manganese
MPa	:	Megapascal
MQL	:	Minimum quantity lubrication
n	:	Machine spindle rotational speed (rev/min)

N	:	Newton
NaOH	:	Sodium hydroxide
OEE	:	Overall Equipment Effectiveness (%)
p	:	Pence
PCD	:	Polycrystalline diamond
PVD	:	Physical vapour deposition
Ra	:	Arithmetic average surface roughness (μm)
rev	:	Revolution
R _{max}	:	Maximum surface roughness (μm)
rev/min	:	Revolutions per minute
Rt	:	Total surface roughness (μm)
R _y	:	Peak-to-valley height surface roughness (μm)
SEM	:	Scanning electron microscopy
Si	:	Silicon
SiC	:	Silicon carbide
SPC	:	Statistical process control
taC	:	Tetrahedral amorphous carbon
Ti	:	Titanium
Ti(C, N)	:	Titanium carbonitride
TiB ₂	:	Titanium diboride
TiC	:	Titanium carbide
TiN	:	Titanium nitride
UCL	:	Upper control limit

USL	:	Upper specification limit
VB_{Bmax}	:	Maximum width of tool flank wear (mm)
V_c	:	Cutting speed (m/min)
W	:	Watt
WC	:	Tungsten carbide
WHU	:	Work holding unit
Zn	:	Zinc

CHAPTER 1: INTRODUCTION

1.1 Background to the project

Process optimisation is one of the many strategies that industries adopt to improve business competitiveness. It is implemented to ensure process effectiveness, reduce costs and improve product quality. The strategy involves making continuous improvements to the existing process in order to maximise productivity without unnecessary acquisition of new equipment or facilities. Manufacturing process optimisation may focus on reduction of process variability and scrap rate through selection of appropriate tooling, use of suitable operating parameters and a full understanding of the process itself. Optimum conditions and parameters during cutting, such as feed rate, cutting speed and depth of cut, together with appropriate cutting tools, should be selected to ensure economy of machining operations, which are often assessed by productivity metrics and total manufacturing costs per unit.

Doncasters Sterling specialises in the machining of aluminium alloy turbocharger compressor impellers used in passenger and commercial vehicles. The company's success relies on its ability to fulfill customer demand in terms of component numbers as well as satisfying stringent component dimensional tolerances. At the outset of the project, the overall machine shop scrap rate of ~17%, excluding foundry work, was considered unacceptable and a burden on the business. Consequently, the company had a need to improve machining processes and productivity in response to customer demand. As a result, this led the project to investigate and assess Sterling's existing machining processes, explore alternative machining strategies and cutting tool materials.

1.2 Company and project overview

Doncasters Ltd. is a leading international engineering group that manufactures precision components and assemblies for the aerospace, power generation, automotive/transportation, petrochemical, construction, and recreation markets. It operates from sites in the UK, Europe, USA, Mexico and China with an estimated annual turnover of \$1billion [1]. Doncasters Sterling is one of the group companies, based in Coventry (UK), which manufactures turbocharger impellers in aluminium for passenger and commercial vehicles. It produces around 5 million impellers annually with diameters ranging from 30mm-300mm. The company has advanced casting facilities and fully automated machines capable of producing high precision compressor impellers. Component machining operates round the

clock with two identical machine tools producing ~10000 impellers per week. The company is looking to raise its competitiveness by increasing the current level of machining productivity, improving overall quality of the product and reducing operation costs.

In order to optimise the existing compressor impeller machining processes, it was proposed that the project undertake tooling trials/performance studies of different types of cutting tool materials suitable for aluminium machining. These involved utilising the company's existing machine tools and standard tooling in order to provide a baseline for future comparison. Special cutting tools were also provided by collaborators. It was anticipated that in-company work would require manpower/operator assistance and consequently disruption of production during machine setup, tool and workpiece assessment, etc. This was cited as a major challenge of the project, because not only would daily production be halted but also a high level of scrap components could be generated with a risk of machine tool breakdown during on-site trials. The work would however allow Doncasters Sterling to build on their relationship with tool manufacturers/suppliers with valuable technical support during and after project completion, and access to the machining database and comprehensive experimental results for use with decision making/machining process optimisation. In addition, the company would gain a number of financial benefits including tool cost savings, enhanced operational efficiency and improved output volume and machined component quality.

1.3 Project collaborators

The research was carried out as part of an Engineering Doctorate (EngD) degree programme with much of the preliminary work undertaken within Doncasters Sterling (assessment of in-company data, workpiece preparation, tooling trials, etc). University of Birmingham School of Mechanical Engineering facilities were also utilised for experimental based machinability tests, and analysis of results, etc. The project also involved collaboration with Element Six Ltd., Ireland, (PCD product manufacturer) and Mapal Ltd., UK, (cutting tool manufacturer) which provided tooling and specialist technical knowledge in their relevant fields as well as financial support. Supplementary involvement with Teer Coatings Ltd., UK (now part of the Miba Group), and CemeCon, Germany, was sought for the provision of specific cutting tool coatings and associated technical support. In addition, the Engineering and Physical Sciences Research Council (EPSRC) provided finance in relation to tuition fees. See Appendix A for details of collaborators and academic supervisors.

1.4 Specific aims and objectives

Specific objectives of the work were to:

- Carry out a comprehensive assessment of the existing aluminium compressor impeller machining processes within Doncasters Sterling, entailing details of machine tools and equipment, machine operations, cutting tools and parameters, production and scrap levels, etc.
- Establish baseline process capability indices (C_p and C_{pk} values) for the current machining processes.
- Undertake a detailed literature review of machinability and tool materials in aluminium machining.
- Identify appropriate tooling for the impeller machining operations through experimental evaluation of various cutting tool materials including tungsten carbide (WC), polycrystalline diamond (PCD), diamond-like carbon (DLC) and other chemically vapour deposited (CVD) diamond products. Assess associated key performance indicators including tool wear/life, tool cutting forces (thrust and torque), workpiece geometrical accuracy and surface integrity (surface roughness, microhardness and microstructure).
- Perform a cost analysis of alternative tooling and manufacturing practices for the production of compressor impellers.

CHAPTER 2: ALUMINIUM COMPRESSOR IMPELLER PRODUCTION AND REQUIREMENTS AT DONCASTERS

2.1 Introduction

Exhaust gas turbochargers, see example in Figure 1, are used with internal combustion engines to increase power output, lower emissions and improve fuel consumption. They comprise a number of parts/elements, one of which is the compressor wheel/impeller, see Figure 2, which draws in and pre-compresses air during rotation of the turbine shaft driven by the exhaust gas energy. The component operates at a high velocity, up to 150,000rev/min, and is subjected to high stresses and temperatures ($\sim 200^{\circ}\text{C}$ discharged temperature) during operation [2, 3].

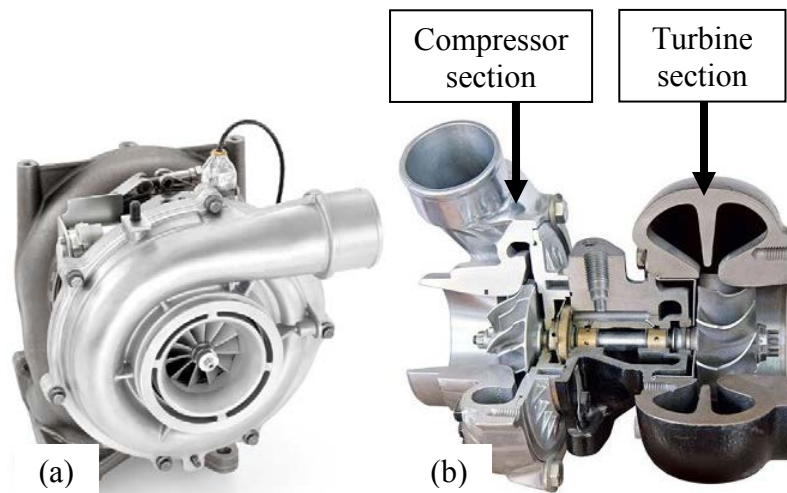


Figure 1: Turbocharger (a) whole assembly and (b) cutaway

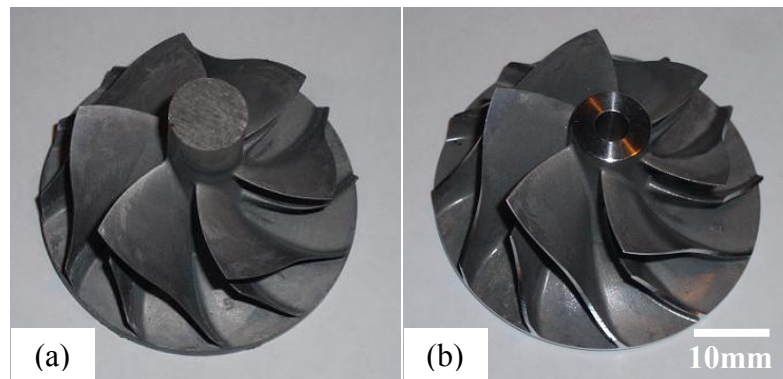


Figure 2: Compressor impellers (a) cast and (b) machined

2.2 Compressor impeller machining operations, design and varieties

Like other engineered components, the aluminium compressor impeller is required to be machined to specified tolerances for safety and functionality purposes. The necessary fit of the turbine shaft requires a minimum hole surface roughness $<0.2\mu\text{m Ra}$, with cylindricity of $<5\mu\text{m}$, to ensure appropriate balance of the impeller-turbine assembly. Essentially, compressor wheels are made from either aluminium alloy (American Aluminium Association) C355 or P354 with respective silicon contents of 5% and 9% and workpiece material hardness of 114-117HB and 129-138HB. Quality control and inspection of the compressor impellers is carried out during production. Defects which are evident during and after machining include those produced by the casting operation: inclusions, positives/porosity, blowholes, together with machine defects such as marks on the component caused by trapped swarf, burrs, bent blades, etc. due to wrong setups and non-conformance tooling/fixtures (multi-pin, back stop, etc.). Examples of casting and machine defects are shown in Figure 3. The production of compressor impellers, ranging from 40mm-70mm diameter, at Doncasters Sterling involves a total of nine machining operations. The breakdown of these operations is shown in Figure 4 while Figure 5 details the compressor impeller machining process flowchart giving the sequence of operations. These include the loading/unloading of components by the ALMA jaws/work holding unit (WHU) to and from the machine main spindle for operations 1-5 and the counter spindle operations numbered 6-9.

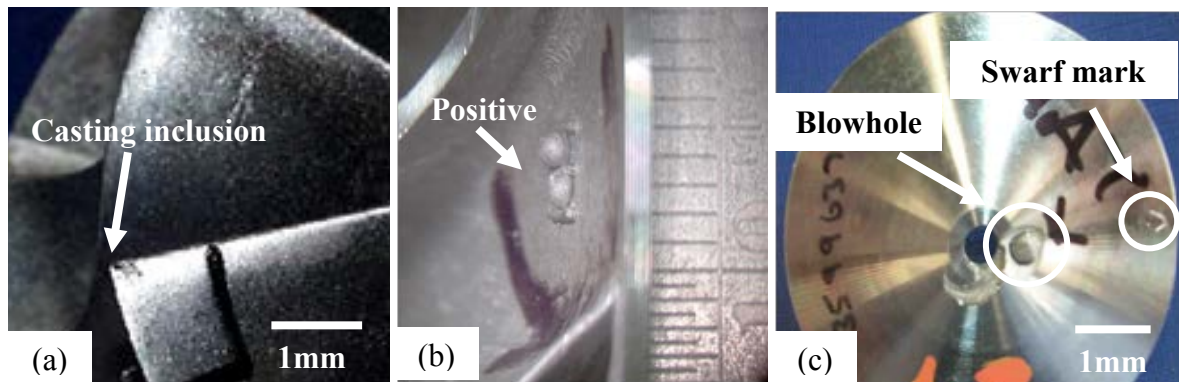


Figure 3: Details of casting and machine defects (a) casting inclusion, (b) positive and (c) blowhole

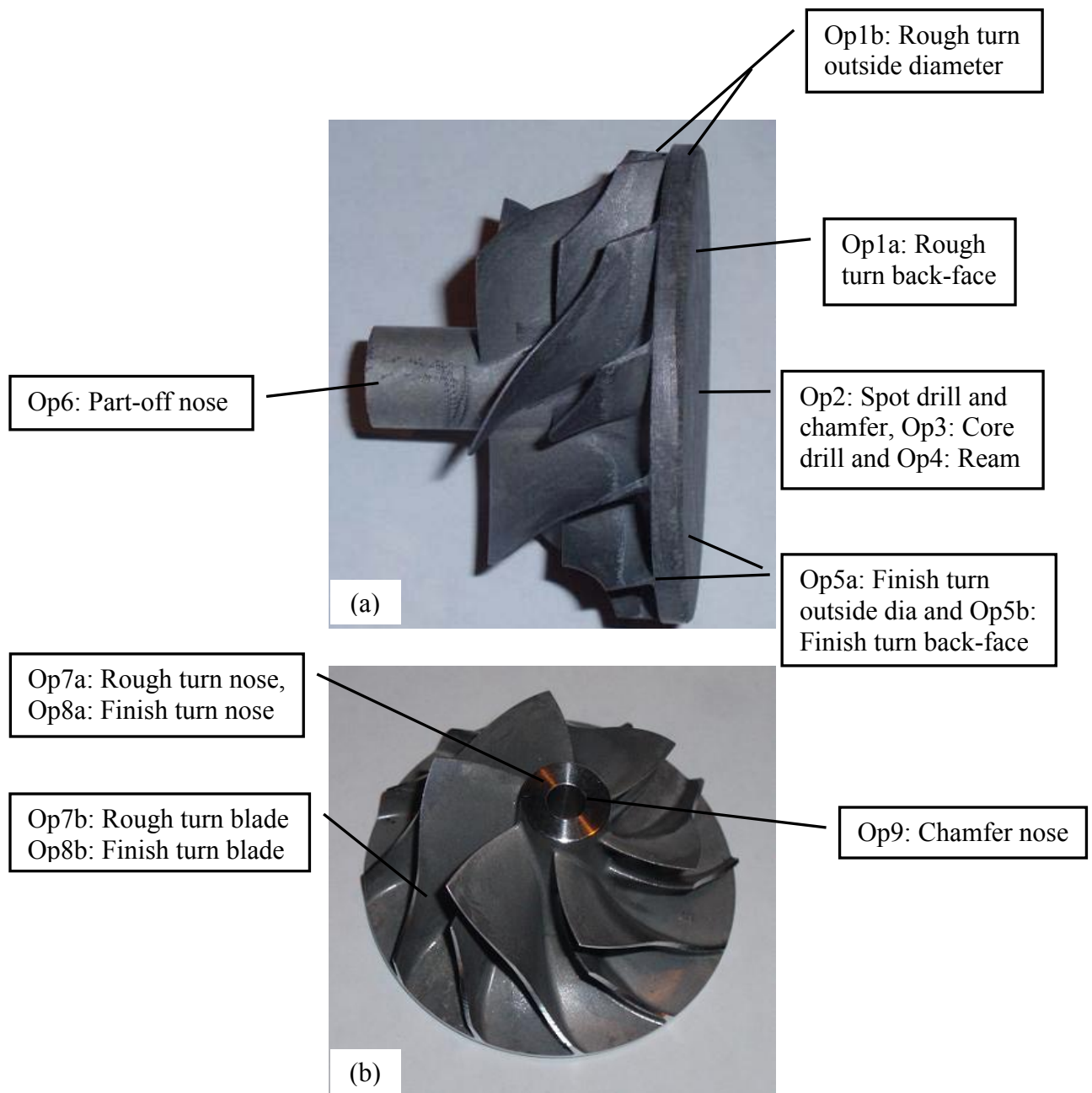


Figure 4: Breakdown of impeller machining operations (a) Op1-6 and (b) Op7-9

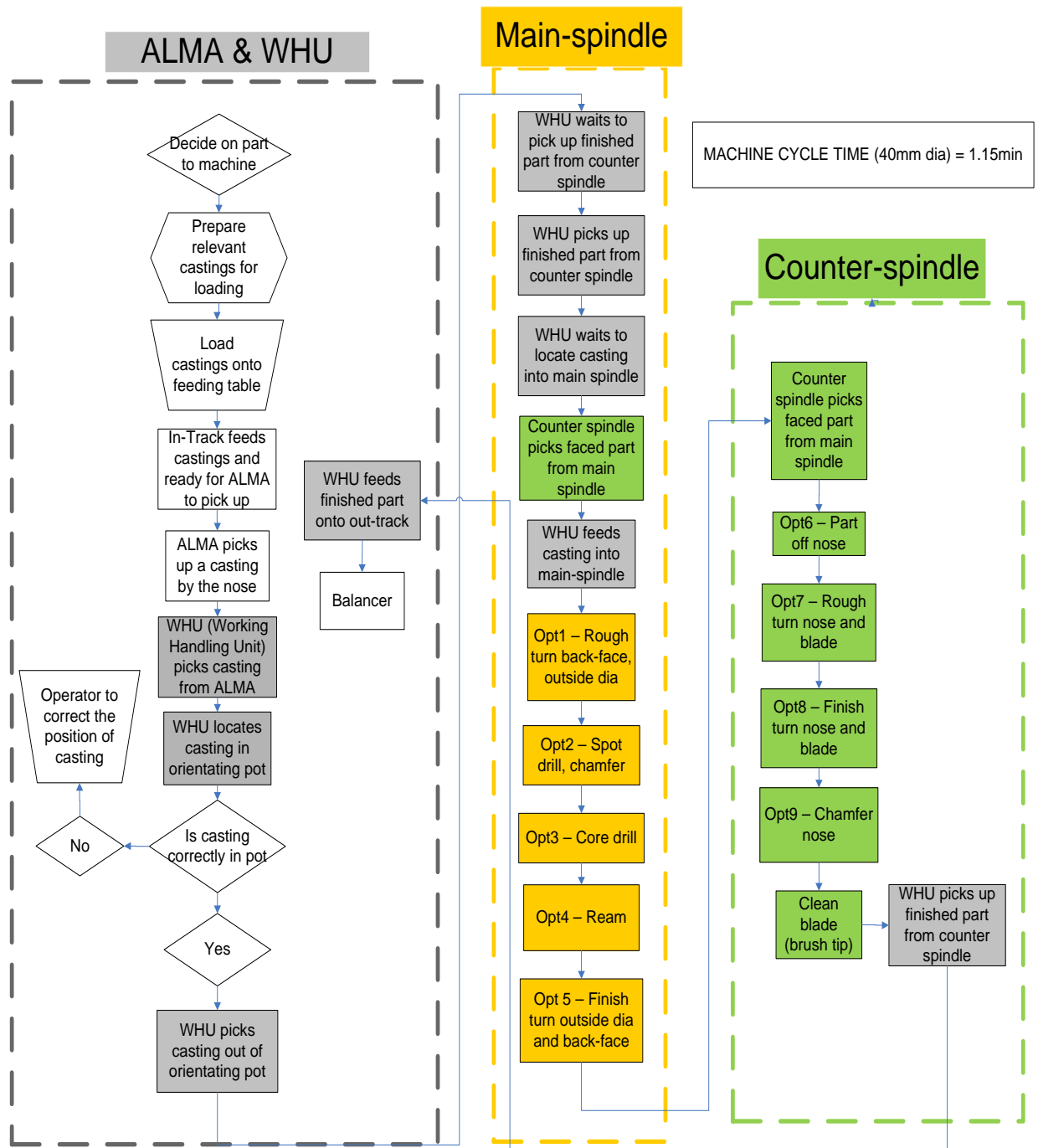


Figure 5: Compressor impeller machining process flowchart

2.3 Machine tools

Two Index G200 centre lathes, supplied by Geo Kingsbury Machine Tools Ltd. in 2000, are currently used to machine the required compressor wheels, see example in Figure 6. These are horizontal CNC centre lathe type machines with twin-opposed spindles, having a power rating of 20kW per spindle, and twin turrets. Figure 7 [4] and Figure 8 show a schematic and photographic details of the spindles and turrets. Each machine is capable of producing ~6000 compressor wheels per working week. The overall machine cycle time to produce one component is approximately 1.15 minutes. The machine tools operate in a wet/flood condition and are fitted with a conveyor belt which automatically removes the chips/swarf during operation. They are regularly maintained by the in-house maintenance engineers as well as external contractors to avoid unnecessary machine downtime and expensive repairs.



Figure 6: Index G200 CNC centre lathe

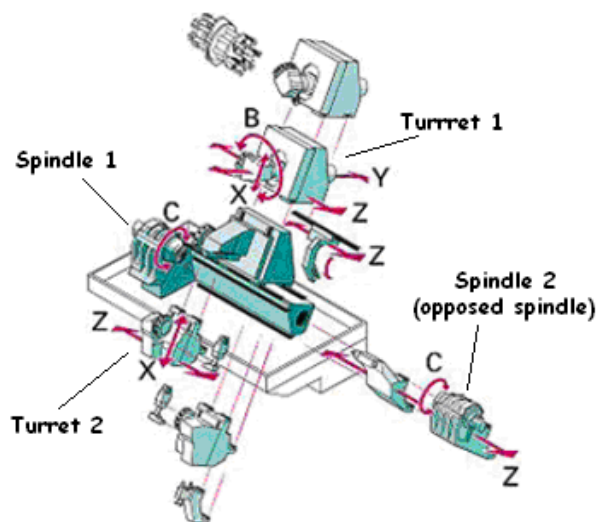


Figure 7: Schematic layout of Index G200 [4]

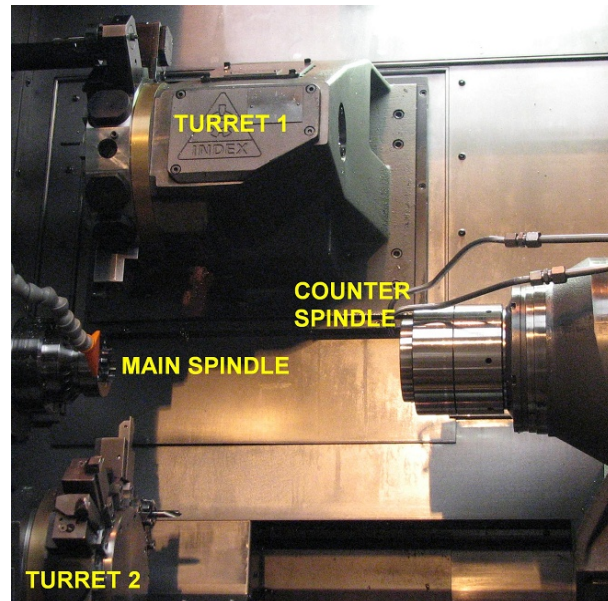


Figure 8: View of the spindles and turrets on the Index G200

2.4 Machine fixtures

A collet is used together with a multi-pin unit to hold impeller castings. These are fixed onto the machine main spindles to ensure rigidity and accuracy of the work holding position during cutting operations 1 to 5. Figure 9 shows examples of the fixtures. The nose of the component is held hydraulically in the collet (variety of sizes are available for different impeller diameters) whilst its blades are positioned between the multi-pin unit (component holding unit). Similarly for operations 6 to 9, a workpiece holding assembly comprising a back stop unit and a collet are used on the counter spindle for operations 6 to 9. Figure 10 shows an example of the counter spindle work holding assembly and units.

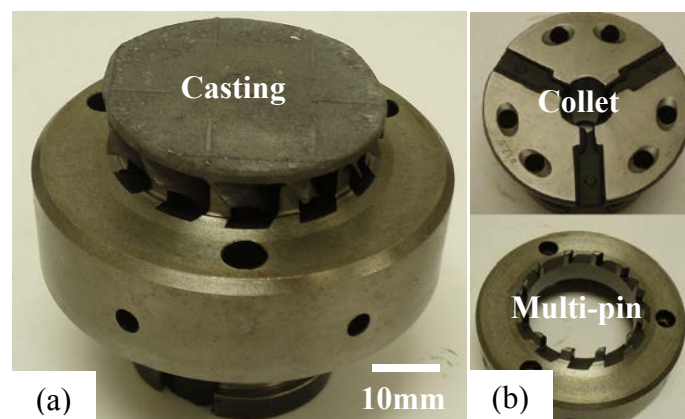


Figure 9: Main spindle workpiece holding (a) assembly and (b) collet and multi-pin unit for Operations 1 to 5

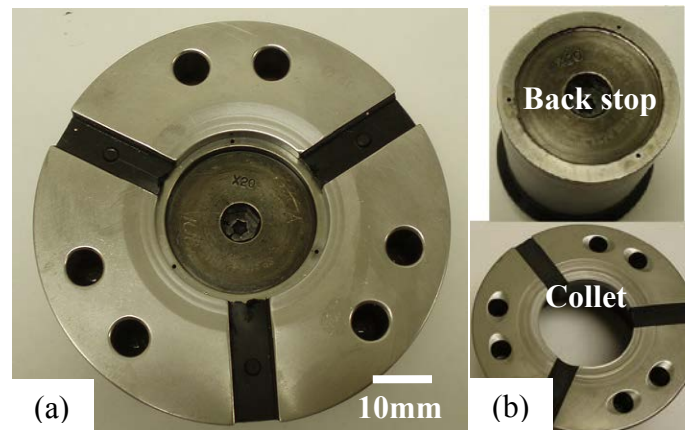


Figure 10: Counter spindle workpiece holding (a) assembly and (b) back stop unit and collet for Operations 6 to 9

2.5 Cutting tools and parameters

When the project commenced, the main cutting tool supplier was the MSC Industrial Supplier Co. which supplied standard carbide tools manufactured by Kennametal. Other carbide tools were directly purchased from Walter Titex and Mapal UK while PCD products were supplied by Exactaform. Cutting tools were purchased in bulk corresponding to machine shop three-monthly consumption in order to prevent stock shortages, with the stock held at the supplies and delivered/invoiced as and when required.

Standard carbide cutting tools were scrapped when they could no longer produce acceptable required tolerance, hole diameter, surface finish, etc. Used PCD products however were dispatched back to the supplier (Exactaform) for a tool regrind, which could typically be carried out up to three times, and supplied at a lower price (~40% less than the new tool). In terms of supplier quality, cutting tools were generally not inspected when received, though components were regularly checked as and when a new cutting tool was employed on the machines. Due to the high tool costs associated with Mapal products, tools were segregated and kept for further investigation in the event of producing unacceptable parts.

Assessment of the existing machining operations provided an insight into the overall machining process. Analysis also provided a baseline of existing machining performance for the subsequent cutting tool development work (evaluation of alternative cutting tool materials, workpiece machinability tests, etc.) and tooling trials undertaken in the project. Examples of

the cutting tools used in each machining operation together with tables listing tool details are given in the following subsections.

2.5.1 Operation 1 (1a and 1b): Rough turn back-face and outside diameter

Figure 11 details the carbide insert while Table 1 details product and process information.

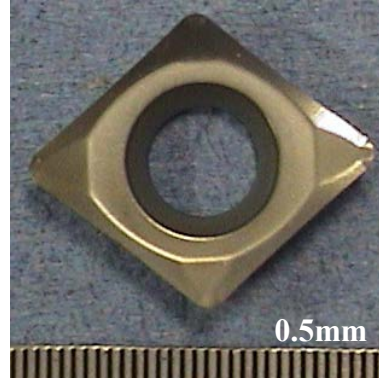


Figure 11: Carbide roughing insert

Table 1: Product and process information for Operation 1

Supplier = Kennametal
Part No. = CCGT09T308HP KC5410
Tool holder = Indexa Seiki
Material = Carbide KC5410 (polished TiB ₂ coating)
Number of cutting edges = 2 (not reground)
Nose radius = 0.8mm
Rake angle = 15°
Component rotational speed = 6000rev/min (faster for smaller wheel)
Feed rate = 0.06-0.15mm/rev (faster for smaller wheel)
Cutting speed ~ 750-1320m/min (maintained at constant speed all through, with no hole in middle)
Depth of cut = average of 1mm
Cost = £4.62
Tool life per insert ~800-1000 components

2.5.2 Operation 2: Centre (spot) drill and chamfer

Centre drill example is given in Figure 12 while the tool details and operating parameters are included in Table 2.

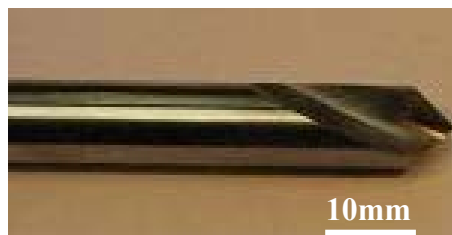


Figure 12: Centre/spot drill

Table 2: Product and process information for Operation 2

Supplier = Cromwell
Part No. = SHR025-2531C
Tool holder = Hoffmann Group
Material = HSS
Diameter = 10mm x 90° point geometry
Overall length = 89mm
Flute length = 24mm
Component rotational speed = 6000rev/min
Feed rate = 0.06mm/rev
Cutting speed ~100m/min
Penetration depth = 2.75mm
Cost = £ 7.58
Tool life ~ 5000 components

2.5.3 Operation 3: Core drill (blind-hole)

Figure 13 shows the core drill and Table 3 lists tool and process parameter details.



Figure 13: Core drill

Table 3: Product and process information for Operation 3

Supplier = Walter Titex
Part No. = A1167B
Tool holder = Hoffmann Group
Material = Solid Carbide K30F
Type = Twist, 3-Flute
Diameter = 4.8mm
Overall length = 62mm
Flute length = 35mm
Rotational speed = 6000rev/min + driven (2500 to 3000rev/min)
Feed rate = 0.15 mm/rev
Cutting speed = 110-120m/min
Penetration depth = 27 - 36mm (blind hole)
Cost = £16
Tool life = 2800-3000 components

2.5.4 Operation 4: Ream (blind-hole)

The tool and its operating parameters for operation 4 are given in Figure 14 and Table 4 respectively.

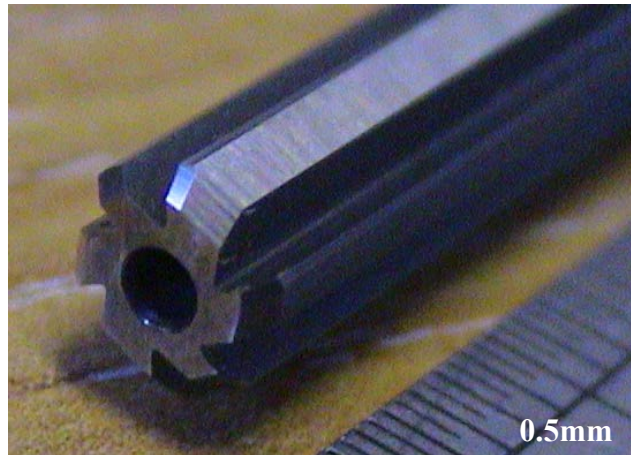


Figure 14: Reamer

Table 4: Product and process information for Operation 4

Supplier = Mapal/Beck
Part No. = RV3188
Tool holder = SMP (floating/adjustable)
Material = Carbide K10
Type = Straight, 6-flute
Overall length = 80
Flute length = 35
Rotational speed = 1500-2000rev/min
Feed rate = 0.06(in), 0.3(out) mm/rev
Cutting speed = 24-32m/min
Depth of cut ~0.2mm (diameter of reamer)
Penetration depth = 1-2mm less than core drill
Cost = £49
Tool life ~ 2,500-3,000 components

2.5.5 Operation 5: Finish turn outside diameter and back-face

Figure 15 shows the finishing insert while Table 5 details the product and process parameters.

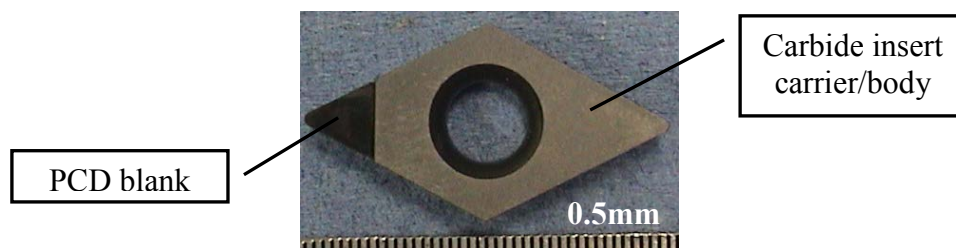


Figure 15: PCD finishing insert

Table 5: Product and process information for Operation 5

Supplier = Exactaform
Part No. = DCGT11T304
Tool holder = Indexa Seiki
Material = PCD 002
Number of cutting edges = 1 (not reground)
Nose radius = 0.4mm
Rake angle = 12°
Component rotational speed = 5000-6000rev/min (faster for smaller wheel)
Feed rate = 0.1mm/rev (faster for smaller wheel)
Cutting speed = 630-1320m/min (maintained at constant speed all through, with 5mm hole in middle)
Depth of cut = 0.2mm
Cost = £20.70
Tool life per insert ~ 2000 components

2.5.6 Operation 6: Part-off nose

Figure 16 gives example of the part-off insert and Table 6 details the tool and operating parameters.



Figure 16: Part-off insert

Table 6: Product and process information for Operation 6

Supplier = PHHorn
Part No. = LS223.0820.CO T125
Tool holder = PHHorn
Material = Carbide
Number of cutting edges = 2 (not reground)
Rotational speed = 5000rev/min
Feed rate = 0.05mm/rev
Cutting speed = 140-250m/min (maintained at constant speed all through, with 5mm hole in middle)
Cost = £8.79
Tool life per insert ~5,000 components

2.5.7 Operation 7 (7a and 7b): Rough turn nose and blade

The tool and cutting parameter details for operation 7 are given in Figure 17 and Table 7.

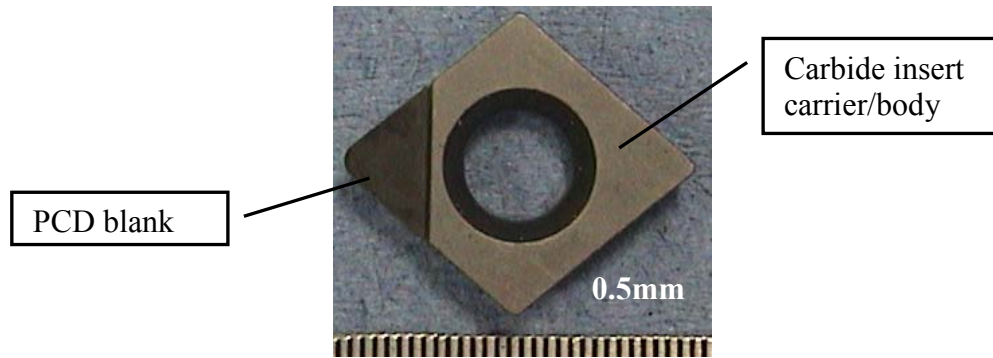


Figure 17: PCD roughing insert

Table 7: Product and process information for Operation 7

Supplier = Exactaform
Part No. = CCGT09T308
Tool holder = Indexa Seiki
Material = PCD 010
Number of cutting edges = 1 (not reground)
Nose radius = 0.8mm
Rake angle = 12°
Component rotational speed = 6000rev/min (faster for smaller wheels)
Feed = 0.06-0.15mm/rev (faster for smaller wheel)
Cutting speed ~235m/min (nose), 715m/min (inducer diameter) (maintained at constant speed all through, with 5mm hole in middle)
Depth of cut = average of 1mm
Cost = £23
Tool life per insert ~5,500-6,000 components

2.5.8 Operation 8 (8a and 8b): Finish turn nose and blade

Figure 18 shows the finishing insert used in operation 8 and Table 8 details the tool and operating parameters.

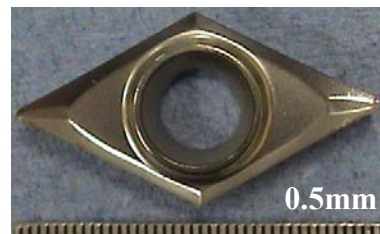


Figure 18: Carbide finishing insert

Table 8: Product and process information for Operation 8

Supplier = Kennametal
Part No. = DCGT11T304HP KC5410 (polished TiB ₂ coating)
Tool holder = Indexa Seiki
Material = Carbide KC5410
Cutting edges = 2 (not reground)
Nose radius = 0.4mm
Rake angle = 15°
Component rotational speed = 5000rev/min (faster for smaller wheel)
Feed = 0.1 rev/mm (faster for smaller wheel)
Cutting speed ~ 195m/min (nose), 590m/min (inducer diameter) (maintained at constant speed all through, with 5mm hole in middle)
Depth of cut = 0.2mm
Cost = £6.05
Tool life ~4,000 components

2.5.9 Operation 9: Chamfer nose

The cutting tool used for this operation is the same as that detailed in Figure 12 while Table 9 provides associated product and process information.

Table 9: Product and process information for Operation 9

Supplier = Cromwell
Part No. = SHR025-2531C
Tool holder = Hoffmann Group
Material = HSS
Component rotational speed = 6000rev/min
Diameter = 10mm x 90° point geometry
Feed rate = 0.15mm/rev
Cutting speed ~100m/min
Overall length = 89mm
Flute length = 24mm
Penetration depth = 2.75mm
Cost = £ 7.58
Tool life = 5,000 components

2.6 Remarks on the current compressor aluminium impeller production at Doncasters Sterling

Machine downtime as a result of tool breakage, maintenance/service of the spindles, incorrect machine setup, etc., was found to be a significant factor in the low productivity at Doncasters Sterling. Tool breakage (drill and reamer) together with a long setup time of the reaming operation were major factors contributing to downtime in the machine shop. The breakage of tools was mainly caused by incorrect tool setup or defective castings containing

blowholes, which led to regular tool changes and expensive machining. Suggested changes to the methods used in impeller casting inspection (ultrasonic/non-destructive testing), prior to component machining should minimise this issue, however this aspect was outside the remit of the present work. Hole surface finish ($<0.2\mu\text{m Ra}$) was observed to be difficult to achieve when changing the carbide reamer leading to lengthy/fiddly adjustment of the machining parameters (cutting speed and feed rate) and the floating tool holder. A part solution to reducing machining time was the use of fixed/standardised tool change/setup procedures and defined operating parameters for each job.

The tooling currently employed at Sterling was a combination of high-speed steel, uncoated tungsten carbide and PCD cutting tools, all of which were supplied by different suppliers/manufacturers. With more suitable tool geometry it was felt that it should be possible to use PCD tooling for rough turning/facing (heavy cutting) operations and potentially allow the machine tool to operate for longer periods without halting for a tool change and/or parameter adjustment.

Frequent change/switch of the tool suppliers was observed to be a common, but unwise, practice at the company. Such practice was an attempt at minimising capital costs without any scientifically based systematic evaluation. This not only undermined the supplier relationship, but also compromised technical performance and created inconsistency in the product quality being produced in the machine shop. Furthermore, tooling and operating parameters were often replaced on operator whim rather than according to assessment/procedures.

In general, the current machine tools, existing tooling and fixtures had the capability to produce precision products of high tolerances. However, education and training for the metrology/measuring equipment (Surftest, Talyrond, Go-No Go gauge, etc.) was needed by the operators on a regular basis so that they could gain a better understanding of the equipment and its use. Inadequate care when handling and storing high precision tooling, such as the reamers and PCD tools, was also experienced leading to damage/chipping of cutting edges and non-conformance of components and/or unnecessary downtime.

CHAPTER 3: LITERATURE REVIEW

3.1 Machining of aluminium

3.1.1 Background

Aluminium alloys are used in many applications and industry sectors, for transportation, food and beverage, building/construction, machinery, electrical appliances, etc. There are two classes of aluminium alloys namely wrought alloys (initially cast as ingots or billets of simple round, regular cross-sections) and cast alloys (directly cast into final form of complex shapes). The automotive industry in particular has substituted many steel and cast iron components for aluminium as a means to improve fuel economy due to aluminium's high strength-to-weight ratio. Aluminium casting alloy products include automotive cylinder heads, gears and cogs, crankshafts, bicycle frames, etc while wrought products include rolled plates, sheet, foil, extruded bars and rods, etc. Aluminium alloys are classified in a numerical series in accordance with the International Alloy Designation System (IADS). The classification divides aluminium alloys into groups associated with the principal alloying elements as detailed in Table 10 [5, 6].

Table 10: Aluminium classifications [5, 6]

IADS designation	Main alloying elements
1xxx	Unalloyed aluminium, mainly used in electrical and chemical industries
2xxx	Copper is the principal alloying addition, widely used in aircraft construction
3xxx	Manganese is the major alloying addition, used for architectural applications
4xxx	Silicon is the main alloying element, such alloys are commonly used for welding and brazing
5xxx	Magnesium is the main alloying element and alloys are widely used in marine applications
6xxx	Silicon and Magnesium are the principal alloying elements and the alloys are used for marine and automotive applications
7xxx	Zinc is the main alloying element and the associated alloys are used for aerospace structural components and in high strength applications
8xxx	Series of alloying elements with miscellaneous compositions

Each series of alloy may also comprise a letter followed by four digit numbers which designates various heat treatments. Pure aluminium is relatively weak and ductile and is

commercially used in applications that favour excellent workability and corrosion resistance, for example cooking utensils, chemical equipment, etc. The 2xxx – 8xxx groups have good machinability, chemical and mechanical properties with alloying elements such as copper (Cu), manganese (Mn), silicon (Si), zinc (Zn), magnesium (Mg) and iron (Fe). Aluminium silicon alloys (Al-Si) containing less than 11% silicon are termed hypoeutectic, those with 11-13% silicon are called eutectic and those with more than 13% silicon are commonly known as hypereutectic alloys [7].

Aluminium alloys with silicon as the major alloying constituent form the basis for the casting alloys used in the automotive industry. Aluminium C355 is a commercial casting alloy which is used extensively due to its good casting characteristics, high strength-to-weight ratio and corrosion resistance. It is a cast and heat treatable aluminium alloy containing 93.2%wt Al with 1.2%wt Cu, 0.5%wt Mg, 0.1%wt Mn and 5%wt Si. In addition, it is considered to have good machinability with curled, easily broken chips and excellent surface finish can be achieved [8]. Table 11 [1, 9] lists physical and mechanical properties of standard (permanent mould) and Sterling cast C355 alloys.

Table 11: Properties of cast C355 aluminium alloys [1, 9]

Property	Standard C355 [9]	Sterling C355 [1]
Density (g/cm^3)	2.71	2.71
Hardness (HV)	~100	120-140
Ultimate tensile strength (MPa)	290	366
Yield strength (MPa)	185	271
Modulus of elasticity (MPa)	-	67.6×10^3
Shear modulus (MPa)	-	26.2×10^3
Thermal conductivity (W/mK)	167	151
Coefficient of thermal expansion ($\mu\text{m/mK}$)	22.3	22.4

3.1.2 Machinability of aluminium alloys

The majority of components manufactured from aluminium require machining and surface polishing to ensure functionality and performance. Generally, aluminium alloys are relatively easy to shape and are considered as offering the highest levels of machinability, with low cutting forces, high material removal rates and good workpiece surface finish, compared to other lightweight metals. Table 12 [10] gives an example of power and thrust force requirements of aluminium alloys against other materials.

Table 12: Power and cutting force requirements in machining of different materials [10]

Material	Hardness (HB)	Average unit power hp/in³/min requirement for drilling with HSS (kW/m³/sec)	Thrust force, lb 1/4 in diameter drill (N)
Aluminium alloys	30-150	0.16 (~121)	38 (~169)
Steels	85-200	1.0 (~758)	130 (~579)
Titanium	250-375	1.1 (~834)	-
Nickel alloys	80-360	1.8 (~1365)	-

It is known that aluminium, due to its soft nature, tends to bond/adhere to the cutting tool either as a built-up layer (BUL) or built-up edge (BUE) [11]. Shen [12] described the process of BUE formation and break-away which may be continuous and unpredictable over the duration of the machining operation. He suggested that BUE is usually formed under extreme compressive stresses and its adhesion to the tool surface can cause the tool to chip, hence shortening tool life. List et al. [13] determined typical tool-chip interface cutting pressures for aluminium 2024-T351 using uncoated carbide tools to be between 300 to 500MPa at 30 to 60m/min cutting speeds with maximum BUE height of 650µm obtained at lower speed. Sanchez et al. [14] concluded that BUE is developed by mechanical adhesion processes and can grow until it reaches a critical thickness before plastically deforming over the tool rake face. Experimentally, Nouari et al. [15] illustrated the successive stages in the evolution of workpiece adhesion and showed that a built-up layer develops at the start of cutting before the onset of a built-up edge.

The repeatability and consistency of the machined part becomes difficult to achieve in the presence of BUE and reports [16, 17] show that it has adverse effects not only on workpiece surface finish, but also on component geometrical size. Rubio et al. [17] found that both BUL and BUE play a role in alteration of the initial tool geometry that affects the surface finish quality of the workpiece. Farid et al. [18] studied high speed drilling of A383 Al-Si alloy and found that adhered aluminium material tended to plough the machined surface producing irregular surface roughness profiles. Basavakumar et al. [19] showed that when the built-up edge reached a critical size, it either slipped away or adhered to the machined workpiece surface increasing the roughness of the new surfaces. Yousefi and Ichida [20] and Smith [21] reported that an increase in cutting speed decreased the likelihood of a secondary cutting edge forming due to greater chip velocity and lower pressure at the interface between the chip and the tool, thus avoiding any pressure welding tendency, which is also in agreement within work by List et al. [13].

Cutting fluid is widely used in machining operations to aid transportation of the chip, provide cooling and help lubricate the tool-workpiece interface, this latter aspect being critical in minimising the formation of BUE [22, 23]. Minimum quantity lubrication (MQL) can also help reduce the amount of aluminium adhesion and clogging on the tool. Bhowmick and Alpas [24] performed drilling experiments on aluminium silicon 319 using an uncoated HSS tool with water spray (H_2O -MQL) and showed that both BUE and adhered aluminium to the drill bits decreased by 36% and 60% respectively compared with dry cutting. Optical images shown in Figure 19 [24] clearly demonstrate the benefit of cutting fluid application. The authors observed that the use of low coefficient of friction (<0.2 , under an ambient atmosphere) diamond-like carbon coated cutting tools, also proved to be an effective strategy for minimising adhesion and workpiece material built-up edge. Recent work by Gangopadhyay et al. [25] demonstrated a significant reduction in build-up/adhesion when using diamond tools, CVD diamond and PCD, even at a low speed of 200m/min during turning of AA6005 aluminium alloy.

Aluminium based metal matrix composites (MMC) which contain hard particles of silicon carbide (SiC), typically around 20%, as reinforcement are also important engineering materials being lightweight but with high strength and stiffness, high-temperature operating capability and abrasion resistance [9]. Such materials have been developed to help overcome aluminium's poor high-temperature performance and low wear resistance [26]. The machinability of MMC, however, is not as good as traditional aluminium-based alloys due to rapid tool wear caused by the abrasive reinforcement of SiC, (2700-3500HV), and evidence of substantial workpiece adhesion on the tool [27]. Conventional cutting tool materials such as cemented carbide and high speed steel are reported to be unsuitable for cutting Al MMC [28]. The typical flank wear of a TiN coated carbide K10 tool (1.5min of cutting) at a cutting speed of 50m/min with a feed rate of 0.1mm/rev is ~ 0.4 mm [29], while workpiece surface roughness values are quoted as ranging from 0.2 to 5 μ m Ra depending on the machining parameters and the particle ratio. In contrast, PCD tools have been reported to exhibit exceptional all round cutting performance [27, 29-32]. An effective strategy for least wear damage and the good surface finish is reported to be the employment of high cutting speeds and feed rates, but at the expense of extended depth of the machining-affected layer [32, 33].

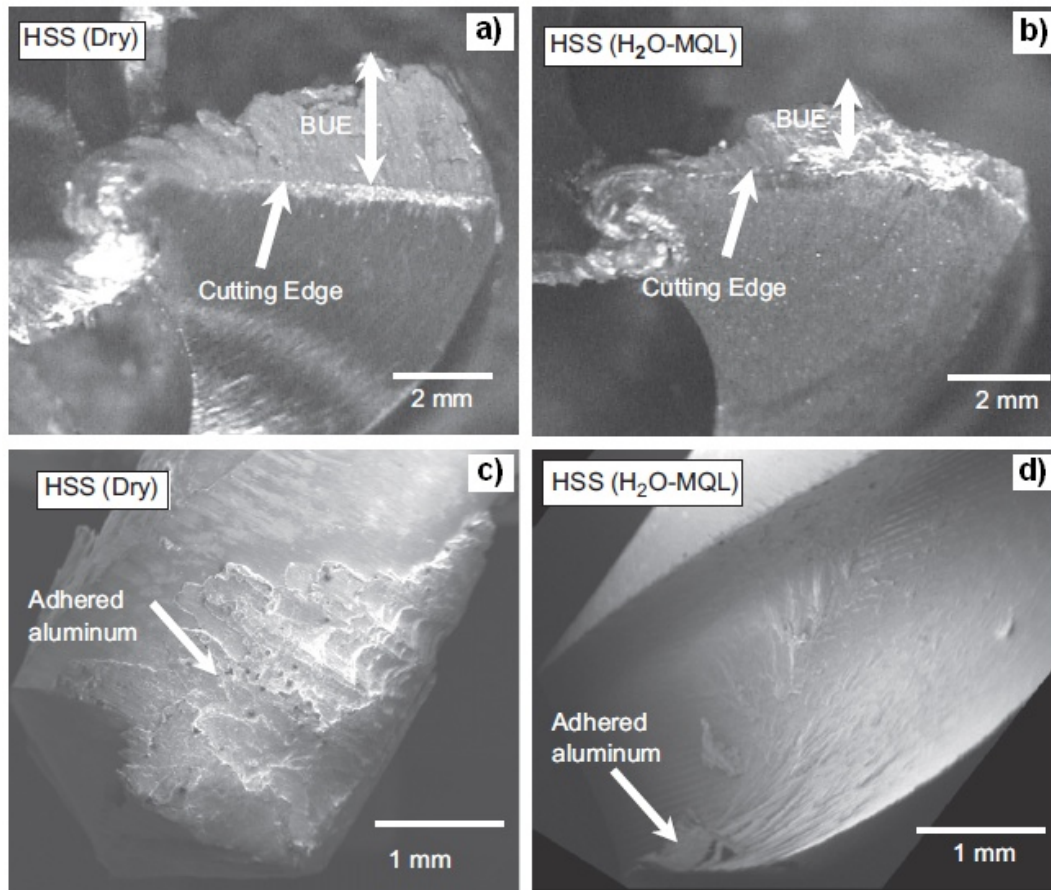


Figure 19: Optical images of aluminium BUE on HSS drill cutting edges in (a) dry and (b) H₂O-MQL conditions and aluminium adhesion to HSS drill flutes in (c) dry and (d) H₂O-MQL conditions [24]

3.1.2.1 Effects of silicon in aluminium

Silicon addition in aluminium aids castability/stimulates flow, enhances tensile strength, corrosion and wear resistance, helps minimise shrinkage during solidification and reduces thermal expansion of the cast component [6, 34]. In the temperature range 27-427°C, the coefficient of linear thermal expansion for aluminium is lowered to $20 \times 10^{-6} \text{K}^{-1}$ and $12 \times 10^{-6} \text{K}^{-1}$ by adding 10% and 40% of silicon, respectively [35]. A study by Dwivedi et al. [36], results of which are shown in Figure 20, highlights the significant influence silicon has on tensile strength and hardness of aluminium alloys.

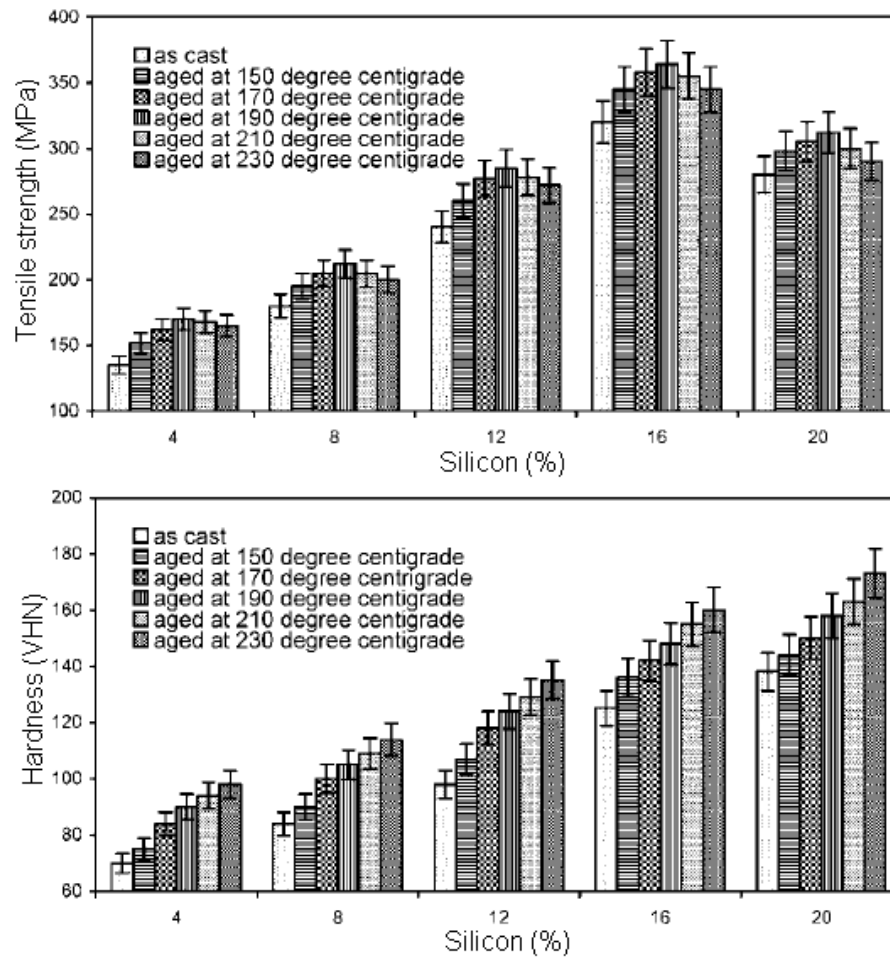


Figure 20: Mechanical properties of Al-Si alloys as function of silicon content [36]

The hard particles of silicon however increase wear resistance of the workpiece material [37] and cause abrasive wear to the cutting tool, thus reducing tool life and making machining more expensive [38, 39]. Roy et al. [40] carried out a machinability study of cast pure aluminium and cast aluminium with 12% silicon. Not surprisingly it was found that a more severe flank wear land was experienced when machining AlSi12 compared with pure aluminium, see Figure 21 (a) and (b). Figure 21 (c) and (d) show curl and broken chips obtained from machining pure aluminium and AlSi12 respectively.

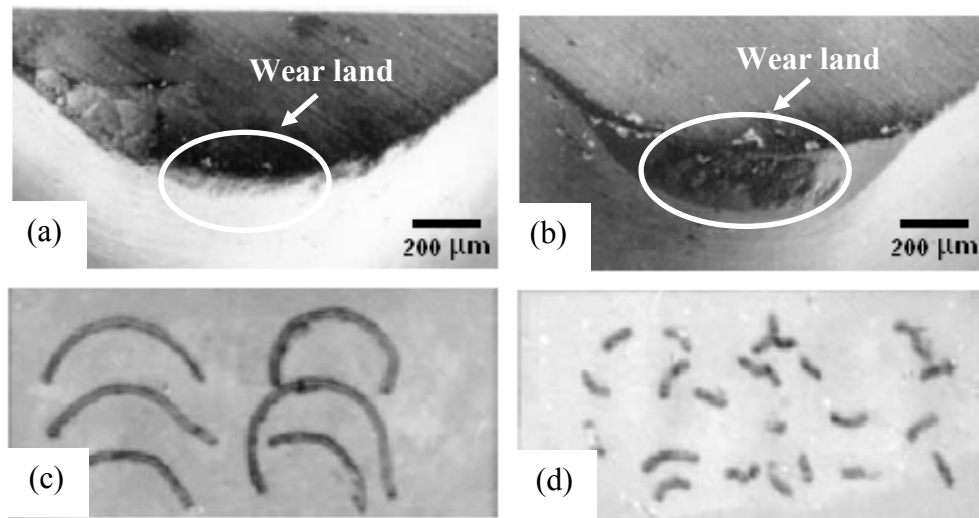


Figure 21: SEM pictures of conditions of carbide K10 tools after machining (a) pure aluminium and (b) AlSi12 for 30seconds and chip morphology after machining (c) pure aluminium and (d) AlSi12 for 30seconds [40]

Dwivedi et al. [41] studied the influence of eutectic (12%Si) and hypereutectic (17%Si) cast Al-Si alloys on machinability and observed that higher silicon content increased the bulk hardness of the workpiece material by ~5%, from 105 to 117HV. The increase in material hardness also contributed to higher cutting forces, of ~70%, and cutting temperature, which increased by ~12%. Uhlmann et al. [42] analysed tool wear mechanisms using nanocrystalline chemical vapour deposition diamond coated tools to machine aluminium with 9%Si and 17%Si. The work showed that the harder and more brittle hypereutectic AlSi17 alloy was highly abrasive which led to fretting of the tool coating and displacement of the tool cutting edge. In contrast, the softer hypoeutectic AlSi9 alloy had a high tendency to adhere to the tool surface causing built-up edge, and lower workpiece surface quality. Grum and Kisin [43] also demonstrated that aluminium with 5%Si produced the poorest workpiece average surface roughness of 3.62μm Ra compared with 2.30μm Ra and 1.67μm Ra achieved with AlSi12 and AlSi20, respectively, under the same machining conditions. The author explained that the higher surface roughness obtained was due to plastic deformation of the soft Al phase in the cutting zone and the change in tool geometry during machining.

3.1.2.2 Tool life and wear

Tool life investigation has been the focus of much of the machinability research over the past decade. Presently, tool life/wear testing methods in metal cutting are based on the use of flat-faced as well as complex shaped (with chip breaker, modified edges) cutting tools that commonly follow criterion where the maximum depth of the flank wear land (VB_{Bmax}), on the clearance side of the tool, is typically between 0.3 or 0.6 mm for ceramics, ISO 3685: 1993

[44]. Typical average tool flank wear curves of a cutting tool used to machine 6061 aluminium alloy are included in Figure 22 [45].

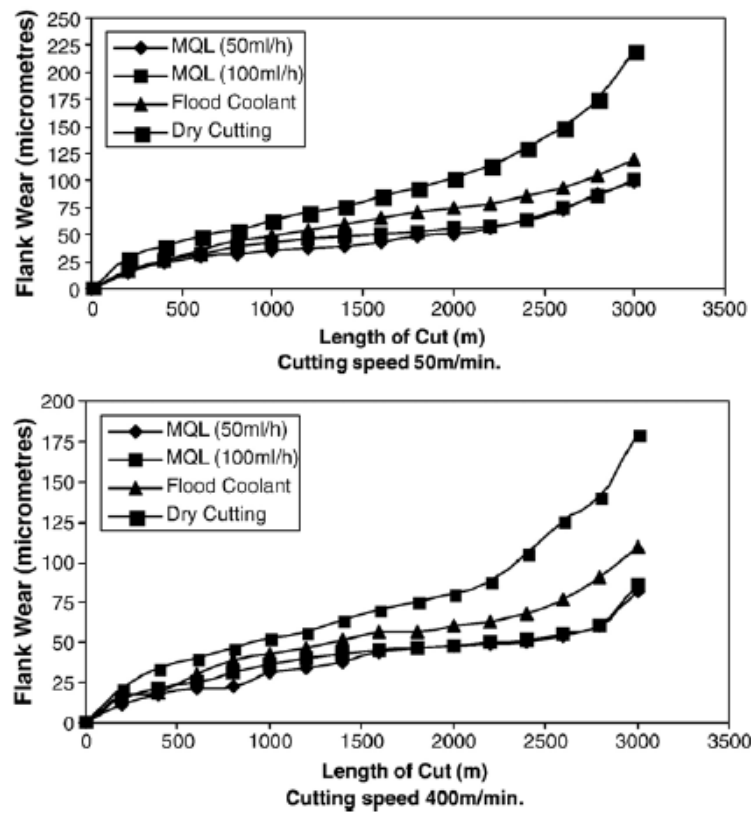


Figure 22: Average tool flank wear for different cutting speeds and conditions when machining 6061 aluminium alloy. Feed rate $f = 0.15\text{mm/rev}$ and depth of cut $d = 1.0\text{mm}$ [45]

The wear experienced by the tool consists of three distinctive regions, see Figure 23 [26], which are normally observed in experimental wear curves. The first region is at the start of the wear curve (new tool condition) where initial wear takes place at high wear rate. The second region is the normal operating region for the cutting tool which contains steady-state wear. The last region of the wear curve is known as the accelerated wear region, which is often associated with high cutting forces, high temperatures and severe tool vibrations that indicate the end of tool life.

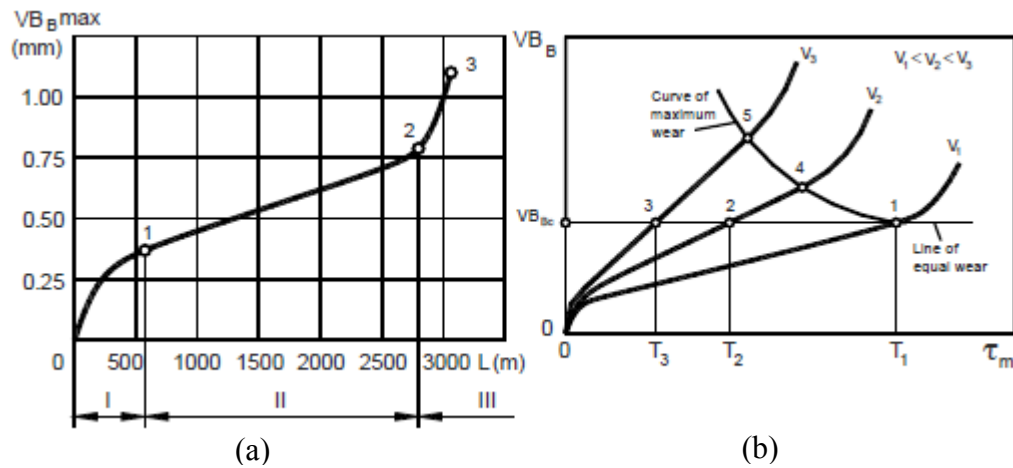


Figure 23: Wear curves (a) normal wear and (b) evolution of flank wear land VB_B at different cutting speeds [26]

The energy dissipated by metal deformation and sliding friction during cutting appears as heat and the resulting temperatures may be sufficiently high to affect tool life. Temperatures, measured using a linear array of photoconductive mercury-cadmium-tellurium (HgCdTe) detectors, in excess of 200°C have been observed during machining of 6061-T6 aluminium alloy, at a cutting speed of 850m/min with $+5^\circ$ rake angle and 1.5mm depth of cut [46]. Recent experimental work by Kazban et al. [47] also produced a result which is in agreement with this when machining the same workpiece material. Deng et al. [48] also found the maximum temperature in the cutting zone to be $\sim 345^\circ\text{C}$ when modeling the machining of aluminium alloy A356 at a cutting speed of 450m/min. It is crucial that the optimum cutting speed is employed to ensure minimum machining costs [49]. A study by Leep and Eldridge [50] showed a 40% increase in mean tool wear (for 460 holes) from 0.287 to 0.411mm, when the cutting speed was doubled from 60 to 120m/min, during a drilling experiment of aluminium 380 containing 9%Si with HSS tools. Experimental results of tool flank wear by Heath [51] using cemented carbide on AlSi20 alloy workpiece also experienced a substantial decrease in tool life with an increase in cutting speed.

3.1.2.3 Drilling of aluminium alloys

Of all the methods used to produce holes, twist drilling is the most important and is often carried out as one of the last steps in the manufacture of parts. This means that the workpiece has already undergone extensive machining prior to any drilling operation and, therefore, incorporates significant value. For this reason, high process reliability is placed on the drilling operation. Typically, a twist, or spiral, drill with multiple cutting edges is used in

the process to produce either through or blind-holes in a workpiece material or to enlarge an existing hole.

During cutting, the drill chisel edge is an important feature that acts to guide the drill as it penetrates into the workpiece affecting the applied cutting forces and subsequent wear experienced by the tool. Eccentric chisel edges lead to alternating torque and bending stresses of the tool body that can cause premature tool failure [52]. The flute of the drill aids the flow of the chips, or swarf, in an upward direction. Formed chips, examples of which are shown in Figure 24 [52], have various sizes and shapes and they are governed by many factors, such as drill design geometry, the rate of material removal, cutting conditions, workpiece materials, etc. Small chips are desirable as large chips do not flow easily through the drill flutes, thus increasing the torque requirement for material removal and causing tool breakage [52]. In addition, the chip becomes more difficult to evacuate with increased drilling depth. Jayal et al. [23] observed that drilled hole cylindricity generally deteriorated by as much as 40% when drilled hole depth was doubled. Liu and Matsuda [53] performed experiments on drilling of an AlSi17 and reported that surface roughness increased six fold when the depth of the drilled hole was doubled.

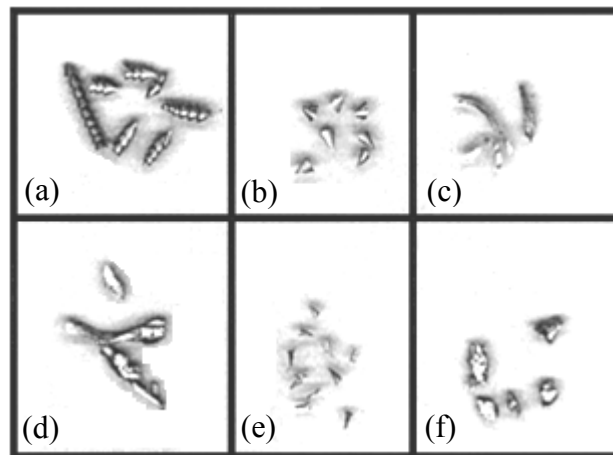


Figure 24: Typical formed chips (a) conical, (b) fan shaped, (c) chisel edge, (d) amorphous, (e) needle, f) impacted when drilling cast SAE 308 and 390 aluminium alloys [52]

Workpiece material clogging in the drill flute is a major issue when machining soft materials such as aluminium. Cutting fluid application is necessary for producing chips of the required shape and for efficient chip disposal as well as for achieving workpiece dimensional accuracy and long tool life in addition to protecting against oxidation and corrosion during machining [23]. Conversely, dry machining of aluminium may help lower environmental impact and overall operational cost [54]. However, such an approach leads to inferior tool life and accuracy of workpiece when drilling aluminium alloys [23]. Haan et al. [22] concluded

that average surface roughness R_a values, double when drilling without cutting fluid, while Jayal et al. [23] and Bono and Ni [55] suggested that thermal effects resulting from drill material expansion in the absence of cutting fluid contributes to oversized holes. The work also showed that dry cutting promoted BUE ahead of the tool tip together with entrapment of abrasive chips between the tool and the hole wall, leading to large deviation of hole size. Furthermore, thermal distortions of the drill have been reported to produce bell-shaped holes near the bottom [55], while Dasch et al. [56, 57] demonstrated that dry cutting promotes aluminium heat build-up and swarf packing in the drill flutes leading to tool breakage. The author also showed that high cutting speed minimised clogging of the material and lowered the workpiece surface roughness. Figure 25 is from Dasch et al. [57] and shows material build up in drill flutes at different cutting speeds. It is, therefore, essential that some level of cooling/lubrication is applied during the aluminium machining processes. In the absence of lubrication, cooling the cutting tool by supplying high pressure air helps increase the drill tool life by a factor of 2 [58]. Even small quantities of cutting fluid supplied at the rate of 20ml/hour have proven to prevent built-up edge and improve tool life [59].

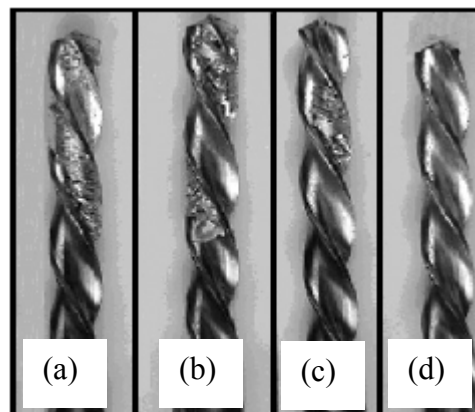


Figure 25: Photos of material build up in drill flutes at speeds (a) 2500rev/min, (b) 5000rev/min, (c) 7500rev/min and (d) 10000rev/min [57]

With regard to tool life, wear of a tool is generally a gradual process and can be attributed to many factors, such as independent cutting parameters such as cutting speed, feed rate and depth of cut, tool geometry, workpiece material, cutting fluids and machine tool characteristics [26]. The tool life of a drill is also governed by the requirements of the part being produced, hole diameter, surface roughness, etc. When drilling aluminium, both chisel edge wear and flank wear are evident and increase with the number of holes produced. The principal tool wear mechanism experienced when cutting aluminium alloy is abrasion with the formation of BUE and material adhesion/clogging being common [24, 60]. It is not however

unusual for a drill to fail prematurely during use. For instance, Dasch et al. [56] shows an example of a catastrophic drill failure that was not due to gradual wear at the cutting edge, but the build up of aluminium in the drill flutes. Thangaraj and Wright [61] suggested that the physical limits of a twist drill are governed by fracture/chipping and excessive wear. Visual inspection may be used to determine the useful life of a cutting tool, but it is not recommended if a detailed study of tool life is to be carried out. Work by Jantunen [62] suggests that direct tool wear monitoring methods involving visual inspection or camera systems are not economically or technically attractive for drill life assessment. Astakhov [49] also stated that hole dimensional assessment should not be the sole tool life criteria in metal cutting tests. This is because it does not allow the optimal control of cutting operations, assessment of different tool materials, or comparison of different cutting regimes. Wear land measurement is a direct method frequently used for comparative work in evaluation of tool life performance.

In addition to flank wear, Kanai et al. [63] classified drill wear of various types at other locations, which are illustrated in Figure 26. They commented that the outer corner wear is the easiest to measure, because other areas are often hindered by the presence of adherent workpiece material. Early work by Lenz et al. [64] also identified that wear on the drill outer corner is a useful criterion to use for assessing drill life. Wain et al. [58] assessed drill wear using optical microscopy, scanning electron microscopy (SEM) and energy dispersive x-ray spectroscopy (EDX) methods. Recent work by Dasch et al. [57] involved drill life testing by drilling holes in aluminium alloy plates until the tool fractured. Chou [65] also used the same tool breakage method together with Go and No-Go gauges for assessing hole quality in determining drill life. Braga et al. [66] measured drill flank wear against feed length using an optical microscope with image analyser software. Similarly, Lin [67] analysed the reliability of cutting tools through average tool flank wear graphs plotted using five point flank wear values measured using a tool microscope.

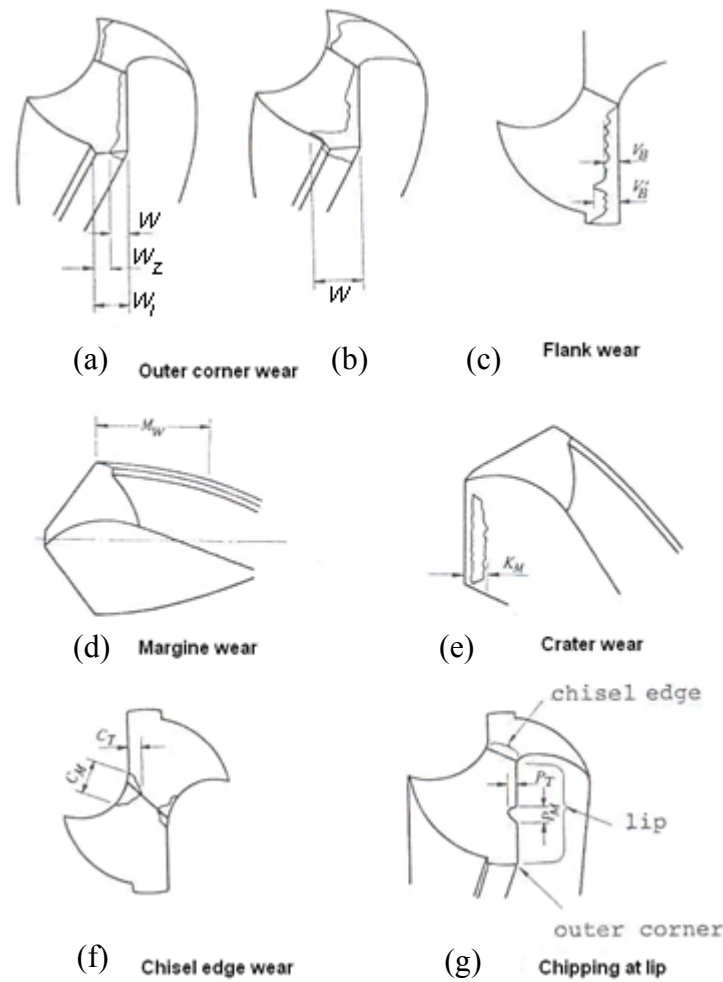


Figure 26: Various types of drill wear [63]

3.1.2.4 Cutting forces associated with drilling operations

Drill performance is normally defined in terms of tool life, e.g. tool wear, cutting forces, or hole quality such as roundness and surface roughness. Drill torque and thrust force are commonly assessed in conjunction with wear assessment as a criterion to characterise the drill condition. Force measurement involving a piezoelectric dynamometer, or force-platform, is well known with results published by many authors [68, 69]. Three distinct drill areas/features contribute to force values [70-72], the main cutting edge accounting for 40% of the thrust force and 80% of the torque, while the chisel edge contributes ~50% and 8% respectively. The margin or land cutting edge produces around 10% of the torque and even less of the thrust force.

Commercial pure aluminium is difficult to machine and cutting forces may be significant. The reason for this is that the contact area between the chip and the tool rake tends to be large and chips are thick/strong. Consequently the shear plane angle is small and chips

tend to move away more slowly [73]. However, aluminium with alloying additions, such as silicon, aids the fracture of the chip which results in minimum contact and reduced tool forces. Typically, the thrust force and torque for LM25 (BS 1490: 1988) [74] aluminium alloy with 7% silicon and a measured hardness of 122HV are ~350N and ~110Ncm under flood conditions respectively [75]. Bhowmick and Alpas [24] evaluated the drilling of 319 aluminium alloy with 6% silicon under MQL conditions of 30ml/hour using uncoated high speed steel (HSS) tools and showed that the respective maximum thrust force and torque were less than 273N and 320Ncm.

Drilling forces are governed by factors such as workpiece material, machining parameters and cutting conditions, etc. Lin and Ting [68] studied tool wear and showed that both thrust and torque are functions of tool wear, drill diameter and feed per revolution. The authors stated that, for the same cutting speed and feed, thrust and torque increased dramatically by 500% and 33% respectively when flank wear progressed from 0.1mm to 0.9mm. Liu and Matsuda [53] found that thrust and torque values increased with hole depth due to high levels of friction generated at the end of the drill. Increased cutting speed is beneficial to reducing cutting forces. Kelly and Cotterell [70] observed lower forces with an increase in cutting speed when drilling aluminium plate, while Hamade et al. [76], showed that an increase in feed rate from 0.04 to 0.64mm/rev, contributed to higher thrust force and torque when drilling 6061 aluminium. The application of cutting fluid also has a significant impact on cutting forces. Williams and Tabor [77] established that the role of a cutting lubricant is to reduce the region of sticking friction between the tool rake and chip surface which reduces the sticking length and increases the shear angle. The authors also found that cutting lubricants are most effective only if they are able to penetrate from the tool periphery and prevent sticking friction, which is in agreement with conclusions by Trent and Wright [73]. Haan et al. [22] experienced a reduction in drilling torque, associated with the margins of the drill and the workpiece, by half when using cutting lubricant.

3.1.2.5 Reaming of aluminium alloys

Reaming is classed as a secondary operation that employs a multi-edge cutting tool to improve accuracy and reduce roughness of a hole surface by removing a small amount of material from the hole wall following a drilling operation. The principle of the reaming process is similar to that of drilling, where the tool rotates and feeds into the workpiece. Figure 27 [38] illustrates a multiple-edge reamer. There is a limited amount of literature on

tool life/wear when reaming aluminium alloys. Work by Lugscheider et al. [78] investigated reamer tool life with various tool materials, including uncoated WC, TiB₂, TiBN and TiAlN coated WC, operating at a cutting speed of 150m/min. They found that the highest tool flank wear was <25µm after 5m of cutting length in AlSi12.

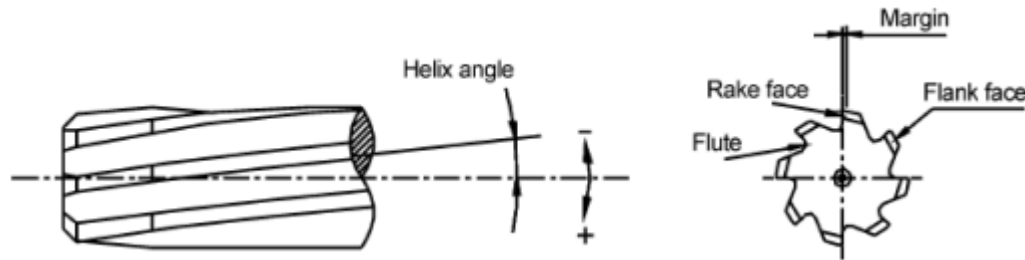


Figure 27: Schematic diagram of a reamer [38]

Since stock removal is small, it is important that the pre-bore condition provides good roundness, parallelism, and surface finish. Typically the roundness of the reamed hole is larger at entry region than that at exit [79]. This roundness error is caused by factors such as misalignment between the axis of the bore and the reamer itself, inaccurate rotation of the spindle, or setting errors. Bezzera et al. [38] observed larger measured diameters than the nominal value when reaming aluminium silicon SAE322 alloy (6% silicon) with semi-synthetic cutting fluid. The authors found that larger depths of cut up to 0.8mm tended not only to deteriorate roughness (by ~20%), but also the roundness (by ~95%) and cylindricity (by ~33%) due to increases in component forces and vibration. The work showed that the best hole roundness and cylindricity was achieved with a depth of cut of 0.2mm. A similar result was found by Zeng [80] who suggested that large depths of cut had a negative influence on hole quality as BUE increased due to the large uncut chip thickness.

While hole quality depends on machine set up and stock removal, it is also sensitive to the types of cutting fluid being employed during reaming, even more so with larger depths of cut [81]. In general, average surface roughness <0.2µm is achievable when machining aluminium alloys with a PCD reamer [82]. Although the absence of lubrication/cooling agents help minimise environmental pollution, reaming aluminium alloy dry is not recommended due to pronounced workpiece material adhesion on the tool flanks and main cutting edges. This undermines cutting geometry and process stability, thus making it more difficult to achieve close tolerances [78, 83]. Cutting fluid may be applied, internally or externally, to aid cutting efficiency in terms of increased tool life, improved tolerances, reduced cutting forces, vibration and surface finish. Early work by Ohgo et al. [84] demonstrated that BUE is

significantly minimised with cutting fluid application irrespective of reaming geometries or conditions.

3.2 Cutting tool materials for aluminium alloys

While employing suitable machining parameters is good practice, selecting appropriate cutting tool materials is equally important. The three main classes of tools are high speed steels (HSS), cemented carbides and ceramics/superhard materials [85]. HSS have been used since the turn of the last century and the typical room temperature hardness of an M2 HSS tool (0.85%C, 4%Cr, 5Mo, 6%W, 2%V, 0.85%Co) is 836HV, however significant loss of strength takes place when cutting temperatures exceed 650°C [73]. Cemented carbides are the most versatile cutting tool materials and are widely used in metal cutting due to a combination of high hardness (~1550HV medium grain with 6%Co) and toughness (10MPa m^{1/2} medium grain with 6%Co) [51, 73]. Figure 28 [51] shows the relationship between hardness and toughness for different tool materials, while Figure 29 [86] shows hot hardness for tools and selected workpiece materials. For aluminium alloy machining the high hot hardness characteristics of conventional alumina and mixed alumina ceramic materials offer no advantage. In terms of high volume production of aluminium silicon alloy components however, the abrasive resistance and durability of PCD, diamond and diamond like coatings are preferred characteristics. The following section deals solely with carbides, polycrystalline diamond and diamond coated tools.

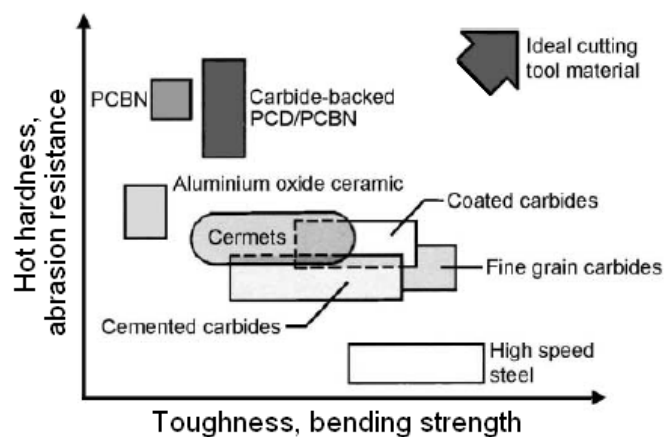


Figure 28: Hardness and toughness of cutting tool materials [51]

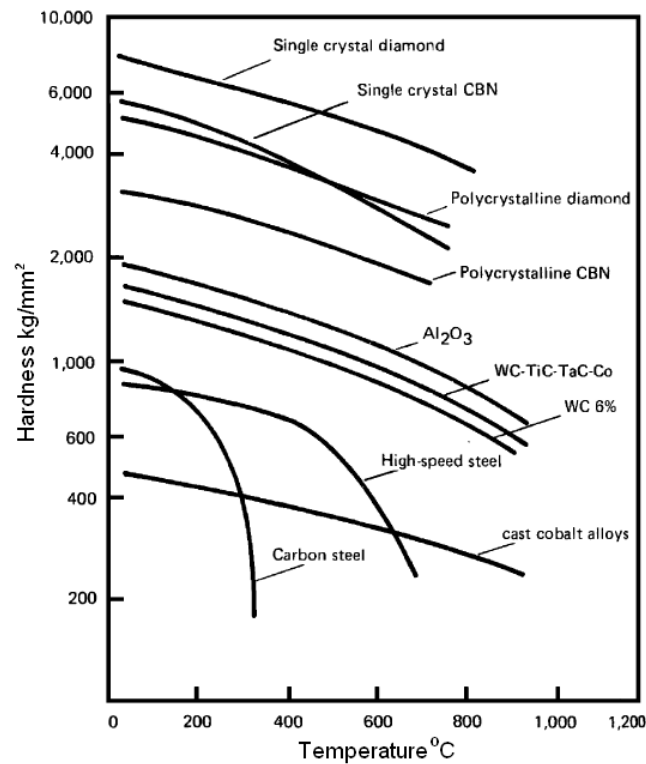


Figure 29: Typical hot hardness characteristics of various tool materials [86]

3.2.1 Cemented carbides

Cemented carbides comprise hard particles, mainly tungsten carbide (WC), which are held together by a metallic binder, usually cobalt (Co). Carbide particles are sintered, above 1300°C [87], in a cobalt matrix, typically 6-12wt%. The international standards organisation guide (BS 7662: 1993) [88] for the selection of carbides according to use details their relative chip production characteristics, metallurgical characteristics, hardness and tensile strength with colour coding for ease of identification of subgroups. Hardmetal products indentified as K type carbides are intended for the machining of short chipping grey cast irons, non-ferrous alloys such as Al-Si and non-metallic materials [89]. The mechanical and physical properties of WC-Co tool materials depend on the cobalt content and carbide grain size and typically a 6%Co, 94%WC alloy has a thermal conductivity of ~100W/mK. In contrast HSS is much lower at ~31W/mK [73]. Yang et al. [90] and Saito et al. [91] summarised average values of hardness, fracture toughness and wear rate as a function of carbide size and showed that wear rate increases when the carbide grain size increases. Sample mechanical properties for tungsten carbide are given in Table 13 [73]. Their maximum operating temperature is ~500°C [92-94], beyond which oxidation occurs. Carbide tools are well documented and they are widely used for producing holes, drilled and reamed, in abrasive aluminium silicon alloy workpieces [20, 23, 38, 60].

Table 13: Properties of WC-Co tool materials at room temperature [73]

% Co	Mean WC grain size (μm)	Hardness (HV)	Transverse rupture strength (MPa)	Compressive strength (MPa)	Young's modulus (GPa)	Fracture toughness ($\text{MPa m}^{1/2}$)
3	0.70	2020	1000	-	-	-
	1.40	1820	-	-	-	8
6	0.70	1800	1750	4550	-	-
	1.40	1575	2300	4250	630	10
9	0.70	1670	2300	-	-	-
	1.40	1420	2400	4000	588	13
	4.00	1210	2770	4000	-	-
15	0.70	1400	2770	-	538	-
	1.40	1160	2600	3500	-	18

A large proportion of the carbide tools employed (~85%) are coated. The coatings are intended to improve tool life and productivity as well as offer advantages in high-speed and dry machining applications. The coating typically provides solution and abrasive wear resistance, a thermal barrier to reduce the thermal energy flow into the tool and decreased friction coefficient to aid sliding of the chip, and minimise built-up edge [26, 95]. There are four major groups of hard coating materials, but the most popular is the group of titanium-based materials, including TiN, TiC and Ti(C,N) [96]. These coatings have high hardness, 2000-3500HV [97-99] with thermal stability up to ~1000°C [73], and have proved their benefits in machining of ferrous materials, such as steels [100-102]. However, such coatings offer no significant advantage in terms of frictional coefficient being typically ~0.5 [97], and provide no significant advantage in the machining of aluminium alloys [25, 40]. In contrast, new low-friction coatings such as Graphit-iC™ and Dymon-iC™ have values of ~0.05 and are becoming more established for the machining of light-alloys and the wear protection of mechanical parts [103, 104]. More details of these coatings are included later on in this report.

3.2.2 Polycrystalline diamond

3.2.2.1 Introduction

Diamond has high thermal conductivity, ~600-2000 W/mK which is some four times that of copper and twenty times that of tungsten carbide at room temperature, extreme hardness, ~50-100 GPa (approximately 5000-10000HV), and low coefficient of thermal expansion properties, ~1.5-4.8x10⁻⁶/K [105-108], which have been exploited in cutting tools [109-117]. Polycrystalline diamond (PCD) was developed in the early 1970's and is well

established as a cost effective alternative to more conventional tool materials for the machining of non-ferrous metals, such as aluminium alloys [118]. It is produced by sintering micron-sized diamond grits together with a metal catalyst/binder, such as cobalt, at high temperatures between 1200-1600°C and at high pressures of ~6GPa [117, 119, 120]. The resulting polycrystalline structure contains randomly orientated crystals providing isotropic properties and greater resistance to cleavage than monocrystalline diamond [89]. A typical processing route for the production of PCD cutting tools involves laser cutting blank segments to near net shape followed by brazing to a steel or cemented carbide tool body and shaping to the required geometry/size using electrical discharge grinding (EDG), or mechanical grinding or lapping [28]. The PCD layer is commonly produced on a cemented carbide backing/substrate (blank, up to ~70mm diameter) to provide additional strength, aid sintering and ease fabrication. Abrasive grinding is used for shaping the majority of indexable insert tools however with more complex form tools and round tools, such as drills, EDM is the preferred fabricating method. PCD tool blanks are commercially available from Diamond Innovations (Compax[®]), Element Six (Syndite) and Sumitomo Electric (Sumidia). A typical 5mm diameter twin lipped PCD tipped drill on a solid carbide body costs in excess of £350. Figure 30 [121] provides an example of PCD blanks and a PCD cutting insert.

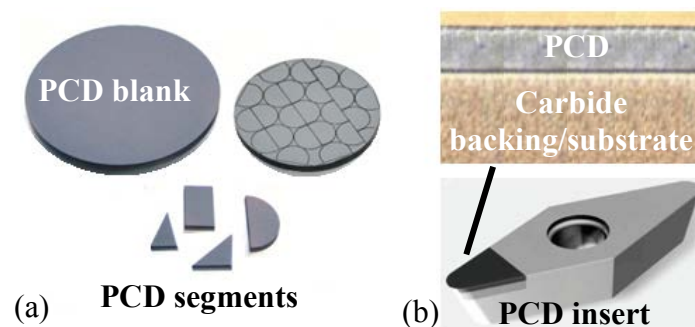


Figure 30: Polycrystalline diamond (a) blanks and (b) cutting insert [121]

3.2.2.2 Properties and performance

The properties of PCD depend not only on the final grain size, but the degree of diamond intergrowth and distribution/quality/cleanliness of the catalyst/matrix material [120, 122-125]. The bonding matrix should have the ability to support the diamond particles firmly, but also to wear to some extent to allow the tips of the diamond particles to be exposed for maximum cutting efficiency [122]. PCD blanks are available in different grades having different structures and properties. Table 14 [108, 126] gives properties of PCD while Figure 31 [73] details wear performance of different PCD grades and Figure 32 [121] shows

structures for different PCD grades. Coarser grades have larger diamond particles than fine grades of PCD. Best wear performance is achieved with larger diamond grains, whereas smaller diamond particles will result in a sharper cutting edge, and provide a better workpiece surface finish [127]. The thermal stability of PCD is reduced at temperatures exceeding 700°C, due to the presence of cobalt in its structure which promotes back-reversion of diamond to graphite [128]. Therefore, neither fabrication nor usage of a PCD tool should approach such high temperatures.

Despite the high hardness of PCD it is relatively brittle this makes it unsuitable for very heavy interrupted cutting operations. As a guide the toughness, or the ability to absorb energy before fracture, of a PCD is typically ~40% less than that of a K10 tungsten carbide tool [108, 126]. As a general comment, PCD tool geometry designs are more limited compared with carbide materials due to the nature of the diamond structure. It is recommended that the tool design incorporate small rake and clearance, angles of 1-7°, thus minimising tensile stresses and fatigue failure/chipping of the diamond particles during cutting [129-131]. Recently, new grades of polycrystalline diamond, such as CTM302 have been developed by Element 6, and employ mixed diamond particle sizes of 2 to 30 microns, see Figure 32 [121]. This provides increased packing density, where the area between the coarse grains is filled by the finer grains, thus providing improved (~15% higher compared with Syndite™ 010) cutting edge quality and tool toughness [121].

Table 14: Physical properties of polycrystalline diamond [108, 126]

Physical properties	Syndite™ 002	Syndite™ 010	Syndite™ 025
Density g cm ⁻³	4.24	4.12	3.86
Fracture toughness MPa m ^{1/2}	6.86	8.81	8.89
Knoop Hardness GPa (HV)	50 (~5000)	50 (~5000)	50 (~5000)
Young's modulus GPa	749	776	810
Thermal conductivity W m ⁻¹ K ⁻¹	-	560	560
Coefficient of thermal expansion 10 ⁻⁶ K ⁻¹	-	4.2	4.6

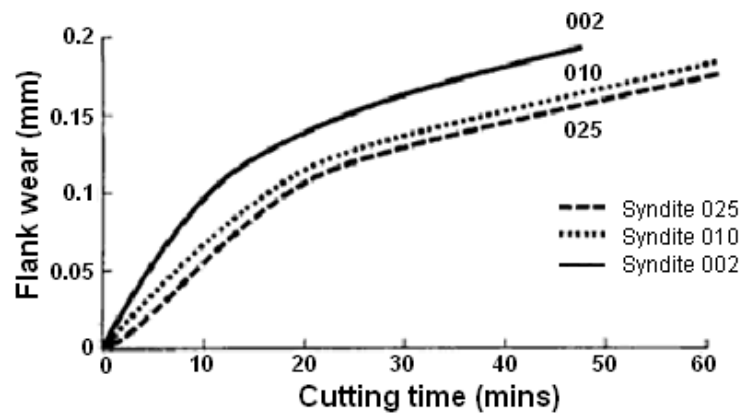


Figure 31: Tool wear for different polycrystalline diamond grades when machining Al-Si alloy (18%Si) [73]

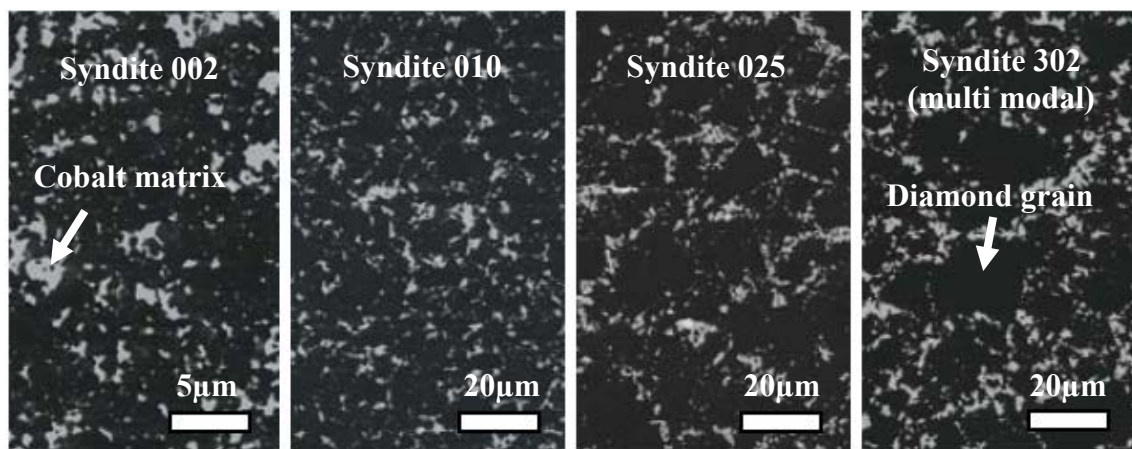


Figure 32: Structure of different PCD grades [121]

Polycrystalline diamond has largely replaced tungsten carbides together with natural diamond in a range of high performance applications when turning, drilling, boring, etc [132, 133], most notably in high volume manufacture of Al-Si automotive parts. Here the life of PCD tools has been shown to be much longer than conventional uncoated and thin film diamond coated tungsten carbides at high cutting speed typically by a factor of 10 to 100. Figure 33 [115] shows tool life performance of PCD when cutting hypereutectic Al-Si. The low rate of wear associated with PCD makes it possible to hold workpiece tolerances to within very close limits. Furthermore, workpiece surface quality produced by PCD has been found to be better than produced by uncoated and diamond coated carbides. Figure 34 [129] shows surface roughness, average (R_a) and total (R_t), performance of WC, PCD and diamond coated WC tools. The high chemical inertness of diamond for aluminium is also beneficial, producing low cutting forces and less workpiece adhesion problems [40].

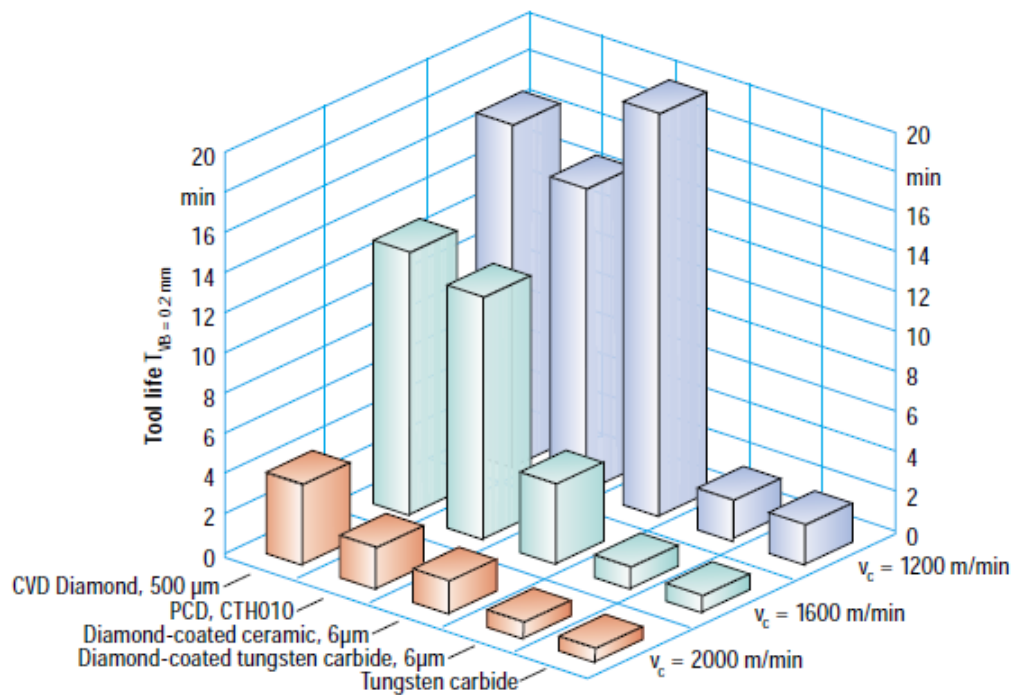


Figure 33: Tool life performance of PCD against other cutting tool materials in the machining of hyper-eutectic Al-Si die casting alloy [115]

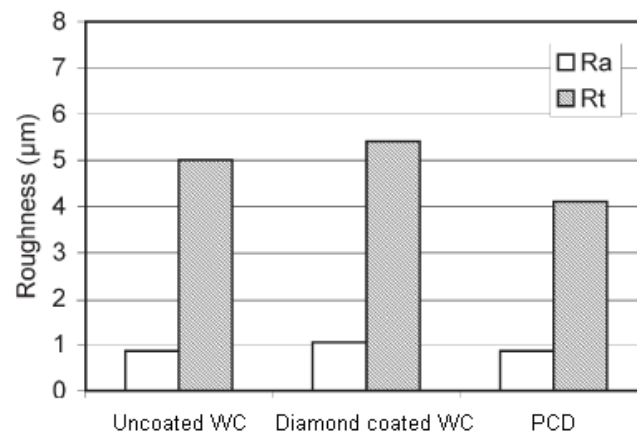


Figure 34: Surface finish performance of Uncoated WC, Diamond coated WC and PCD on cutting aluminium alloy 6351 [129]

3.2.3 Diamond and diamond-like carbon coated tools

3.2.3.1 Diamond coated tools

Demand for improved production rates together with advances in workpiece materials have contributed to the extensive development of coatings for cutting tools. Chemical vapour deposition (CVD) has, since the late 1980s, been the preferred method for producing diamond films. The process takes place at/below atmospheric pressure and involves the use of starting materials, or precursors, typically a mixture of hydrogen and a hydrocarbon component such as methane, to provide the source of carbon from which the diamond is formed. The gas

mixture is excited in an energy-intensive reaction chamber to form plasma above a solid substrate. A variety of CVD methods, such as hot filament, microwave plasma and DC plasma, are used to grow diamond. To ensure good diamond growth the substrate temperature is required to be in the range 700-1000°C [134]. Lower cobalt content leads to greater adhesion, smooth/uniform films, low surface friction coefficient and small grain size when coating cemented carbide [135]. Such high substrate temperatures preclude the CVD diamond coating of low melting point materials such as aluminium and plastics [136]. Kamo and Sato [137] attempted to deposit diamond on substrate at lower temperatures with the aid of microwave plasma CVD system, but the growth rate proved to be extremely slow, typically a 30µm thick film required a processing time of several days [138].

When machining aluminium silicon alloys, CVD diamond coated tools provide significantly lower workpiece surface roughness, less material build-up and lower cutting forces than when using uncoated carbide tools [19]. In comparison with PCD, CVD diamond contains no metallic binder which results in a higher hardness of ~75 GPa [139], hence it has enhanced wear resistance. The absence of a second phase also means that there is less tendency for BUE formation and lower cutting forces, consequently better workpiece surface finish is achieved [140]. Furthermore, the CVD techniques allow diamond films to be deposited on geometrically complex cutting tools of any style and shapes, such as drills, reamers, etc, [134, 141-144], that are difficult to fabricate with PCD. Heaney et al. [143] detailed the CVD diamond coating of small micro-scale tools used in the channel machining of 6061-T6 aluminium. Where cutting performance is concerned, CVD diamond tools have matched or exceeded the life provided by conventional PCD and WC-Co [134, 145, 146]. CVD diamond is also recognised as being suitable for machining high silicon aluminium alloys under wet or dry conditions [65, 147-150]. Machinability problems, associated with BUE, of aluminium are minimised when employing higher machining speeds together with CVD diamond tools [151].

The main disadvantage associated with CVD diamond coatings on WC concerns the adhesive-bond strength of the material to the substrate due to carbon-cobalt interaction, however Polini [152] and Polini et al. [153] demonstrated that substrate modification can improve adhesion of the diamond film. Raghuveer et al. [154] also showed that cleaning and removing cobalt from the substrate surface regions, by chemical etching combined with the addition of an intermediate coating layer of TiN/TiC and a larger tool edge radius, enhanced the diamond adhesion. Hanyu et al.[155] modified drill geometry and demonstrated that a

rake angle of 20° provided the best performance for cutting high silicon content aluminium alloys, while multi-layered coating improved the tool durability. Thin-film, $<30\mu\text{m}$, CVD diamond is favoured where edge preparation and cost are important. Conversely, thick-film ($>30\mu\text{m}$) diamond has been shown to provide longer machining times when compared with conventional tungsten carbide and sintered PCD tools [156]. Fracture toughness of the thick-film CVD diamond ($\sim 5.5\text{MPa m}^{1/2}$) however is relatively poor compared to PCD ($8.85\text{MPa m}^{1/2}$) and is recommended to be used primarily for low cutting force/finishing operations [157]. In addition, increased film thickness results in increased rounding of the tool cutting edge and higher cutting forces. The strength of the diamond coated substrate was observed by Kanda et al. [158] to decrease with increased film thickness and therefore intermittent cutting conditions are not recommended.

Recently, a diamond coating structure termed “nanocrystalline” has been developed in an attempt to improve durability of the tool. The nanocrystalline surface morphology is composed of ultra fine grains, with an average size <100 nanometres ($<0.1\mu\text{m}$) compared with $1\text{--}5\mu\text{m}$ in size found in a microcrystalline diamond coatings. This gives a lower tool surface roughness of $R_a 0.33\mu\text{m}$ compared with $0.47\mu\text{m}$ for a conventional diamond coated tools [89, 159, 160]. Smoother tool surfaces mean that there are fewer opportunities for workpiece material BUE at the tool/chip interface, thus significantly improving both the chip flow across the tool rake face and producing a better machined surface finish. Hanyu et al. [161] examined the drilling of aluminium alloy under dry and minimum quantity lubricant conditions using ultra fine diamond coated tools. They demonstrated excellent anti-sticking properties together with longer tool durability compared to a conventional diamond coating.

3.2.3.2 Diamond-like carbon coated tools

Industry has recently identified the potential benefits of minimising/discarding the use of lubrication agents, despite their positive effect on extraction of swarf, workpiece quality, tool life, etc. By adopting dry or minimum quantity lubrication (MQL) approaches, benefits can be accrued in relation to environmental impact, health risk due to lubricant exposure [23], and costs for lubricant disposal [162]. Conversely, dry metal cutting raises the prospect of BUE formation, increased cutting temperatures and the need for higher cutting power compared with MQL and fully lubricated conditions. Davim et al. [163] experimented with dry drilling of aluminium AA1050 using uncoated K10 carbide tool and showed that

~25% higher cutting power was generated when compared with MQL and flood lubrication due to tool ploughing on the work material.

Diamond-like carbon (DLC) films are reported to have enhanced tribological properties, including a combination of low wear rate, $1 \times 10^{-17} \text{ m}^3/\text{Nm}$ and low coefficient of friction, ~ 0.01 in vacuum [164] and ~ 0.1 under a dry atmosphere [165, 166], giving improved performance in respect of protective coating and dry machining [167]. Such DLC, or hard amorphous carbon films containing significant fractions of sp^3 bonds [168, 169], cover a wide range of different types of carbon-based coatings, but the two major groups are amorphous hydrogenated (a-C:H) and amorphous non-hydrogenated tetrahedral (ta-C) [168]. The non-hydrogenated carbon coating is found to be denser in nature, and therefore higher wear resistance, although friction coefficient increases with decreased hydrogen content [170]. Work by Fukui et al. [171] involving the use of a non-hydrogenated amorphous carbon film with $<4\%$ hydrogen for the dry machining of aluminium alloy, demonstrated that the smooth ($0.01 \mu\text{m Ra}$) surfaces of DLC ($0.1 \mu\text{m}$ thickness, 0.1 coefficient of friction) coated tools reduced the formation of built-up edge and cutting resistance, while increasing cutting length when compared with conventional uncoated tools.

In spite of the advantages DLC coatings offer, they unfortunately suffer from poor levels of adhesion, high brittleness and internal stresses [172]. The addition of various metals to the coating (metal-containing carbon, Me:C), has been shown to reduce such problems [173]. Examples of these are non-hydrogenated amorphous Graphit-iC™ with a combination of carbon and 20% chromium, and hydrogenated amorphous Dymon-iC™ with additional butane in the carbon and chromium composition. These coatings have proved successful in a wide range of applications, many of which are in the field of dry metal cutting.

Carbon-based solid lubricant coatings, Graphit-iC™ and Dymon-iC™, have been extensively developed over the last decade. Stallard et al. [174] and Stallard and Teer [175] studied the tribological behaviour of Graphit-iC™ and Dymon-iC™, and demonstrated that the DLC performed less favourably when tested under high load-bearing ($>2.1 \text{ GPa}$), with the lowest specific wear rates achieved with Dymon-iC™. However, the opposite was found in work by Wain et al. [58], in which the Graphit-iC™ coating provided the longest tool life with the least amount of adherent material when machining Al-Si against MoST (a mixture of molybdenum disulfide, MoS_2 , and titanium) and Dymon-iC™ coatings. Work, by Fox et al. [103], showed the tool life of Graphit-iC™ in dry drilling of low alloy steel (34CrNiMo6,

250HB) to exceed by 20 times that of uncoated tools. Bhowmick and Alpas [24, 176] confirmed that both Graphit-iC™ and Dymon-iC™ were preferable over uncoated tools for machining Al-Si alloys using minimum quantity lubrication. The friction coefficient of these coatings is low, typically reported values between 0.05-0.3 depending on the environment and applied load [103, 104, 172, 174, 175, 177, 178], which is expected to be beneficial for swarf dispersion/removal during operations such as drilling and reaming.

3.3 Workpiece quality

3.3.1 Hole dimensional accuracy

Workpiece hole diameter is commonly analysed in line with other quality assessment parameters by a micrometer or co-ordinate measuring machine (CMM). Bono et al. [55] measured dry drilled holes, 9.92mm diameter and 25mm depth, in aluminium 319 using a CMM. They identified oversized holes with dimensional variations for individual holes ranging from 17-26µm. Kalidas et al. [179] also used the same method for measuring holes with a diameter of 9.13mm when dry drilling of as-cast aluminium 356 workpiece and found that the hole size was larger and tapered towards entry. Work by Kurt et al. [180] when drilling Al 2024 alloy showed that an increase in cutting speed led to larger hole size at the entry, due to vibration and chatter. The author also stated that the dynamic behaviour of the drill and the drilling temperature played an important role in the accuracy of the holes. In contrast, Bono and Ni [55] concluded that thermal distortions of the drill and workpiece, account for only a fraction of the dimensional errors.

3.3.2 Cylindricity and out-of-roundness

The form and size of a hole have a considerable effect on the overall performance of the mechanical system it serves. Even with high-precision machine tools, deviation from design specifications occurs due to inherent variability, fluctuating air pressure, etc. Out of roundness is assessed by using a number of types of reference circle namely least square, ring gauge (minimum circumscribed circle), plunge gauge (maximum inscribed circle) and minimum zone, see Figure 35 [181]. These reference circles are used to establish the centre of the component and the least-square method is used to establish the centre. Out of roundness is considered to be the radial deviations from the component centre. Figure 36 (DD CEN ISO/TS 12181: 2007) [182] shows a form deviation of a roundness feature where A is the reference circle, a_1 and a_2 are positive and negative local deviations respectively for an

internal feature and vice versa for an external feature. In the previously detailed paper by Kurt et al. [180] roundness errors in holes 10mm diameter and 30mm depth, deviated up to $\sim 60\mu\text{m}$ with increased cutting speeds (30-45m/min) and feeds (0.15-0.25mm/rev).

Cylindricity describes the cylindrical quality of form and has been defined as the radial separation of 2 co-axial cylinders fitted to the total surface and is a 3-dimensional analysis of rotation that combines the characteristics of axial and radial form and overall shape [183]. The types of cylinder fits, to which measured data is analysed, are the same as the ones previously mentioned for the roundness. The least square cylinder/circle is the most common and used in many general purpose applications. Figure 37, adapted from [183] and [184], illustrates types of cylinder fits while deviations of cylindrical parts are categorised as banana, barrel, bell-mouth, hourglass and taper, see Figure 38 [185].

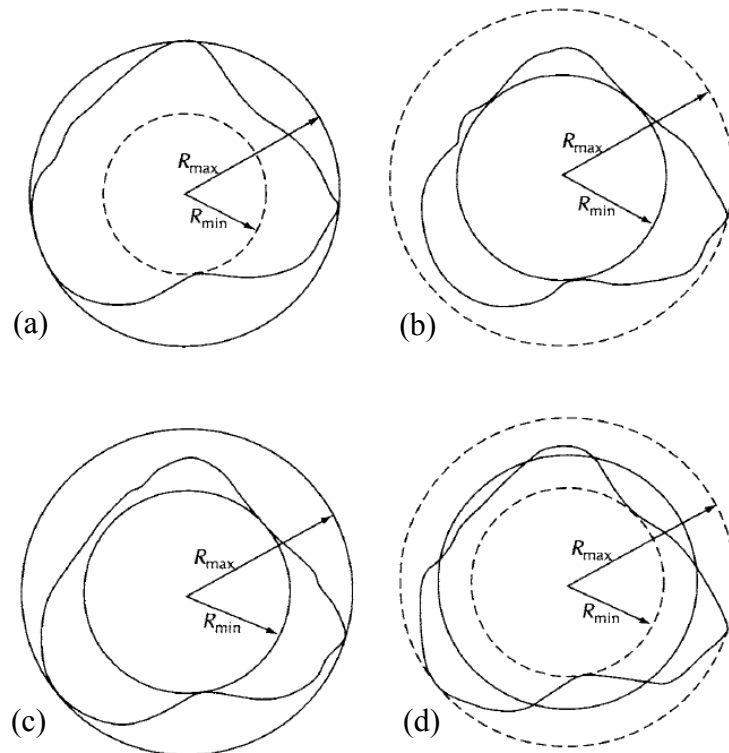


Figure 35: Assessment of roundness (a) ring gauge, (b) plug gauge, (c) minimum zone and (d) least squares [181]

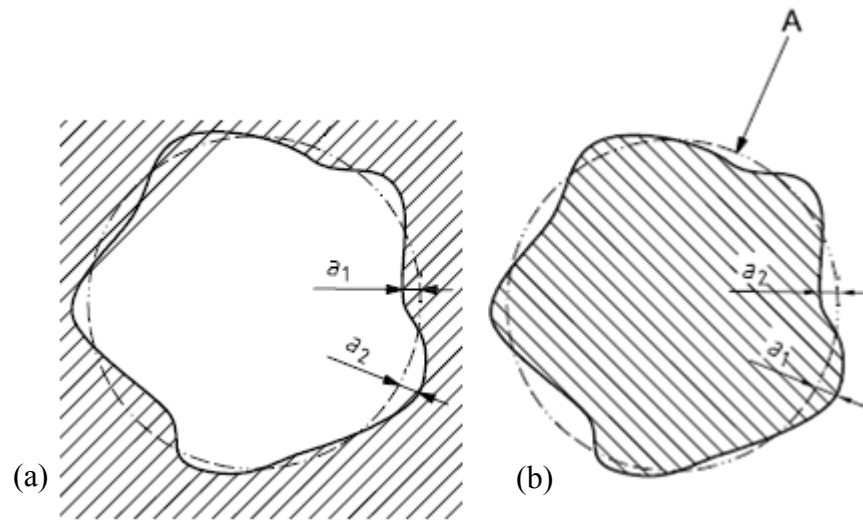


Figure 36: Form deviation of (a) internal and (b) external roundness features [182]

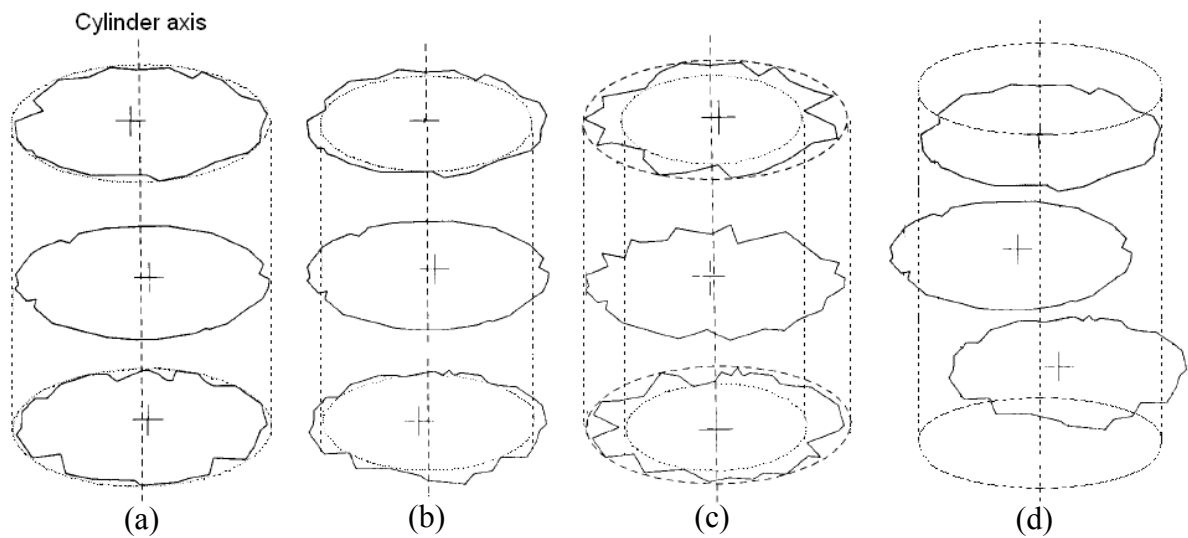


Figure 37: Reference cylinders used for cylindricity analysis (a) minimum circumscribed, (b) maximum inscribed, (c) minimum zone and (d) least square [183, 184]

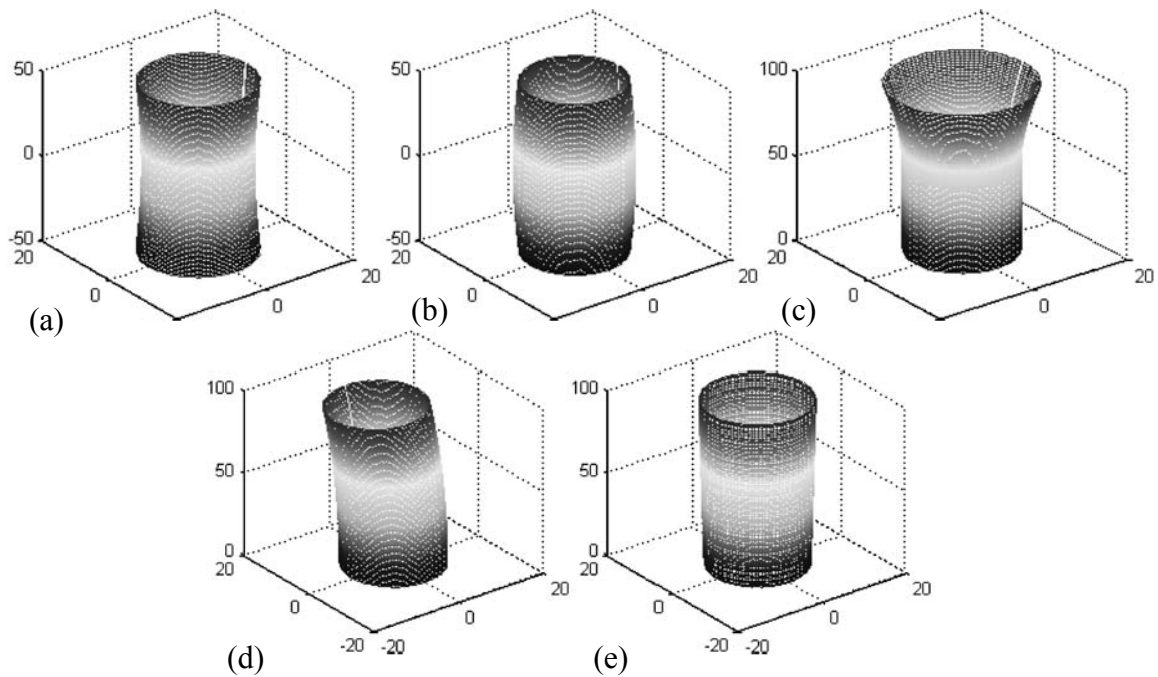


Figure 38: Variations in shape of cylindrical features (a) hourglass, (b) barrel, (c) bell-mouth, (d) banana and (e) taper [185]

3.3.3 Workpiece surface finish and integrity

Mechanical parts are often subjected to severe conditions of stress, temperature and hostile environments. For example, a small turbocharger impeller used in modern automotive diesel engines operates under a high compression ratio (5:1), with rotational speeds up to 150000rev/min, that create high stresses and fatigue in the shaft bore [2]. Failure of such components during operation would cause inevitable damage to the housing and/or the engine. By comparison, failure of a structural components used in an aircraft engine would lead to catastrophic consequences. Here, component reliability and safety are the most important features driving manufacturers to engage in assessment of manufacturing processes. Final machining directly influences the quality and integrity of a workpiece and can have a direct bearing on the performance of a product [186].

Surface integrity (SI) is the term, first introduced by Field and Kahles [187], and is defined as “the inherent or enhanced condition of a surface produced in machining or other surface generation operation”. It encompasses the study of component surface texture, which is a measure of surface roughness or surface topography, and surface metallurgy, which is a study of the component subsurface produced in machining. Such aspects affect the functional performance of a manufactured part [188]. A manufactured component comprises several surface features which are demonstrated in Figure 39 [189]. All material removal processes

change the nature, both topography and metallurgy, of the surface as well as its properties, e.g. fatigue, corrosion resistance, etc, due to the existence of temperatures, plastic deformation and chemical reactions [190]. Subsequently, such surface alterations compromise the SI of the component leading to poor functionality and service life. Typical types of surface alterations during metal removal are listed in Table 15 [188].

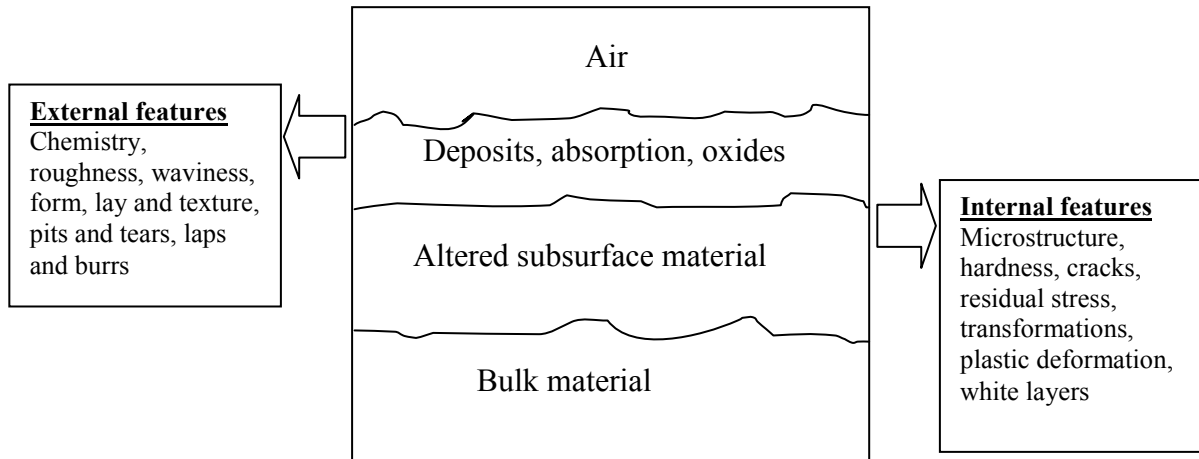


Figure 39: Schematic surface features of a manufactured component [189]

Table 15: List of surface alterations during material removal [188]

Types of surface alteration
Plastic deformation as a result of hot/cold work
Microcracking/macroc cracking and surface irregularities
Intergranular attack and preferential solution of microconstituents
Tears, laps, and crevice-like defects due to built-up edge
Recrystallisation
Change in hardness of the surface layer
Phase transformation
Residual stress distribution in the surface layer
Embrittlement due to chemical absorption of hydrogen
Spattered coating of re-melted deposited on the surface during electrical discharge, laser machining, etc

Field et al. [191] and Kahles and Field [192] outlined experimental procedures for defining surface integrity problems together with details of measuring methods for SI inspection. Three different levels of data sets for evaluating the characteristic features of machined surfaces are specified in Table 16 [191, 192]. The minimum surface integrity data set represents the least expensive approach whereas more critical applications may necessitate the standard or extended data set of SI to obtain additional in-depth data.

Table 16: Different levels of surface integrity data tests [191, 192]

Minimum SI data set	Standard SI data set	Extended SI data set
Surface finish Microstructure up to 10x Microcracks Macrocrack indications Microhardness Microstructure including microcracks, plastic deformation, phase transformation, intergranular attack, pits, tears, laps, protrusions, built-up edge, melted and re-deposited layers, selective etching	Minimum SI data set Fatigue test (screening) Stress corrosion test Residual stress and distortion	Extended SI data set Standard SI data set Fatigue test (extended to obtain design data) Additional mechanical tests Tensile Stress rupture Creep Other specific tests including bearing performance, sliding friction evaluation, sealing properties of surface

The study of surface integrity is well documented and there are numerous studies published on the turning and grinding of hardened materials ~45-65HRC, in respect of fatigue performance [187, 193]. Surface integrity assessment is standard practice in relation to the machining of advanced aerospace titanium and nickel-based super alloys [194]. Recently, Jawahir et al. [186] published a comprehensive review of current developments in surface integrity evaluations including modeling for a wide range of material removal processes. However, the number of papers relating to surface integrity evaluation with aluminium alloys appears limited.

Byrne et al. [195] carried out surface integrity assessment of AlSi9 alloy in a dry cutting environment with PCD tools, and showed that surface topography was characterised by a distribution of small pits and micro grooves with no hardness alteration between the sub-layer and the bulk material. The work also found that hardness results vary largely due to the inhomogeneous nature of the alloy, which contains secondary phases as well as the aluminium matrix. Jasinevicius et al. [196] suggested that hard silicon inclusions are the limiting factor in achieving an ultra fine surface finish in machining. This was because they were difficult to cut and tend to get dragged causing small scratches within the cutting grooves. Figure 40 [195] gives an example of the surface topography of an Al-Si alloy machined surface. More recently, Farid et al. [18] evaluated the surface integrity of an Al-Si alloy which had been high speed drilled and found fracture/dislodgement of silicon particles contributing to poor workpiece surface finish, see Figure 41.

Hardness values close to the surface of machined aluminium alloy workpieces are generally high and tend to decrease with an increase in depth until the bulk material is

reached. Farid et al. [18] demonstrated that microhardness values increased with an increase in cutting speed due to increased cutting temperatures in the deformation zone promoting subsurface plastic flow. Tool geometry also plays an important role on the integrity of the workpiece surface. Yuan et al. [197] demonstrated that a sharp tool generates lower machined surface hardness, 167HV compared with 207HV, and roughness, R_{\max} 0.035 μm compared with 0.06 μm , than a dull tool. Jeelani and Musial [198] studied the effect of cutting speed and tool geometry on the fatigue life of an aluminium alloy workpiece material. The authors concluded that fatigue life was poor with decreased cutting speed or reduced tool rake angle, and that compressive residual stresses are preferred in the machined surface region. Figure 42 [198] details data on workpiece surface roughness and fatigue life as a function of cutting speed when machining Al-Si alloy.

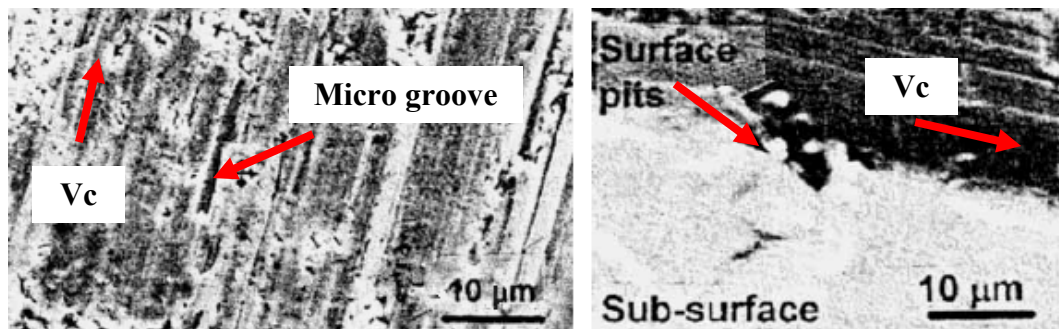


Figure 40: Micrograph of AlSi9 machined surface [195]

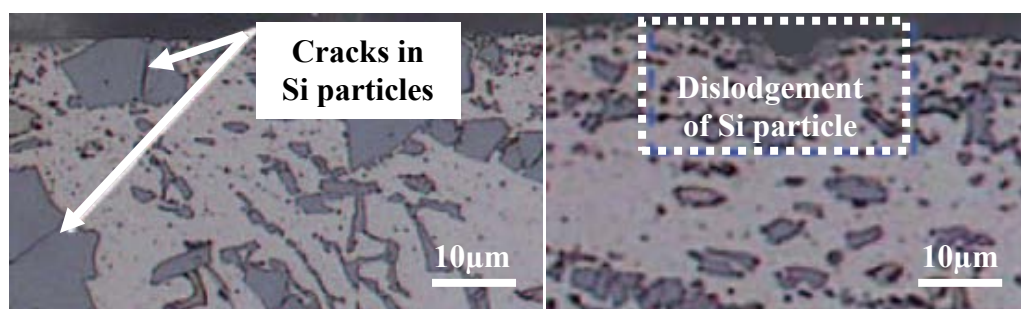


Figure 41: Optical micrograph of Al-Si drilled workpiece subsurface [18]

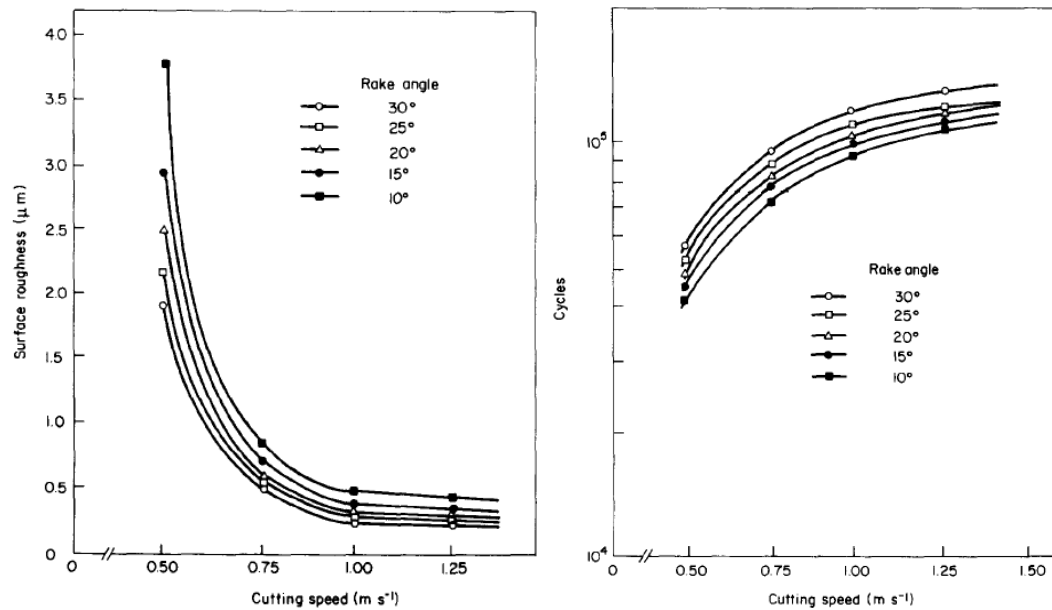


Figure 42: Workpiece surface roughness and fatigue life as a function of cutting speed [198]

Achieving good surface integrity is challenging when machining aluminium MMC due to the hard and abrasive nature of the reinforcement within the material. Even so, surface roughness when Al/SiC machining was found to be better compared to that of Al machining, due to the increased flow ability of the work material at high temperatures [199]. Figure 43 [199] gives comparative surface roughness results for Al and Al/SiC. Pull-out, fracture and dragging of the hard particles, such as SiC, is common during machining of such materials. Ge et al. [200] showed that workpiece surface roughness of 0.02μm Ra could be obtained during the machining of 2024Al/SiCp 15%Vol, but that finer roughness values were extremely difficult to achieve. Grooves/scratches, cracks and voids are surface imperfections which are commonly found in a machined surface of an Al MMC reinforced with 25% SiC [200, 201]. El-Gallab and Sklad [33] and Kannan and Kishawy [202] observed machined workpiece surface defects in the form of pits, voids and interfacial cracking which increased with an increase in cutting speed when machining such types of material. Typical machined defects found with an Al MMC are shown in Figure 44 [33, 202]. Variations in microhardness as a result of work hardening, were found in the machined subsurface and were more pronounced in the MMC reinforced with course particles [202]. Their values peaked within 20μm of the surface however the extent of the alteration was typically up to 100μm below the machined layer. An example of a work hardened layer is given in Figure 45 [202]. Suresh et al. [199] carried out machining experiments on Al and Al/SiC and showed residual stress

values $\sim 5\mu\text{m}$ below the subsurface of -40MPa and -350MPa respectively. The author suggested that the higher compressive stress of Al/SiC was due to higher temperatures in the cutting region.

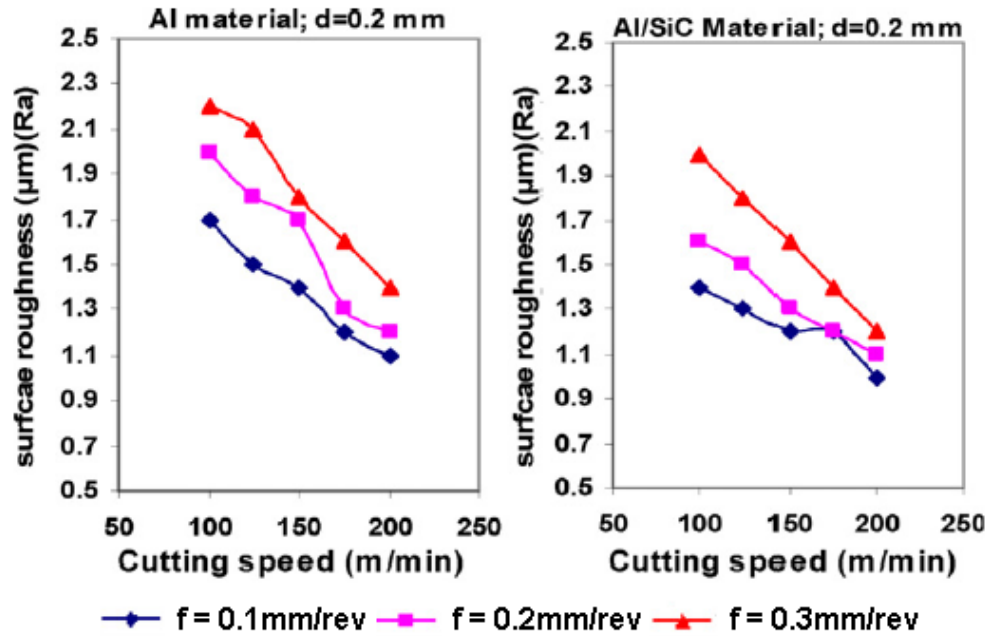


Figure 43: Variation of surface roughness with different cutting speeds and feeds for Al and Al/SiC [199]

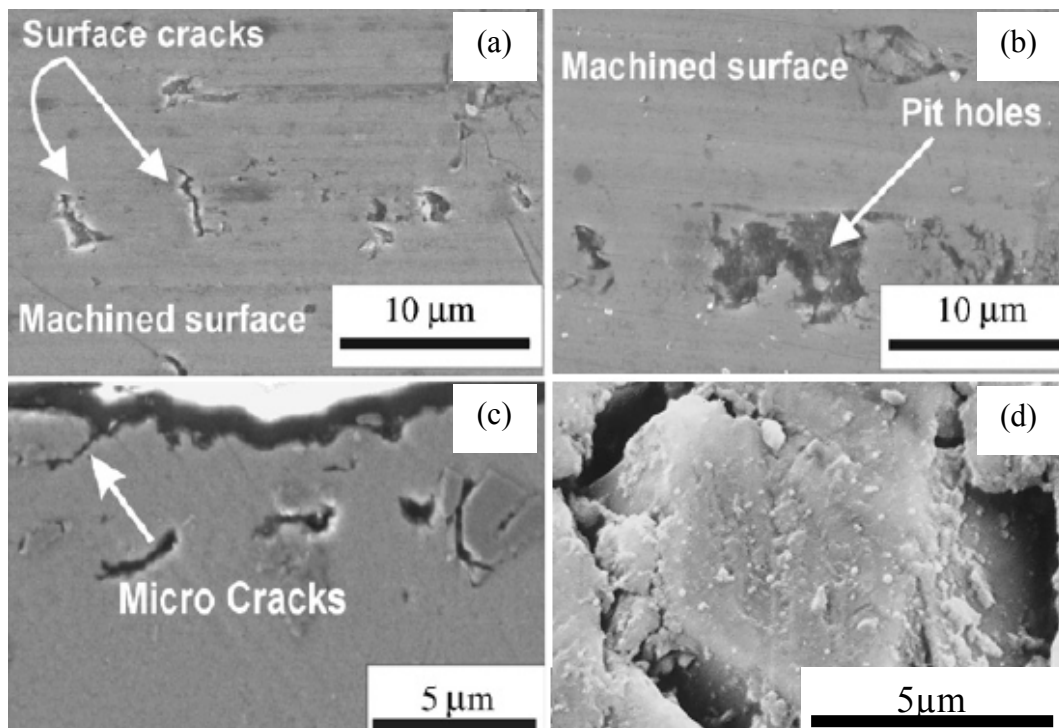


Figure 44: SEM images of Al MMC machined surface showing (a) cracks, (b) pits, (c) micro cracks and (d) fracture/crushed SiC particle [33, 202]

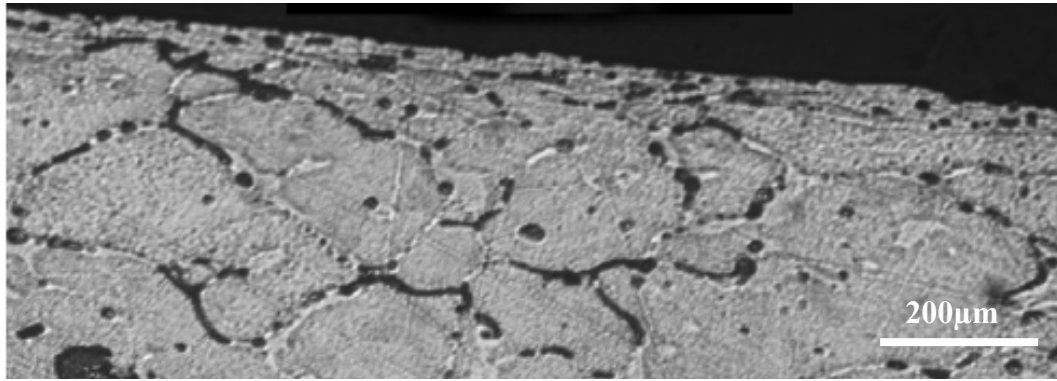


Figure 45: Machined subsurface of Al MMC [202]

3.3.3.1 Techniques for surface roughness and integrity measurement

Non-contact and contact methods are widely employed for determining surface texture or topography. Optical techniques have been used for assessing the quality of a surface which date back to 1927 and involved projecting light onto a surface [203]. The contact method for assessing surface characteristics is performed by profilometry through the use of a stylus-based measurement system. The stylus, commonly employing a small diamond tip, is drawn across a line or an area of a surface providing a useful 2D/3D surface profile. Traditionally, characterisation parameters, such as arithmetic average roughness (R_a), total roughness (R_t), peak-to-valley height (R_y), etc., of a contour or profiles obtained from the motion of the stylus are recorded into a computer for traceability and further analysis. Standard topography roughness and waviness assessments frequently contain the presence of some unintentional irregularities or flaws, such as cracks, inclusions, blowholes, that whenever possible, should not be included in the analysis [10]. Figure 46 [204] displays a typical surface profile trace and parameters, adapted from ANSI B46.1 1978. The roughness of a machined workpiece is generally a result of the inherent action of the cutting tool or machining process, whereas, the waviness exhibits a larger wavelength of periodicity resulting from machine or workpiece vibration, deflection, chatter or run-out of the cutting tool.

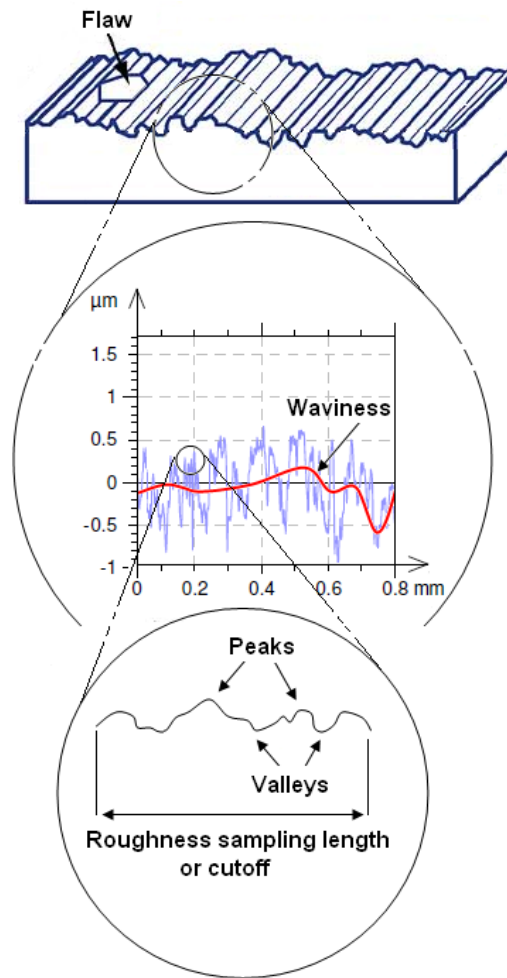


Figure 46: Schematic of typical surface roughness profile parameters [204]

Other equipment which is used for surface examination includes the scanning electron microscope (SEM), transmission electron microscope (TEM), scanning tunneling microscope (STM), atomic force microscope (AFM) and x-rays systems. Details of the associated measurement techniques, though not included in this section, are discussed in Whitehouse's report [205].

Evaluation of workpiece surface metallurgy is commonly carried out using metallographic techniques. Optical examination of microstructural alterations and microcracks requires specimen preparation through means of sectioning, mounting, grinding and polishing in a manner that produces the least possible surface distortion. Standard procedures and metallographic techniques for examining the surface of metals are detailed by Ormandy [206]. Aluminium specimen are usually mounted in cold resin rather than in hot-pressed bakelite to avoid thermally activated microstructural changes. Keller's reagent with 0.5-1% hydrofluoric acid (HF) [207, 208] is the common etching medium used on aluminium alloys. Microhardness determination is carried out using an instrument with a Knoop or

Vickers indenter for indentifying sub-layer work hardened/softened zones. Loads of 25-50 grams are preferred for hardness readings to within $12\mu\text{m}$ (0.0005inch) [191]. The publication by Hashimoto et al. [209], suggests that lack of support at the edge of the mounting contributes to untrue microhardness results. In addition, the mixed phase structure of aluminium workpieces also makes microhardness determination difficult.

3.4 Statistical process control

3.4.1 Introduction

Quality is used to signify excellence of a product or service. It has been described by various authors as *meeting the requirements of the customer* (J.S. Oakland), *“fitness for purpose or use”* (J.M. Juran), *“doing it right the first time”* (P. Crosby), and many more. The ability to meet customer requirements is vital not only for profitability, but also for business survival. Consequently, manufactured parts are traditionally inspected at the end of the production process by means of visual examination, physical measurement, computer input data validation, etc, to ensure quality. Nowadays, statistical process control (SPC) is widely employed in manufacturing [210]. It is an effective problem-solving process improvement tool used for achieving process stability as well as improving capability, through the reduction of variability within the process. Reduced manufacturing costs due to less waste, rescheduling and rework, and increased competitiveness are expected as a result of SPC implementation. Major SPC tools include histograms, check sheets, Pareto charts, cause and effect diagrams, defect concentration diagrams, scatter diagrams and control charts. Of these, control charts are the most technically sophisticated and are used for monitoring quality characteristics that have been measured or computed [211]. Figure 47 shows a typical control chart with a centreline (CL) that shows the average value of the quality characteristic. The other two horizontal lines are the upper and lower control limits (UCL and LCL) respectively, which are specified so that the state of the process can be identified as in control or out of control. For instance, if any of the plotted data fall outside the UCL and/or LCL lines the process is assumed to be out of control and investigation may be necessary in order to find and eliminate the cause/causes responsible for such behaviour. A control chart also presents process trends, from which the future of the process can be predicted, i.e. the process is performing normally, drifting out of control, etc.

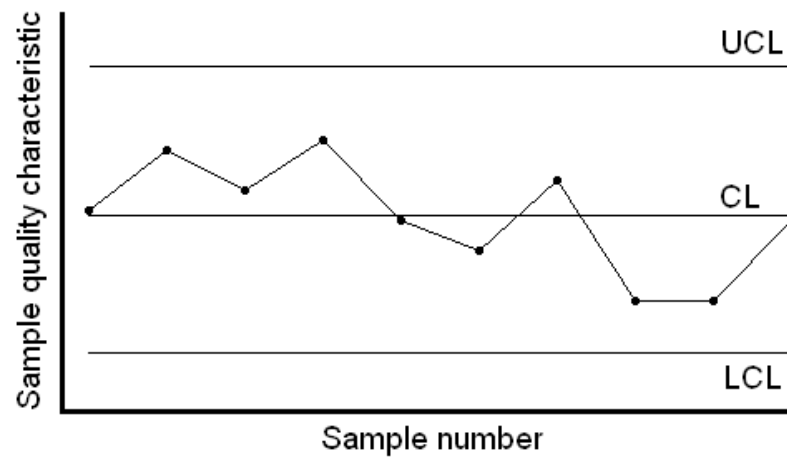


Figure 47: Typical control chart

3.4.2 Causes of quality variation

No two manufactured items are the same, because any production process regardless of how well it is designed or maintained, contains a certain amount of variability that arises from many sources. Some sources of variation in the process cause short term process drift, piece-to-piece differences, while others may cause changes to the output over a period of time. These changes may be sudden or gradual, procedural or irregular depending on the state and environment the process is in. Therefore, the time period and conditions over which measurements are made are critical to the overall variation observed [212].

There are two types of causes of variation, an inherent part of the process, called “common causes”, or an external part of the process, called “special causes”. Common causes of process variation refer to those sources that are consistently acting on the process, such as atmospheric pressure, or temperature changes, equipment vibrations or power fluctuation, etc. Although undesirable and unavoidable, common causes within a process produce a stable and repeatable distribution over time, referred to as “in statistical control”, thus a proportion of in-specification parts can be estimated from the distribution. The other causes of variability are assignable, but are intermittent and unpredictable. These causes are signalled by one or more points beyond the control limits and they may continue to affect the process output over time, unless identified and eliminated. For instance, special causes of variability may be from improper set up of machines, defective materials, or operator error, etc.

3.4.3 Types of control charts and design

There are two types of control charts depending on whether the data relates to variables or attributes. An attribute type of control chart is used with data that have a discrete

nature, such as go or no-go, accept or reject, 0, 1, 2, etc, whereas a variables type chart is suitable for data of a continuous nature, such as dimensions, lengths, etc. The attributes chart may be viewed as a tolerance-based chart that enables an organisation to control and monitor processes and ensure the output conforms to specification. However, Dale and Shaw [213] considered such a chart as providing no incentive for improving the process. Conversely, a performance-based variables chart was viewed as providing more information about the process in terms of process variation, piece-to-piece variation as well as process average, and should be used, when possible, in preference to attributes. Variable control charts are analysed in pairs and the most common consider the average (\bar{X}) and range (R).

Xie et al. [214] affirmed that the use of samples of a fixed subjective size with a traditional attributes type chart is not suitable for continuous inspection in modern manufacturing processes. This is because non-conforming items may be produced if a decision is made only when a sufficient number of items are inspected. Effective control charts require careful design with rational sample groups and sampling frequency. The main goal is to select subgroups or samples so that the chance for variation due to special causes occurring is minimised within each subgroup, but maximised between subgroups. Subgroup size is dictated by the type of process under investigation [212]. Although the larger the subgroup size the easier it is to detect small process shifts, subgroup size or samples need to be at least of two to give an estimate of residual variability, but four is recommended in Oakland's book [215]. Sufficient numbers of subgroups need to be defined so that the major sources of variation that affect the process have an opportunity to occur. Equally important is that subgroups should also be collected frequently enough so that they are able to reflect the potential opportunities for change [212]. Dale and Shaw [213] stated that a sample size of 5 at a frequency of 1 hour is the general rule adopted by the motor industry. A subgroup size of five with twenty subgroups is cited in Dudek-Burlikowska's work [216], which investigates bolt diameter values.

3.4.4 Process capability analysis

Process capability is a measure of the ability to satisfy customer requirements. Process capability analysis involves an engineering study commonly carried out to establish a baseline that is used for process monitoring using histograms, or probability plots, and control charts. Process capability is expressed as a ratio; either PCR and PCR_k [211] or capability indices C_p

and C_{pk} [217], which indicate how well the process satisfies the variability requirements. The formulae for calculating capability indices are as follows [211, 218];

$$C_p = \frac{USL - LSL}{6S} \quad - \quad - \quad - \quad - \quad - \quad - \quad - \quad - \quad \text{Equation 1}$$

$$S = \frac{\bar{R}}{d_n} \quad - \quad - \quad - \quad - \quad - \quad - \quad - \quad - \quad \text{Equation 2}$$

$$C_{pk} = \min \left(\frac{USL - \bar{\bar{X}}}{3S} \right) \text{ or } \left(\frac{\bar{\bar{X}} - LSL}{3S} \right) \quad - \quad - \quad - \quad - \quad - \quad - \quad - \quad \text{Equation 3}$$

The upper and lower specification limits are detailed as USL or LSL. The estimated process standard deviation is S while \bar{R} is the average of the total range R within subgroups and Hartley's constant d_2 is dictated by the selected sample number, i.e. for a sample of five d_2 is 2.326 and for a sample of ten is 3.078 [211]. The symbol $\bar{\bar{X}}$ represents the grand average of the total subgroup average \bar{X} , i.e. $\bar{\bar{X}} = \text{average sum of } X_1 \text{ to } X_5$. Clearly, from the equations, the C_p index compares the total variation with the specified tolerances. In order to have a capable process the process variation needs to be less than the specified tolerance band and the C_p value needs to be at least 1. Recommended index values are shown in Table 17 [211]. Values of C_{pk} take into account both the process variation and centring and this is useful when there is only one specification limit or a one-sided specification [215]. Ultimately, the values of the capability indices should closely match. When $C_p = C_{pk}$ the process is centred and when C_p is significantly greater than the corresponding C_{pk} this indicates an opportunity for improvement.

Table 17: Recommended minimum values for process capability C_p [211]

	Two-sided specifications	One-sided specifications
Existing processes	1.33	1.25
New processes	1.50	1.45
Safety/critical parameters, existing processes	1.50	1.45
Safety/critical parameters, new processes	1.67	1.60

CHAPTER 4: EXPERIMENTAL WORK

The research essentially comprised four main phases of work. Phase 1 and 2 were conducted at Doncasters Sterling as part of initial assessment and benchmarking of existing compressor impeller machining operations and production tooling trials together with the establishment of machine tool and process capability levels. This was followed by laboratory based experiments performed at the University of Birmingham in order to investigate the influence and performance of advanced diamond-like carbon (DLC) coatings and polycrystalline diamond (PCD) tooling when drilling (Phase 3A and 4A) and reaming (Phase 3B and 4B) aluminium alloys, see details below.

Phase 1: Assessment and capability study of current aluminium compressor impeller machining processes (industry based work).

Phase 2: Production tooling trials and comparative work of Doncasters Sterling standard tools against alternative cutting tool materials (industry based work).

Phase 3A: Evaluation of diamond-like carbon coated tools when drilling cast C355 alloy (laboratory based work).

Phase 3B: Evaluation of diamond-like carbon coated tools when reaming 6082-T6 aluminium alloy (laboratory based work).

Phase 4A: Evaluation of diamond tools when drilling cast C355 alloy (laboratory based work).

Phase 4B: Evaluation of diamond tools when reaming cast C355 alloy (laboratory based work).

4.1 Workpiece materials

4.1.1 Industry based work

4.1.1.1 Aluminium compressor impellers for Phase 1 and Phase 2 trials

Tests in Phase 1 and 2 were carried out on production compressor impellers, see examples in Figure 48, made of C355 aluminium alloy, LM16 equivalent/BS 1490:1988 [74], which were cast and heat treated by Sterling. The material has a typical nominal chemical composition (weight percent, wt%) of 1.2Cu, 0.5Mg, 0.1Mn and 5Si (remainder Al). Table

18 [1] lists the physical and mechanical properties of the cast C355 alloy used at Doncasters Sterling while Table 19 [1] details the stages of material heat treatment as well as corresponding temperatures and duration.

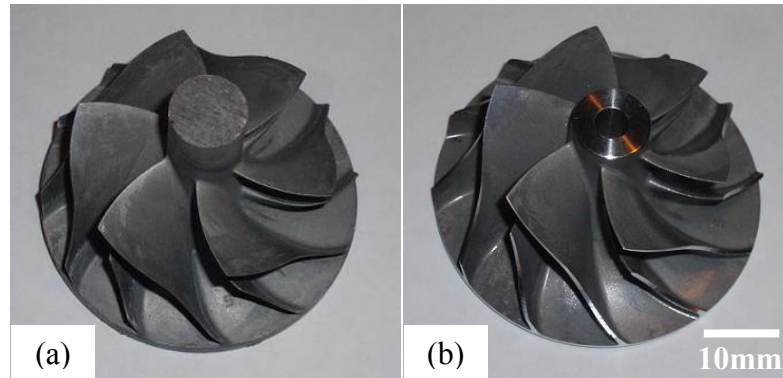


Figure 48: C355 aluminium compressor impellers in (a) cast and (b) machined condition for Phase 1 and 2 trials

Table 18: Mechanical and physical properties of cast C355 Al alloy [1]

Property	Value
Density (g/cm^3)	2.71
Hardness (HV)/(HK)	140/154
Ultimate tensile strength (MPa)	366
Yield strength (MPa)	271
Modulus of elasticity (MPa)	67.6×10^3
Shear modulus (MPa)	26.2×10^3
Thermal conductivity (W/mK)	151
Coefficient of thermal expansion ($\mu\text{m/mK}$)	22.4

Table 19: Heat treatment times and temperatures for C355 material used at Doncasters Sterling [1]

Stage	Time (min)	Temperature ($^{\circ}\text{C}$)
1. Solution heat treatment	1 st 30	500
	2 nd 480	530
2. Quenching in hot water (followed by air cool)	2 (45)	40 (20)
3. Artificial ageing/hardening	480	160

4.1.2 Laboratory based work

4.1.2.1 Aluminium blocks for Phase 3A tests

Workpiece material in the form of flat, rectangular blocks were required for the laboratory based experiments in order to suit the machine tool/test setup and work holding arrangements. The workpiece material was made from C355 Al alloy having the same

chemical composition as the compressor impellers used in Phase 1 and 2. A total of 12 Al blocks were cast, heat treated at Sterling and machined to size for wear (260mm x 115mm x 32mm) and cutting force (260mm x 20mm x 32mm) trials at the University of Birmingham. Figure 49 (a) and Figure 49 (b) show examples of the cast and machined workpiece samples. Individual plaster moulds were fabricated for each block of Al cast, which were adapted from the mould pattern used for casting impeller components at Sterling. Figure 50 shows the adapted mould employed. Destructive testing of the cast workpieces (over a small area) was conducted to verify conformance of the material properties. The average data over the entire batch is shown in Table 20 [1], which was found to be within acceptable tolerances.

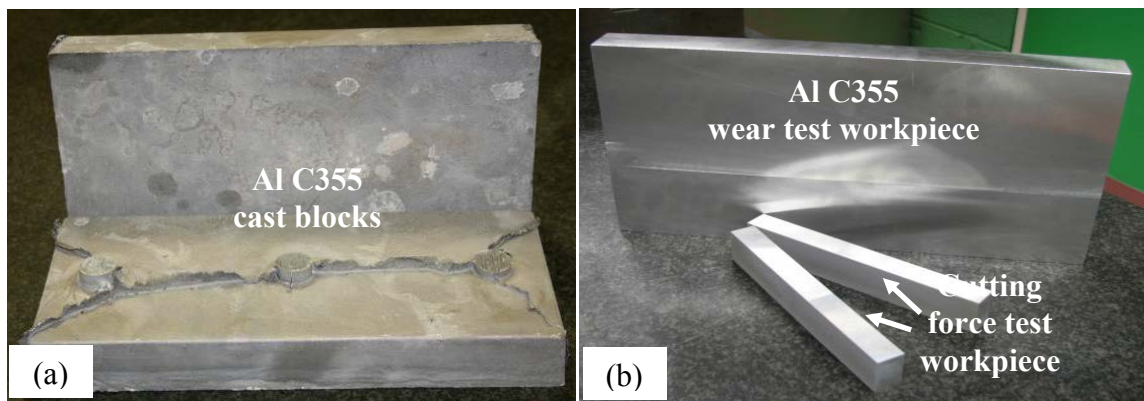


Figure 49: Al workpiece blocks in (a) cast and (b) cast/machined form for Phase 3A tests

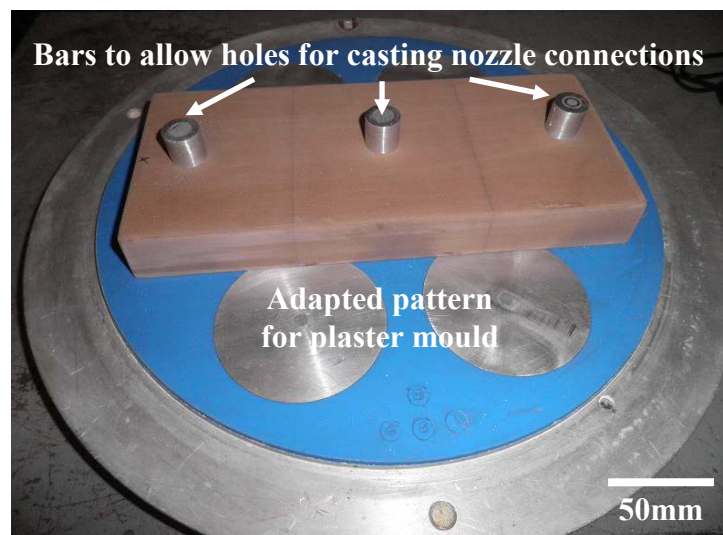


Figure 50: Adapted mould for casting workpiece blocks

Table 20: Average mechanical properties of the cast C355 Al alloy made using the adapted plaster mould [1]

Property	Value
Hardness (HV)/(HK)	140/154
Ultimate tensile strength (MPa)	335.9
Proof stress (MPa, 0.2%)	248.6
Modulus of elasticity (MPa)	71.67×10^3
Elongation to failure (%)	5.78

4.1.2.2 Aluminium blocks for Phase 3B experiments

Phase 3B trials, involving the evaluation of diamond-like carbon coatings for reaming, were conducted on commercial aluminium 6082-T6 alloy (BS EN 573) [5] instead of C355 Al alloy. This was because the latter material was not available for the planned trials and in order for the work to meet the scheduled availability for the machine tool, technical assistance, laboratory equipment, etc., a suitable substitute alloy (commercially available with close matching chemical composition to that of the cast C355 alloy) had to be selected. The material was supplied by Smiths Metal Centres Ltd. (UK) in the form of extruded bar, which was then machined into several rectangular pieces with dimensions of 255x130x33mm and 20x130x33mm for wear and cutting force experiments respectively, see Figure 51. Table 21 [1] details the average measured mechanical properties of the 6082-T6 alloy.

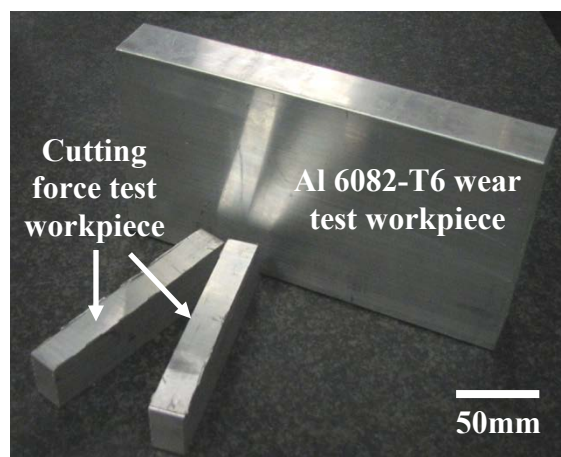


Figure 51: Machined aluminium 6082-T6 test pieces

Table 21: Mechanical properties of commercial aluminium 6082-T6 alloy [1]

Property	Value
Hardness (HV)/(HK)	114/126
Ultimate tensile strength (MPa)	342.3
Proof stress (MPa, 0.2%)	320.6
Modulus of elasticity (MPa)	79.68×10^3
Elongation to failure (%)	10.22

4.1.2.3 Aluminium blocks for Phase 4 tests

Workpiece material for this phase of tests was again C355 Al alloy, which was formed into a number of rectangular blocks by casting in a permanent grey cast iron die, supplied by K.B Elsmore & Sons Ltd., due to the relatively slow oven drying procedure and workpiece cracking problems experienced when using the plaster moulds in Phase 3A. Figure 52 shows the permanent cast iron die, corresponding assembly and an example of the cast aluminium workpieces following machining. The sides of the die were fitted with thermocouples connected to a digital data logger unit to monitor and maintain the die temperature (constant at 80°C) during the casting process for optimum solidification of the aluminium blocks. Each of the blocks produced was then heat treated accordingly to the procedures used for the impellers at Sterling as detailed previously in Table 19. The cast aluminium blocks were subsequently face-milled and machined to size for wear and cutting force tests at the University of Birmingham. Table 22 [1] includes average mechanical properties of the cast workpieces.

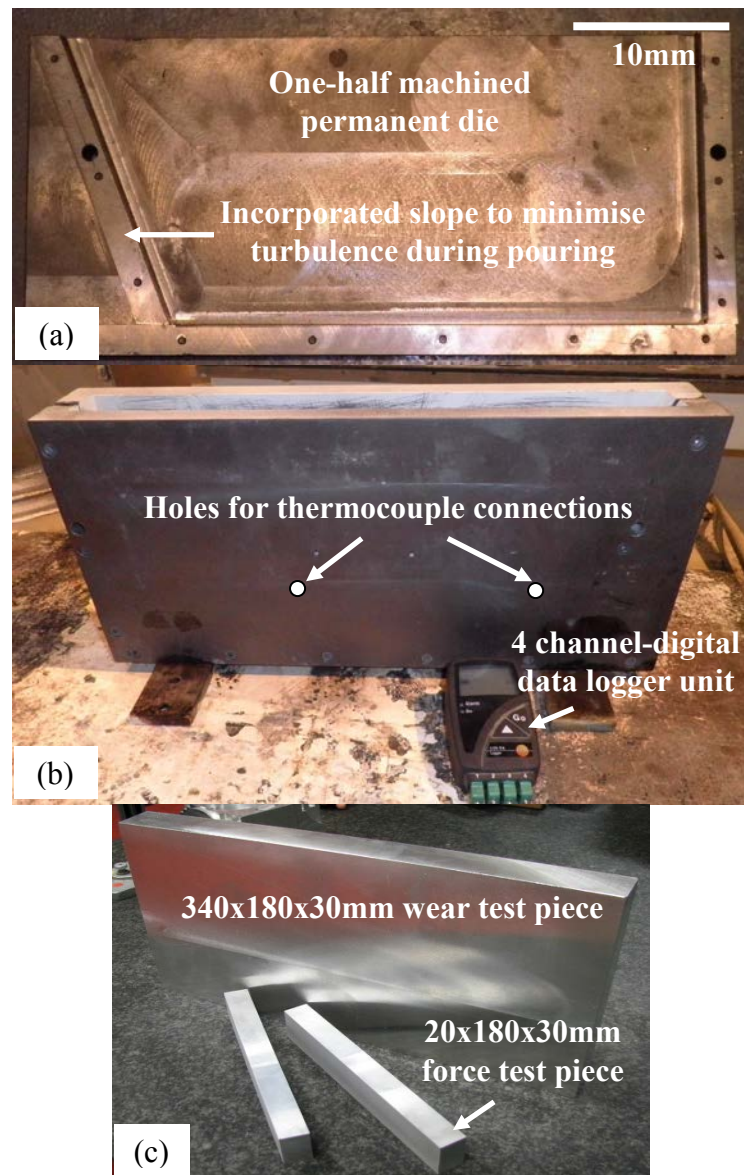


Figure 52: Phase 4 workpiece preparation for (a) permanent cast iron die, (b) die assembly and (c) cast/machined aluminium blocks

Table 22: Mechanical properties of the C355 alloy produced using the cast iron permanent die [1]

Property	Value
Hardness (HV)/(HK)	140/154
Ultimate tensile strength (MPa)	346.3
Proof stress (MPa, 0.2%)	271.7
Modulus of elasticity (MPa)	65.31×10^3
Elongation to failure (%)	6.5

4.2 Tool geometries, materials and coatings

Conventional uncoated K10 fine grained tungsten carbide (10%Co) twist drills (operation 3) sourced from Walter Titex (A1167B) and uncoated K10 tungsten carbide ($\varnothing 5.09\text{mm}$) Beck RV3188 reamers (operation 4) supplied by Mapal (UK), were used for hole machining operations in Phase 1 and 2 as well as a benchmark in Phase 3 and 4. The drill was 3-fluted with a diameter of 4.8mm, see Figure 53. The point and helix angles were 150° and 15° respectively, with a flute length of 35mm, see schematic in Figure 54. The tool material had a room temperature hardness of 1550HV [219] and a maximum operating temperature/oxidation limit of 600°C [73]. The recommended maximum cutting speed and feed rate when wet drilling Al alloys with $<10\%\text{Si}$ was 150m/min and 0.12mm/rev [219] respectively for a typical $\varnothing 4.8\text{mm}$ tool. The reamers, shown in Figure 55, had 6 straight flutes with a chamfer dimension of $0.5 \times 45^\circ$ and through-hole feature for internal cutting fluid supply. Figure 56 shows a schematic of the Beck reamer and associated details of geometry. The typical recommended maximum values of cutting speed and feed rate for reaming Al with $<10\%\text{Si}$ in a wet environment were 16m/min and 0.2mm/rev [219] respectively for a $\varnothing 5.09\text{mm}$ tool. A summary of the hole machining tools is detailed in Table 23. The drills and reamers were also employed as the substrate for the deposition of DLC and CVD diamond coatings, which were evaluated in Phase 3 and 4 trials.

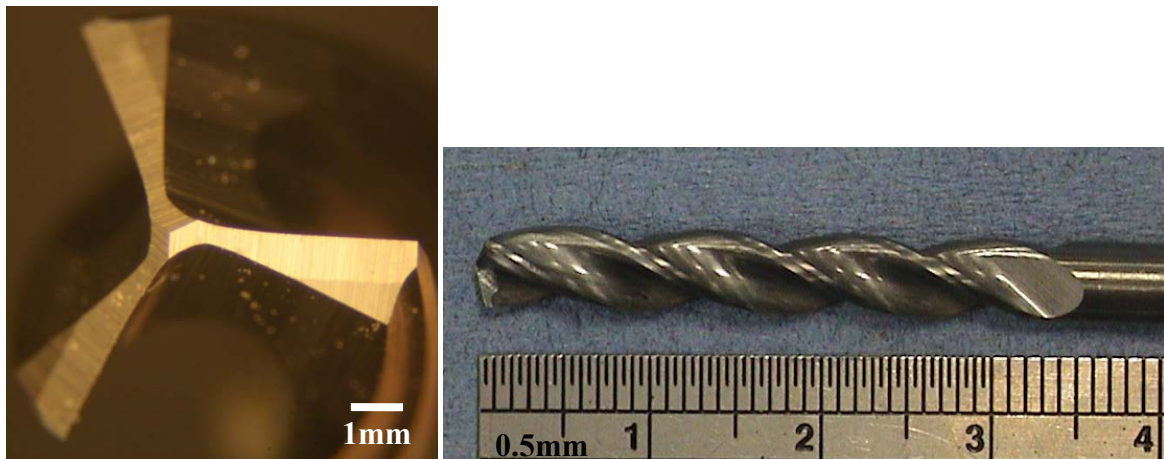


Figure 53: Walter Titex A1167B uncoated carbide twist drill

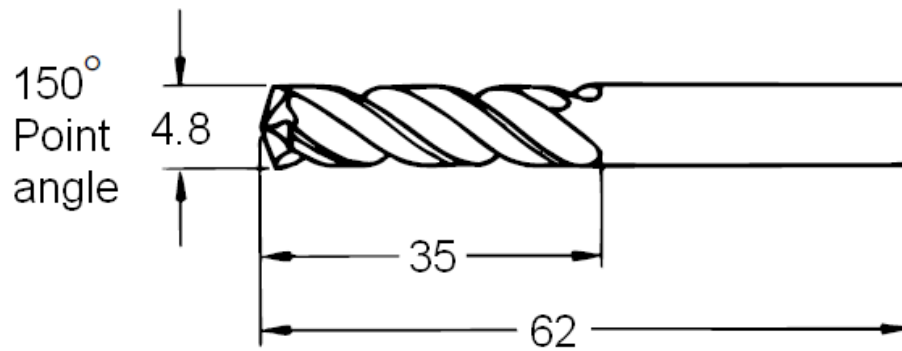


Figure 54: Walter Titex A1167B cemented tungsten carbide drill geometry details, dimensions are in mm [219]

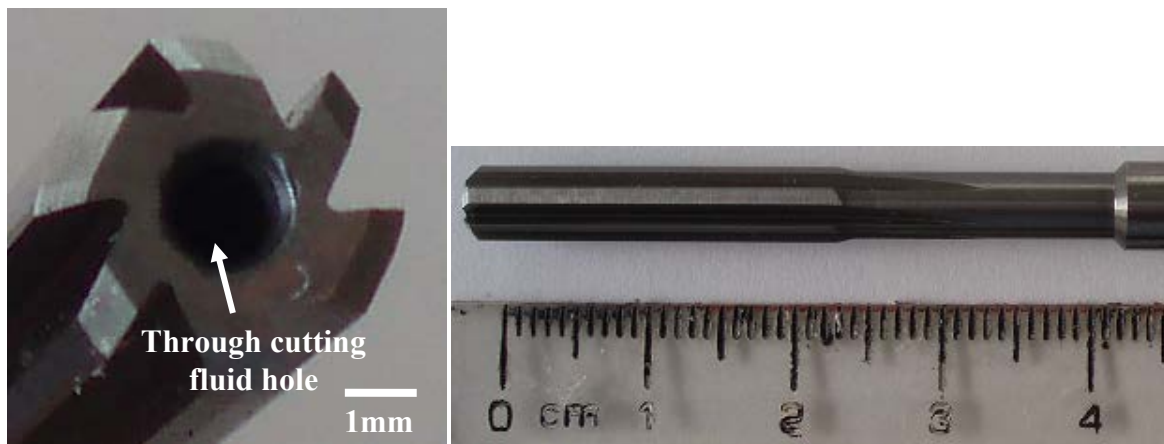


Figure 55: Mapal Beck RV3188 cemented tungsten carbide reamer

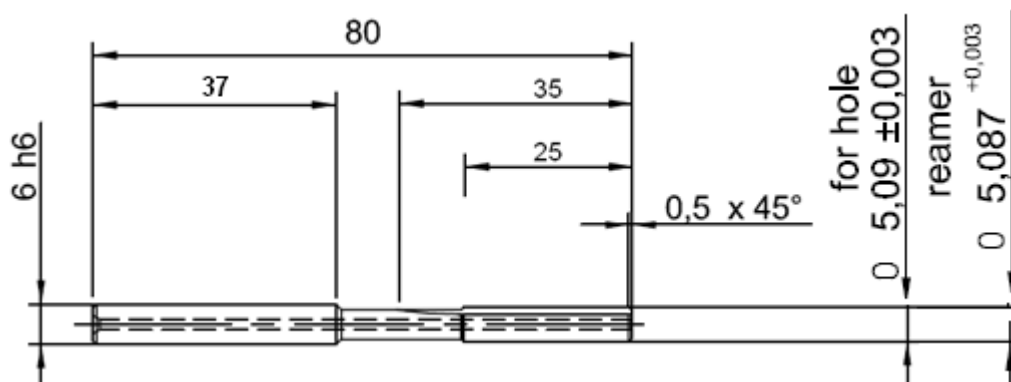


Figure 56: Mapal Beck RV3188 uncoated carbide reamer geometry details, dimensions are in mm [220]

Table 23: Tool details for hole machining operations [219, 220]

Tool	Supplier	Material	Dia.	No. flute	Helix angle	Point angle	Chamfer	Cost (inc. VAT)
Drill A1167B	Walter Titex	WC K10 10%Co	4.8mm	3, twist	15°	150°	N/A	£16
Reamer RV3188	Mapal Beck	WC K10 10%Co	5.09mm	6, straight	0°	N/A	0.5x45°	£49

4.2.1 Industry based work

4.2.1.1 Phase 1: Assessment and capability study of current compressor impeller machining processes

The work was principally carried out to establish baseline performance of the existing machining processes. All of the cutting tools involved in this assessment were commercial products employed for the production of aluminium compressor impellers at Sterling when the project commenced. The assessment and capability study of the reaming operation (operation 4) involved the use of uncoated carbide drills and reamers detailed previously in Table 23. For turning/facing operations, indexable K10 tungsten carbide coated with titanium diboride (TiB_2) CCGT09T308HP KC5410 inserts supplied by Kennametal were used for roughing (operation 1) while polycrystalline diamond tipped inserts (DCGT11T304) from Exactaform were utilised for finishing (operation 5), see Figure 57. Further details of the tooling used in Phase 1 are shown in Table 24 [221, 222].

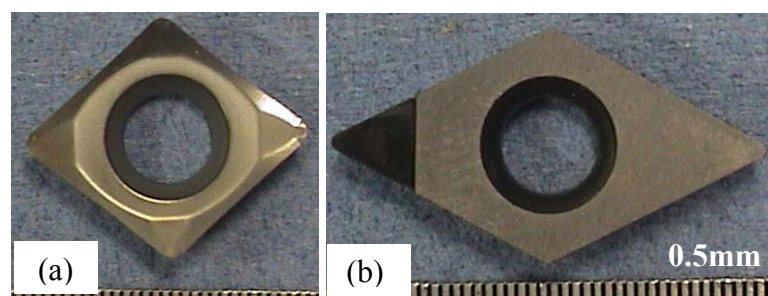


Figure 57: Turning inserts (a) Kennametal CCGT09T308HP KC5410 TiB_2 coated carbide for roughing and (b) Exactaform DCGT11T304 PCD for finishing

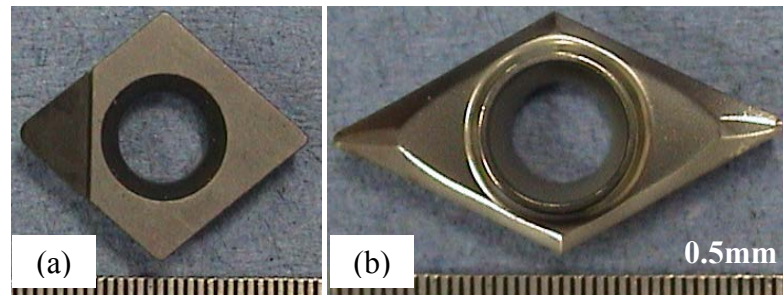


Figure 58: Turning inserts (a) Exactaform CCGT09T308 and (b) Kennametal DCGT11T304HP KC5410 TiB₂ coated carbide

Table 24: Tool details of roughing and finishing indexable inserts used in Phase 1 [221, 222]

Tool	Supplier	Material	Rake angle	Relief angle	Nose radius	Cost per edge (inc. VAT)
Roughing insert CCGT09T308HP KC5410	Kennametal	WC K10 +TiB ₂	15°	7°	0.8mm	£2.31
Finishing insert DCGT11T304	Exactaform	PCD 002	12°	7°	0.4mm	£20.70
Roughing insert CCGT09T308	Exactaform	PCD 010	12°	7°	0.8mm	£23.00
Finishing insert DCGT11T304HP KC5410	Kennametal	WC K10 +TiB ₂	15°	7°	0.4mm	£3.02

4.2.1.2 Phase 2: Production tooling trials and comparative work of Sterling standard tools against alternative cutting tool materials

This work was carried out to establish the feasibility and operational cost of alternative cutting tool materials against the standard carbide tools utilised at Doncasters Sterling, as part of the research programme. Kennametal CCGT09T308HP KC5410 TiB₂ coated carbide and Exactaform CCGT09T308 PCD roughing inserts, see details in Phase 1, were utilised in the production tooling trials for the rough turning/facing (operation 1) operation. Two alternative PCD tipped inserts were also assessed, which were fabricated by Mapal Ltd. (UK) using Syndite CTB010 blanks (10µm average grain size) supplied by Element Six Ltd. (E6, Ireland). The roughing tool designated CCGW09T308F01N 0AA had a plain rake face (0°) while the CCGT09T308F01N C2A insert incorporated a chip breaker feature to prevent swarf entrapment, see Figure 59. Both inserts had equivalent relief angle of 7° and a corresponding nose radius of 0.8mm. Table 25 [121, 220] provides details of the PCD roughing tools. Blind holes (Ø4.8mm) were produced using the Titex A1167B 3-fluted carbide drill (detailed in Table 23) and an alternative Guhring 611 titanium nitride (TiN, 2400HV) [223] coated (see

Figure 60) twist drill. The drilled holes were subsequently machined to size ($\varnothing 5.09\text{mm}$) using a standard uncoated carbide Beck RV3188 reamer (detailed in Table 23) and an alternative reaming tool with fine grained PCD cutting edges (Syndite CTB002, $2\mu\text{m}$ grain size) brazed onto a K10 WC substrate, see Figure 61. The PCD tool was manufactured by Mapal with through-tool coolant holes. Figure 62 [220] details the geometry and associated tolerances of the reamer (all dimensions are in millimetres), while Table 26 [121, 220, 223] provides details of the alternative tools used for hole machining operations.

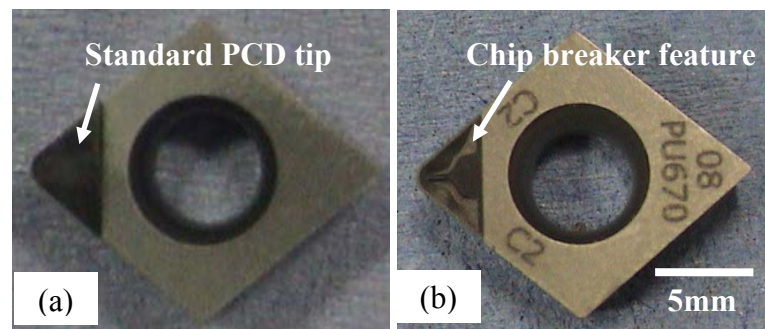


Figure 59: PCD roughing inserts (a) standard Mapal CCGW09T308 F01N 0AA and (b) Mapal with chip breaker geometry CCGT09T308F01N C2A

Table 25: Tool details for Mapal PCD roughing inserts used in Phase 2 [121, 220]

Tool	Supplier	Material	Rake angle	Relief angle	Nose radius	Cost per edge (inc. VAT)
Roughing insert CCGW09T308F01N 0AA	Mapal	Syndite CTB010 PCD, $10\mu\text{m}$ average grain standard feature	0°	7°	0.8mm	£36.14
Roughing insert CCGT09T308F01N C2A	Mapal	Syndite CTB010 PCD, $10\mu\text{m}$ average grain with chip breaker feature	0°	7°	0.8mm	£40.91

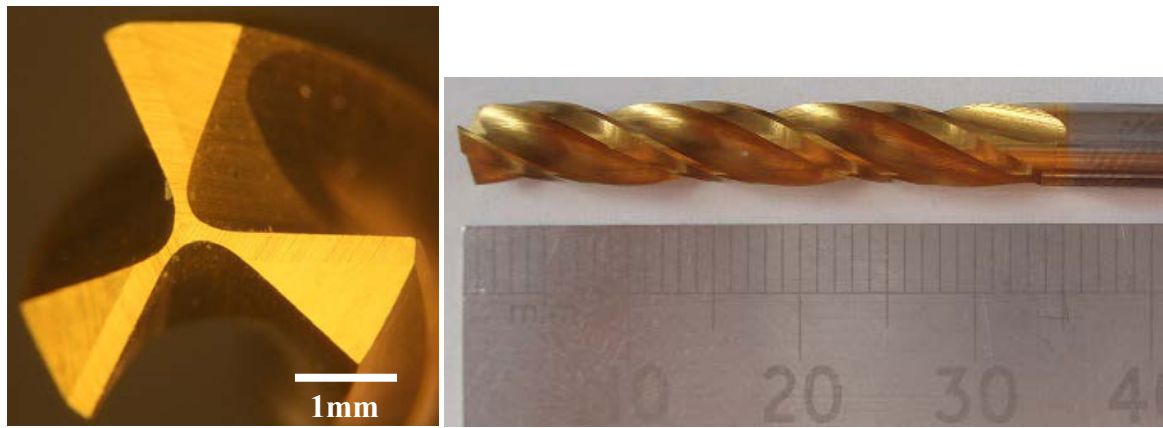


Figure 60: Guhring 611 TiN coated carbide drill



Figure 61: Mapal brazed Syndite CTB002 PCD reamer

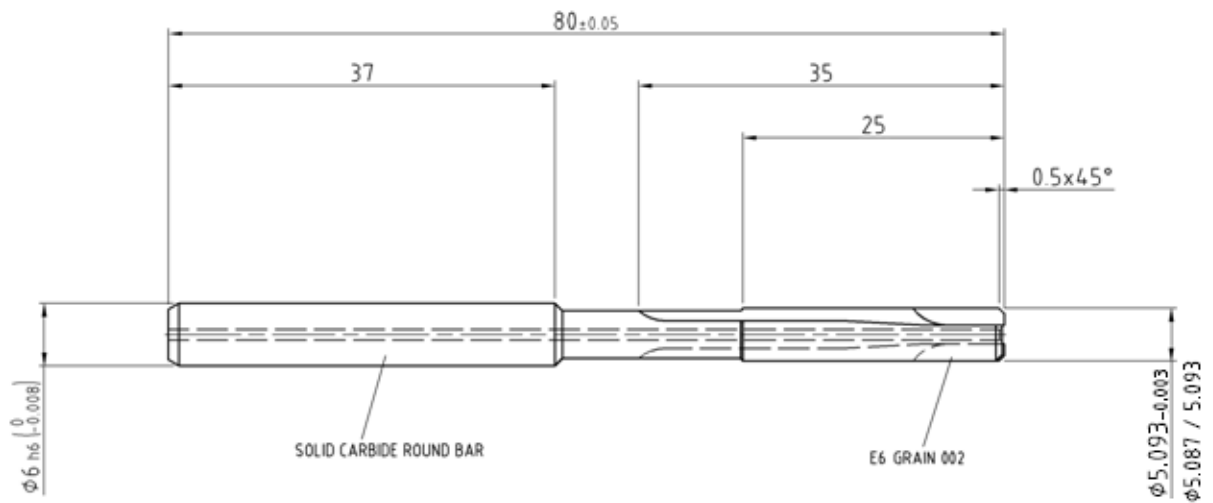


Figure 62: Mapal brazed PCD CTB002 reamer geometry details [220]

Table 26: Details for alternative tools used for drilling and reaming operations in Phase 2 [121, 220, 223]

Hole machining tool	Material	No. of flute	Diameter	Rake angle	Point angle	Chamfer	Cost per edge (inc. VAT)
Guhring 611 drill	WC+TiN	3, twist	4.8mm	28°	150°	N/A	£24
Mapal CTB002 reamer	Syndite CTB002 PCD, 2µm average grain	2, straight	5.09mm	N/A	N/A	0.5x45°	£356.93

4.2.2 Laboratory based work

4.2.2.1 Phase 3: Evaluation of diamond-like carbon coated tools when drilling and reaming aluminium alloys

The performance of two commercial, low friction, diamond-like carbon based coatings (developed by Teer Coatings Ltd.) were evaluated against conventional uncoated carbide for the drilling and reaming of C355 aluminium alloy. The coatings [224], Graphit-iC™ (non-hydrogenated amorphous) and Dymon-iC™ (hydrogenated amorphous), were applied by physical vapour deposition (PVD) onto Walter Titex A1167B drills and Beck RV3188 reamers. Details of the substrates were previously described in Section 4.2. Examples of the drills and reamers used are shown in Figure 63 and Figure 64 respectively, while Table 27 [73, 224] provides details of physical properties and costs of the tools/coatings.

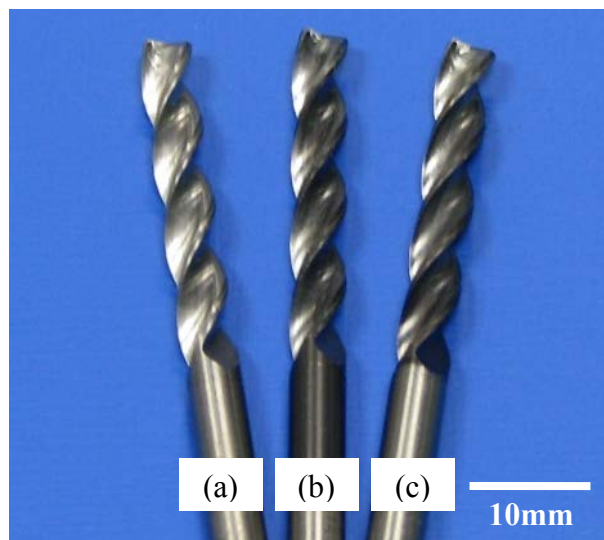


Figure 63: Tools used in Phase 3A (a) uncoated WC, (b) Graphit-iC™ and (c) Dymon-iC™

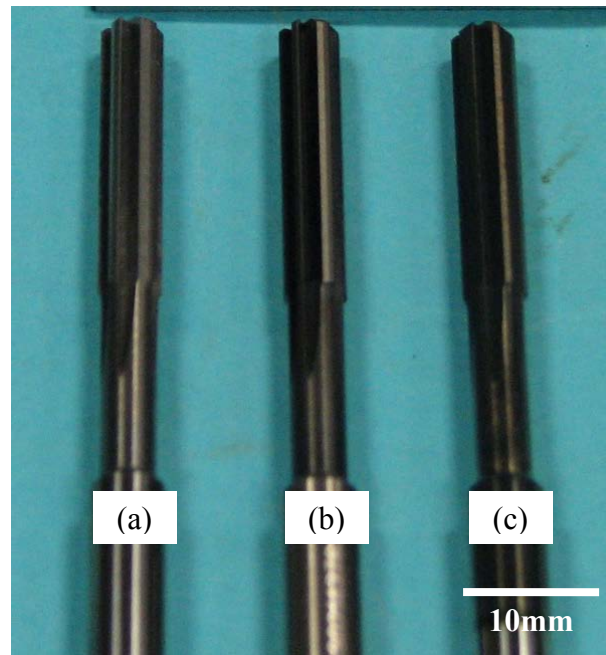


Figure 64: Tools used in Phase 3B (a) uncoated WC, (b) Dymon-iC™ and (c) Graphit-iC™

Table 27: Details of tools and coatings used in Phase 3 [73, 224]

Tool	Supplier	Hardness @ room temp. (HV)	μ	Max. operating/ oxidation temp.	Cost per tool (inc. VAT)
Uncoated WC drill	Walter Titex	1550	0.2	600°C	£16
Uncoated WC reamer	Mapal Beck	1550	0.2	600°C	£49
WC, 2 μ m thick, Dymon-iC™	Teer Coatings	1500	0.03-0.1	450°C	£32.13
WC, 2 μ m thick, Graphit-iC™	Teer Coatings	1800	0.05-0.09	500°C	£32.13

4.2.2.2 Phase 4: Evaluation of diamond coated and PCD tools when drilling and reaming cast C355 aluminium alloy

The final phase of experimental work involved assessing the performance of CVD diamond coatings and polycrystalline diamond tool materials when drilling and reaming C355 Al alloy in comparison to standard uncoated WC products. An ~8 μ m thick multi-layer commercial CVD diamond coating (CCDiaFiberSpeed) was deposited onto Walter Titex A1167B drills while an alternative ~3 μ m CVD diamond coating (MultiSpeed04) was applied on Beck RV3188 reamers. Two different grades of PCD involving a medium grained CTB010 (~10 μ m average grain size) and a mixed modal CTM302 (30 μ m and 2 μ m grains) were brazed

onto solid carbide substrate drills. These were straight-fluted (0° helix) with an overall tool length of 80mm and corresponding cutting length of 40mm. Examples of the uncoated carbide, CVD diamond coated carbide and brazed PCD drills are shown in Figure 65 while Figure 66 and Figure 67 [220] detail the design and geometry of the PCD cutter. Table 28 [73, 121, 225] summarises details of the coated drills used in Phase 4. As for tests with the brazed PCD reamers, a fine grained CTB002 ($2\mu\text{m}$ grain size) was evaluated together with the mixed modal CTM302. Figure 68 shows the various reamers utilised while a schematic of the PCD reamer design is detailed in Figure 69 [220]. Table 29 [73, 121, 225] details the coated reamers used in Phase 4. All of the PCD tooling employed was fabricated by Mapal with the diamond blanks supplied by Element 6.



Figure 65: Uncoated, CVD diamond coated carbide and PCD drills

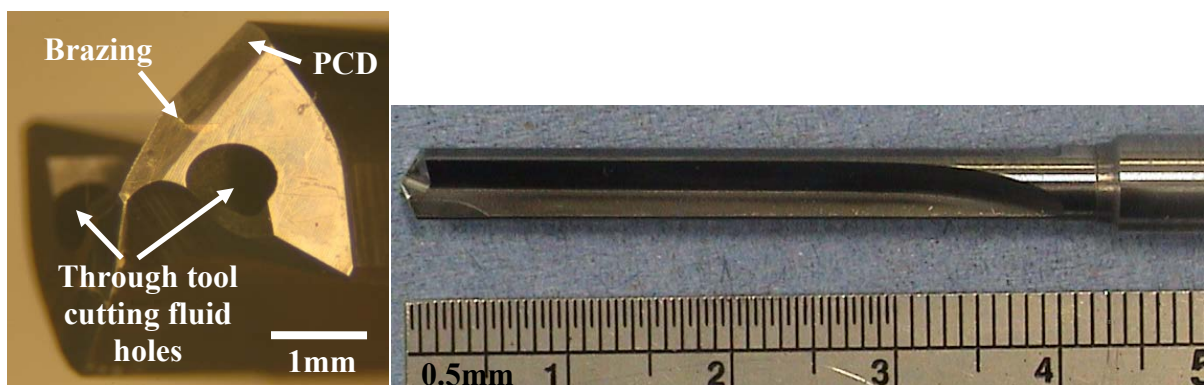


Figure 66: Brazed Syndite CTB010 PCD drill

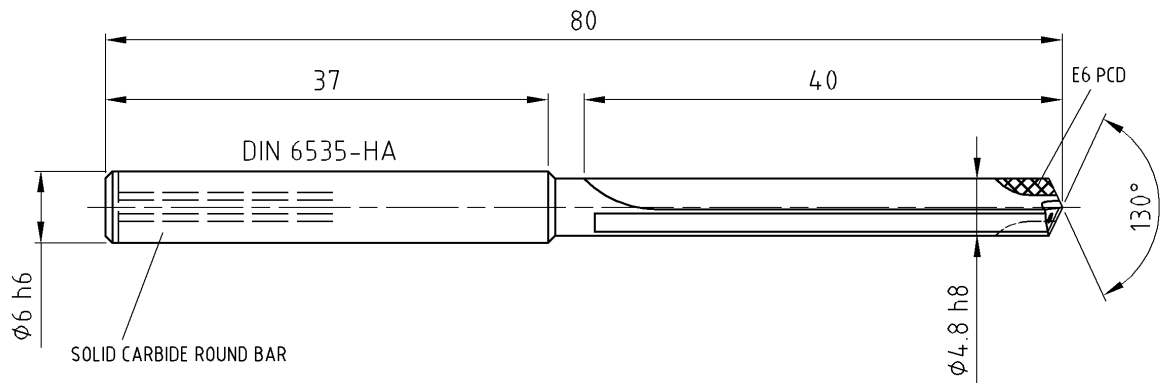


Figure 67: Geometry details of brazed PCD drill [220]

Table 28: Details of drills used in Phase 4 [73, 121, 225]

Tool	Supplier	Material	Hardness @ room temp.	μ	Max. operating/ oxidation temp.	COE (K ⁻¹)	Cost per tool (inc. VAT)
A1167B	Walter Titex	WC K10	1550HV	0.2	600°C	5	£49
CVD CCDiaFiberSpeed	CemeCon AG	CVD diamond	Up to 10,000HV	0.1	700°C	1.1 $\times 10^{-6}$	£76
CTB010	Mapal Beck	PCD	-	-	700°C	-	£212
CTM302	Mapal Beck	PCD	-	-	700°C	-	£371



Figure 68: Uncoated, CVD diamond coated carbide and brazed PCD reamers

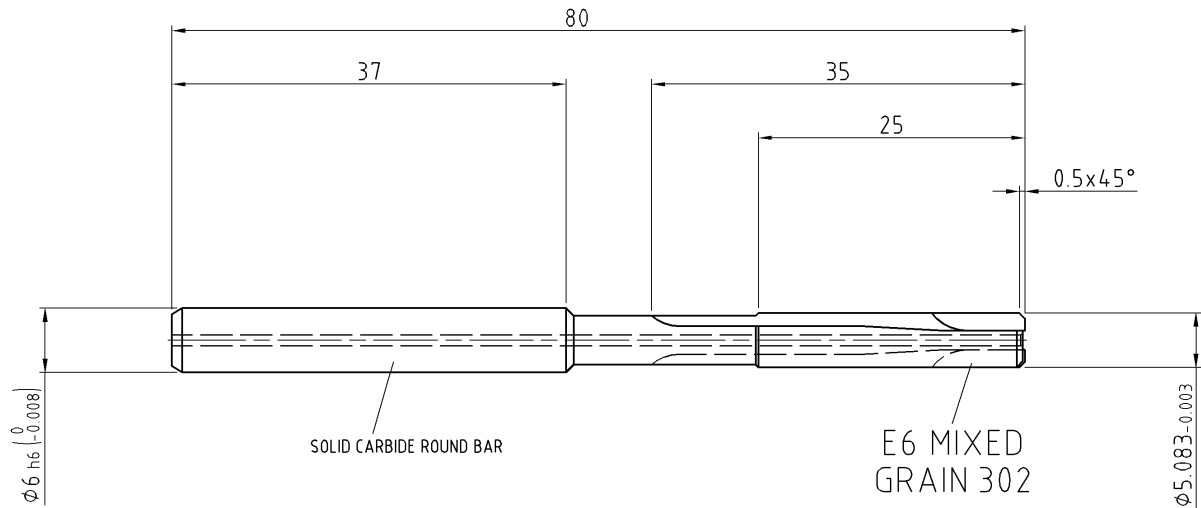


Figure 69: Geometry details of brazed PCD reamer [220]

Table 29: Details of reamers used in Phase 4 [73, 121, 225]

Tool	Supplier	Material	Hardness @ room temp.	μ	Max. operating/ oxidation temp.	COE (K ⁻¹)	Cost per tool (inc. VAT)
RV3188	Mapal Beck	WC K10	1550HV	0.2	600°C	5	£49
MultiSpeed04	CemeCon AG	CVD diamond	Up to 10,000HV	0.1	Up to 700°C	1.1 $\times 10^{-6}$	£66
CTB002 PCD	Mapal Beck	PCD	-	-	Up to 700°C	-	£371
CTM302 PCD	Mapal Beck	PCD	-	-	Up to 700°C	-	£355

4.3 Equipment

4.3.1 Machine tools and fixtures

Preliminary experimental work and production tooling trials in Phase 1 and 2 were carried out on an Index G200 horizontal CNC twin-spindle lathe at Doncasters Sterling, each with a variable speed of 6000rev/min and a total power rating of 40kW (20kW per spindle). See Section 2.3 in Chapter 2 for further details of the Index G200 CNC lathe and layout. The work holding unit and related fixtures were identical to those employed for production work. A collet was used in conjunction with a multi-pin unit, see Figure 70, for holding the impellers. Further details of fixtures which were used during the industry based testing were included previously in Chapter 2. Testing in Phase 3 and 4 (laboratory based experiments)

were conducted on a Matsuura FX-5 high speed CNC vertical machining centre fitted with a Renishaw probe and tool setter based at the University of Birmingham. The machine tool was capable of variable rotational spindle speeds up to 20,000rev/min rated at 15kW together with a maximum corresponding feed rate of 15m/min. Figure 71 shows the Matsuura FX5 unit located in the Machining Research Group laboratory.



Figure 70: Workpiece and work holding unit used in Sterling



Figure 71: Matsuura FX-5 high speed machining centre

4.3.2 Cutting fluid application

All tests in Phase 1 and 2 were carried out wet using Braemar Aquacare G-60 water/oil emulsion with 15-17% mineral oil concentration at a fluid pressure of ~3bar (12l/min) in accordance with standards/procedures in place at Sterling. Similarly, work in Phase 3 and 4 was undertaken in a wet environment but with Houghton Hocut 3380 water based emulsion containing 7-10% volume solution mineral oil. Here the concentration of the

cutting fluid was monitored regularly using a refractometer. For drilling experiments in Phase 3A and 4A, the influence of flood (3bar) and high pressure (70bar) cutting fluid application was investigated. This was supplied externally via suitable pipes/nozzles at flow rates of 25 and 24l/min respectively. High pressure cutting fluid was delivered using a high pressure pump unit supplied by Pumps & Equipment Warwick Ltd. Figure 72 shows the fluid delivery setup on the FX-5. In contrast, the reaming work in Phase 3B and 4B involved through-tool high pressure cutting fluid also at 70bar delivered via a retrofit Bristol-Erikson spindle, incorporating a BT40 tool holder, at a flow rate of 12l/min. Figure 73 shows the through-tool cutting fluid arrangement employed.

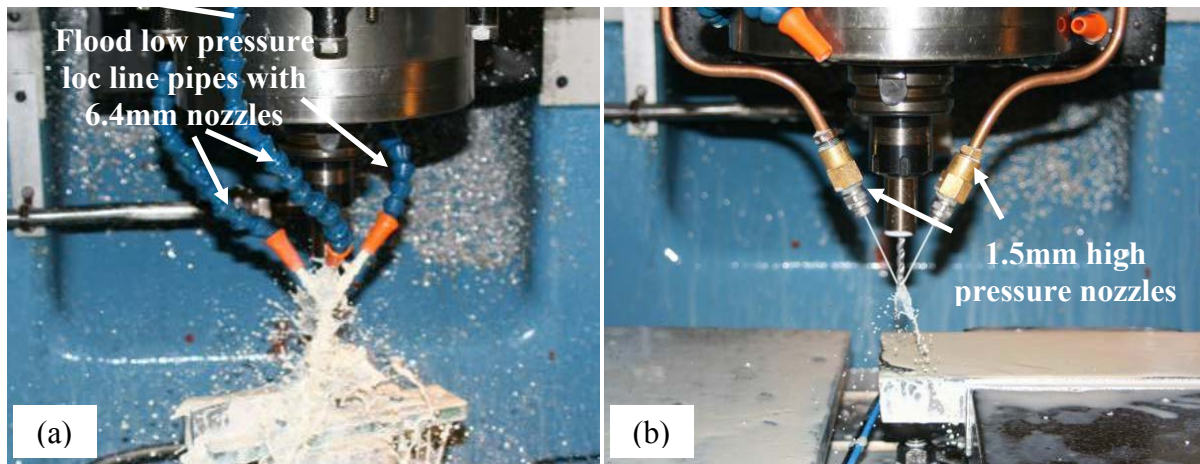


Figure 72: Cutting fluid arrangements on FX-5 (a) flood and (b) high pressure cutting fluid

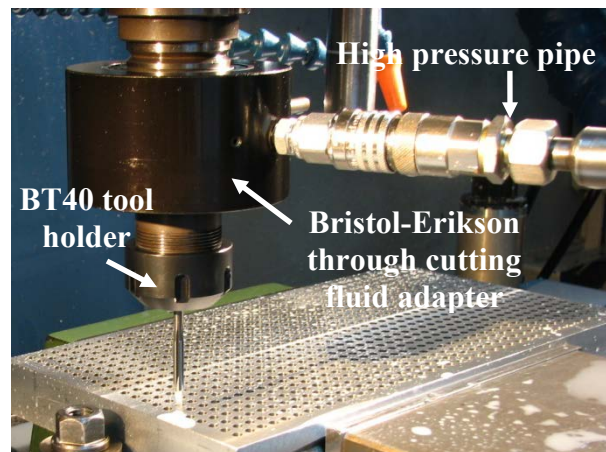


Figure 73: High pressure through-tool cutting fluid arrangement on FX-5 for Phase 3B and 4B

4.3.3 Tool wear evaluation

Tool flank wear was measured using a WILD M3Z microscope equipped with a X-Y digital micrometer platform (0.001mm resolution) connected directly to a Canon 400D DSLR digital camera for image capture of new/worn drills and reamers. A tilting table fitted with a bespoke fixture was employed to accommodate the through-tool cutting fluid spindle adapter

arrangement (to avoid removing tool from collet) as well as to compensate for varying tool cutting edge angles in order to maintain optimum image focus. Similarly, a machined block was used for holding the cutting inserts, see Figure 74.

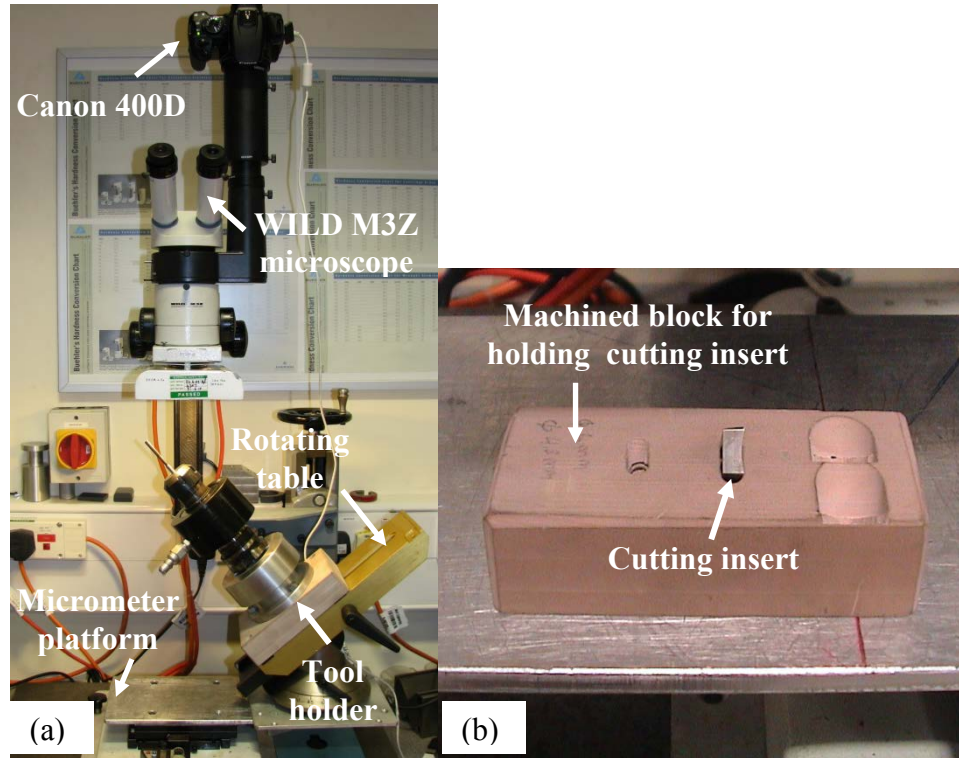


Figure 74: Typical tool flank wear measurement setup for (a) round cutting tools and (b) inserts

4.3.4 Force measurement

Cutting forces in Phase 2 involving comparative turning (Operation 1 and Operation 5) experiments were measured using a 3-component Kistler platform dynamometer (type 9257A), which was attached to modified Indexa Seiki tool holders. Conversely, thrust forces and torque during drilling (Operation 3) and reaming (Operation 4) in Phase 3 and 4 testing were carried out using a 4-component Kistler model 9273 drilling dynamometer, with maximum measurable loads of 5kN for F_x and F_y , 20kN in F_z and 200Nm for M_z (torque). Signals recorded from both dynamometers were processed through a bank of Kistler type 5011 charge amplifiers connected to a computer running Dynoware software. Figure 75 details the platform and drilling dynamometers together with their respective experimental arrangements. A weight (equivalent to 5N) was used for calibration of the dynamometers, see Figure 76 for an example of the calibration setup. Sampling rate used for the turning tests was 24000Hz, while the same for drilling and reaming trials were in a range of 8000-24000Hz and

1333-12000Hz respectively, depending on the corresponding rotational speeds and number of cutting edges. A ‘long’ time constant was chosen for the charge amplifiers for all tests.

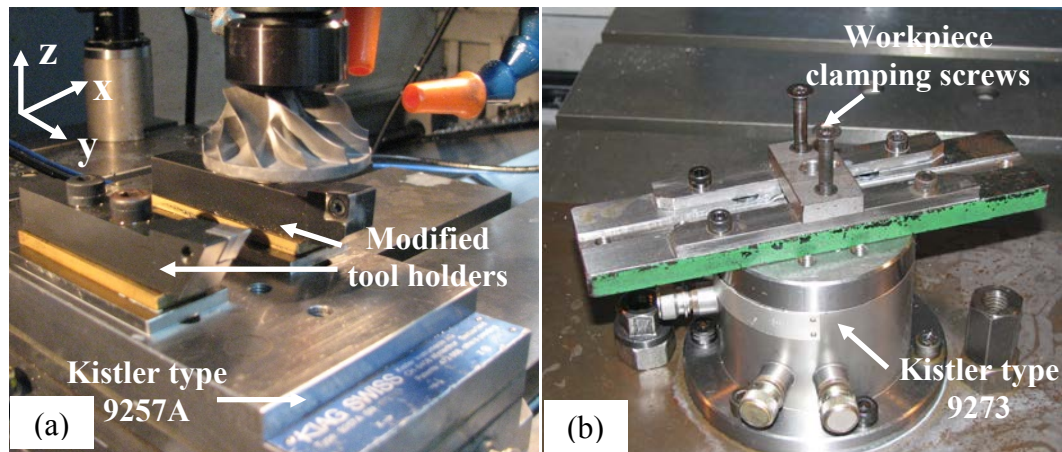


Figure 75: Force measurement setup and equipment (a) Kistler turning dynamometer and (b) Kistler drilling/reaming dynamometer



Figure 76: Typical force calibration on the dynamometer

4.3.5 Workpiece feature geometrical accuracy measurement

Workpiece quality assessment following Phase 1 and 2 trials was conducted at Doncasters Sterling. Hole diameter measurement was carried out using a Mahr Dimensionair air gauge (see Figure 77) with 0.0001mm resolution. The squareness of the component back and nose faces were evaluated using a MG test unit integrated with a Mitutoyo dial having 0.001mm divisions, see Figure 78 (a). Hole surface roughness measurement was performed on a Mitutoyo Surftest series SJ400 with a 2 μ m radius diamond tipped stylus, see Figure 78 (b). Conversely, the roughness of turned surfaces was evaluated using a Taylor Hobson Talysurf 120L, which is further described in the next section. Cylindricity was measured using a Taylor Hobson Talyrond series 131 equipped with a 1mm ruby ball stylus, see Figure 79 (a).

For Phase 3 and 4 experiments, the diameter of drilled and reamed holes was measured using a Diatest split ball probe (4.7-5.5mm range) fitted with a Mitutoyo ID-C112MB digital indicator having a resolution of 0.001mm, see Figure 79 (b). Geometrical parameters of the holes (roundness, cylindricity and parallelism) were assessed on a Taylor Hobson Talyrond series 300 system equipped with a 3mm ruby ball stylus, see Figure 80.

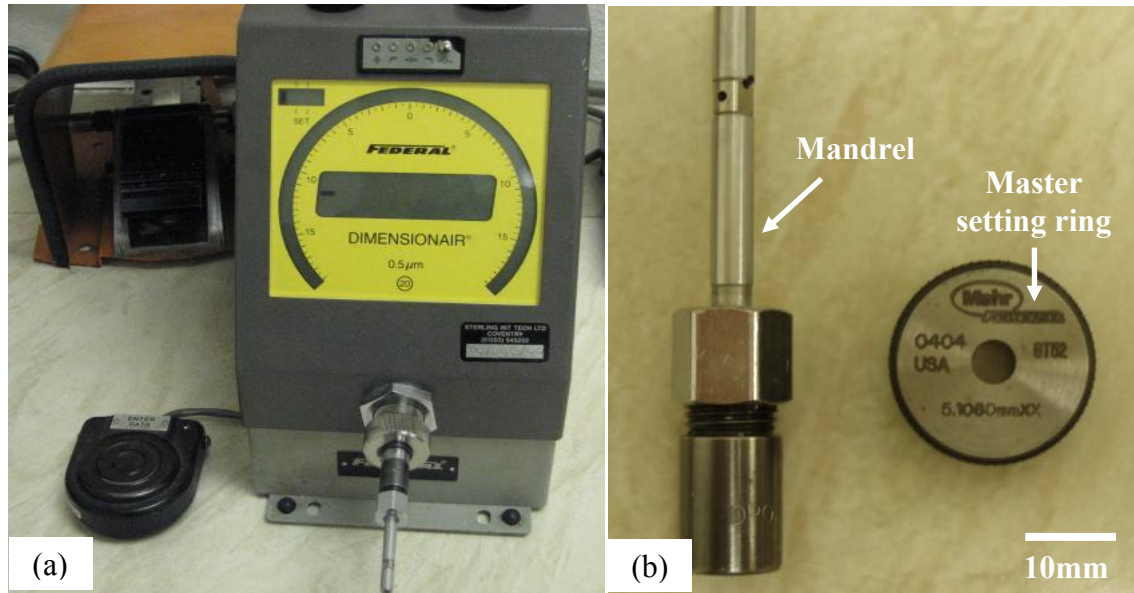


Figure 77: Hole diameter measurement equipment (a) Mahr air gauge unit and (b) mandrel with setting ring

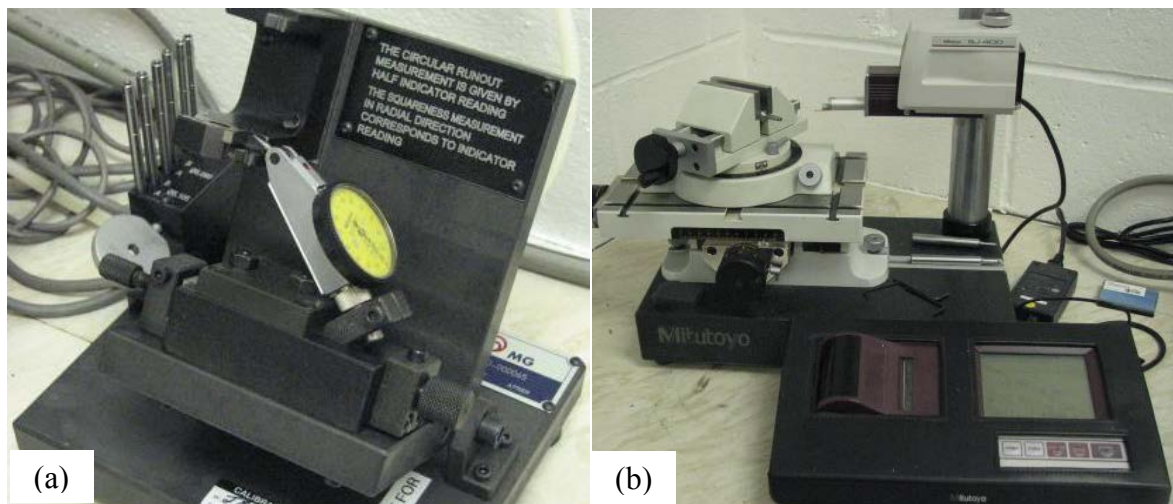


Figure 78: Images of (a) MG squareness test unit and (b) Mitutoyo Surftest series SJ400

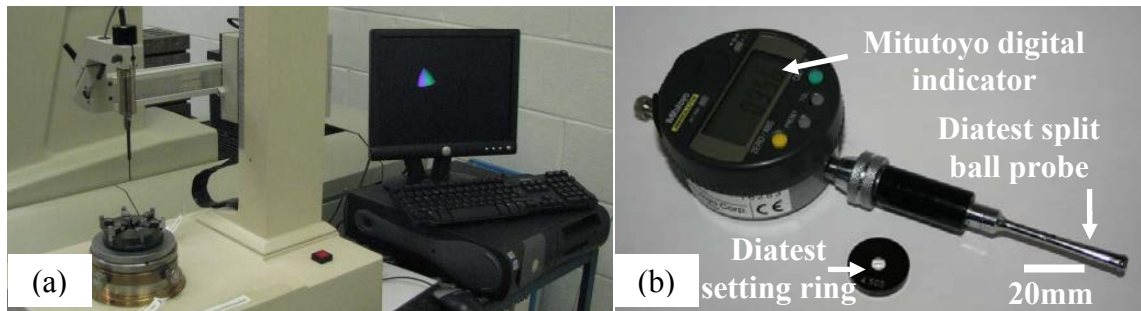


Figure 79: Images of (a) Taylor Hobson series 131 and (b) hole diameter measuring equipment

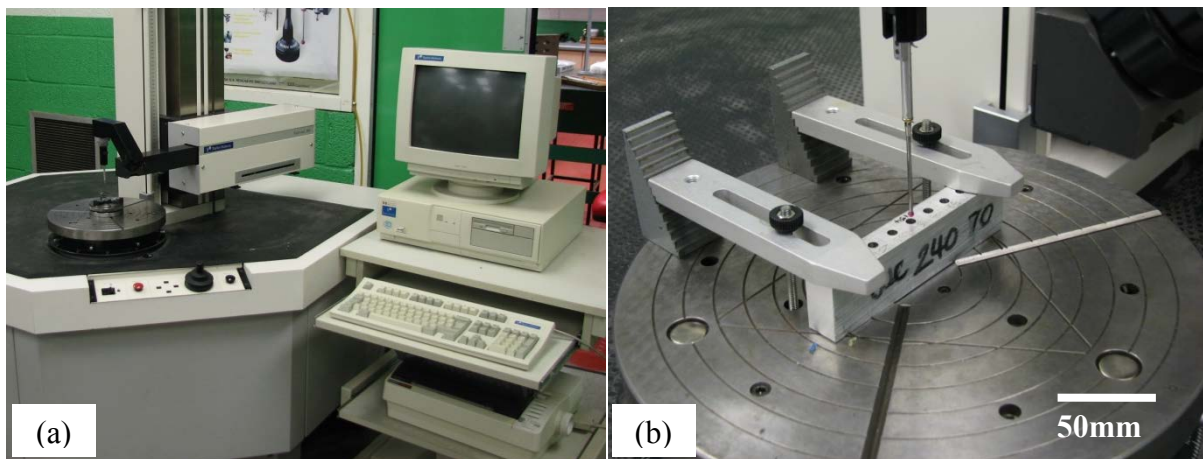


Figure 80: Illustration of (a) Taylor Hobson Talyrond series 300 and (b) hole assessment setup

4.3.6 Workpiece surface roughness and integrity assessment

Following geometrical analysis of the holes, specimens were sectioned approximately 500 μ m from the hole centerline using wire electrical discharge machining (WEDM). The internal hole surface roughness was measured on a Taylor Hobson Form Talysurf series 120L attached with a 2 μ m radius diamond tipped stylus, see Figure 81. The sectioned specimens were subsequently cold mounted in Epoxicure resin mixture to avoid any metallurgical changes prior to the microhardness tests and microstructural analysis. Figure 82 shows a mounted sample and schematic of hole sectioning arrangement. The mounted samples were then ground and polished according to Buehler's four-step procedure for aluminium alloys using a Buehler Alpha twin-speed grinding/polishing unit. The respective applied force and speed per specimen during grinding were 22N at 240rev/min and 27N at 120rev/min for fine polishing. The direction of the grinding/polishing discs in each step was complementary except for final polishing, which used contra rotation. Silicon carbide P1200 grit paper was used to grind down specimens leaving ~80-100 μ m of material above the hole centreline. This

was followed by the polishing process involved using various cloths and diamond suspensions, including 6 μm diamond suspension on Ultra-Pol, 3 μm diamond suspension on Trident and 0.06 μm colloidal silica on Micro cloths. Figure 83 shows the grinder/polisher unit together with the associated SiC paper and cloths, while Table 30 details the grinding and polishing procedure.

Microhardness depth profile measurements of the cross-sectioned holes were undertaken using a Mitutoyo HM series 124 microhardness test unit with a Knoop diamond indenter. Optical investigation of subsurface damage and microstructural alterations of the workpiece was performed on a Leica Type DM LM microscope system fitted with a PixeLink camera connected to a computer operating Omnimet 8.7 digital imaging software. Figure 84 details the microhardness and optical microscopy equipment utilised.

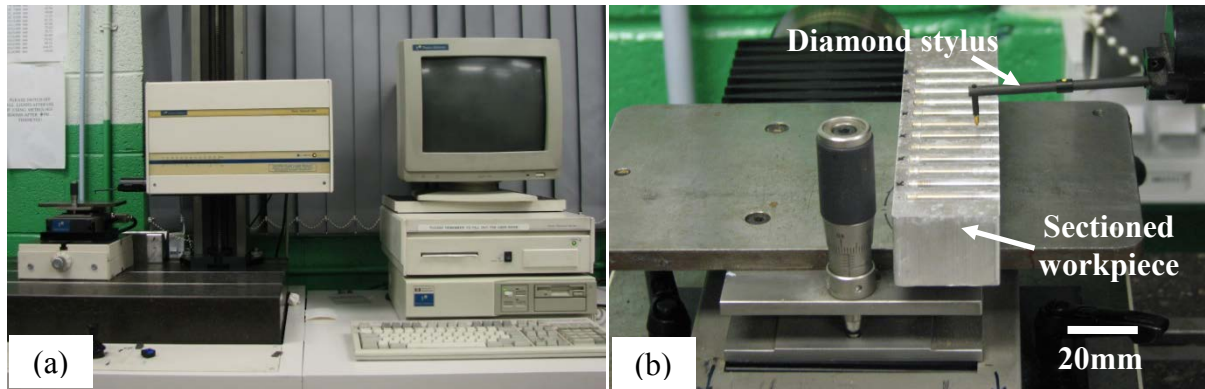


Figure 81: Illustration of (a) Taylor Hobson Form Talysurf series 120L and (b) surface roughness setup

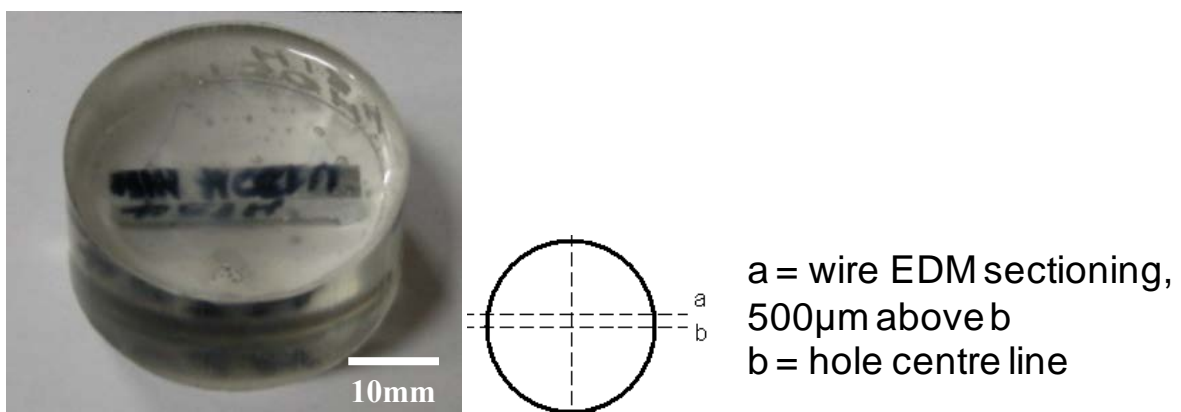


Figure 82: Typical cold resin mounted sample with schematic layout of drilled hole sectioning

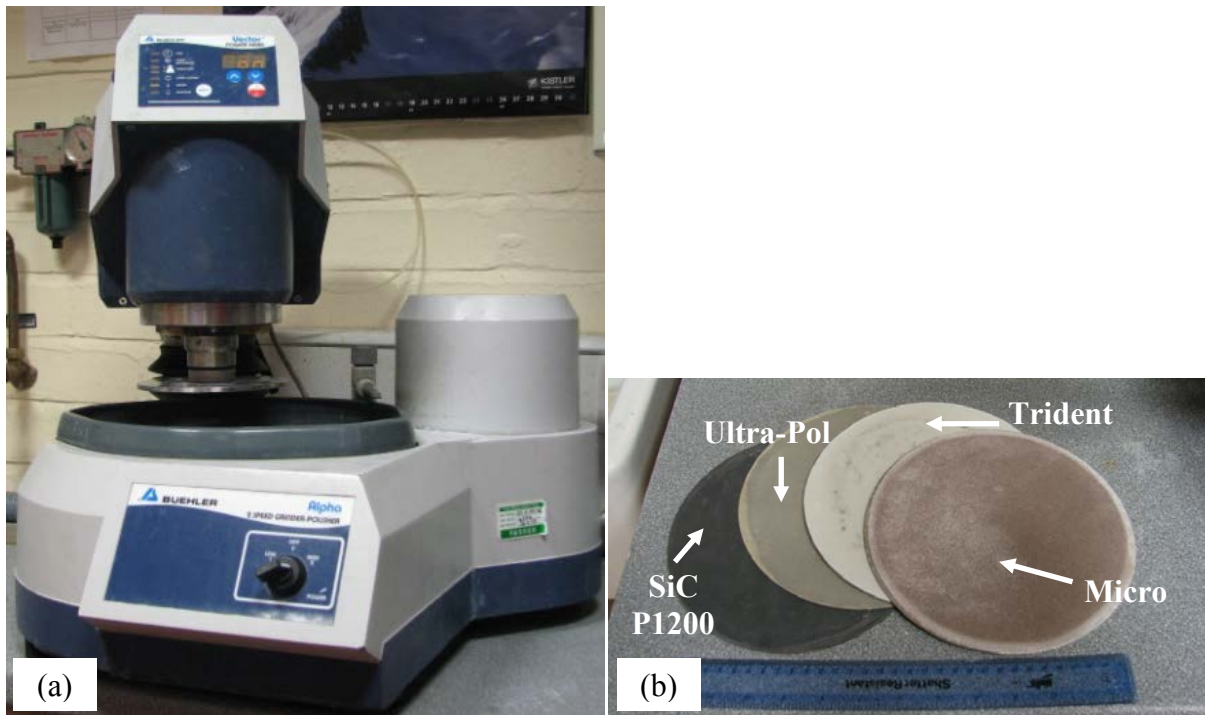


Figure 83: Illustration of (a) Buehler grinder/polisher and (b) SiC paper and polishing cloths

Table 30: Buehler grinding and polishing procedure for Al alloy

Surface	Abrasive/size	Load/specimen, speed and direction	Time (sec)
Carbimet abrasive disc	SiC P1200 grit	22N, 240- 300rev/min, Complementary	Until ~100 μ m above required size
Ultra-Pol cloth	6 μ m Metadi Supreme diamond suspension	27N, 120- 150rev/min, Complementary	120
Trident cloth	3 μ m Metadi Supreme diamond suspension	27N, 120- 150rev/min, Complementary	40-60
Micro cloth	0.06 μ m colloidal silica	27N, 120- 150rev/min, Contra	15-30

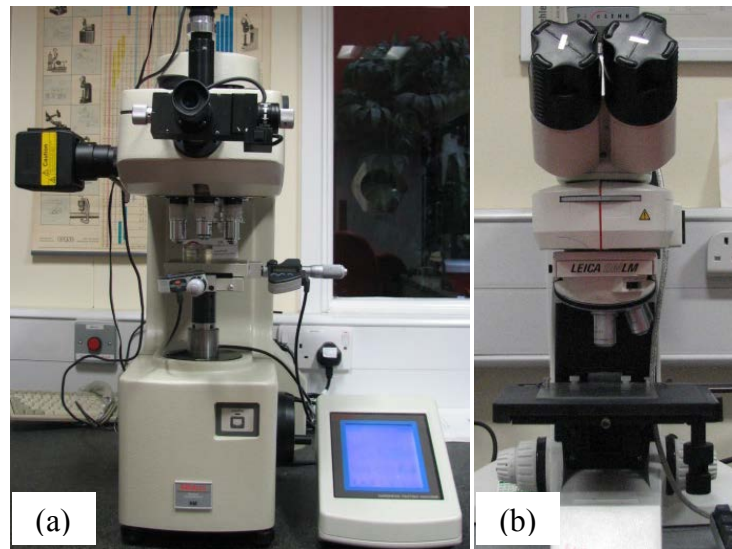


Figure 84: Illustration of (a) Mitutoyo microhardness test unit and (b) Leica DMLM microscope

4.4 Experimental design, procedures and test arrays

4.4.1 Industry based work

4.4.1.1 Phase 1: Assessment and capability study of current compressor impeller machining processes

Machining process capability studies on the Index G200 were performed according to ISO 22514: 2007 [218] incorporating a sample size of 50 which was divided into 10 batches of 5. A new set of tools/inserts were employed for the investigations. The process capability (C_p) and process performance indices (C_{pk}) were calculated using Equations 1 to 3 detailed in Section 3.4.4. Measurements focused on the critical features (operations 1, 3, 4, 5, 7 and 8) of the impellers which primarily relate to the quality of the hole and component squareness. Figure 85 illustrates the critical quality features of the components (marked CR1 to CR5) and Table 31 lists the component critical features and associated limits. Machining conditions and cutting parameters, see Section 2.5 were identical to those utilised for production at Doncasters Sterling. The calculated C_p and C_{pk} values for the hole machining process (geometrical size) were used as baselines in conjunction with drilling/reaming process control charts, which are similar to those used by DaimlerChrysler Corp., Ford Motor Company and GM Corp according to ISO 7870: 2007 standard [212, 226]. Machine shop scrap level and capacity were also observed using the Doncasters machine shop daily record sheets, and resource planning system (SYSPRO).

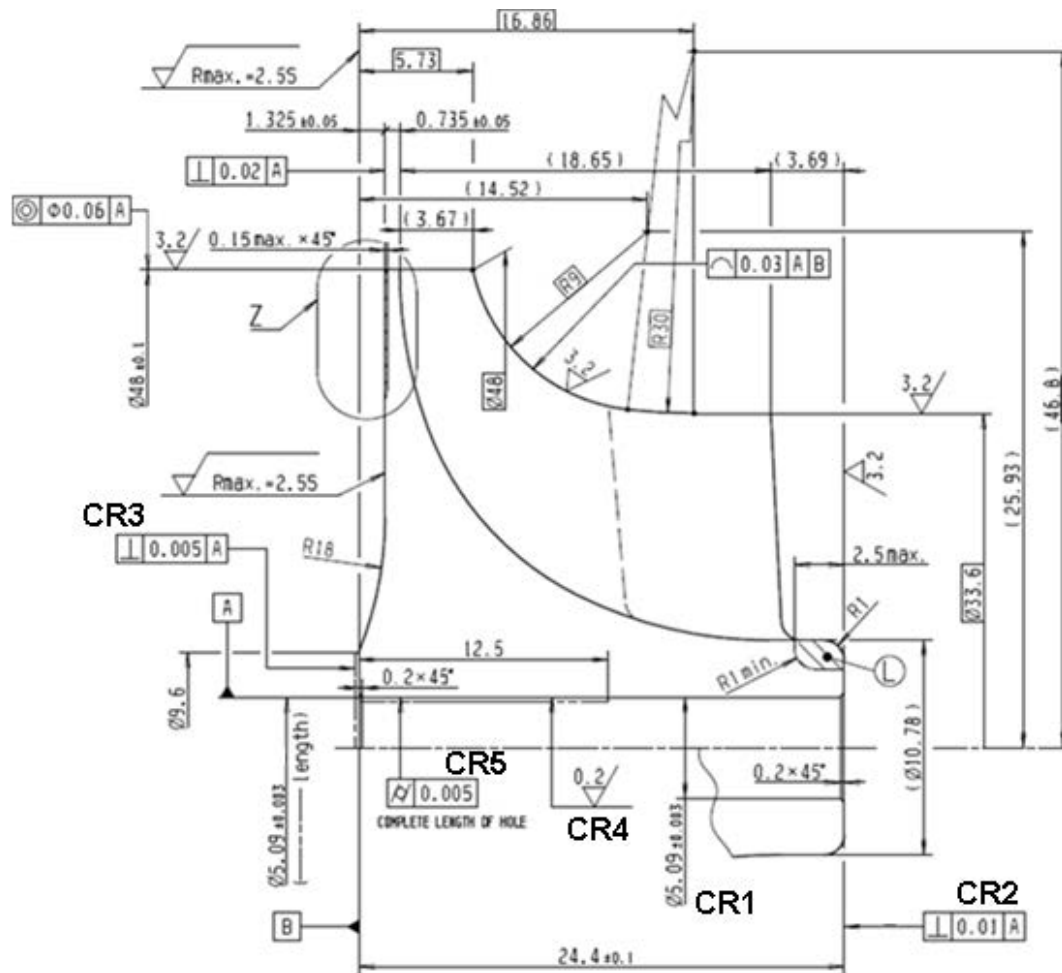


Figure 85: Compressor impeller critical quality features/dimensions

Table 31: Component critical features and associated limits

Critical component feature	Specification limit
Hole diameter (CR1)	$\pm 3\mu\text{m}$
Squareness of nose (CR2)	$\leq 10\mu\text{m}$
Squareness of back-face (CR3)	$\leq 5\mu\text{m}$
Hole surface roughness (CR4)	$\leq 0.2\mu\text{m}$
Hole cylindricity (CR5)	$\leq 5\mu\text{m}$

4.4.1.2 Phase 2: Production tooling trials and comparative work of Sterling standard tools against alternative cutting tool materials

Preliminary comparative evaluation of cutting tools was conducted in three different production tooling trials (Phase 2A, B and C). Assessment parameters involving the

measurement of cutting forces, workpiece surface roughness, tool life and cost analysis. In terms of tool life trials, new tools were utilised for each run with the customer specified component tolerances (see Figure 85) used to determine the end of tool life criterion. However, cutting forces (thrust and torque) of Phase 2C were thought insignificant and not considered. In Phase 2A both carbide and PCD tooling were assessed. Blind-hole drilling (operation 3) in Phase 2B was performed followed by the reaming (operation 4) operation, Phase 2C. The total cutting length in the former was ~28mm whilst the latter was 25mm. Depth of cut for the roughing operation (operation 1) was 1mm with a total of three passes (3mm) per machining cycle. Maximum cutting force (F_x) and torque (M_z) were recorded. The roughness evaluation was performed on the turned surface of the component as per ISO 4288: 1998 [227] with a 0.8mm cut-off over a 4mm evaluation length. An example of the roughness measurement setup for operation 1 is shown in Figure 86. The machining parameters employed were equivalent to those used in Sterling's production operations and are detailed in Table 32. Test matrices for the production tooling trials are detailed in Table 33 to Table 35.

Table 32: Test operating parameters

Parameters	Rough facing	Drilling	Reaming
Speed m/min (rev/min)	850 (6000)	130 (8500)	32 (2000)
Feed mm/rev (mm/min)	0.15 (900)	0.1 (850)	0.12 (240)
Depth of cut (mm)	1, 3 passes	4.8	0.28
Cutting environment	Low pressure flood 3bar, external	Low pressure flood 3bar, external	Low pressure flood 3bar, internal

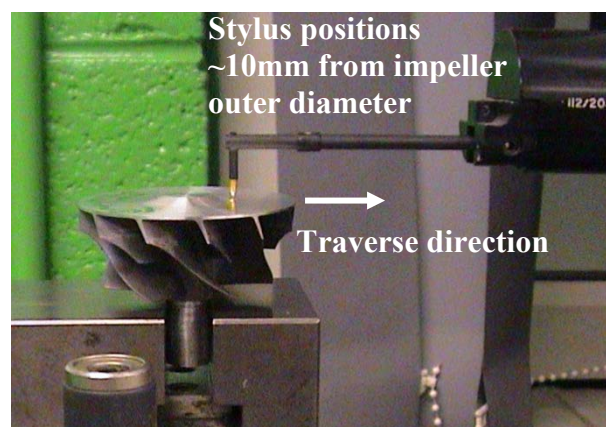


Figure 86: Surface roughness measurement setup for rough turning operation 1

Table 33: Test matrix for Phase 2A rough facing

Test number	Tool coating	Tool supplier/manufacturer	Tool code	Cutting speed/environment
1	WC K10 +TiB2 (Type 1)	Kennametal	CCGT09T308HP KC5410	See Table 32
2	PCD 010 (Type 2)	Exactaform	CCGT09T308	See Table 32
3	PCD CTB010 (Type 3)	Mapal	CCGT09T308F01N C2A (chip breaker)	See Table 32
4	PCD CTB010 (Type 4)	Mapal	CCGW09T308F01N 0AA (standard)	See Table 32

Table 34: Test matrix for Phase 2B drilling

Test number	Tool coating	Tool supplier/manufacturer	Tool code	Cutting speed/environment
1	WC	Titex	A1167B	See Table 32
2	TiN	Guhring	611	See Table 32

Table 35: Test matrix for Phase 2C reaming

Test number	Tool coating	Tool supplier/manufacturer	Tool code	Cutting speed/environment
1	WC	Beck	RV3188	See Table 32
2	PCDCTB002	Mapal	30349250	See Table 32

4.4.2 Laboratory based work

4.4.2.1 Phase 3A: Evaluation of diamond-like carbon coated tools when drilling cast C355 aluminium alloy

Phase 3A involved 3 variable factors of cutting speed, cutting tool material and machining environment with specific parameter levels detailed in Table 36. The drilling feed was kept constant at 0.1mm/rev throughout the experiment. The main workpiece blocks for blind-hole drilling (to a depth of 28mm) were held in place with a standard vice, see Figure 87 for the experimental setup. The hole positions were initially marked using a carbide centre drill to a depth of 1mm prior to the mainstream operation, each in a single plunge movement i.e. no pecking. Tool overhang was ~36mm with measured runout <0.01mm. The pattern of holes employed for the test was a square array with an 8mm pitch in both directions. Each workpiece block could accommodate a maximum of 300 holes spread over 12 rows.

Table 36: Test matrix for Phase 3A

Test number	Tool coating	Cutting speed m/min (rev/min)	Cutting environment
1	Uncoated WC	130 (8500)	Low pressure flood 3bar
2	Uncoated WC	260 (17000)	Low pressure flood 3bar
3	Graphit-iC™	130 (8500)	Low pressure flood 3bar
4	Graphit-iC™	260 (17000)	Low pressure flood 3bar
5	Dymon-iC™	130 (8500)	Low pressure flood 3bar
6	Dymon-iC™	260 (17000)	Low pressure flood 3bar
7	Uncoated WC	130 (8500)	High pressure 70bar
8	Uncoated WC	260 (17000)	High pressure 70bar
9	Graphit-iC™	130 (8500)	High pressure 70bar
10	Graphit-iC™	260 (17000)	High pressure 70bar
11	Dymon-iC™	130 (8500)	High pressure 70bar
12	Dymon-iC™	260 (17000)	High pressure 70bar

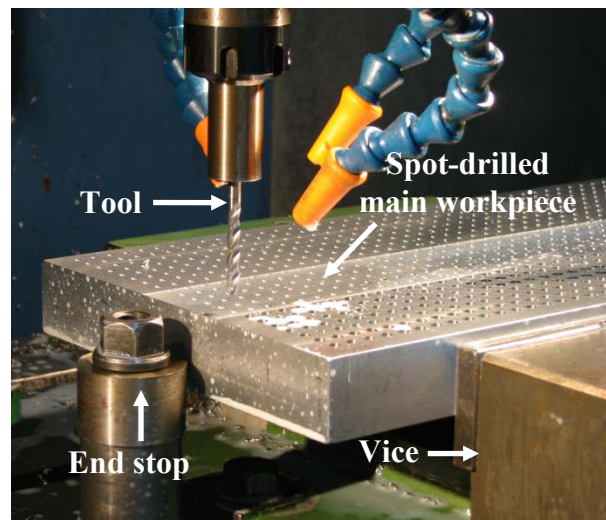


Figure 87: Test setup for blind hole drilling trials

Tool wear and thrust force/torque were measured after the first hole and at intervals of 51 holes thereafter (readings were taken at holes 1, 52, 103, 154, 205, 256, and 307 respectively). The holes for assessment were produced in the strip samples attached to the drilling dynamometer as shown in Figure 88. The maximum flank wear (VB_{Bmax}) of each cutting edge (3-flute) was measured and then averaged in accordance to ISO 3685: 1993 [44] standard. Tools were immersed for ~1 minute in sodium hydroxide (NaOH 25%) as and when necessary to remove any adhered material in order to allow for the measurement of wear scars. End of test criterion was either an average maximum flank wear of 0.3mm, catastrophic failure of the drill or upon completion of 307 holes. The first hole was drilled in the small workpiece clamped on the Kistler dynamometer in order to determine the cutting force of the

new tool upon commencing the drilling test and at a 51 hole interval thereafter until hole 307 was reached. Maximum thrust force (F_z) and torque (M_z) values were recorded.

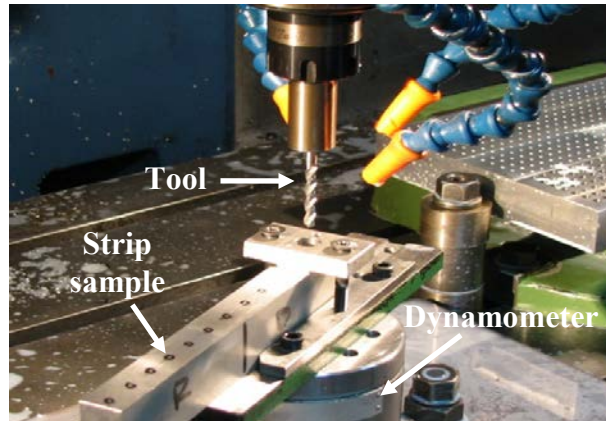


Figure 88: Force measurement setup

Following the end of each trial, the holes of the strip samples were cleaned prior to geometrical accuracy assessment. Hole diameter was measured at depths of 2mm, 12mm and 23mm from the hole entry and averaged. Roundness, cylindricity and parallelism parameters were similarly averaged from 3 measurements made at holes 1, 154 and 307 for each test. Surface roughness measurements however were carried out at intervals of 100 holes at the entry (2mm from entry) and bottom (25mm from entry) location of every hole evaluated. Procedures for the surface roughness assessment were in accordance with ISO 4288:1998 [227] standard. Investigation of workpiece subsurface alteration/damage and microstructural analysis were carried out on holes 1, 154 and 307 in trials which provided the longest tool life and the best hole quality. Knoop microhardness measurements using a 0.025kg load with a 15s duration were performed on sample cross-sections perpendicular to the feed direction, and were taken at 12mm from the hole entry. Diamond indentations were made at depths of 10, 20, 30, 40, 50, 75, 100, 150, 200, 300, 400, 500 and 750 μ m from the machined surface respectively. Three measurements were performed at each depth and averaged, with appropriate spacing defined to avoid overlaps/interference between the indents. Figure 89 shows the typical diamond indentation pattern during microhardness assessment. Samples were subsequently etched at room temperature using Keller's reagent (2.5% HNO_3 , 1.5% HCL , 1% HF , 95% H_2O) for ~20s immersion to enable optical investigation of subsurface damage or microstructural alterations within the workpiece.

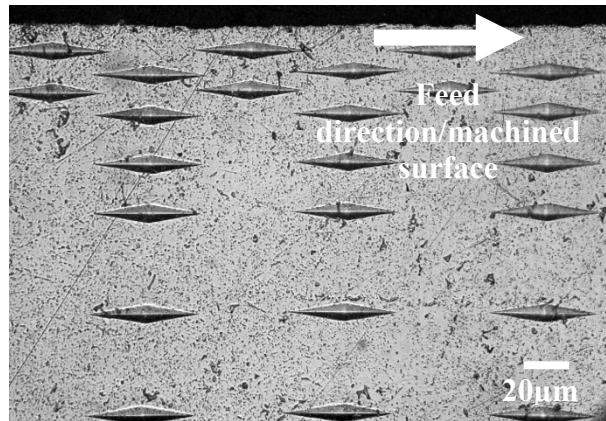


Figure 89: Typical measurement of workpiece microhardness

4.4.2.2 Phase 3B: Evaluation of diamond-like carbon coated tools when reaming 6082-T6 aluminium alloy

A full factorial experimental design involving variation of tool coating (uncoated, Dymon-iC™ and Graphit-iC™) and cutting speed (32 and 96m/min) was utilised for the reaming tests in Phase 3B, see Table 37. Feed rate was kept constant at 0.12mm/rev during the experiment while the workpiece setup for tool wear and cutting force evaluation was identical to that employed in Phase 3A. Through-hole high pressure cutting fluid of 70bar was supplied throughout the test. An array of pre-drilled blind holes (28mm deep) was produced in the workpiece with a new WC drill ($\varnothing 4.8\text{mm}$) prior to each test in order to minimise any deviation in reaming depth of cut resulting from prior drill wear. Tool overhang was $\sim 42\text{mm}$ with a corresponding 0.01mm maximum runout. The holes were reamed to a depth of 25mm with the frequency of tool wear and force measurement as well as the end of test criterion being equivalent to that used in Phase 3A (total of 307 holes with tool inspection at 51 hole intervals). Average maximum flank wear was determined from the measurement of six cutting edges. Figure 90 demonstrates the typical reaming force signature obtained in the trials.

Average hole diameter was evaluated from three measurements at 2mm, 12mm and 23mm from hole entry starting with hole 1 and at 51 hole intervals thereafter. A total of 5 profiles along holes 1, 154 and 307 were generated and replicated three times for hole geometrical (roundness, cylindricity and parallelism) accuracy analysis. Workpiece surface roughness was also assessed at 51 hole intervals at the top and bottom of the hole (2mm and 23mm from hole entry respectively). Evaluation of workpiece microhardness was performed at the start and end of each test, while microstructural analysis was carried out on hole 2, 153 and 306. A total of three measurements of workpiece subsurface microhardness were taken at

each depth level according to the intervals adopted in Phase 3A. Similarly, Keller's reagent was used to reveal material grain boundaries for subsequent microstructural assessment.

Table 37: Test matrix for Phase 3B

Test number	Tool coating	Cutting speed m/min (rev/min)
1	Uncoated WC	32 (2000)
2	Uncoated WC	96 (6000)
3	Graphit-iC™	32 (2000)
4	Graphit-iC™	96 (6000)
5	Dymon-iC™	32 (2000)
6	Dymon-iC™	96 (6000)

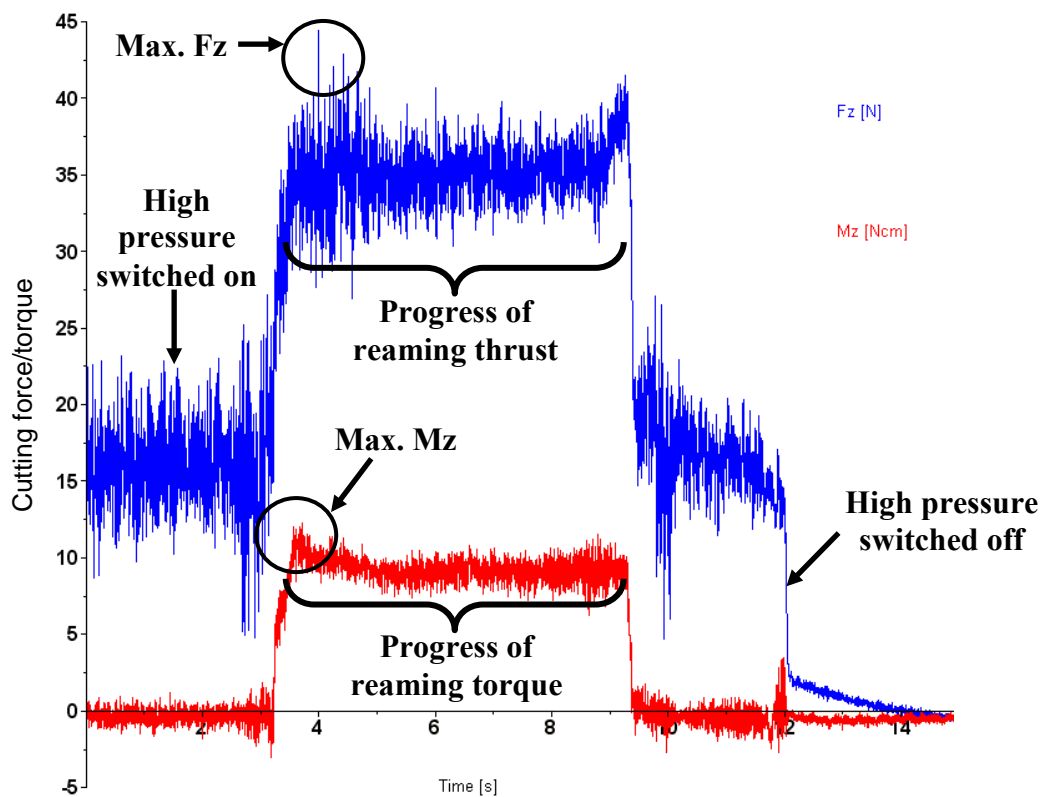


Figure 90: Typical reaming force with high pressure cutting fluid at 32m/min speed and 0.12mm/rev feed rate

4.4.4.3 Phase 4: Evaluation of diamond coated and PCD tools when drilling and reaming cast C355 aluminium alloy

This phase of experimental work involved drilling (Phase 4A) and reaming (Phase 4B) at two different cutting speeds (130m/min and 260m/min for drilling and 32m/min and 96m/min for reaming). The former tests were performed at a constant feed rate of 0.1mm/rev and the latter at 0.12mm/rev. Drilling tests were carried out under low pressure flood conditions (3bar) and the reaming with high pressure cutting fluid application (70bar), which

was similar to the production process in Doncasters Sterling. Drilling procedures were the same as those carried out in Phase 3A. Drill and reamer overhang was ~36mm and ~42mm respectively while runout was <0.01mm in all trials. Unlike the previous phase of experiments, reaming tests were performed on the same workpiece immediately after completion of the drilling trials, i.e. after every 840 drilled holes (one workpiece block), without workpiece removal from the vice. This procedure was utilised in an attempt to minimise deviation of the reamer alignment as well as shorten the experimentation time. The end of test criterion was a total of 1,683 holes (2 workpiece blocks) with measurement of tool wear (maximum flank wear VB_{Bmax}), cutting force/torque, hole geometrical accuracy and surface roughness performed on the first hole and at intervals of 280 thereafter (holes 1, 282, 563, 843, 1123, 1403 and 1683). In terms of hole roundness, cylindricity and parallelism values, a total of 5 profiles were generated for each specimen with measurements repeated three times. Drilled and reamed hole surface roughness was measured at 2mm from hole entry and similarly ~2mm from the bottom of the hole. In contrast, microhardness and microstructural analysis was undertaken on holes 1, 1123 and 1683 according to the procedures detailed for Phase 3A and 3B experiments. Table 38 and Table 39 show the test matrices for the drilling and reaming trials respectively.

Table 38: Test matrix for Phase 4A

Test number	Tool coating	Cutting speed m/min (rev/min)
1	Uncoated WC	130 (8500)
2	Uncoated WC	260 (17000)
3	CVD diamond	130 (8500)
4	CVD diamond	260 (17000)
5	PCD 010	130 (8500)
6	PCD 010	260 (17000)
7	PCD 302	130 (8500)
8	PCD 302	260 (17000)

Table 39: Test matrix for Phase 4B

Test number	Tool coating	Cutting speed m/min (rev/min)
1	Uncoated WC	32 (2000)
2	Uncoated WC	96 (6000)
3	CVD diamond	32 (2000)
4	CVD diamond	96 (6000)
5	PCD 002	32 (2000)
6	PCD 002	96 (6000)
7	PCD 302	32 (2000)
8	PCD 302	96 (6000)

CHAPTER 5: RESULTS AND DISCUSSION

5.1 Industry based work

5.1.1 Phase 1: Assessment and capability study of current compressor impeller machining processes

5.1.1.1 Machine capacity, scrap level and production issues

Scrap rate data was gathered from Doncasters Sterling SYSPRO Enterprise Resource Planning software to determine cumulative scrap level, see Figure 91. The graph shows various sources of machine shop scrap and the respective volume recorded during weeks 11-21 in 2008, which was found to include other types of component flaws that were not directly related to machining, i.e. missing components, material inclusions, etc., which equated to ~26%.

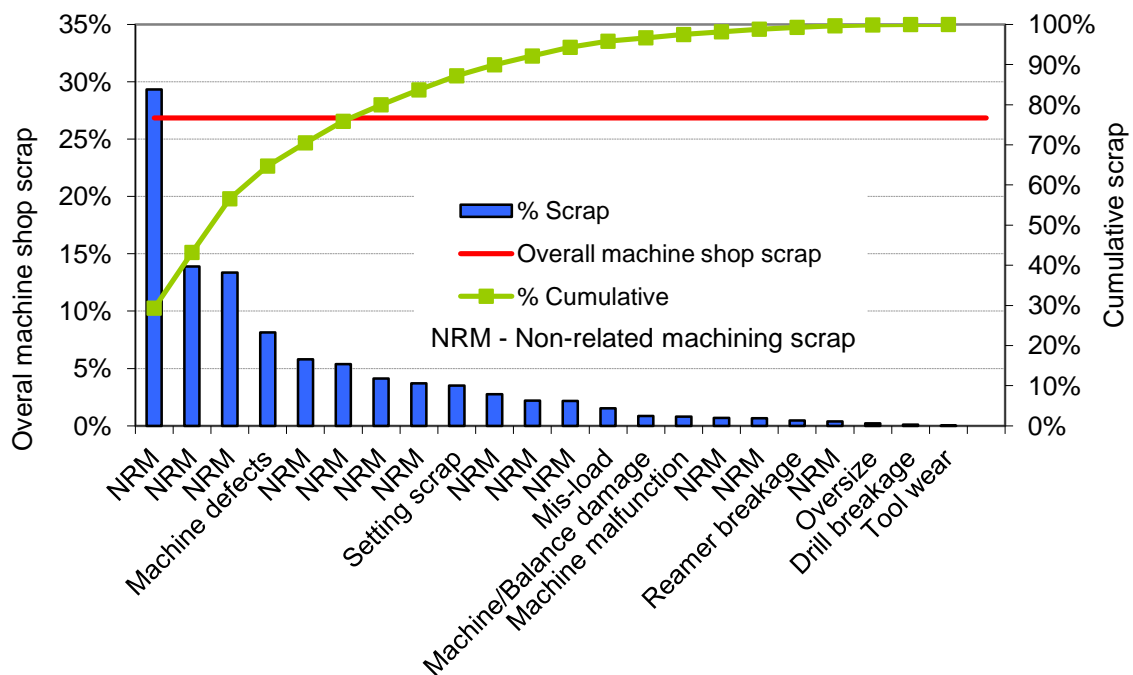


Figure 91: Machine shop scrap analysis for year 2008 over weeks 11-21

Damage categorised as “machining scrap”, or directly related to machining, included machine defects (burrs on blades, score/scuff in bore, over/undersize or out of specification, etc.), setting errors, mis-load, machine damage (marks on component caused by tool fixtures or swarf residual), machine malfunction (low air supply, power cut, insufficient cutting fluid level), tool breakage and excessive tool wear. This equated to ~6% of the overall scrap rate produced in the machine shop. The data on machining related component scrap was

predominantly the result of burr formation on the components and bore defects (scuff/scores, over/undersize, etc.), which demonstrates scope for improvement involving more robust process conditions and more reliable cutting tools.

The overall cycle time required to machine a typical 45mm diameter compressor impeller was approximately 1.25 minutes. Generally, the Overall Equipment Effectiveness (OEE) measure based on two machines working continuously 24 hours a day, 7 days a week was around 80% during the operating period over weeks 41-51 in 2008. Note that the OEE for the machine shop was available during this period and that the data differed from that used for the scrap analysis. See Appendix B for further details of the data and formulae used to calculate the OEE levels observed for the ten-week period. Relatively high percentage (>80%) levels of OEE were achieved in the majority of weeks, which indicates that the machines were effectively utilised and a high ratio of good parts were produced. Low values of OEE were however also observed in weeks 41, 42 and 44, which was mainly due to extended idle time as a result of machine breakdown, a high number of scheduled job changeovers/frequent tool changes and unavailability of the machine operators.

5.1.1.2 Process capability study on Index G200 machining centre

Results from a run of 50 machined impellers and subsequent measurements of the critical features are shown in Appendix B. All measured features were found to be within the design specification. Process capability index (Cpk) is an indication of how close a process is in achieving specified targets relative to process variability. A larger Cpk value reduces the likelihood of a component being produced outside the specifications. Simply put, process capability (Cp) represents the consistency and precision of a process, with higher Cp levels denoting greater process reliability [211]. For processes within the automotive industry, the widely accepted and applied minimum threshold for Cp and Cpk values is 1.66. Table 40 details the calculated Cp and Cpk values for the critical component features based on the 50 machined sample impellers.

Table 40: Process capability indices/values based on compressor impeller critical quality features

Features	Process capability (Cp)	Process capability index (Cpk)
Hole diameter towards nose	3.84	2.16
Hole diameter towards back	6.96	5.45
Hole diameter in middle	10.59	7.27
Squareness of nose	3.88	0.89
Squareness of back-face	2.59	2.03
Hole surface roughness	5.77	3.17
Hole cylindricity (2 nd study)	1.24 (1.79)	1.22 (0.89)

The hole diameter at the back, nose and middle positions was found to show high process capability indices, above 1.66, and suggests that the hole making operations (drilling and reaming) were within the defined control limits (X Bar chart), as shown in Appendix B. The figures also detail hole R charts which indicate that the process was stable and consistent throughout the experiment. The machine surface roughness results of the hole also highlighted acceptable process capability values of Cp 5.77 and Cpk 3.17, with very little variability as shown in Figure B4. Process capability in terms of hole cylindricity however was only 1.24, which was below the automotive industry target, although the process was stable and within the control limits according to the X bar and R charts shown in Figure B5. Additionally, the histograms in Figure B5 indicate high variability within the process, probably due to factors such as alignment of machine spindle, irregular wear of cutting tools or inappropriate calibration of the metrology equipment. A further study of process capability relating to hole cylindricity following calibration (relatively more feasible and cost effective problem solving) of the Talyrond 131 unit, showed an improvement in Cp to 1.79. The distribution/histogram curve was clearly narrower, see Figure B6, but shifted toward the lower specification limit which resulted in a poorer Cpk value of 0.89 compared with the previous result (Cpk 1.22) shown in Figure B5. The squareness of the component on the back-face and nose showed satisfactory Cp values of 2.59 and 3.88 respectively, see Figures B7 and B8. However, the Cpk value in terms of component squareness on the nose was only 0.89 and is reflected in the distribution curve of the capability histogram, Figure B8, which approaching the lower specification, whilst its narrow bell-shape suggests low process variability. Generally, low values of component squareness (5µm max. on the back and 10µm max. on the nose), hole cylindricity (5µm max.) and hole surface roughness (0.2 µm max.) are preferred when machining compressor impellers at Doncasters Sterling. These features have defined

maximum tolerances (single-sided) as opposed to lower and upper limits (bilateral/two-sided) and, therefore, lower Cpk values are generally obtained as the distribution curves lean towards the bottom end of the specification, i.e. zero. While Cpk of the hole surface roughness, nose squareness and hole cylindricity in the current study would improve if the measured parameters were to shift towards the maximum tolerance, this situation is undesirable in practice.

5.1.1.3 Drilling and reaming process control charts

Hole making operations involving drilling and reaming were considered critical compared to all other processes in terms of workpiece quality requirements due to swarf and heat entrapment during drilling/reaming operations. As a result, control charts were introduced in the machine shop for monitoring of the drilling/reaming process. The charts allowed operators to record hourly measurements of impeller hole size together with any actions/activities taken, e.g. lunch break, tool changes, variation to machine setup, etc., during the operation. It was found that the hole machining process, in terms of dimensional accuracy, fluctuated when the machine tool was interrupted or idle, regardless of previous activity and/or the length of time. This may be due to the fact that the idling time allowed the spindles and/or tool holder sufficient time to cool down, thus compromising the overall hole machining operation. A sample of machine shop control charts detailed in Figure B9 clearly show that a continuous machining run led to a more consistent and predictable process, as well as improved component quality (lower variability in hole diameter).

5.1.2 Phase 2: Production tooling trials and comparative work of Sterling standard tools against alternative cutting tool materials

5.1.2.1 Phase 2A: WC and PCD cutting inserts (Operation 1, rough turning/facing)

Flank face wear flat formation, due to abrasion, was the principal wear mode which was generally observed during rough turning/facing of the aluminium compressor impellers at Doncasters Sterling. During the production tooling trials, it was observed that insert replacement was not necessarily due to excessive tool wear. Tool change was initiated when burr formation on the components as shown in Figure 92 was detected, rather than as a result of a change in component geometrical size.

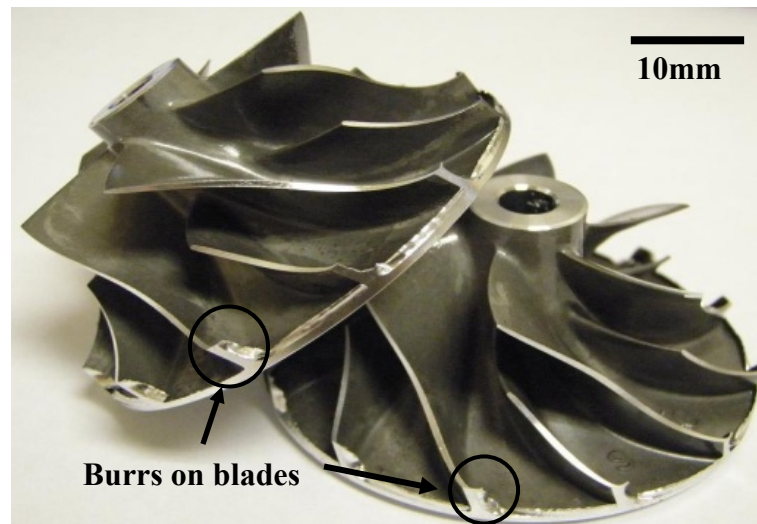


Figure 92: Burr formation on impeller blades

Production tool life per edge of the Type 3 (3433 components) and Type 4 (6363 components) inserts significantly exceeded the performance of both the Type 1 WC+TiB₂ Kennametal (400 components) and Type 2 PCD Exactaform (64 components) products, see Table 33 for details of type of tool. Optical micrographs showing new and worn tool conditions of the tools tested are detailed in Figure 93 to Figure 95.

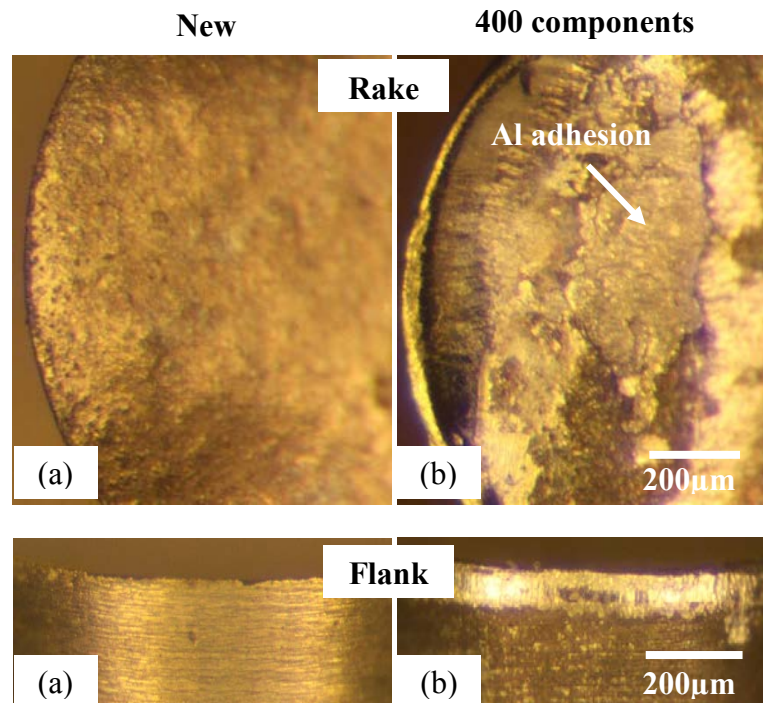


Figure 93: Micrographs of (a) new and (b) worn Kennametal Type 1 WC insert

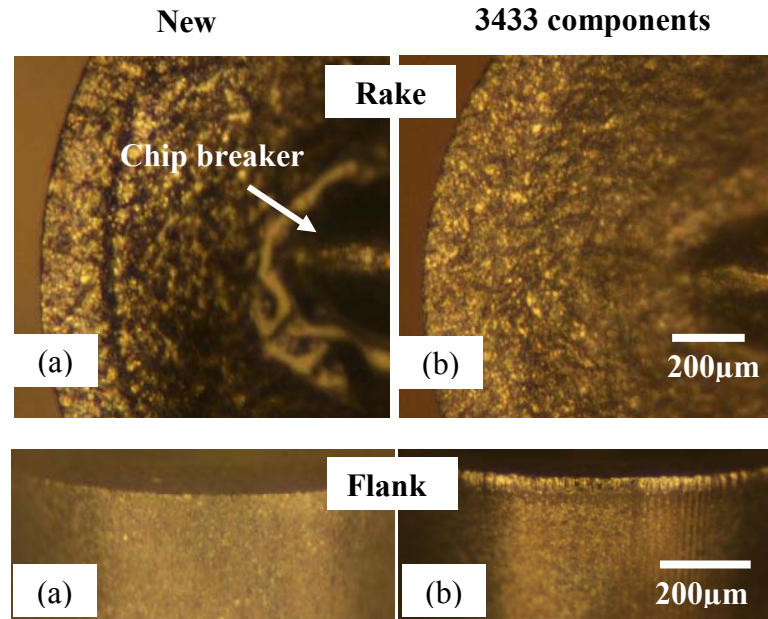


Figure 94: Micrographs of (a) new and (b) worn Mapal Type 3 PCD insert

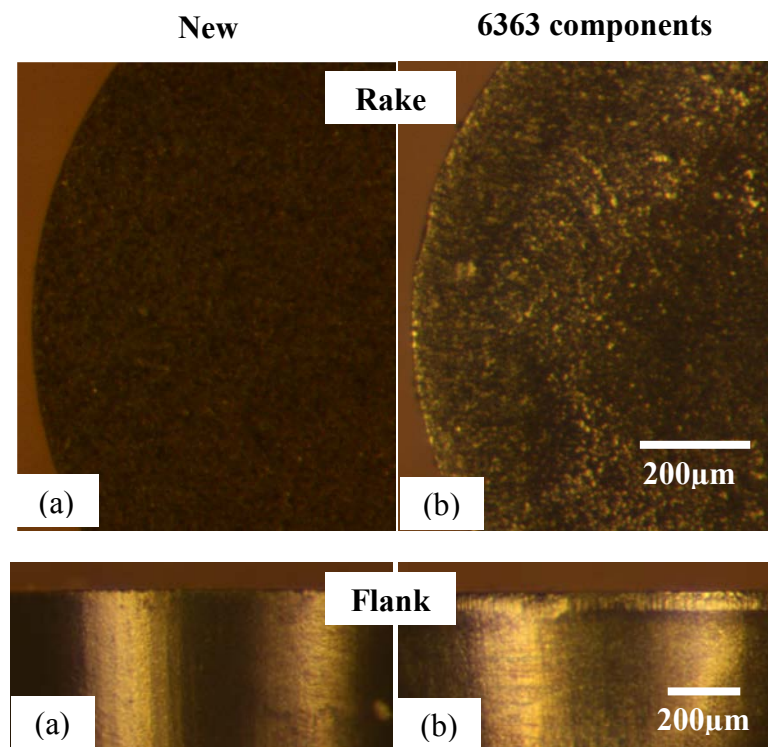


Figure 95: Micrographs of (a) new and (b) worn Mapal Type 4 PCD insert

Flank clearance together with high tool rake angles, 7° and 12° respectively, would result in a weaker edge of the Type 2 insert. This coupled with the interrupted nature of the cutting operation was most likely the reason for the catastrophic tool failure. Figure 96 shows an SEM image highlighting the failure regions of the fractured Type 2 roughing insert.

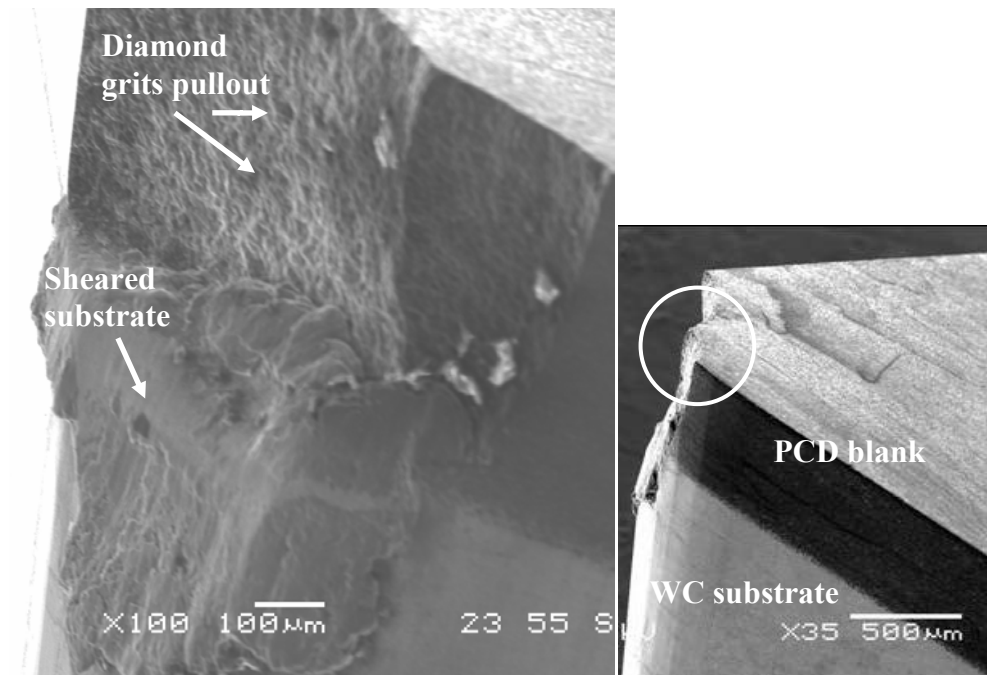


Figure 96: SEM image of failed Exactaform Type 2 PCD insert

The Mapal Type 4 PCD insert lasted the longest with 6363 components compared with the Mapal Type 3 PCD tool at 3433 components. Both inserts used PCD blanks were classified as medium grade (10µm grain size) and the reason the Type 3 (with chip breaker geometry) machined fewer components was possibly due to the different types of compressor impellers produced, some requiring greater material removal/depth of cut per impeller during the operation. Aluminium adhesion was clearly present on the surface of the coated carbide insert, whilst the Mapal PCD inserts did not exhibit any major signs of material sticking. Long, spiral continuous/ribbon-like chips were formed with all inserts tested. The Mapal Type 3 insert however generated closed conical chips, which was beneficial to the machine tool and components as the risk of swarf damage was minimised. The shape of chips produced by each of the roughing inserts is depicted in Figure 97.

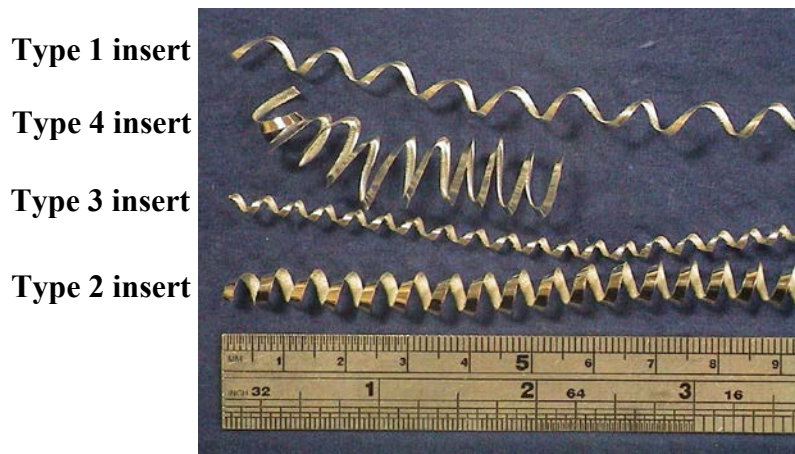


Figure 97: Chips shapes produced by different inserts during rough turning operation

The cutting force F_x was the largest component observed, compared with the feed force F_y and the radial force F_z , during the rough turning tests. Figure 98 shows the cutting force F_x in Zone B acting in the direction of the cutting velocity. Figure 99 shows the average maximum cutting forces produced by the Kennametal, Exactaform and Mapal roughing inserts.

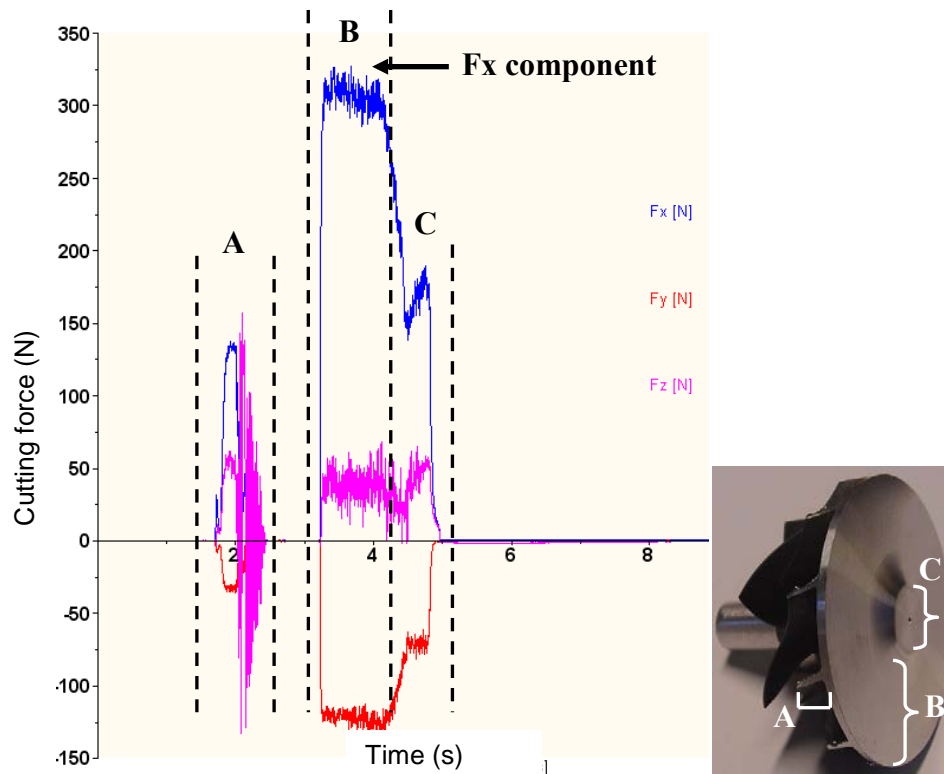


Figure 98: Cutting force during the first turning/facing stages: A-outside diameter, B-main back-face and C-back-face profile

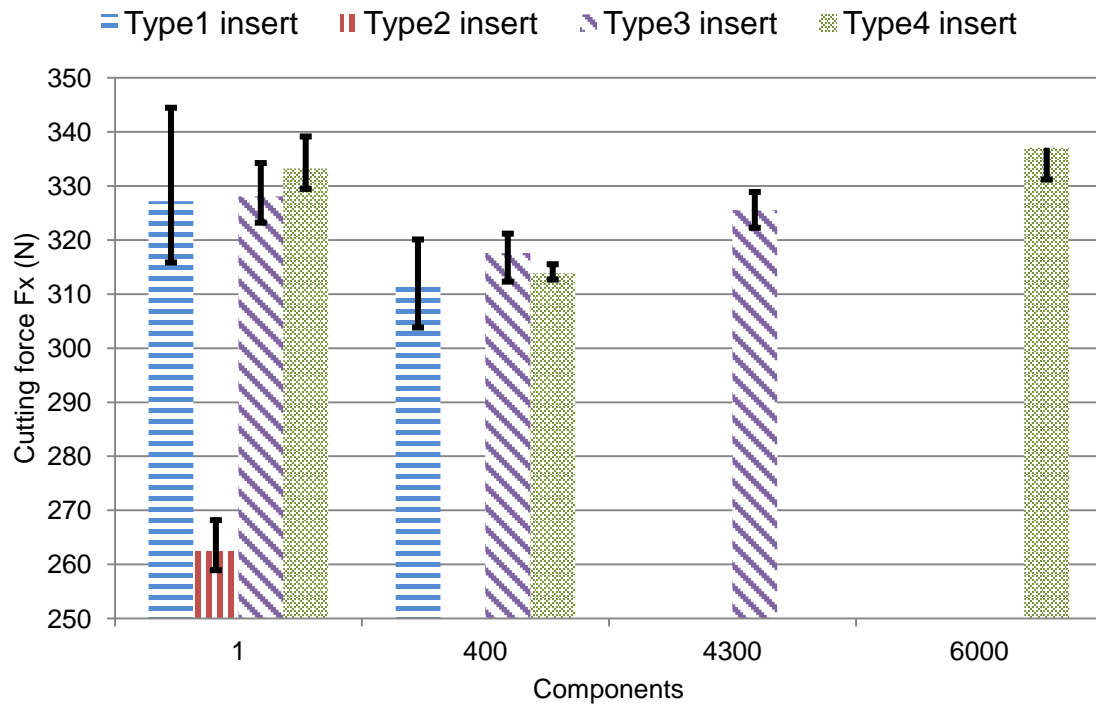


Figure 99: Average maximum cutting forces (F_x) of inserts on roughing operation

Despite its low tool life, the new/as-received Exactaform PCD (Type 2) insert produced ~25% lower cutting forces compared to the other products. The Kennametal WC+TiB₂ (Type 1) insert generated similar force levels (± 3 N) to that observed with the Mapal (Type 3 and 4) PCD tools, both when new and after machining 400 components. The highest average maximum F_x of ~337N corresponding to the worn (after 6300 components) Mapal Type 4 PCD insert was only 8% and 4% higher than the Kennametal Type 1 (after 400 components) and Mapal Type 3 PCD tool (after 4300 components).

Figure 100 shows the average workpiece surface roughness (R_a) measured ~10mm from the impeller's outer diameter from components produced using the new/as-received Kennametal, Exactaform and Mapal inserts. The lowest ($0.66\mu\text{m } R_a$) and highest ($1.80\mu\text{m } R_a$) surface roughness following the rough facing operation (typically $1\text{--}2\mu\text{m}$ is achieved) were obtained with the Mapal Type 4 and Exactaform Type 2 insert respectively. The R_a levels produced however were considered to be very good for a roughing operation, as typical surface roughness expected from a finish turning process is $0.75\mu\text{m}$ to $1.50\mu\text{m } R_a$ [228].

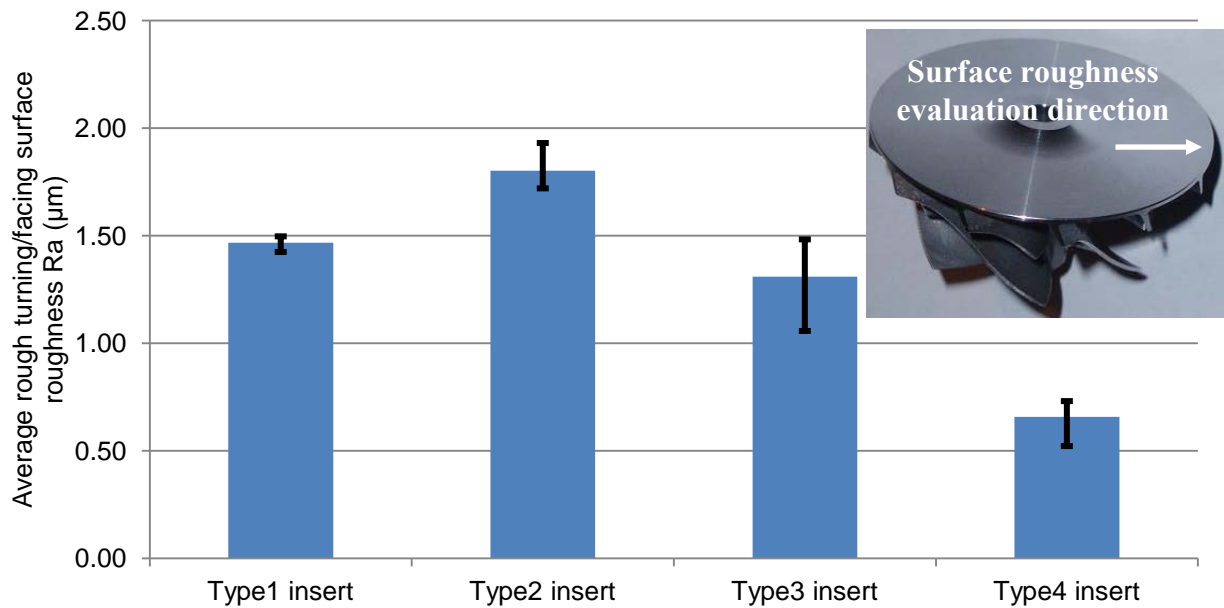


Figure 100: Workpiece surface roughness by different cutting inserts

The Mapal PCD inserts (Type 3 and 4) proved to be economical, despite the substantial capital cost of the inserts compared with the Kennametal and Exactaform products. Table 41 details operational costs for each of the roughing inserts tested. With the possibility for tool regrinding, the Mapal Type 3 and 4 inserts offer further cost benefits. For example a £15 tool regrind would equate to a 58% saving on the insert capital cost, which would reduce the tooling price for the rough turning/facing operation to 0.23p/unit, provided that tool life was not compromised. The number of possible tool regrinds of the Type 3 insert is limited due to the chip breaker geometry, therefore the Mapal Type 4 was considered the most cost effective for the rough turning/facing operation.

Table 41: Operational cost of roughing inserts

Insert Parameter	Type 1	Type 2	Type 3	Type 4
Cost per edge (p)	231	2070	4091	3614
Tool life (components)	400	63	3433	6363
Cost of operation per edge [after 1st regrind] (p/unit)	0.58	32.86	1.19	0.57 [0.23]

5.1.2.2 Phase 2B: WC and TiN coated drills (Operation 3, blind-hole drilling)

The uncoated carbide Titex A1167B and TiN coated Guhring 611 drills machined 3000 and 3300 components respectively before hole cylindricity drifted beyond the allowable tolerance ($>5\mu\text{m}$). This suggested that the harder TiN layer (2400HV) [223] helped prolong the life of the tool. Micrographs detailed in Figure 101 to Figure 104, show evidence of aluminium built-up edge/adhesion on both tools at the end of the trials. The coated tool however experienced substantially greater material adhesion on the cutting edges and chip clogging between the drill flutes compared to the uncoated tool. This was especially pronounced in areas where the coating had been removed/peeled off. Excessive material clogging can eventually obstruct the swarf/chip flow up the drill and has the potential to cause tool breakage, component damage and/or misalignment of the machine spindle. The percentage increase in thrust force and torque between new and worn condition was similar for both the Titex and Guhring drills.

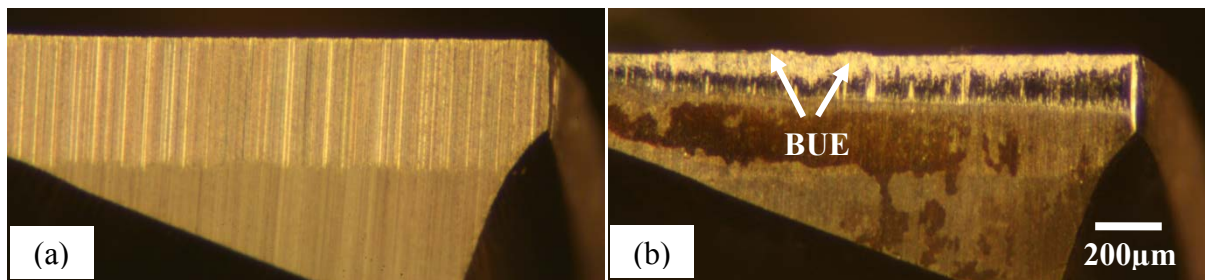


Figure 101: Micrographs of (a) new and (b) worn tungsten carbide Titex A1167B drill

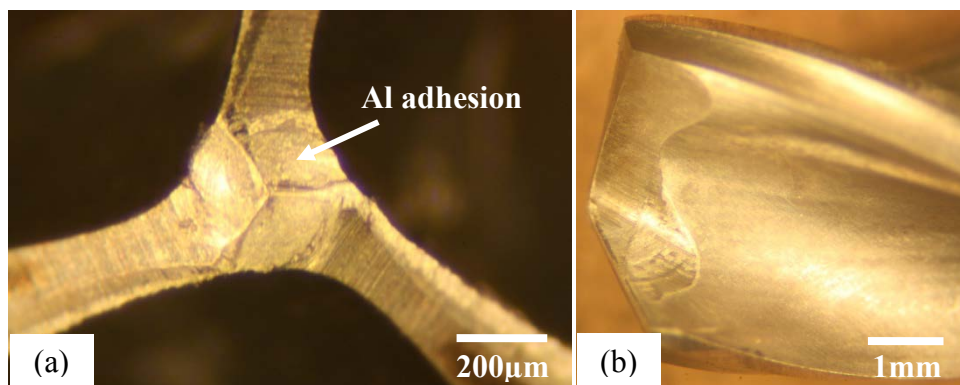


Figure 102: Micrographs of (a) worn chisel edge and (b) worn drill flute

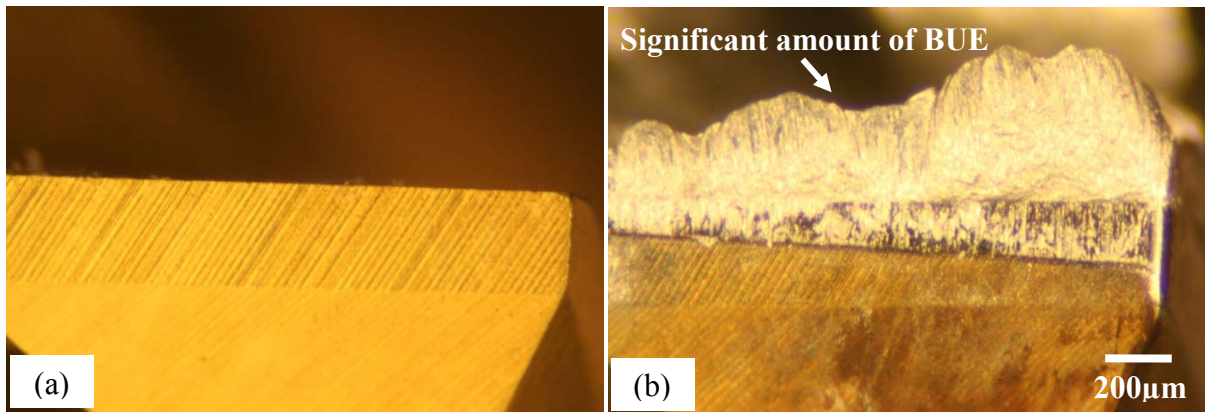


Figure 103: Micrographs of (a) new and (b) worn TiN coated carbide Guhring 611 drill

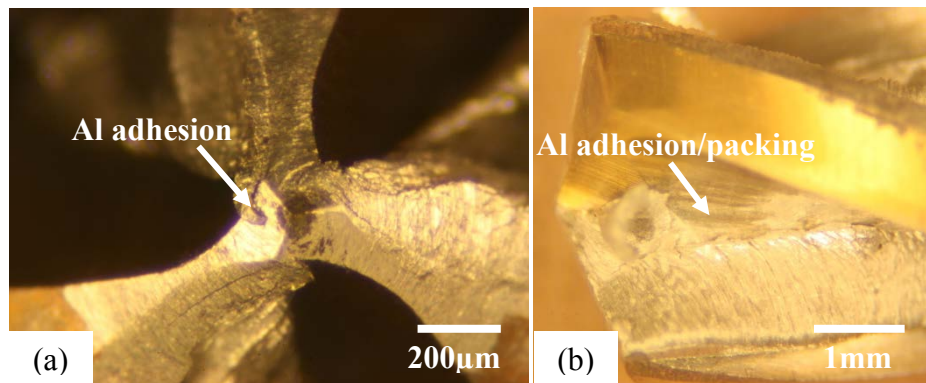


Figure 104: Micrographs of (a) worn chisel edge and (b) worn drill flute

Respective thrust force (F_z) and torque (M_z) of the Guhring drill increased by 68.6%, (470.20N to 792.89N) and 102.4% (49.69Ncm to 100.56Ncm) from new to worn condition, see Figure 105 and Figure 106. The high torque levels reflected the tool condition (Al packing and BUE) observed under the microscope. Despite lower thrust force (~30%) and torque (~18%) levels, the tool life of the Titex drills were ~10% lower than the Guhring tools.



Figure 105: Average maximum drilling thrust force by Titex and Guhring drills

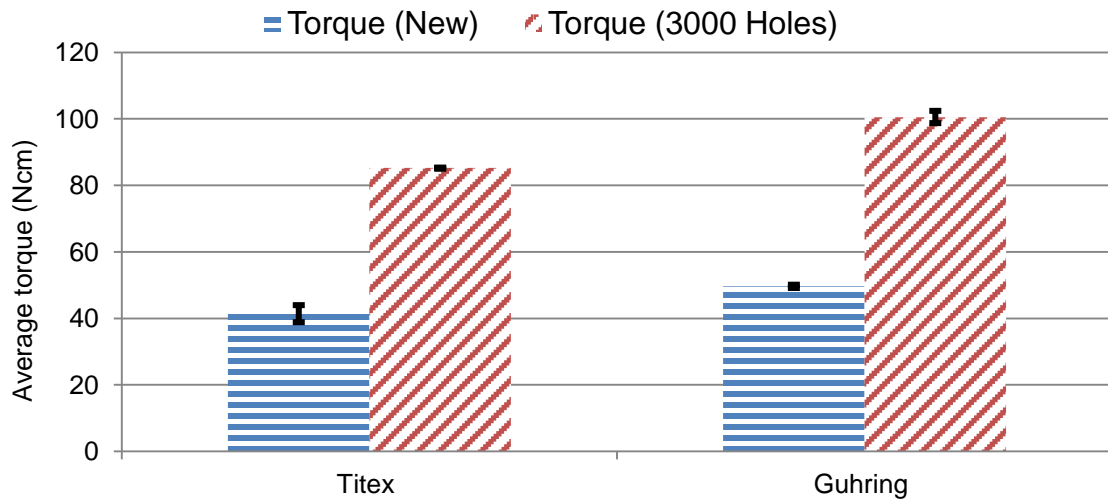


Figure 106: Average maximum drilling torque by Titex and Guhring drills

The average hole surface roughness produced by both the uncoated and coated drills was relatively low with Ra values ranging from 0.23-0.75 μm for the former and 0.31-0.37 μm for the latter during the duration of the trial, see Figure 107. The higher roughness value obtained with the coated tools when new was most likely due to greater amounts of adhered material. Nevertheless, results were within acceptable limits for the drilling operation, as hole roughness is expected to improve following a finishing/reaming operation.

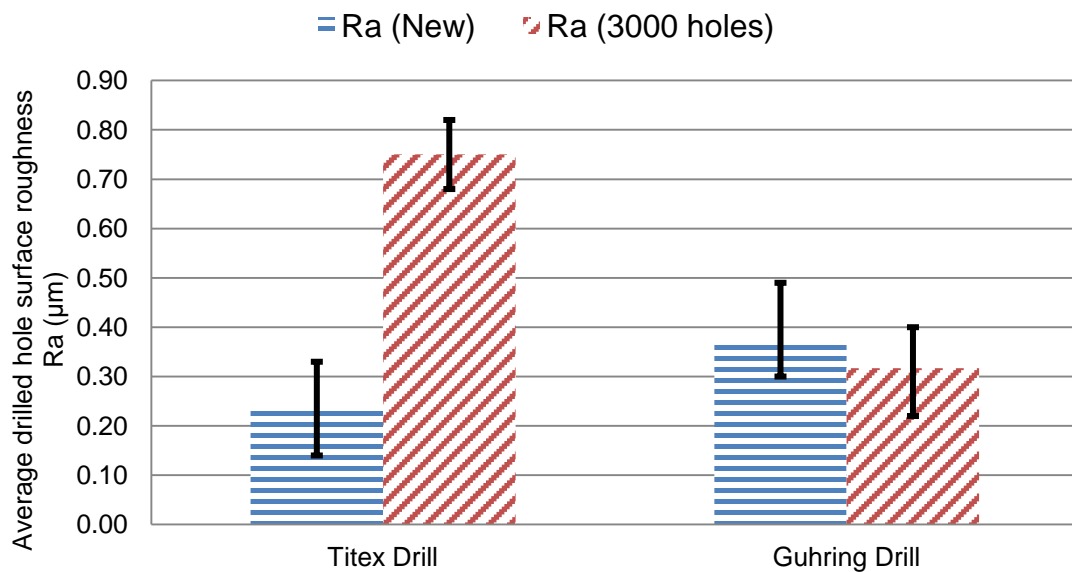


Figure 107: Average workpiece surface roughness by Titex and Guhring drills

Based on the results obtained, an analysis of the cost per component (excluding the cost of tool changing time and labour) showed that the uncoated carbide drill was ~27% lower in comparison to the TiN coated tool (0.53 vs. 0.73p/unit) when blind hole drilling of the aluminium compressor impellers, see Table 42.

Table 42: Operation cost of drills

	Titex A1167B	Guhring 611
Tool cost (p)	1,600	2,400
Tool life (components)	3,000	3,300
Cost of drilling operation (p/unit)	0.53	0.73

5.1.2.3 Phase 2C: WC and PCD reamers (Operation 4, blind-hole reaming)

The tool life for the carbide Beck RV3188 ($\phi 5.090\text{mm}$) Mapal PCD CTB002 ($\phi 5.090\text{mm}$) reamers was 3000 and 4880 components (after which the hole diameter was out of tolerance) respectively. Following regrinding and resizing of the latter to 5.080mm (due to variety/change in impeller production), a second trial resulted in a further 6319 holes giving a total of 11,199 components machined. The relatively large variation in the tool life of the PCD reamer (30%) between the first and second run was due to the difference in the initial geometrical size of the cutter. For the first trial, the reamer was fabricated to approximately $1\mu\text{m}$ below the nominal diameter while for the second trial (first regrind), it was ground oversize by $+2\mu\text{m}$. This meant that the tool life of the PCD reamer could be maximised by ensuring the tool diameter was towards the upper limit of the tolerance band. The third production tooling trial (second regrind) of the PCD reamer was incomplete due to discontinuation of the impeller production with $\phi 5.080/5.090\text{mm}$ bore/hole size. The reamer however machined 900 components prior to the discontinuation. The completion of the third PCD tooling trial required extensive machining hours (~ 135 hours) which was difficult due to the smaller job batches and wider variety of components (hole diameter and/or depth) in place. Figure 108 shows the schematic tool reground area on the PCD blank.

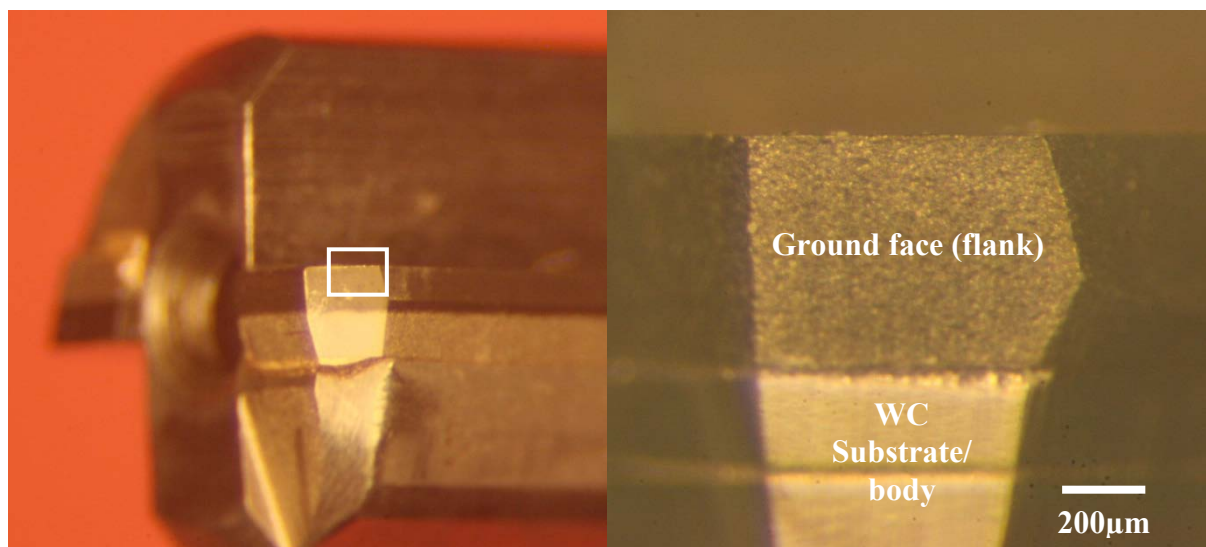


Figure 108: Schematic tool reground area on the PCD blank

In terms of capital cost, the PCD reamer was over 7 times higher than the price of the carbide equivalent (£356 vs. £49). Table 43 details operational costs for the reamers. The PCD tool allowed up to 3 regrinds and assuming that 6200 components could be machined before the hole diameter moved out of specification, the total tool life would be ~24800 components. Hypothetically, based on the production tool life, the Mapal PCD and the uncoated Beck reamers would work out to cost ~1.80p/unit and ~1.63p/unit respectively. Generally, the average tool setup time for the carbide reamer ranged between 20-40 minutes, which includes the time taken for tool holder re-grease and readjustment, in order to achieve hole diameter and surface finish tolerances. In contrast, the average tool setup time for the PCD reamers was <10min, due to relatively higher tool cutting edge precision/quality, which provided considerable benefits (average ~67% setup time saved) towards overall productivity.

Table 43: Operational cost of reamers

	Beck RV3188	Mapal CTB002	Mapal CTB002 (after one regrind)	Mapal CTB002 (after two regrinds)	Mapal CTB002 cumulative
Tool cost (p)	4900	35693	3000	3000	41693
Tool life (components)	3000	4880	6319	900*	12099
Cost of reaming operation (p/unit)	1.63	-	-	-	3.45

* *Incomplete tool life trial*

5.2 Laboratory based work

5.2.1 Phase 3A: Evaluation of diamond-like carbon coated tools when drilling cast C355 aluminium alloy

5.2.1.1 Tool life/wear and workpiece material adhesion

Optical microscope assessment of the drill chisel edges showed extensive wear with coating layers completely removed at the end of the experiment (hole 307). The Graphit-iC™ coating however was seen to minimise workpiece adhesion compared to the uncoated tools, regardless of cutting parameters and environments used. Conversely, a large amount of aluminium packing was evident between the drill flutes of the Dymon-iC™ coated drills, particularly when cutting at lower cutting speed under low pressure/flood conditions. It was expected that material packing would eventually deteriorate swarf extraction and diminish hole quality as the number of drilled holes increased. Furthermore, the material build up on

the drill flutes was thought to be promoted by the rough surface of the carbide substrate after the coating was peeled off. Built-up edge was also observed on all drills (tool flank and chisel edge) but was minimised at the higher cutting speed, as the cutting temperature raised and contact area between the tool rake and the chip/swarf was minimal [73]. Figure 109 to Figure 114 show micrographs of the built-up edge and adhered workpiece material on tools at the end of test in Test 1 to 12. High pressure fluid application noticeably helped minimise BUE of the tools regardless of the cutting speed, as the fluid access/lubrication to the cutting zone and chip clearance improved.

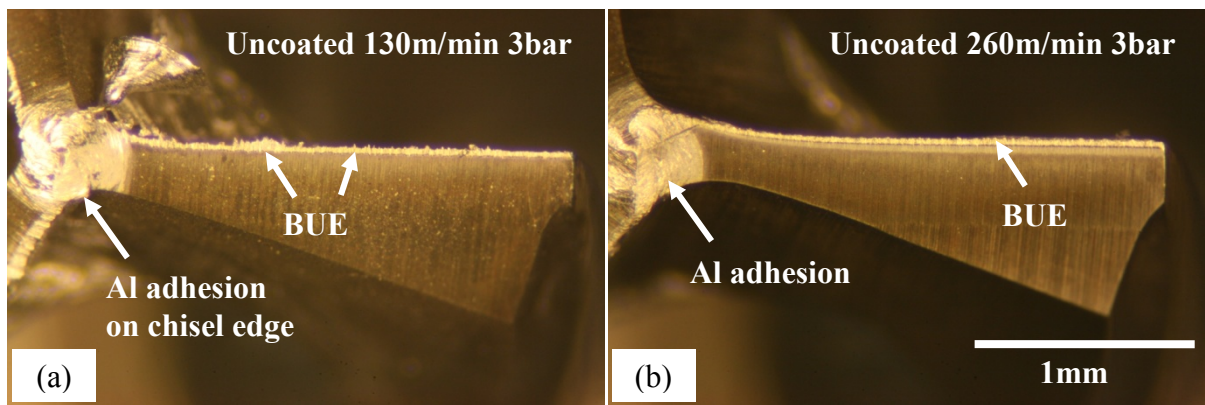


Figure 109: End of test micrographs of uncoated carbide drills in (a) Test 1 and (b) Test 2

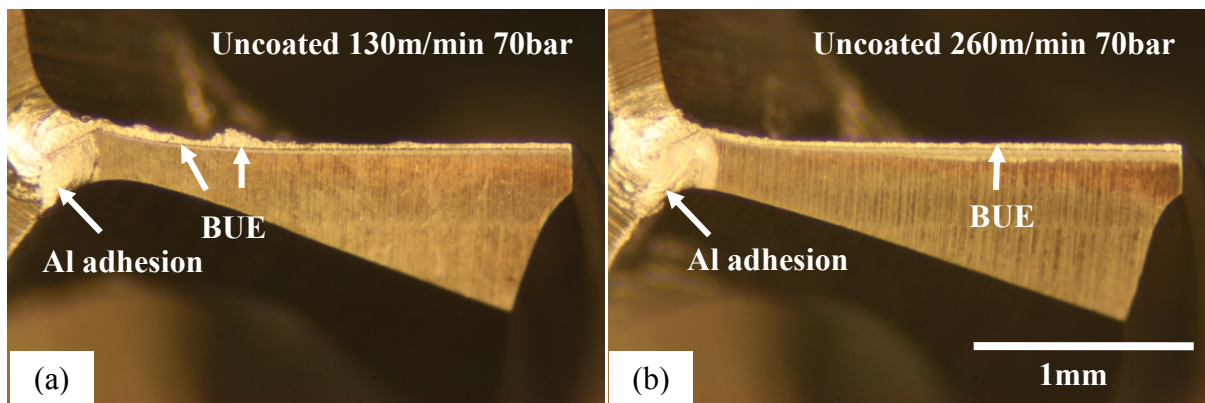


Figure 110: End of test micrographs of uncoated carbide drills in (a) Test 7 and (b) Test 8

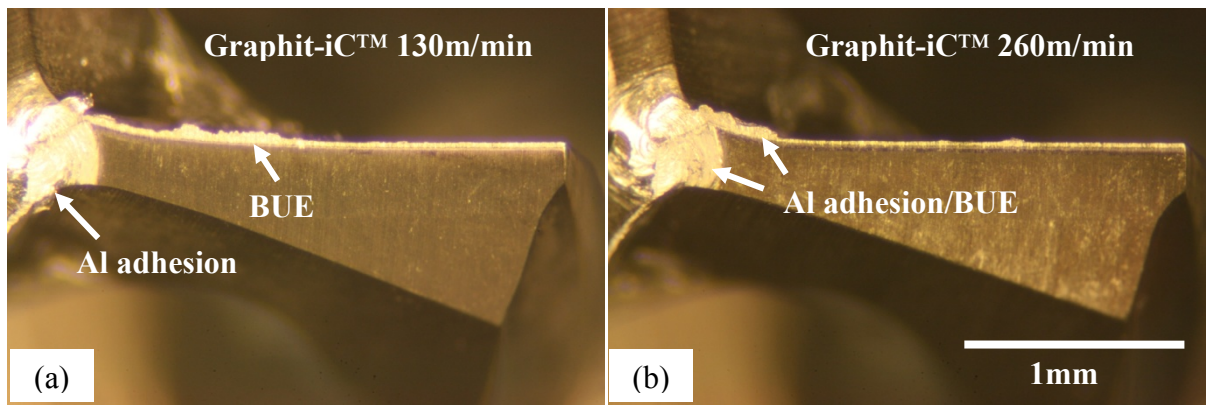


Figure 111: End of test micrographs of Graphit-iC™ coated drills in (a) Test 3 and (b) Test 4

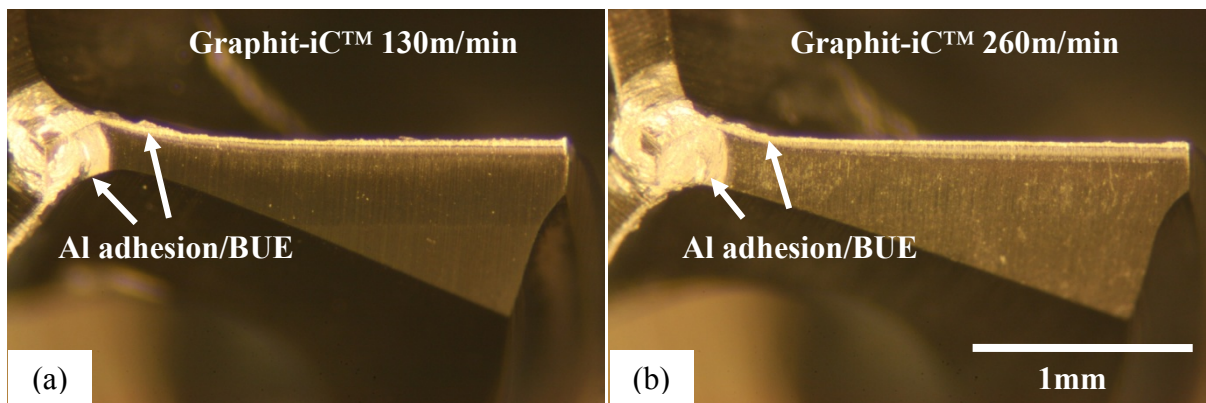


Figure 112: End of test micrographs of Graphit-iC™ coated drills in (a) Test 9 and (b) Test 10

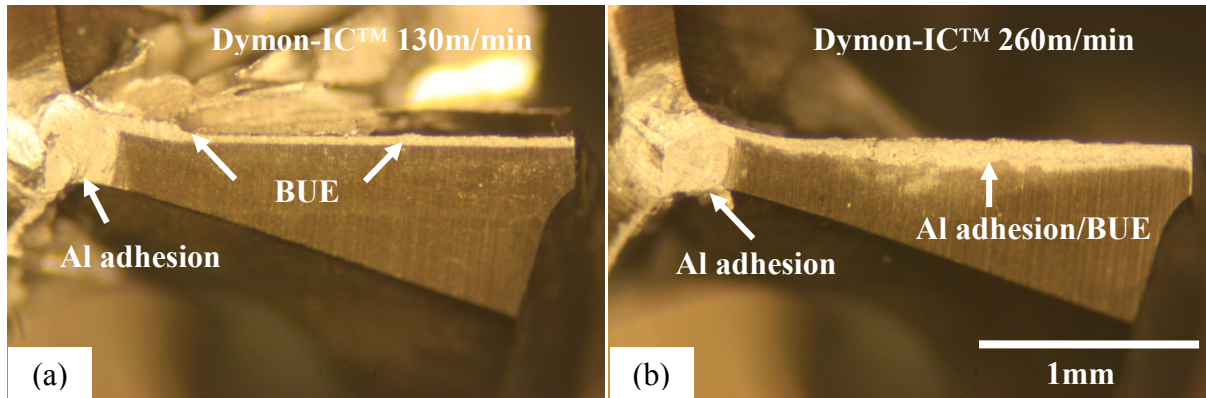


Figure 113: End of test micrographs of Dymon-iC™ coated drills in (a) Test 5 and (b) Test 6

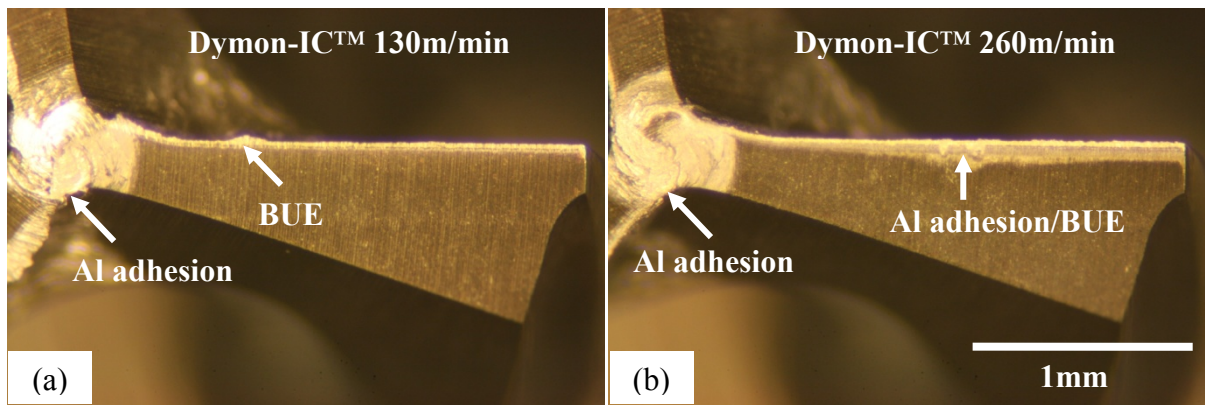


Figure 114: End of test micrographs of Dymon-iC™ coated drills in (a) Test 11 and (b) Test 12

Wear progression on the drill flank and chisel edges was generally gradual in all of the tests performed. No signs of cutting edge fracture were detected irrespective of operating conditions. Figure 115 details the flank wear curves for trials undertaken with low pressure fluid application (Tests 1-6).

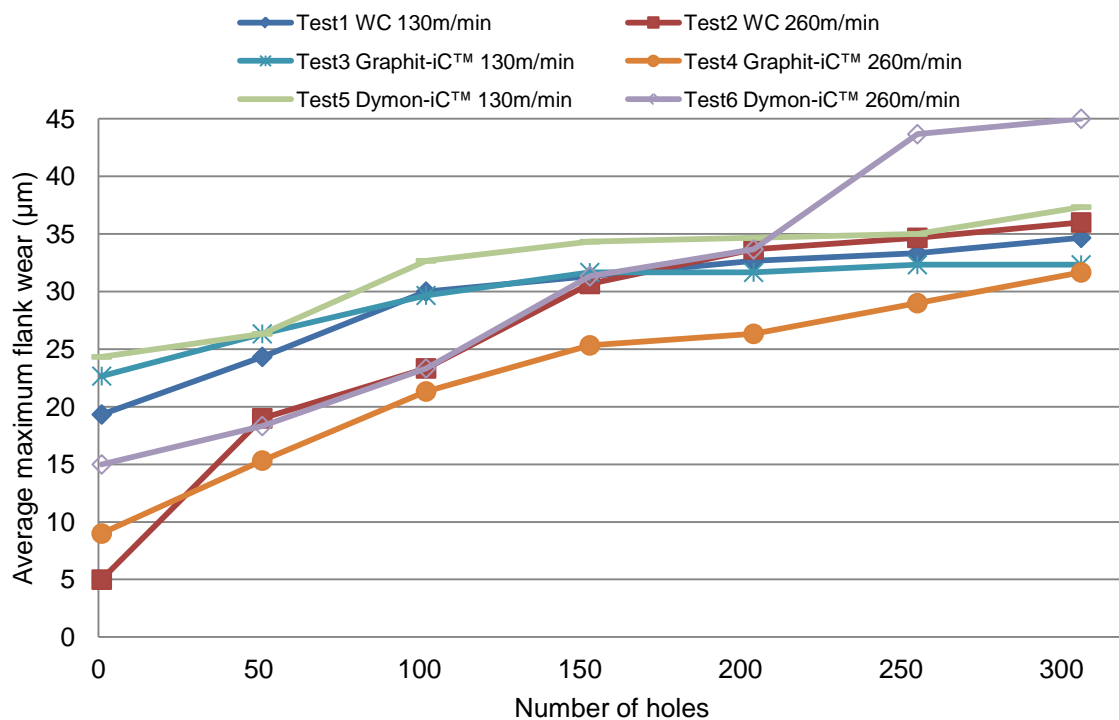


Figure 115: Phase 3A – Drill wear curves under low pressure cutting fluid application

The test involving the uncoated WC drill exhibited an extensive wear rate (up to 50 holes) when operating at 260m/min with low pressure fluid (Test 2). The growth rate of the tool flank wear however gradually slowed down after 150 holes. The initial flank wear ($\sim 20\mu\text{m}$) after drilling the first hole was found to be much higher when drilling under the same test condition with the uncoated WC at a lower cutting speed of 130m/min (Test 1). In

contrast, end of test flank wear was marginally higher (~6%) when machining with the uncoated WC at higher cutting speed (Test 2). The corresponding micrographs in Figure 109 indicate that worn chisel edge and material adhesion/BUE had an effect on the wear progression on the drills, possibly causing tool to chip due to immense compressive stresses and its adhesion to the tool surface [12]. Chisel edge wear and adhered material on the cutting edge were visible after drilling the first hole in Test 1. See micrographs in Appendix C. This resulted in a high initial wear (~20µm), of the uncoated WC in Test 1, while the drill used in Test 2 exhibited minimal chisel edge wear and Al adhesion leading to a lower initial value of flank wear (~5µm). A similar trend was also observed in Tests 3 and 4.

The Dymon-iC™ coated drill (Test 5) exhibited higher initial wear (~24µm) when machining at 260m/min cutting speed with low pressure fluid compared to Test 6 (~15µm) at lower cutting speed under the same environment. The corresponding micrographs in Appendix C show higher initial BUE formation on the drill cutting edge used in Test 5 after drilling the first hole, but there was no significant growth of BUE after hole 150. Despite the absence of initial BUE on the drill employed in Test 6, significant Al adhesion was observed on the flank surfaces of the drill after hole 200. This also reflected the high wear rate shown in Figure 115.

Figure 116 shows flank wear curves for trials under taken with high pressure fluid (Tests 7-12). Regarding the effect of the tool coating, it was observed that the Graphit-iC™ coating consistently exhibited lower (~15%) flank wear compared to that observed with the Dymon-iC™ coating, regardless of the cutting speed and environment. The Graphit-iC™ coating is reported to perform better in a water-based environment, whereas the Dymon-iC™ coating suffered from severe wear [174]. The wear progression in Figure 115 is in agreement with this observation.

The use of high pressure cutting fluid, irrespective of the cutting speed, was found to reduce (~13%) tool wear levels which was attributed to the improved access of cutting fluid to the cutting zone towards the bottom of the hole. Furthermore, the high pressure fluid application effectively allowed better lubrication between the chip and tool cutting edge, thereby limiting the formation of BUE/material adhesion observed in the micrographs. In almost all cases, flank wear did not exceed 41µm at test cessation.

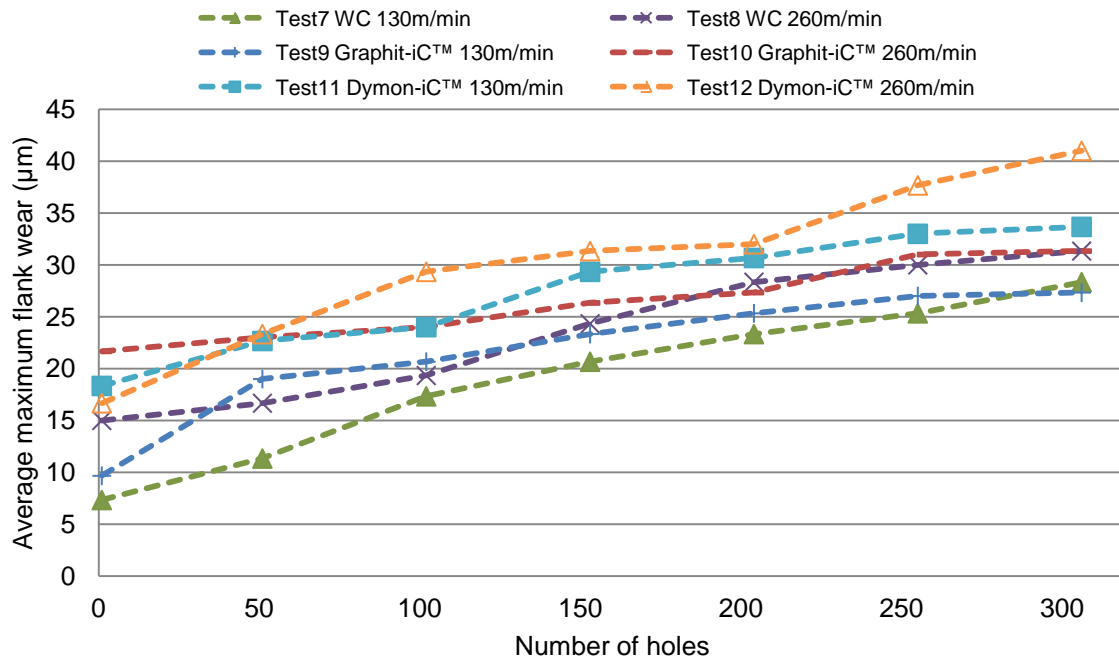


Figure 116: Phase 3A – Drill wear curves under high pressure cutting fluid application

5.2.1.2 Cutting forces

Figure 117 shows thrust force produced during drilling of the cast C355 alloy under the different conditions employed. In general, thrust force gradually increased (<5% on average from start to end of test) with the number of holes drilled due to tool wear progression.

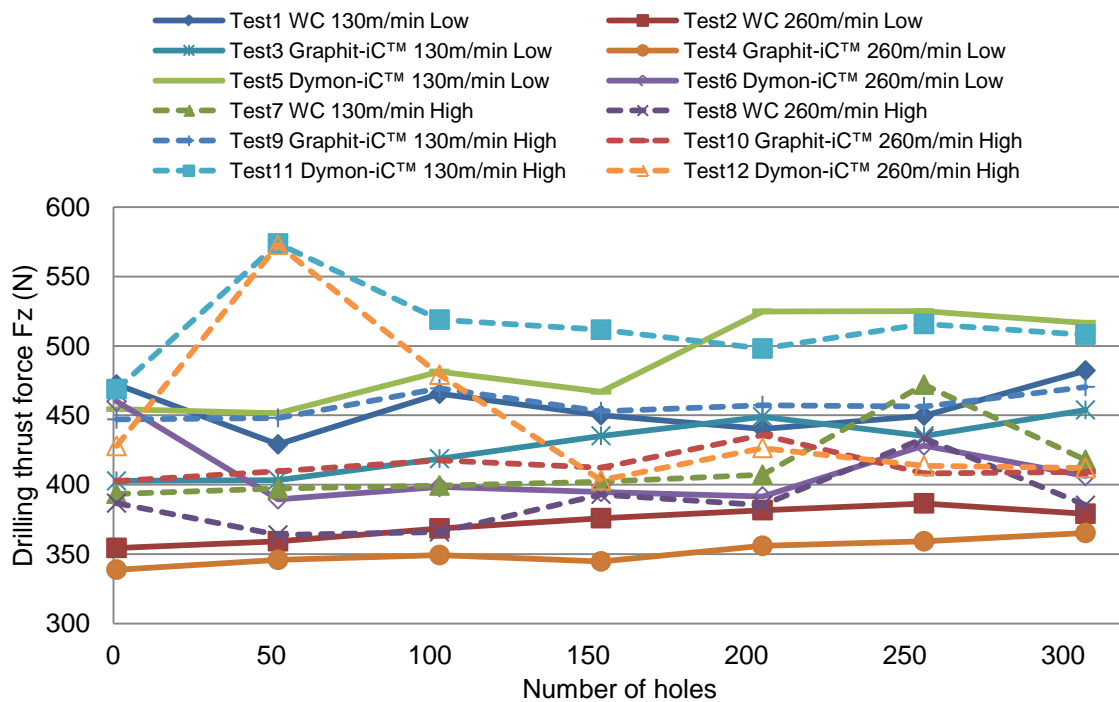


Figure 117: Phase 3A – Drilling thrust force for all tests

Thrust forces produced by the Dymon-iC™ coated drills were higher than for the corresponding Graphit-iC™ and uncoated tools (10% and 19% respectively) with a maximum F_z of 573N when operating at 130m/min speed with high pressure cutting fluid. This was likely due to the extensive adhered material on the chisel edge of the Dymon-iC™ coated drill observed in the micrographs together with high initial wear rate (up to hole 150) previously detailed in Figure 116. Fluctuations in the cutting force patterns however were observed in a number of experiments (Test 11 and 12), which saw a sharp increase after 50 holes followed by a drop after 100 holes. This was thought to be due to possible irregularities in the cast workpiece material properties, together with inclusions, silicon particle, etc., in certain regions. Figure 118 shows the typical example of casting impurity in the workpiece.

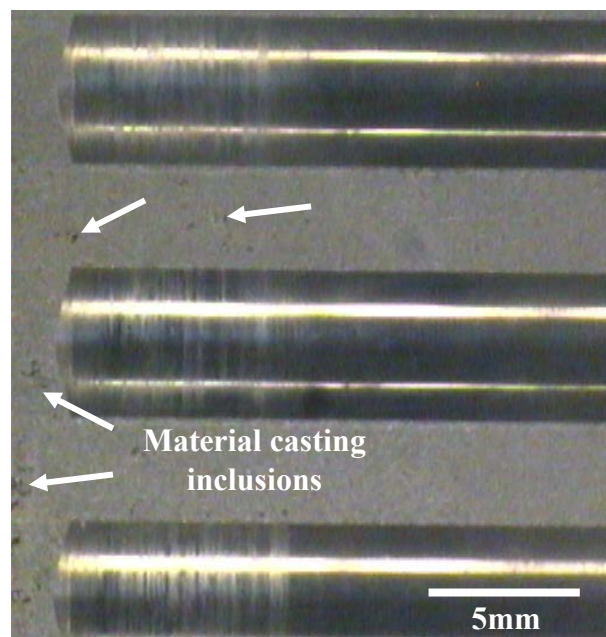


Figure 118: Typical impurity/defect found within the work material

When using low pressure flood cooling, thrust forces were lower (~80N) when the cutting speed increased to 260m/min. Similarly, Kelly and Cotterell [70] reported a reduction in feed force with an increase in machining speed when drilling a 30mm aluminium alloy ACP 5080 plate. In addition, Davim [26] observed a 50% reduction in the cutting force when the cutting speed was increased from 60-420m/min during the machining of Al 2024 T6. He suggested that a reduction in the cutting force was due to lower plastic deformation and increased power spent at the tool-chip interface when at higher cutting speeds. While higher tool wear rates are expected with increasing cutting speed and temperature, a drop in thrust force can occur due to the decrease in contact area and reduction in shear strength of the workpiece material as a result of thermal softening [73].

Drilling torque trends in Figure 119 show a gradual increase with the number of holes drilled. Overall, under low pressure cutting fluid, the torque levels produced in tests under high cutting speed were lower (~16%) than in tests under low cutting speed. Under which condition, the Graphit-iC™ (Test 4) generated the lowest (52Ncm) torque level. The comparatively higher torque levels generated in tests under high cutting speed in combination with high pressure fluid environment (Test 8, 10 and 12) were due largely to the instability of the tool under the action of the latter.

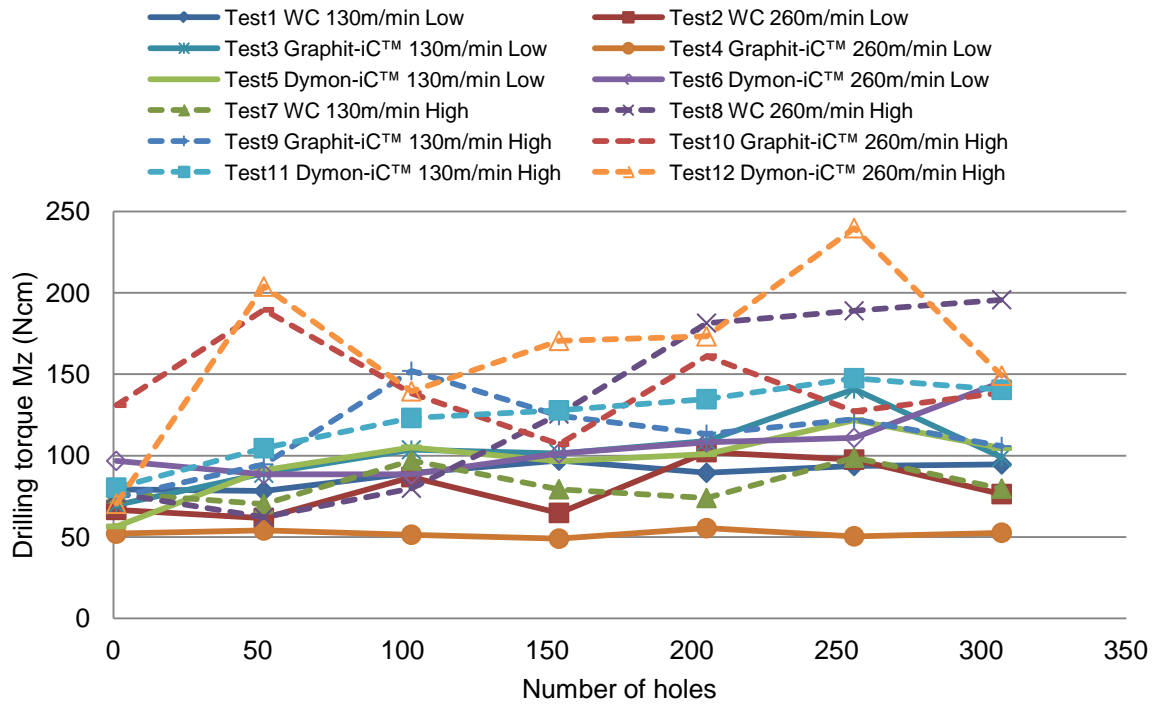


Figure 119: Phase 3A – Drilling torque of all tests

5.2.1.3 Workpiece quality

Drilled hole diameter measured using the Diatest showed that average values for all samples were within $4.8 +0.015/-0.010\text{mm}$, see Figure 120 and Figure 121. The hole size was found to be more consistent (less variation and deviation from nominal diameter) when machined under high pressure fluid application, although the majority of tests produced undersized holes (except Test 7 and Test 12). This was most likely due to enhanced access of fluid into the cutting zone, which minimised thermal expansion effects of the workpiece material [23, 55]. Furthermore, the 70bar fluid pressure was expected to reduce the formation of BUE ahead of the tool tip and entrapment of abrasive Al-Si chips between the cutting edge/flutes and the hole wall. Conversely, holes produced under flood coolant conditions were either oversized or up to $\sim 4\mu\text{m}$ below the nominal diameter.

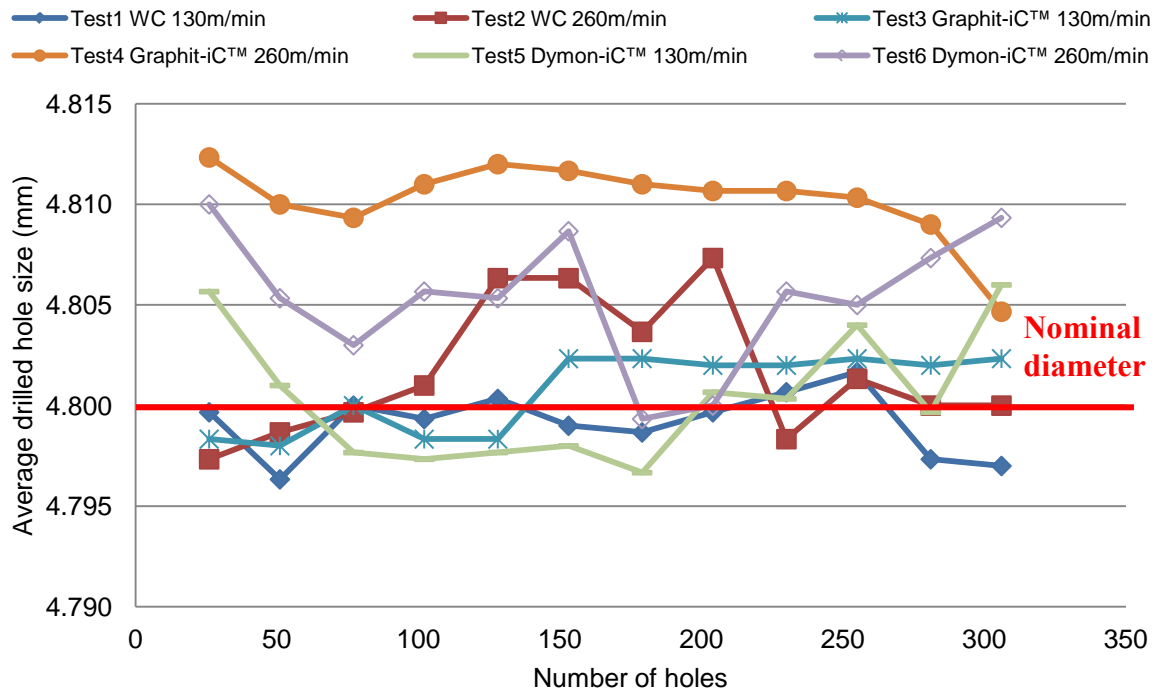


Figure 120: Phase 3A – Drilled hole diameter under low pressure/flood cutting fluid application

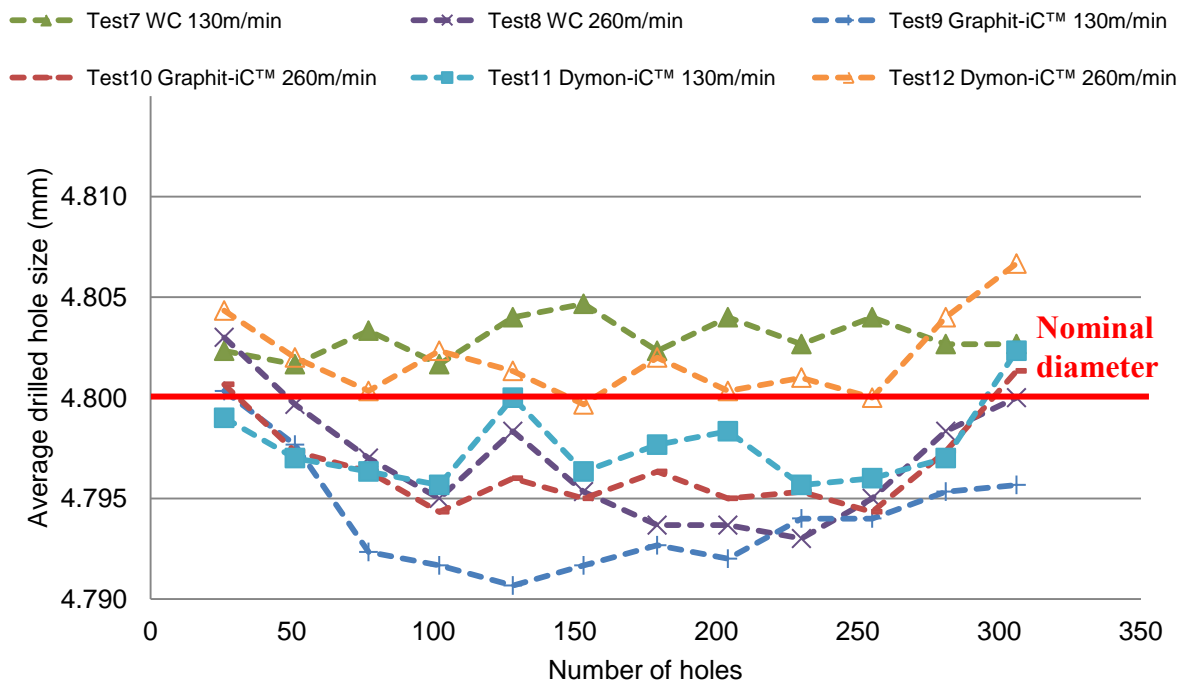


Figure 121: Phase 3A – Drilled hole diameter under high pressure cutting fluid application

Hole roundness produced in all tests were comparable and did not exceed $10\mu\text{m}$. Superior hole cylindricity results were typically obtained when drilling with the coated tools at low ($\sim 7\%$ better) and high ($\sim 30\%$ better) cutting speed under the flood cutting fluid condition. Drilled hole quality results are shown in Figure 122. Increasing the cutting speed

from 130m/min to 260m/min was found to have a detrimental effect on the overall geometrical accuracy of the drilled holes. Particularly, Test 2, 8, 10 and 12 produced poorer roundness (~84% poorer) and cylindricity (~27% poorer) results despite reduced BUE/adhesion observed in micrographs. The reason was possibly due to high pressure cutting fluid mechanical impact during the operation.

In terms of parallelism, Test 4 and 9 produced positive parallelism which suggests the drilled holes were larger at the entry position. The majority of measured specimens however showed negative parallelism values, which indicates that the drilled holes were larger towards the bottom, i.e. bell-shaped. Generally, the coated drills produced better (~70%) parallelism compared to the uncoated drills, particularly under high pressure fluid environment. This was most likely due to reduced adhered material/BUE observed under the micrographs in Figure 112 and Figure 114.

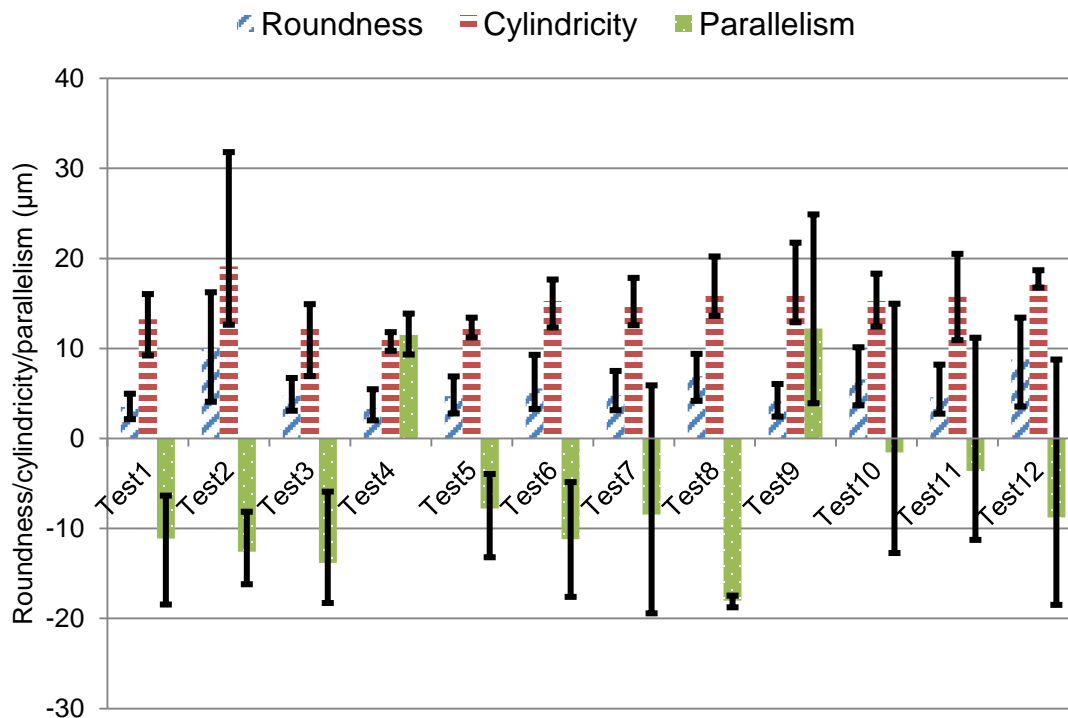


Figure 122: Phase3A – Drilled hole quality

5.2.1.4 Workpiece surface roughness and integrity

Figure 123 and Figure 124 show workpiece surface roughness results measured at the top and bottom positions of holes respectively. In general, initial hole surface roughness was relatively high (up to 2.1μm Ra) particularly with tests involving uncoated carbide tools in Tests 1, 2 and 8, but improved as testing progressed. This was likely due to a combination of high initial tool wear (after hole 1) observed in the previous tool wear profiles, Figure 115 and

Figure 116, together with excessive adhered material on the measured cross-sectioned sample. Further investigation of the cross-sectioned sample in Figure 125 showed evidence of scuff marks/adhered material, which was within the surface roughness evaluation length (4mm) that caused the initial high roughness profile. Overall hole surface roughness was (~ 2.5 times) lower at the hole entry position ($< 0.5 \mu\text{m}$ Ra after ~ 100 holes) compared to the bottom location due to the greater difficulty in swarf extraction further down the drill path. A similar observation was described by El-Khabeery et al. [229] following an investigation into the deep hole drilling of carbon steel. Surface roughness of the drilled holes (Test 7-12) evaluated under high pressure cutting fluid condition was $\sim 23\%$ lower when compared with tests (Test 1-6) performed in flood cutting fluid environment, most likely due to reduced formation of BUE ahead of the tool tip. The improved surface roughness also reflects the optical microscope observation of the cutting tools in Section 5.2.1.1. An unusually high roughness was measured after 200 holes in tests involving uncoated WC (Test 2) under low pressure cutting fluid at high cutting speed. This was also the result of adhered material similar to that shown in Figure 125.

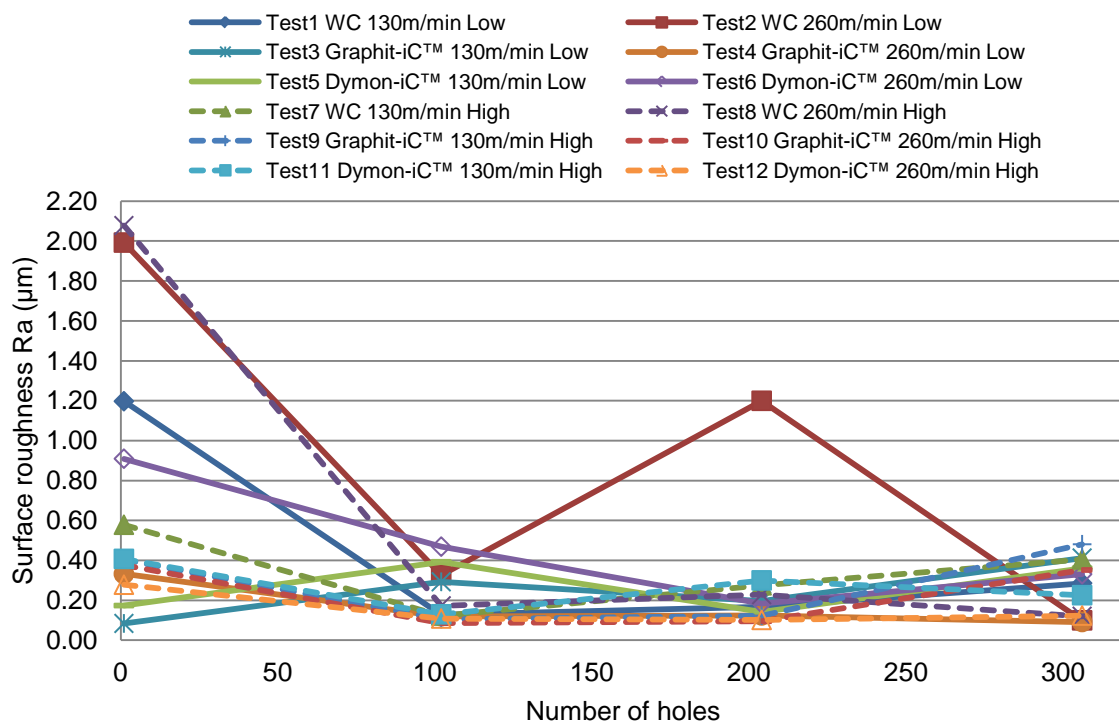


Figure 123: Phase 3A – Drilled surface roughness (2mm from hole entry)

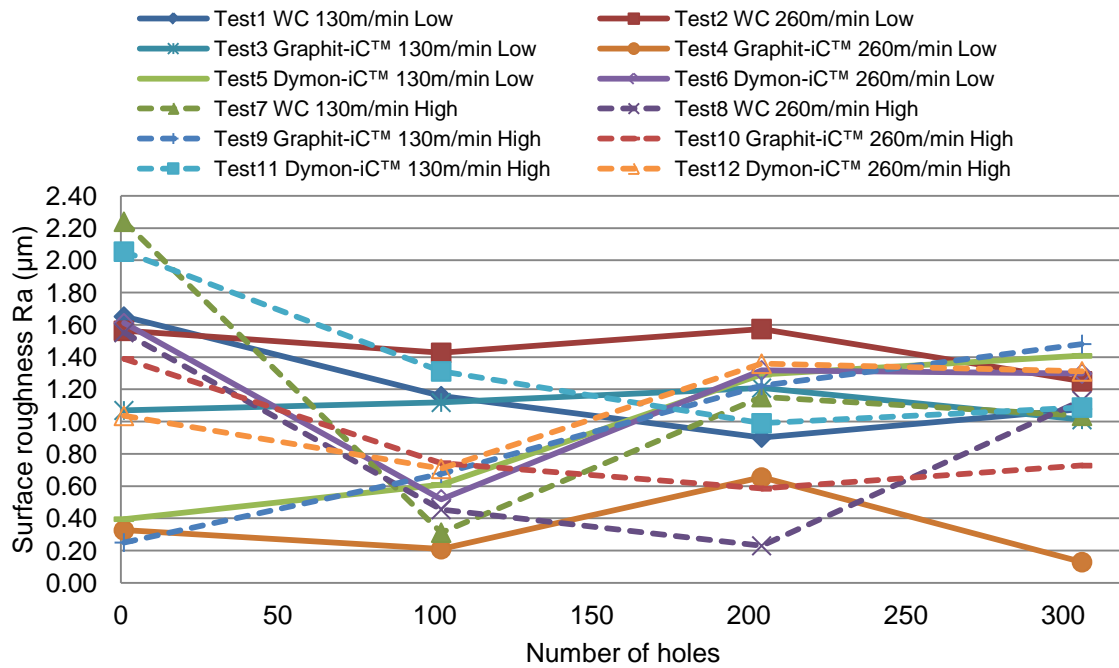


Figure 124: Phase 3A – Drilled surface roughness (23mm from hole entry)

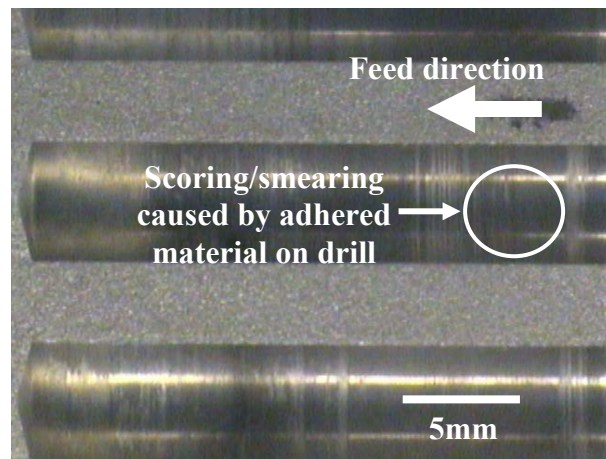


Figure 125: Typical adhered material observed on cross-section of hole

Microhardness evaluation was carried out on selected holes produced at the start (hole 1), middle (hole 154) and end of test (hole 307), for Tests 7, Test 9 and 11, which showed comparatively low tool flank wear and high overall hole quality, in terms of hole geometry. The microhardness depth profiles obtained from drilled hole 1 were close to the material bulk hardness (140HV/154HK), see Figure 126, and suggest no strain hardening. Conversely, the microhardness levels in Figure 127 (drilled hole 154) and Figure 128 (drilled hole 307), to a depth of $\sim 75\mu\text{m}$, show a $\sim 16\%$ increase in hardness, which suggests strain hardening induced by surface deformation [230]. Furthermore, the trend indicates that the hardness increased with the number of holes drilled, owing to the rubbing between the tool and the workpiece as a result of tool wear [231, 232].

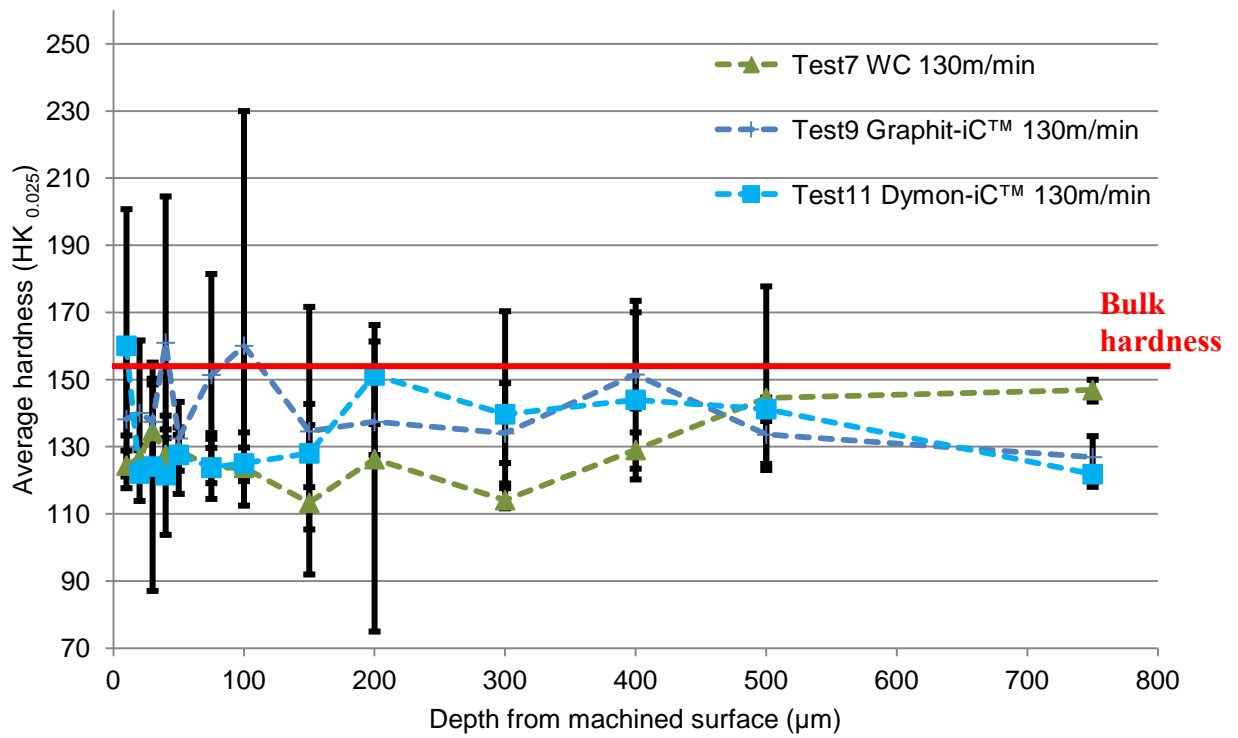


Figure 126: Phase 3A – Microhardness of cross-sections of drilled hole 1 (12mm from entry)

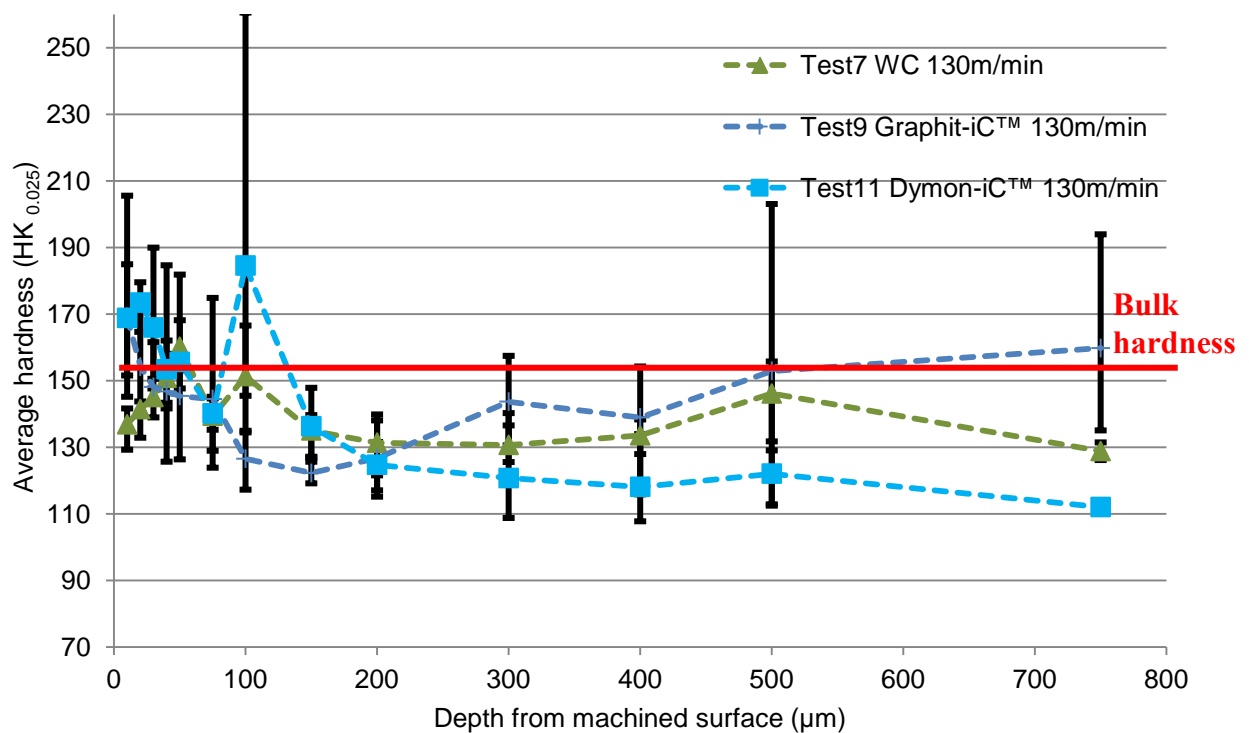


Figure 127: Phase 3A – Microhardness of cross-sections of drilled hole 154 (12mm from entry)

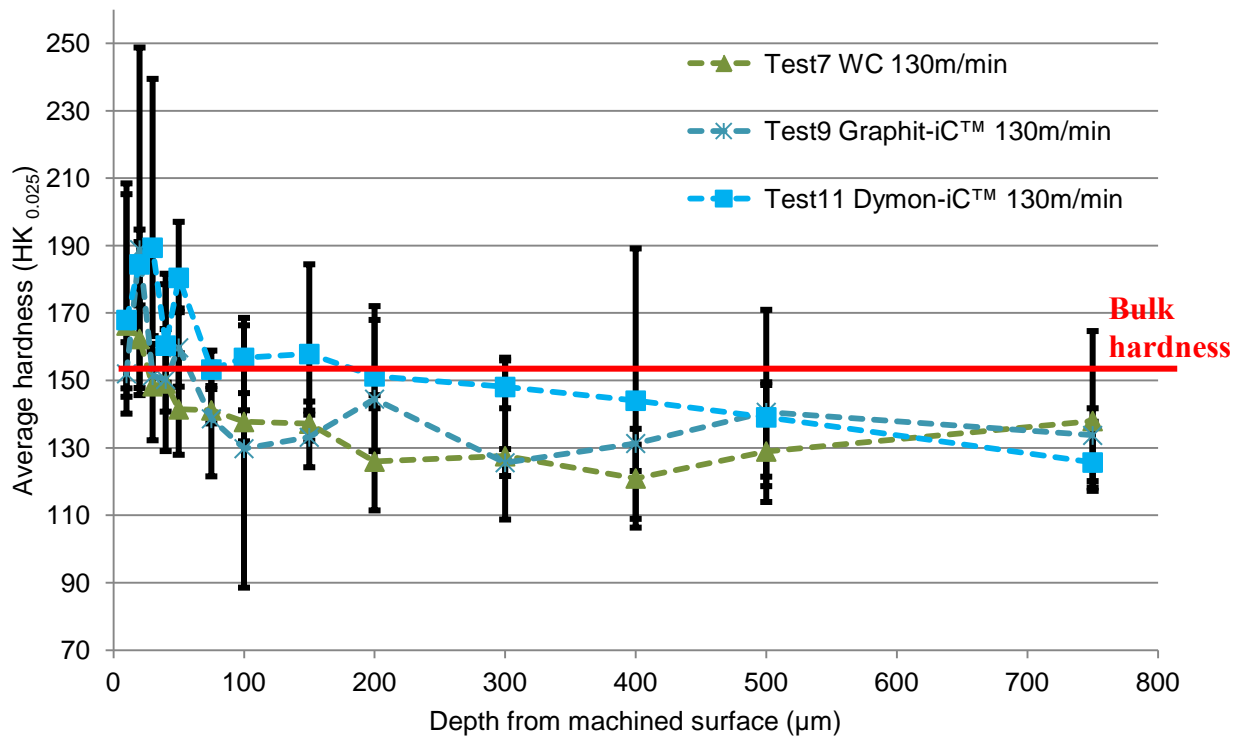


Figure 128: Phase 3A – Microhardness of cross-sections of drilled hole 307 (12mm from entry)

Analysis of the workpiece cross-sectional micrographs in Figure 129 showed that holes machined using the uncoated WC and Dymon-iC™ coated drills experienced small levels (up to 30μm) of pitting and tearing, although there was no evidence of plastic deformation or microcracks. Any microcracks induced during the cutting operation of the relatively ductile Al workpiece would diminish/heal [233]. In contrast, components machined with the Graphit-iC™ coating showed some minor surface irregularities, but no signs of pits or tears were detected.

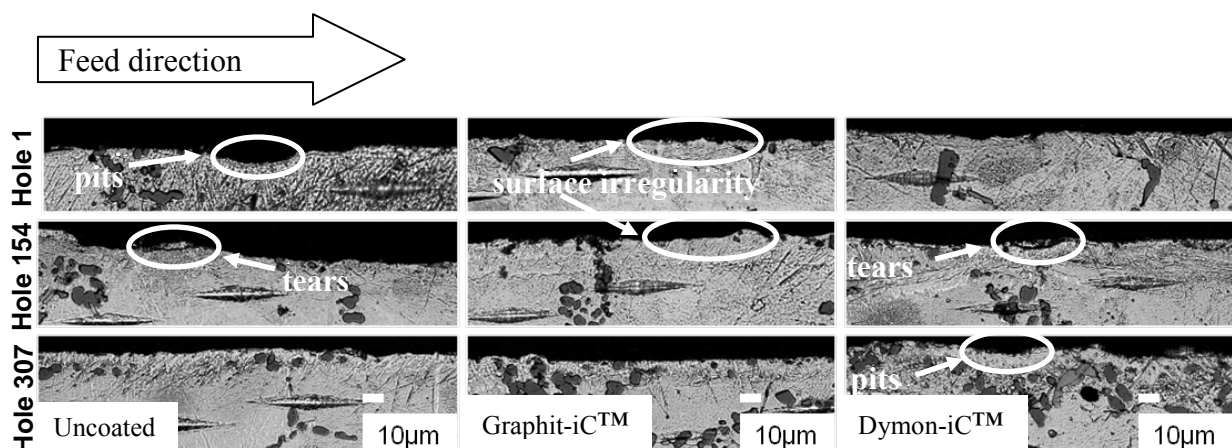


Figure 129: Phase 3A – Microstructure of subsurface of drilled hole (12mm from entry)

5.2.1.5 Production tooling trial of Graphit-iC™ coated drills

Based on the assessed results, the Graphit-iC™ coated drill was found to provide the best performance when drilling compared with the standard uncoated carbide and Dymon-iC™ coated tools. Benefits included the lowest tool wear rate, stable cutting forces, consistent hole geometry/quality and minimum workpiece damage. Graphit-iC™ coated drills were subsequently fabricated and installed on the Index G200 at Doncasters Sterling for production environment tool life trials involving the blind-hole drilling operation. A total of three trials were conducted and all drills produced conforming parts per customer requirement (5µm max. hole cylindricity), based on hourly production measurement records. Figure 130 shows the typical hole cylindricity measured during the trial (generated from Talyrond series 131) with a value of 3.05µm.

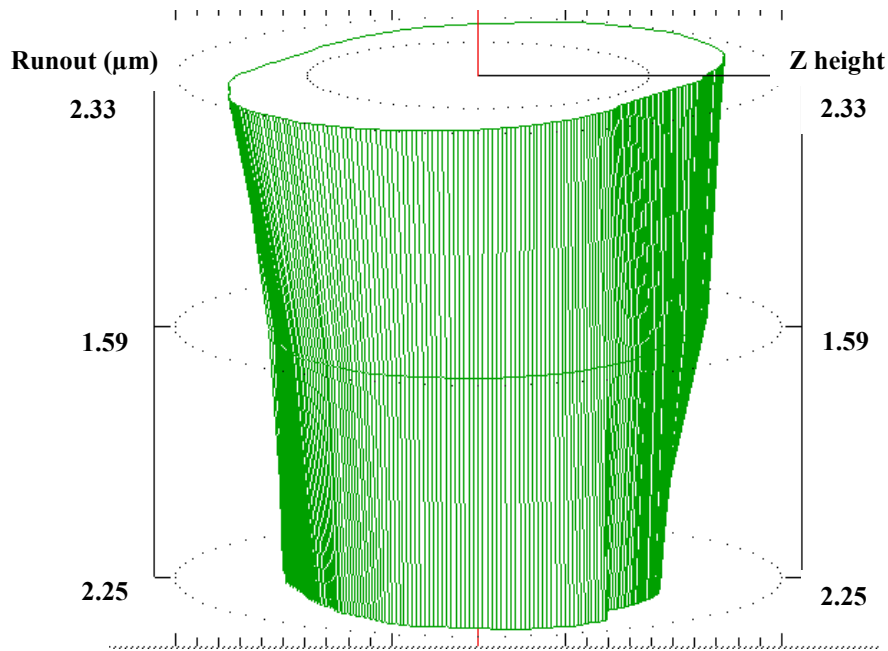


Figure 130: Phase 3A – Production trial hole cylindricity result by Graphit-iC™ (data produced on Talyrond series 131)

Drills in the first and second trial achieved 1826 and 1370 components prior to tool breakage caused by defective components (presence of blowhole and/or porosity). The final tool life trial was not completed due to an incorrect tool setup. Figure 131 shows the broken drills during the trials while Figure 132 shows the defective component together with the broken drill bit. Based on the production tool life study of Phase 2B and the laboratory based tool wear experiment in Figure 115, the uncoated WC drill produced 3000 holes with a wear

rate of $\sim 0.05\mu\text{m}$ per hole. The estimated production tool life of the Graphit-iC™ is 5000 holes per tool for a wear rate of $0.03\mu\text{m}/\text{hole}$. This being the case, the operational cost of drilling the aluminium impellers would be cheaper (0.35p/unit) when employing the Graphit-iC™ coated drill compared to that of the uncoated carbide tool (0.53p/hole).

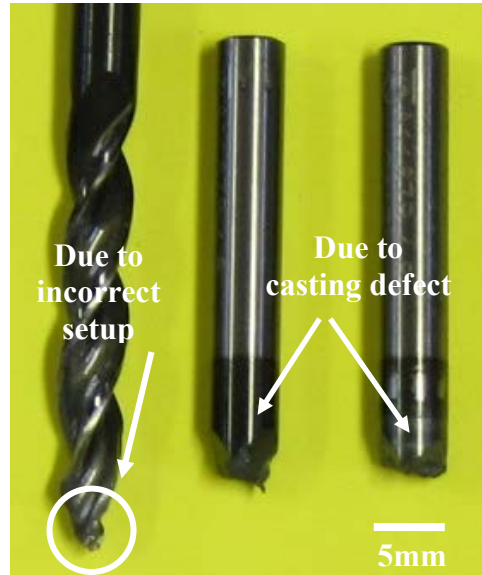


Figure 131: Phase 3A – Breakage of Graphit-iC™ drills during production trial due to incorrect setup and casting material defects

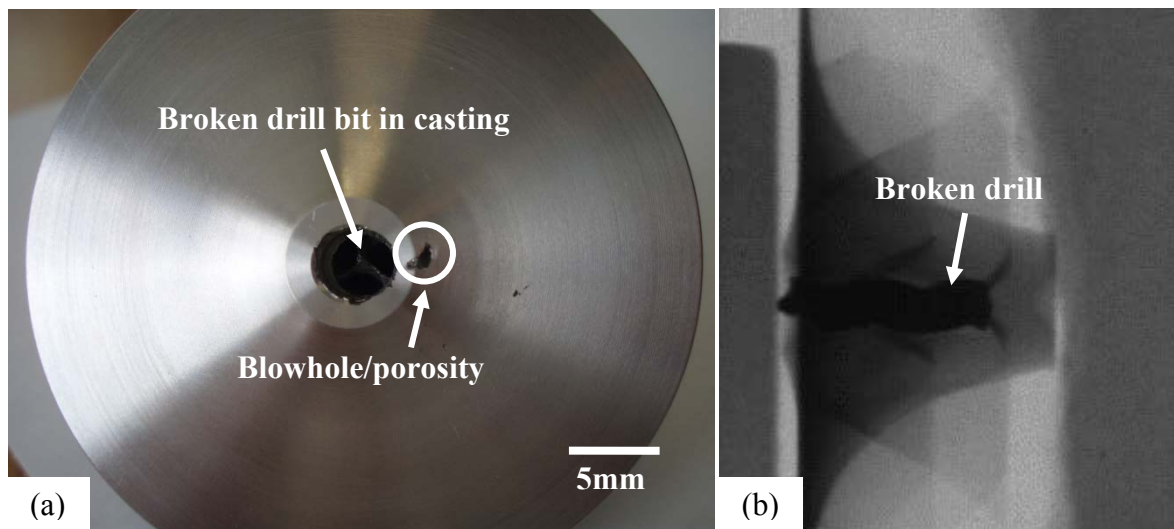


Figure 132: Photograph of (a) defect in material casting and (b) X-ray image of broken drill

5.2.2 Phase 3B: Evaluation of diamond-like carbon coated tools when reaming 6082-T6 aluminum alloy

5.2.2.1 Tool life/wear and workpiece material adhesion

Built-up edge, as a result of low temperature pressure welding, together with swarf deposit on the tool and tool holder were evident during the experiment in all tests performed at the lower cutting speed of 32m/min. Figure 133 details the tool condition and build up of swarf at the end of the trials.

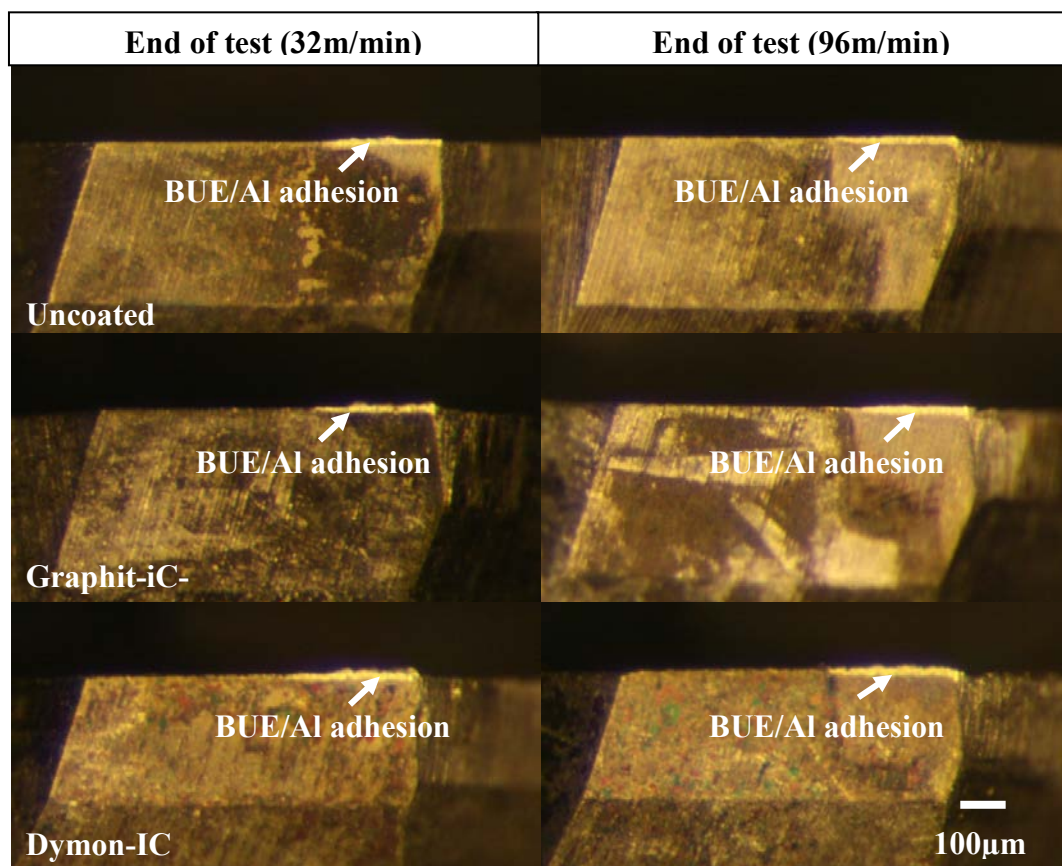


Figure 133: Phase 3B – Micrograph of tool wear and swarf build up at the end of test

Figure 134 shows the gradual tool flank wear progression against number of reamed holes for two different cutting speeds tested under the application of through spindle high pressure (70bar) cutting fluid. The average maximum flank wear scar (VB_{Bmax}) of the reamers was generally greater in experiments (from start to end of test) performed at higher cutting speed, Test 2 (19%), Test 4 (5%) and Test 6 (13%). It was evident that the swarf entrapment was less severe when operating at the cutting speed of 96m/min, see Figure 135.

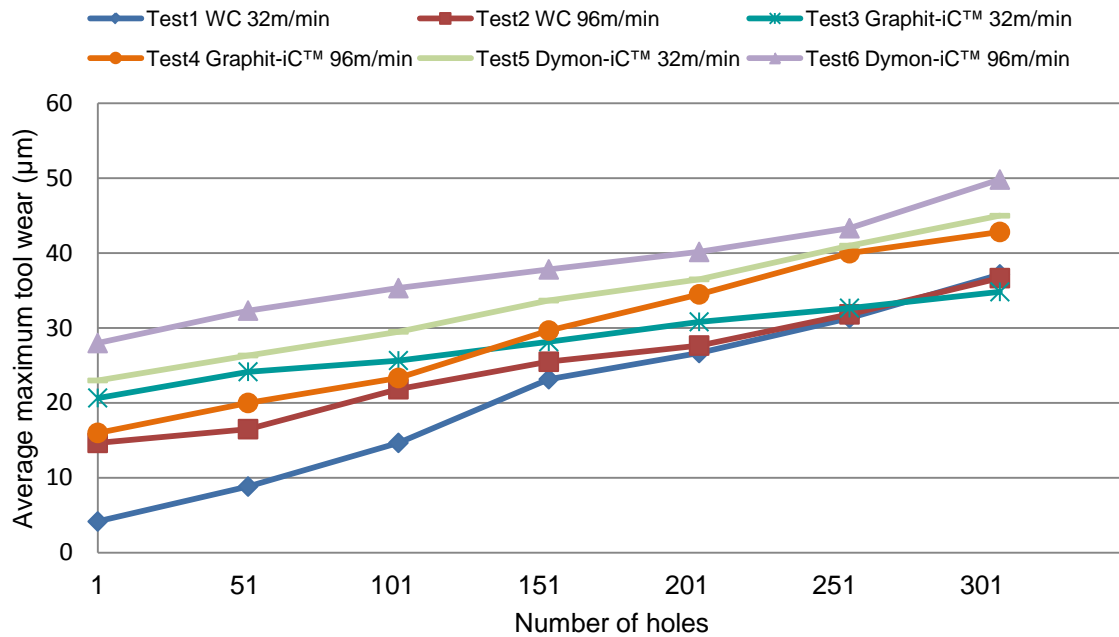


Figure 134: Phase 3B – Wear curve of reamers

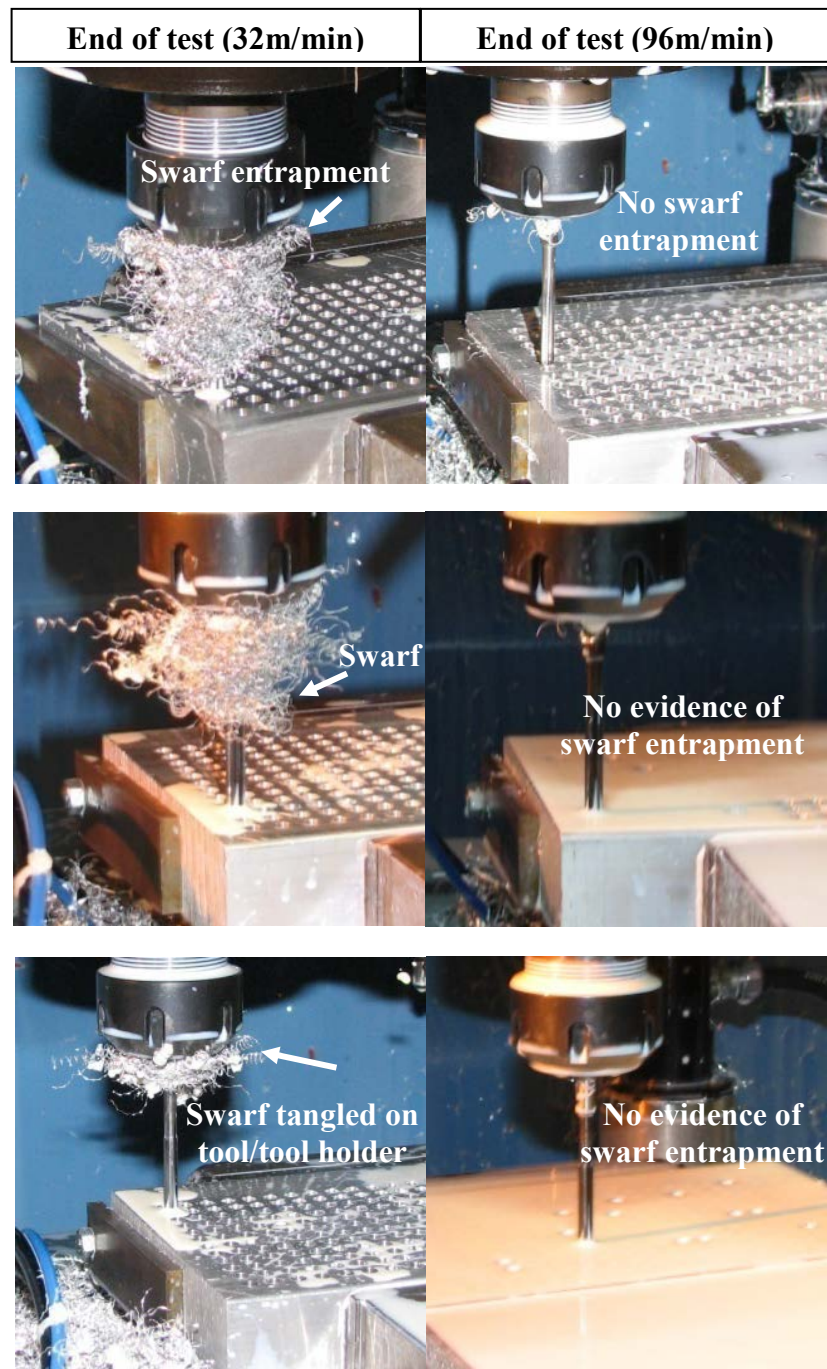


Figure 135: Phase 3B swarf entrapment of cutting tool/tool holder for low and high cutting speeds

Regardless of test conditions, the uncoated carbide reamers (Tests 1 and 2) showed the least initial wear after the first hole, followed by the Graphit-iC™ coated tool (Test 3 and Test 4). The wear rate of the uncoated WC reamer (Test 1) was $0.11\mu\text{m}/\text{hole}$ which was however ~150% and ~57% higher compared with the Graphit-iC™ (Test 3) and Dymon-iC™ (Test 5) coated tools respectively at low cutting speed. While the Graphit-iC™ coating had the lowest wear rate ($\sim 0.04\mu\text{m}/\text{hole}$) at 32m/min cutting speed, the Dymon-iC-IC ($\sim 1500\text{HV}$) coated

reamer was found to be marginally superior ($\sim 0.06\mu\text{m}/\text{hole}$) despite its lower hardness compared to the uncoated WC ($\sim 1550\text{HV}$) and Graphit-iCTM ($\sim 1800\text{HV}$) tools when cutting speed was increased to 96m/min. The calculated wear rate was up to $\sim 30\%$ lower which was attributed to the low friction coefficient (0.03) of the Dymon-iCTM coating. This suggests that the Dymon-iCTM product could potentially offer a significant increase in productivity of the high-volume compressor impellers at Doncasters Sterling, as reaming time per hole would be reduced by 66% by increasing the cutting speed from 32 to 96m/min.

5.2.2.2 Cutting forces

Reaming thrust force and torque profiles are shown in Figure 136 and Figure 137. Force levels generated in Test 1, involving the uncoated carbide, marginally increased by 8% to 35N (up to hole 51) before drifting below the level at which the test commenced. The thrust force significantly increased by $\sim 37\%$ towards the test cessation due to a greater amount of BUE formation, as shown in Appendix D. It was observed that the duration of the force increment was more extensive (up to hole 151) when the cutting speed increased to 96m/min (Test 2). This thrust force level however notably decreased by $\sim 46\%$ after hole 151. Tests 3 and 4 also generated a similar trend for the same test duration. Tests 5 and 6, involving the Dymon-iCTM coated drills, produced higher initial thrust force levels before dropping to the same average level as the other tests after hole 103. The fluctuating trend of the thrust force measured in tests involving Dymon-iCTM coated tools was most likely caused by the greater extent of BUE formation evident in the micrographs shown in Appendix D. The micrographs also show BUE reducing with increased cutting speed in all tests. Higher cutting temperatures associated with greater machining velocity have been known to reduce frictional effects at the tool-chip interface. This was demonstrated by Moufki et al. [234], who observed a decrease in the mean coefficient of friction as the average temperature rose following an increase in cutting speed. Work by Nayebi et al. [235] further supported this conclusion where similar results were obtained with increased feed rate and cutter rotational speed.

Torque levels (Test 1-6) after hole 205 were stable, ranging between 13-17Ncm towards the test cessation. Unusual torque peaks were detected in Tests 3 and 4 at the start of the experiment and in Tests 2 and 4 after hole 154. Micrographs show no excessive material build up on the tool cutting edge and the cause of the sudden peaks was thought to be the variation (hardness property, casting defects, etc.) of the workpiece material. In any case, both

the thrust force and torque levels generated by the reamers were considered to be relatively insignificant.

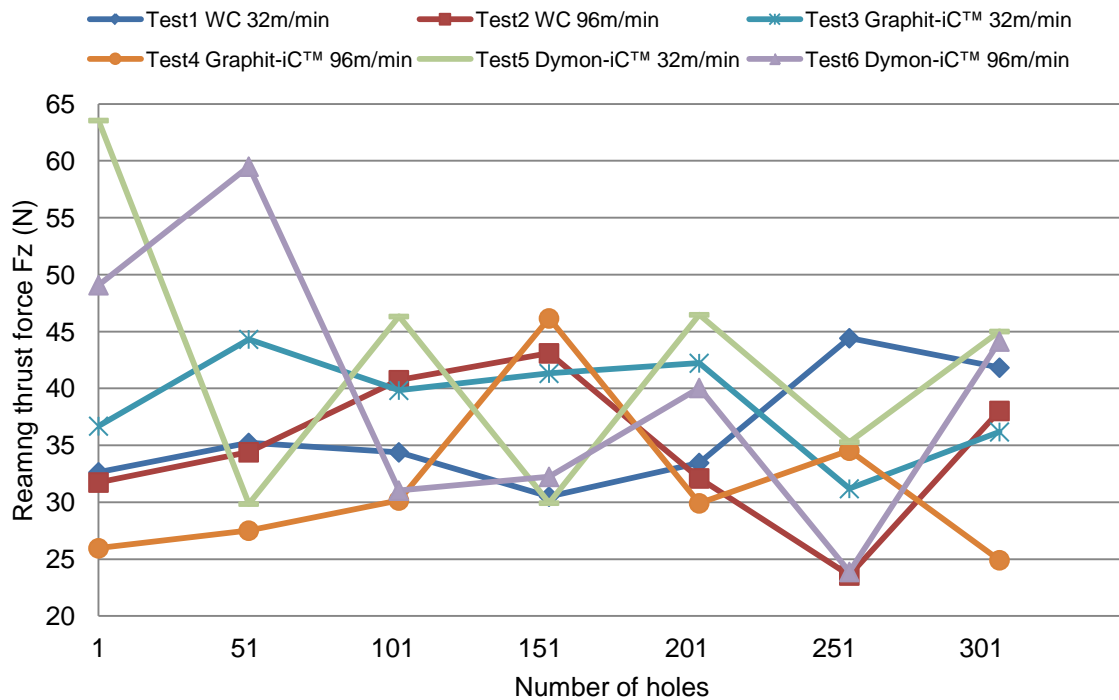


Figure 136: Phase 3B – Reaming thrust force

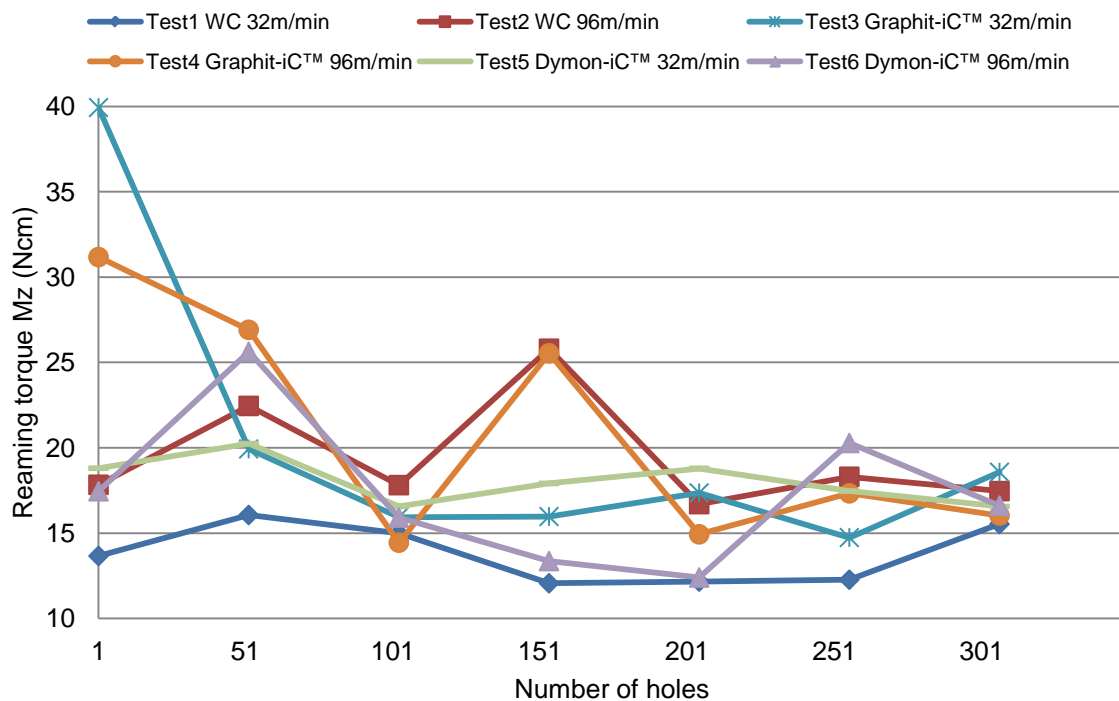


Figure 137: Phase 3B – Reaming torque

5.2.2.3 Workpiece quality

The average diameters of the reamed holes was mostly oversized, $>5.09\text{mm}$, although the values were generally consistent throughout the duration of tests, see Figure 138. The largest holes were produced by the Graphit-iC™ (Test 4) and the Dymon-iC™ (Test 6) coated tools when machining at 96m/min . Conversely, when operating at the lower cutting speed, hole diameters obtained utilising the coated reamers were comparable to those generated using uncoated WC tools ($5.091\text{--}5.094\mu\text{m}$). Data involving hole roundness, cylindricity and parallelism as detailed in Figure 139 further demonstrated that high speed operation appeared to be detrimental to hole quality, with the standard carbide reamers outperforming the coated tools in corresponding tests. However, all of the reamed holes produced at the lower cutting speed were within the roundness and cylindricity tolerance of $<5\mu\text{m}$ specified by Sterling. Positive values of parallelism were observed in most tests which meant that the holes towards the entry were larger than that towards the bottom. This is a common effect as tool deflection is the greatest as the reamer enters the predrilled hole, but improves as the reamed hole depth increases.

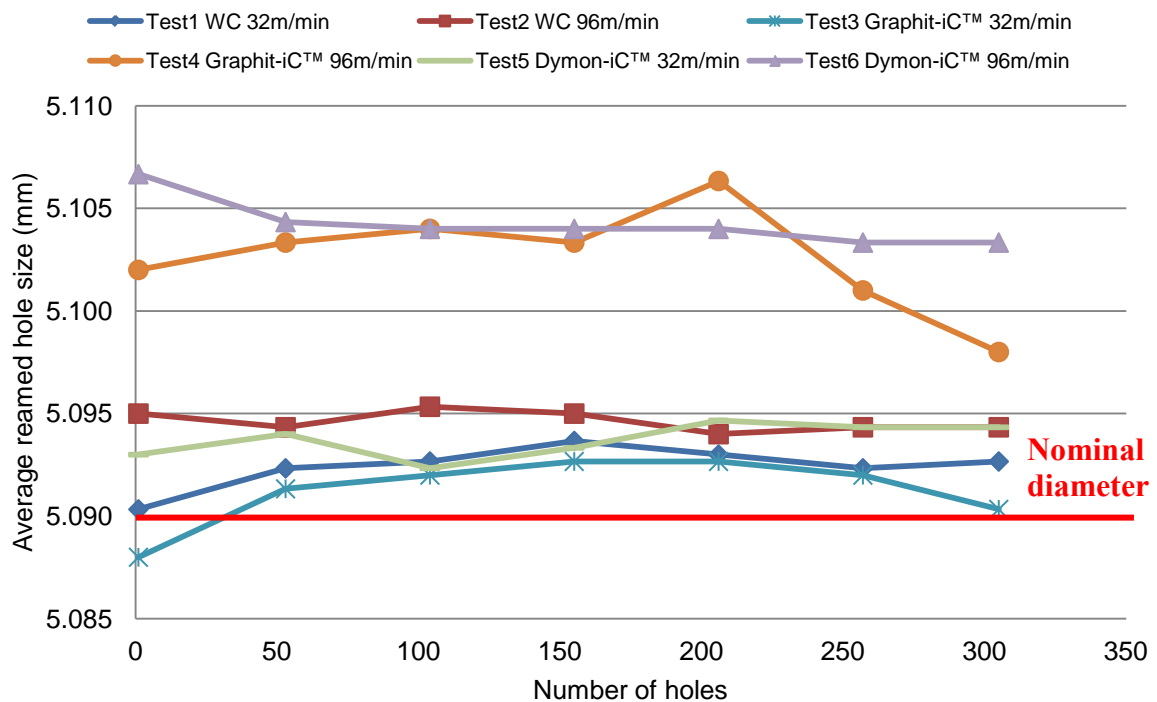


Figure 138: Phase 3B – Reamed hole diameter

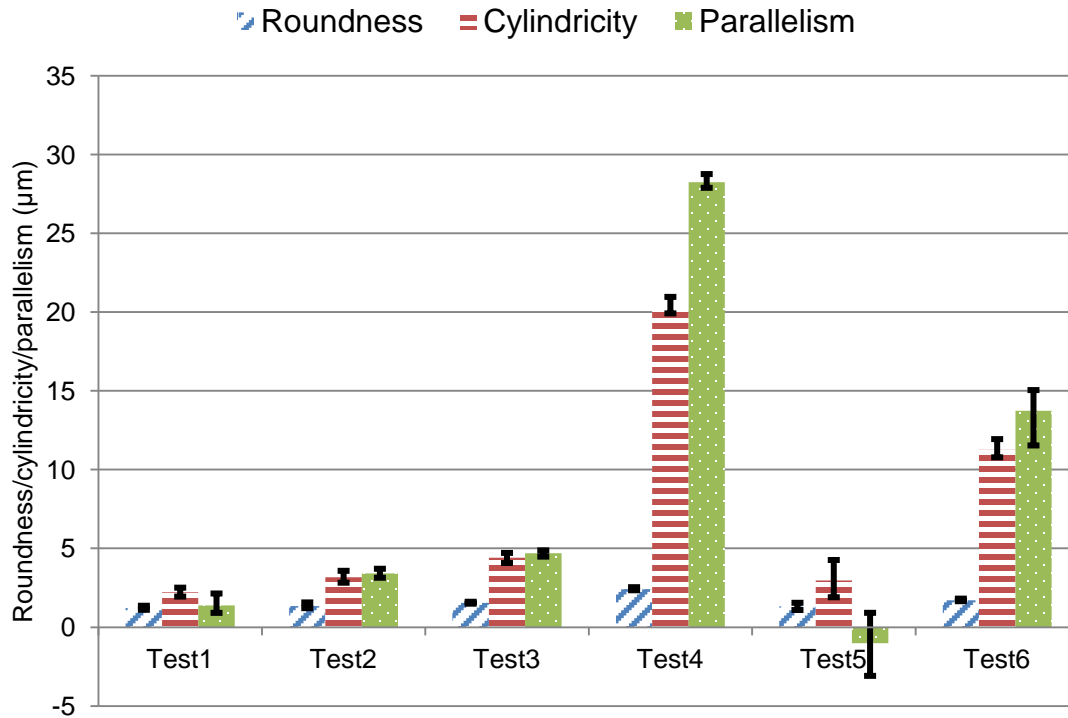


Figure 139: Phase 3B – Reamed hole quality

5.2.2.4 Workpiece surface roughness and integrity

Figure 140 and Figure 141 show workpiece surface roughness results following reaming measured at 2mm and 23mm from hole entry respectively. Workpiece surface roughness towards the hole entry fluctuated but was within 0.1-0.5 μm for the duration of tests. The roughness values towards the bottom of the hole were marginally higher, and reached a maximum of $\sim 0.6\mu\text{m}$ Ra (Test 5) after 307 holes. In general, workpiece roughness reduced as cutting speed increased, which was partly attributed to the lower amounts of smearing/adhered material present, as shown in the micrographs in Figure 133. However, further improvement in surface finish is expected in the production environment where a floating reamer holder is employed instead of the standard fixed configuration used in the present trials. Such tool holders provide greater flexibility of the reamer enabling the tool to enter/follow the pre-drilled hole better, hence reducing chattering.

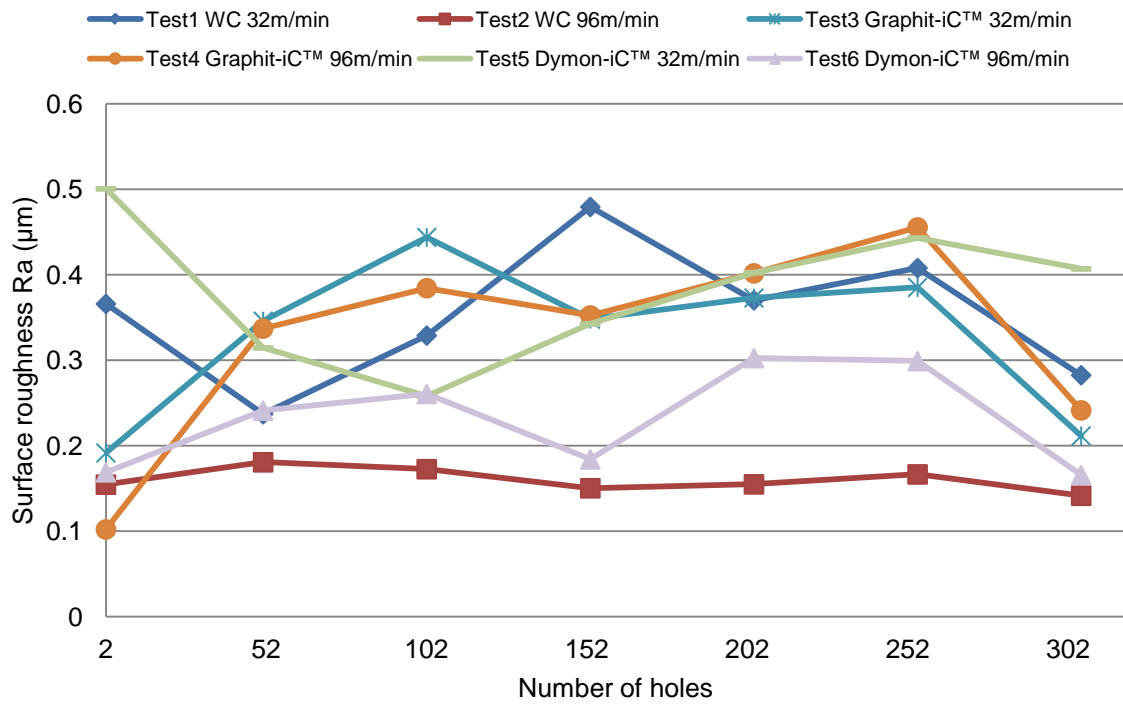


Figure 140: Phase 3B – Reamed surface roughness (2mm from hole entry)

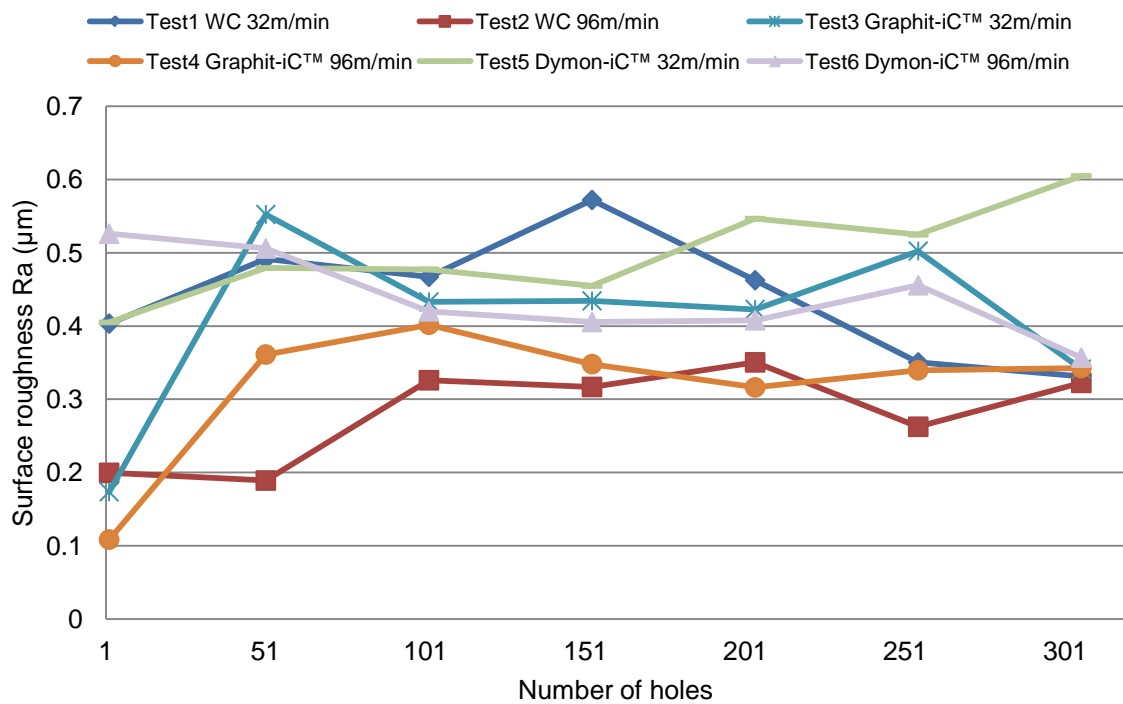


Figure 141: Phase 3B – Reamed surface roughness (23mm from hole entry)

Figure 140 and Figure 141 show microhardness depth profile plots of holes (start and end of tests) reamed at 32 and 96m/min respectively. Evidence of workpiece softening was observed to a depth of $\sim 20\mu\text{m}$ below the surface in the first hole reamed at 32m/min

regardless of the tools employed. In contrast, an increase of up to $\sim 20\text{HK}_{0.025}$ above the bulk hardness at $30\mu\text{m}$ beneath the surface was recorded for the first hole reamed at 96m/min using the uncoated tool. In terms of the last hole machined, hardened layers up to a depth of $90\mu\text{m}$ were seen after reaming with the uncoated and Dymon-iCTM coated tools, irrespective of the cutting speed, although the maximum level achieved was $\sim 10\text{HK}_{0.025}$ higher when operating at 96m/min . This suggests greater strain hardening of the machined surface/subsurface most likely as a result of the higher corresponding tool wear levels at test cessation. No significant variation in workpiece microhardness (from the bulk) however was evident in any of the holes finished using the Graphit-iCTM coated reamer (except for a slight increase in the first hole at 32m/min). Micrograph images of selected cross-sectioned samples (holes 2, 153 and 306) produced with the uncoated, Graphit-iCTM and Dymon-iCTM coated reamers are shown in Figure 144 to Figure 146 respectively. While there were some minor instances of indentations on the reamed surfaces, there were no signs of pits/tears or microcracks in any samples evaluated.

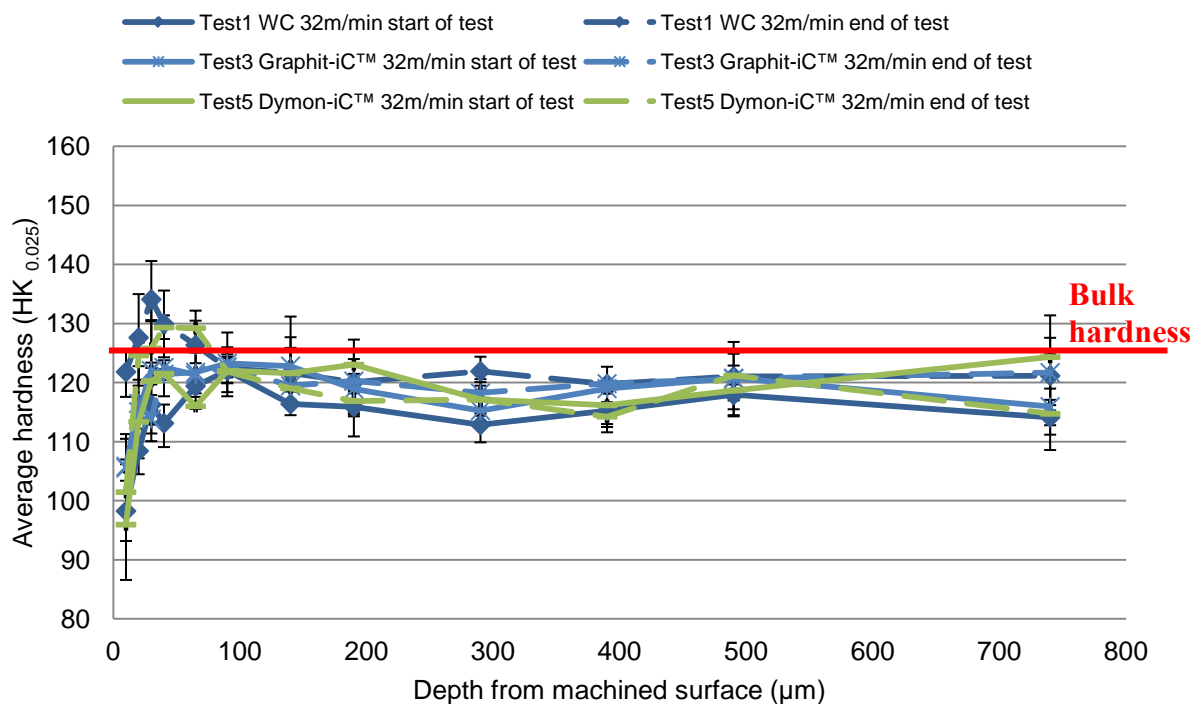


Figure 142: Phase 3B – Microhardness of cross-sections of reamed hole (12mm from entry, reaming speed 32m/min)

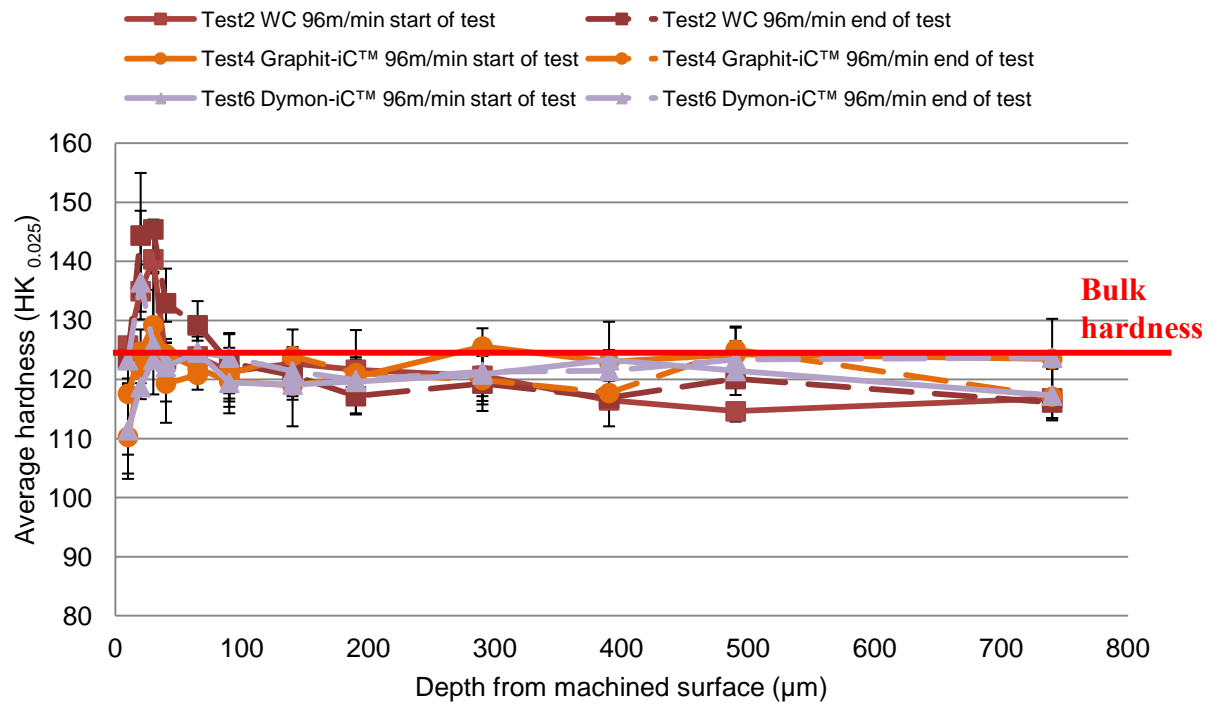


Figure 143: Phase 3B – Microhardness of cross-sections of reamed hole (12mm from entry, reaming speed 96m/min)

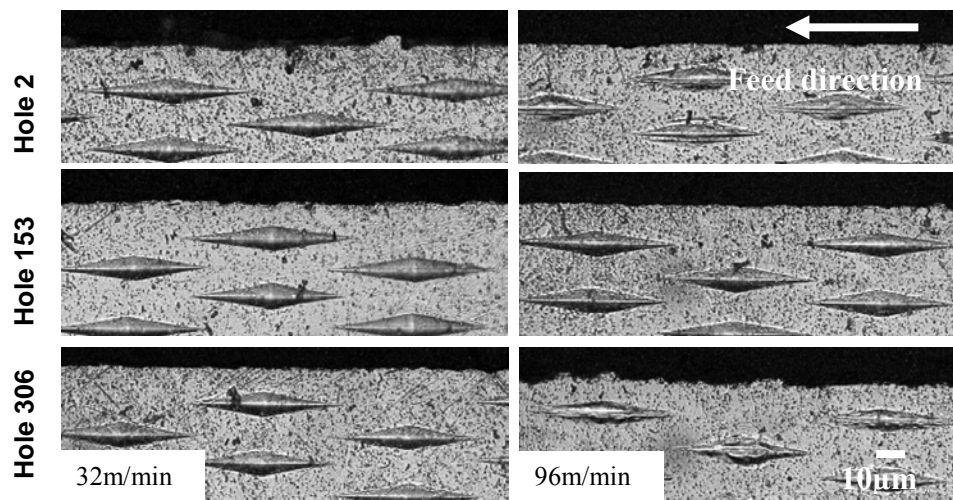


Figure 144: Subsurface microstructure of reamed hole produced with uncoated coated carbide tool (12mm from entry)

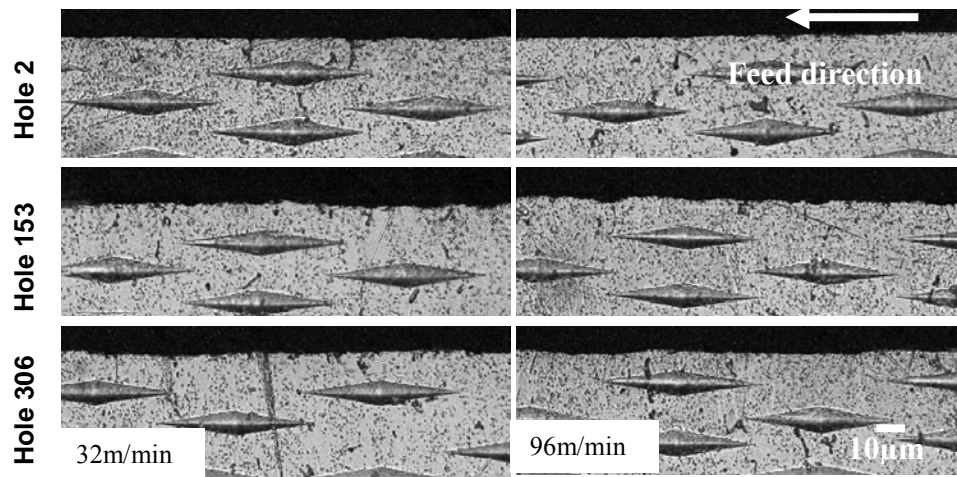


Figure 145: Subsurface microstructure of reamed hole produced with Graphit-iC™ tool (12mm from entry)

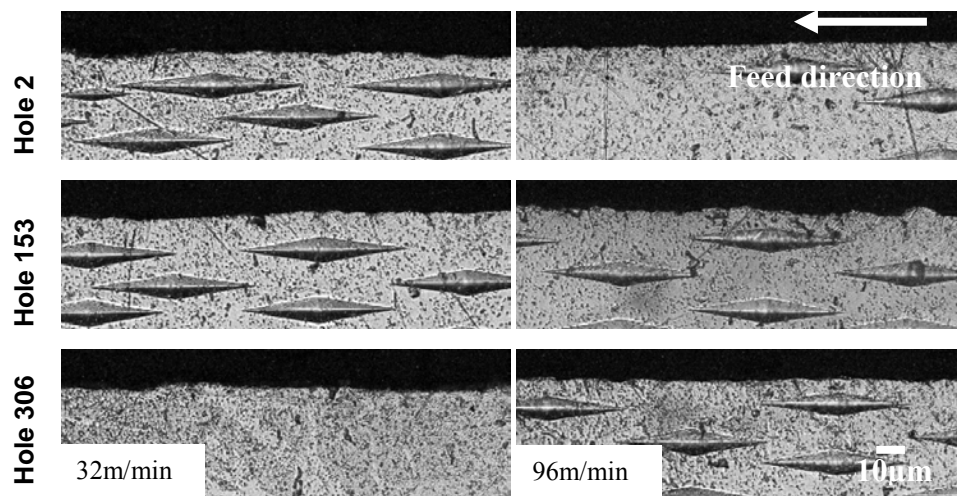


Figure 146: Subsurface microstructure of reamed hole produced with Dymon-iC™ tool (12mm from entry)

5.2.3 Phase 4A: Evaluation of diamond coated and PCD tools when drilling cast C355 aluminium alloy

This phase of experimental work involved drilling of cast C355 aluminium alloy at two different cutting speeds (130m/min and 260m/min) and a constant feed rate of 0.1mm/rev under low pressure flood (3bar) conditions.

5.2.3.1 Tool life/wear and workpiece material adhesion

Significant adhesion of workpiece material and BUE was evident on the flank and chisel edges of uncoated drills irrespective of cutting speed. A high degree of chemical affinity between aluminium and cemented carbide (composite of WC and Co) is acknowledged as one of the main reasons for this [40]. Figure 147 to Figure 150 show optical micrographs of drill edges in the worn condition for each trial (after 1683 holes unless

otherwise indicated). Appendix E further shows the tool wear/condition of the drills used in Phase 4A. In contrast, excessive material adhesion was not observed when employing CVD diamond coated tools, although peeling of the coating layer occurred after hole 282 when operating at the higher cutting speed, which led to premature termination of the test. Figure 151 shows an SEM image of the worn region, which details clear evidence of spalling of the diamond coating. Similarly, no signs of material adhesion or BUE were visible on any of the PCD blanks, although there was accumulated material on the carbide body/chisel edge of the tools. Additionally, adhered Al material was also found to be trapped between gaps in the brazing joints of the PCD blank and the carbide tool substrate, see Figure 152. This was also thought to be partly due to the lack of cutting fluid access (low pressure) at the tool edge.

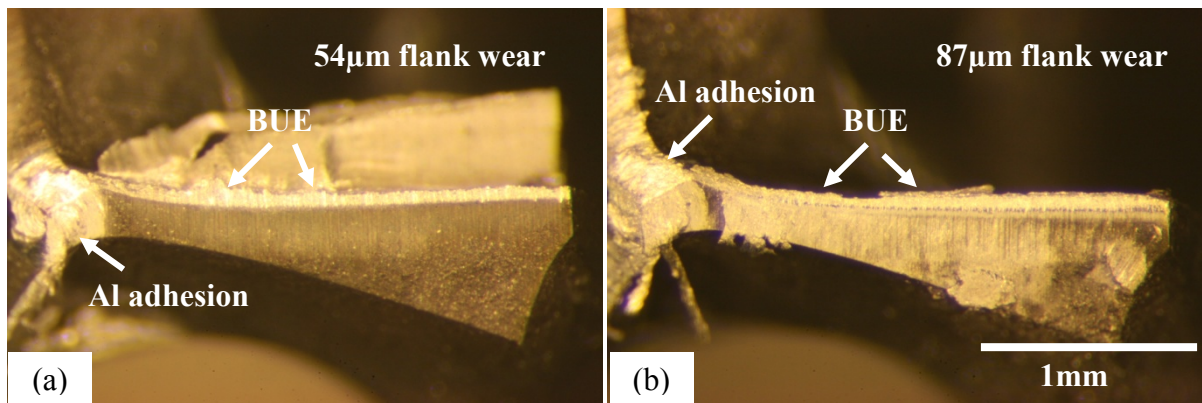


Figure 147: Phase 4A –Micrographs of uncoated carbide drills in the worn condition in (a) Test 1 and (b) Test 2

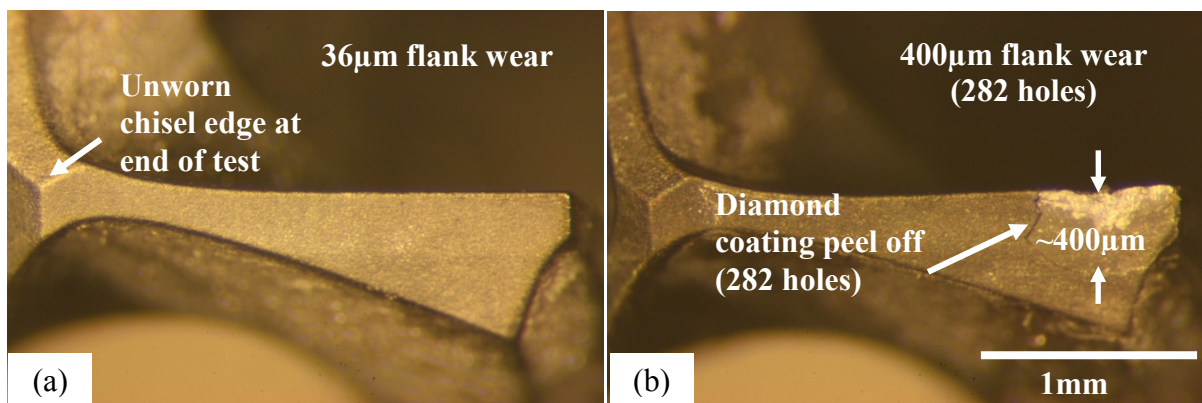


Figure 148: Phase 4A – End of test micrographs for CVD diamond coated drills under (a) Test 3 and (b) Test 4

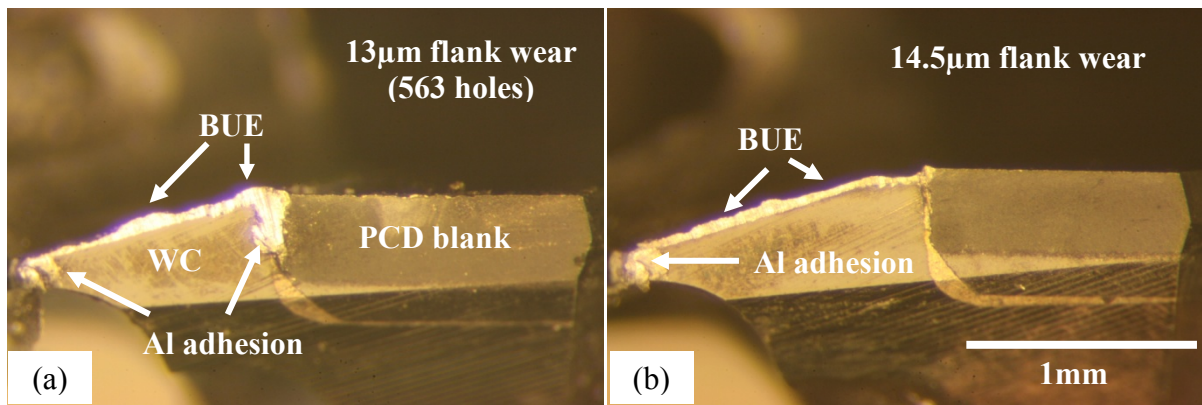


Figure 149: Phase 4A – End of test micrographs for PCD CTB010 drills under (a) Test 5 and (b) Test 6

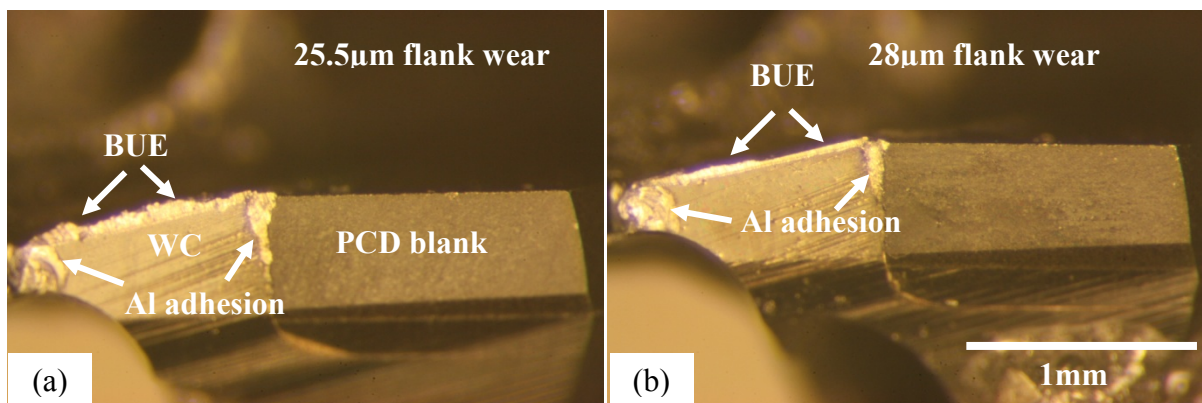


Figure 150: Phase 4A – End of test micrographs for PCD CTM302 drills under (a) Test 7 and (b) Test 8

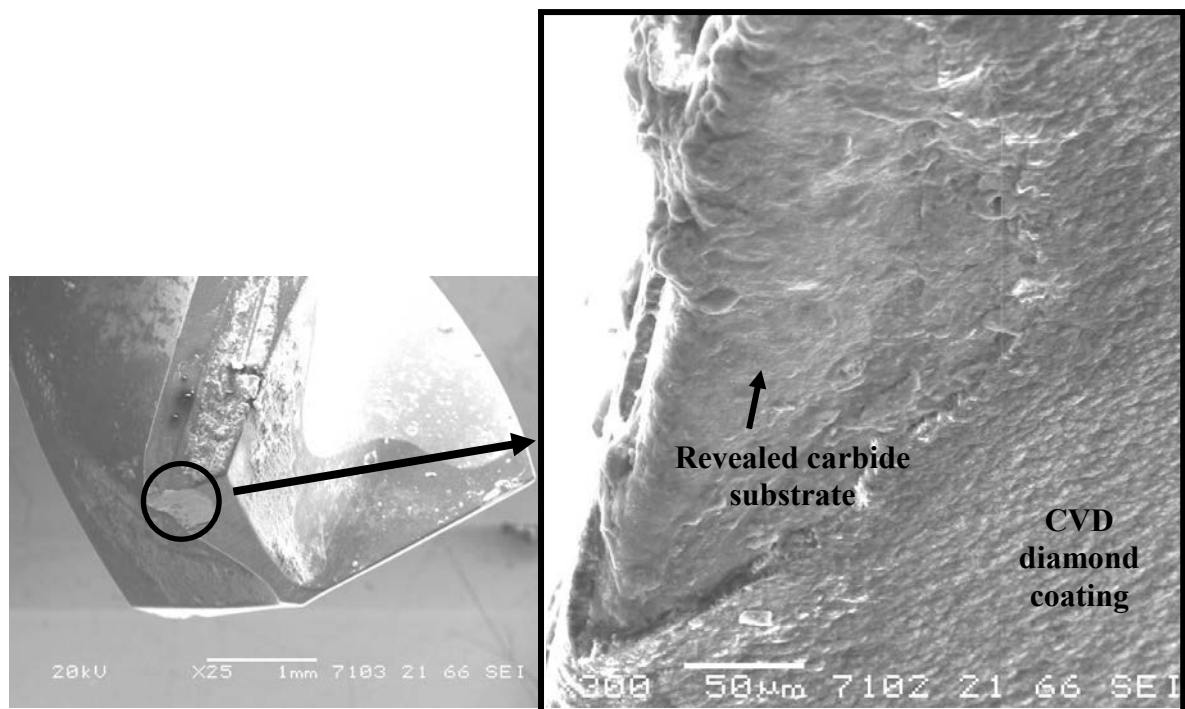


Figure 151: SEM image of worn CVD diamond coated drill in Test 4 (260m/min)

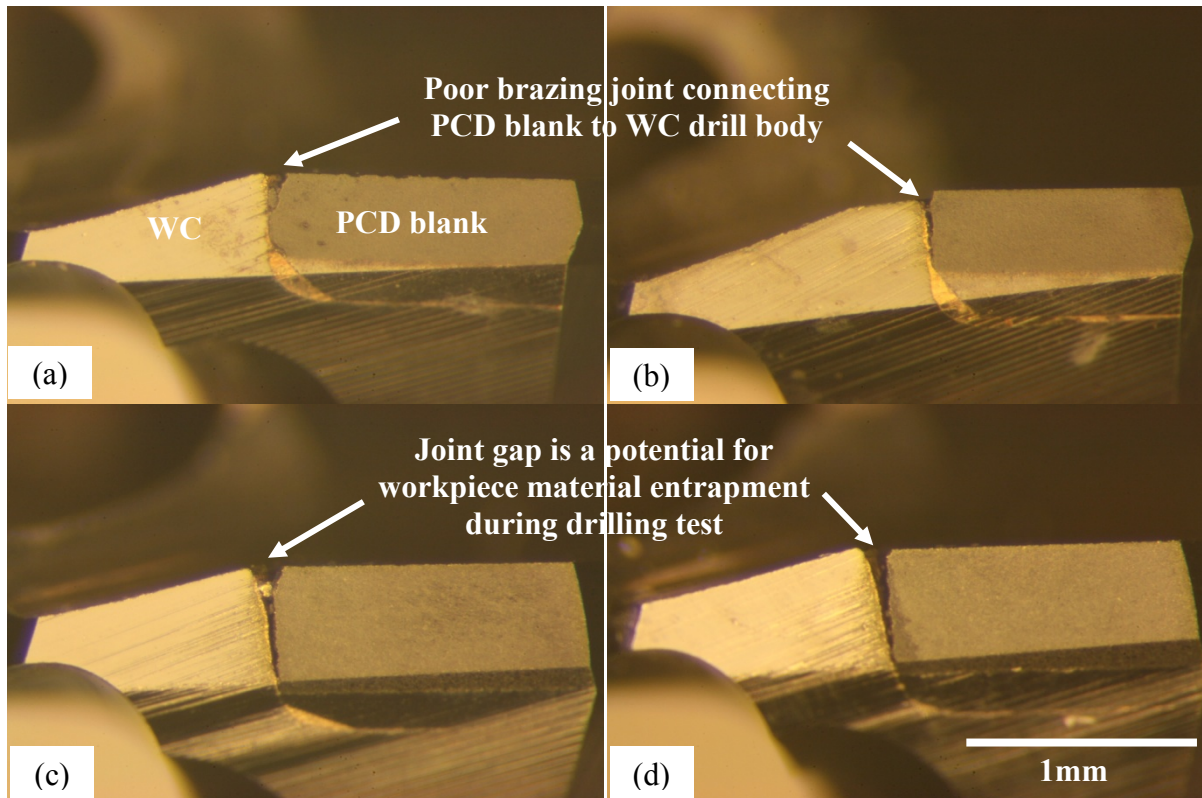


Figure 152: New/as-received condition of PCD drills used in (a) Test 5, (b) Test 6, (c) Test 7 and (d) Test 8

Figure 153 details the flank wear (VB_{Bmax}) progression of each tool over the test duration. Audible/high frequency noise was detected in all tests as the tool penetrated the top of the workpiece, but no tool clogging was evident. Unfortunately, the PCDCTB010 drill in Test 5 suffered catastrophic breakage due to a malfunction in the tool changer during the experiment and hence the trial had to be halted after 563 holes.

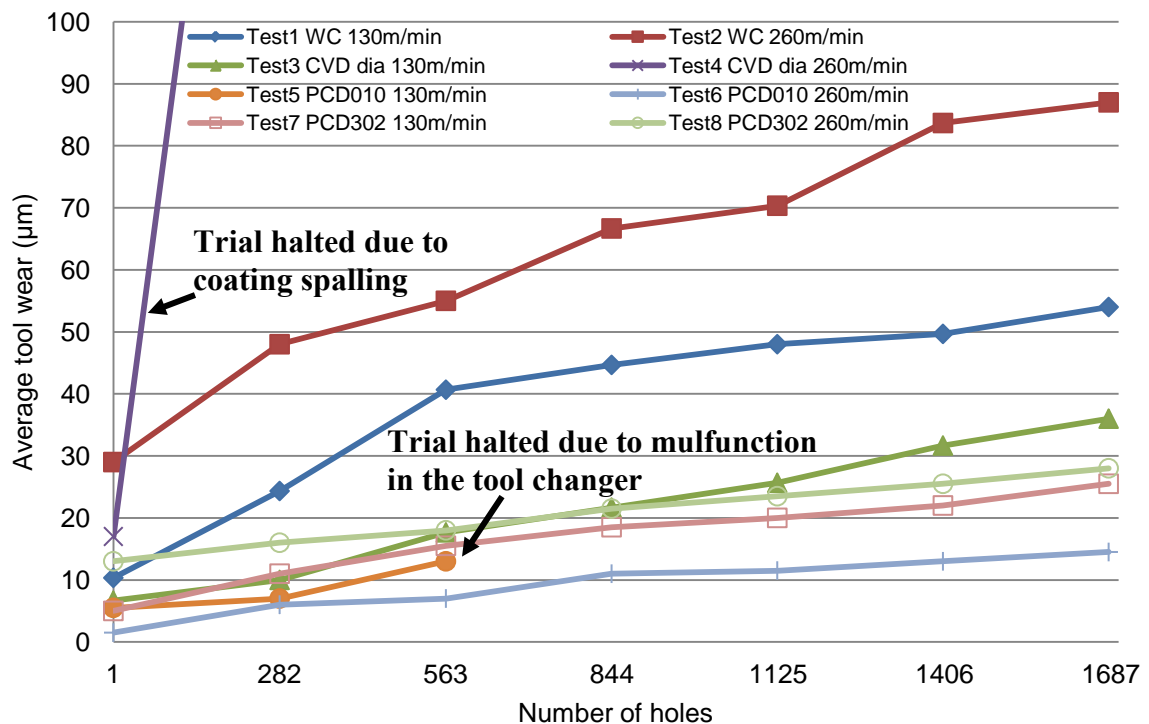


Figure 153: Phase 4A – Drill flank wear curves

Tests (1, 3, 5, and 7) performed at 130m/min (8500rev/min, 0.1mm/rev) generally showed steady tool wear progression (flank and chisel edges) over the duration of the experiment. In general, the PCD drills showed the lowest wear rate, with the CTB010 grade (Test 6) having a maximum flank wear of only 14.5µm after 1683 holes. Conversely, wear on the uncoated WC drills at low (Test 1) and high (Test 2) cutting speeds was 55µm and 87µm respectively at test cessation (~4 and ~6 times higher respectively). Based on the lower tendency for BUE formation, the CVD diamond or PCD tools would be expected to significantly improve hole quality when drilling aluminium compressor impellers at Doncasters Sterling.

5.2.3.2 Cutting forces

Thrust/feed force (F_z) generated when drilling 4.8mm diameter holes in C355 aluminum were measured over 1683 holes with the results illustrated in Figure 154. A significant reduction in forces was observed when employing the PCD drills. Despite a straight fluted geometry, the PCD products (Test 5 to Test 8) generated ~70 to ~125% lower average thrust forces compared with uncoated and CVD diamond coated twist drills (Test 1 to Test 4) under equivalent machining conditions. The higher thrust force values generated by the uncoated tools also reflect the large flank wear levels/scars as illustrated in Figure 147 (a) and (b).

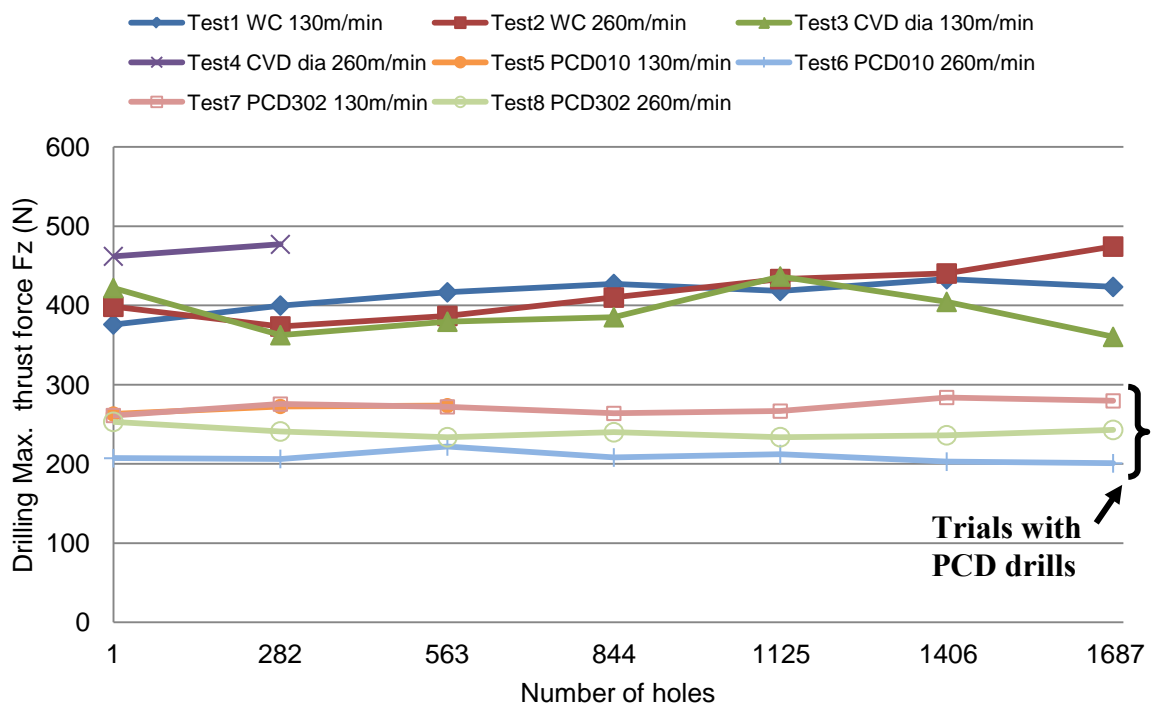


Figure 154: Phase 4A – Drilling force

Typically, thrust forces were seen to decrease with an increase in drilling speed. A reduction of 22% and 12% was observed in tests involving the CTB010 (Test 5 and Test 6) and the CTM302 grades (Test 7 and Test 8) respectively as the speed was varied from 130 to 260m/min. This was in line with results detailed by Kelly and Cotterell [70], who reported a 30% reduction in thrust force following a fourfold increase in rotational speed during the drilling of aluminium alloy plate under flood cooling conditions. This was attributed to an increase in the shear angle and corresponding smaller too-chip contact length at higher cutting speeds [234]. In contrast, only a marginal decrease (~1%) was observed between Test 1 and Test 2 involving the uncoated WC drills.

The maximum drilling torque values generally showed a rising trend with the number of holes drilled, due to tool wear progression, see Figure 155. A number of tests (Test 2, 3, 4, and 8) however exhibited high initial torque levels, which was possibly due to Al material adhering on the drill corners at trial commencement.

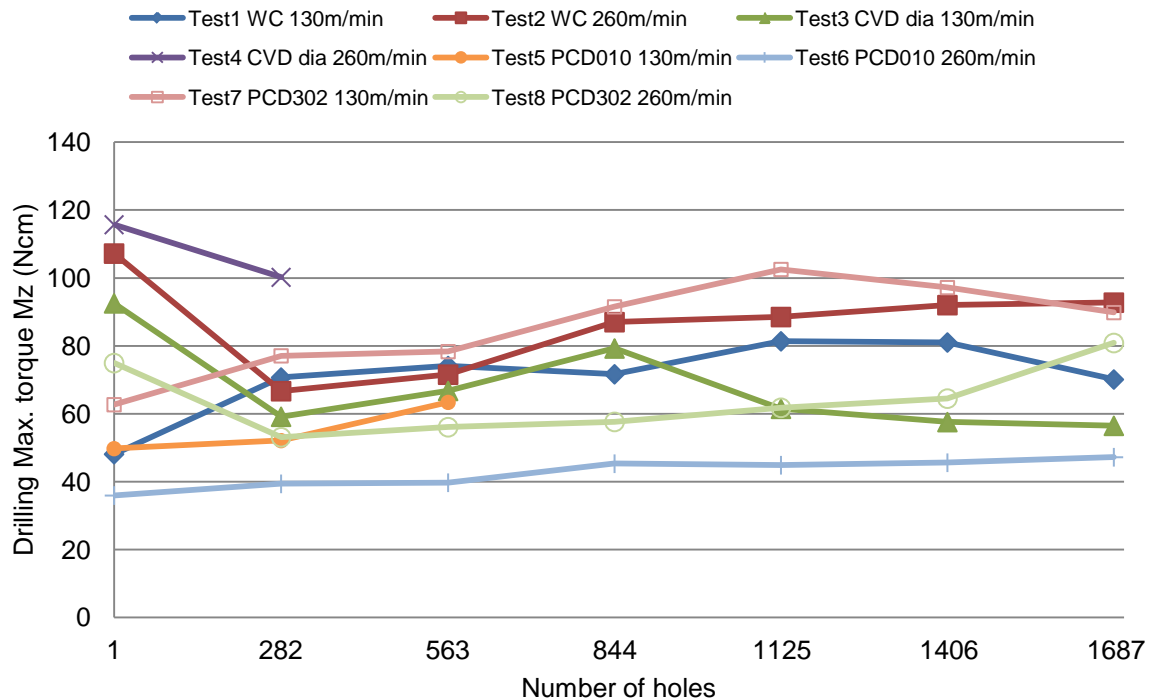


Figure 155: Phase 4A – Drilling torque

Torque produced with the CVD diamond coated drill increased by 33% (from 60Ncm to 80Ncm) between holes 282 and 843 before falling steadily to 56Ncm at the end of the test (hole 1683). Doubling of the cutting speed led to 21% rise in torque when utilising the uncoated carbide drills although this trend was reversed in the case of the PCD tools. The latter was partly due to its lower affinity for workpiece material adhesion and/or BUE formation compared to the uncoated carbide tools, particularly when employing high cutting speeds.

The unexpectedly high torque levels recorded in Test 7 (CTM302 PCD) compared to the uncoated cutters (Test 1 and 2) could have been due to the straight flute geometry of the former. This would typically result in poorer chip evacuation as compared to drills with helical/flutes. A possible solution could be to utilise cutters with internal cutting fluid holes to enable high pressure delivery.

5.2.3.3 Chip/swarf morphology analysis

Typical chips formed during the drilling of C355 aluminium using different tools at cutting speeds of 130m/min and 260m/min are detailed in Figure 156. The uncoated carbide drills in Test 1 and Test 2 produced a mixture of short, continuous conical and fan shaped swarf, see Figure 157. This was similarly observed in trials involving the CVD diamond coated drills in Test 3 and Test 4, see Figure 158. In contrast, the straight fluted PCD tools used in Test 5 to Test 8 produced transitional type chips, as shown in Figure 159 and Figure 160. Such chips displayed initial curling, but fractured prior to achieving a complete revolution or conical shape [52]. Nevertheless, none types of chips produced caused any major flute packing during the machining operation.

In general, small discontinuous chips are preferred as they can be transported easily along the drill flutes, thus reducing torque generation, cutting temperature and risk of tool breakage [52, 236]. There did not appear to be any significant alteration to the chip morphology with respect to changes in drilling speed. Further SEM investigation of sample swarf collected after each experiment detailed in Figure 157 to Figure 160 clearly show the conical and transitional shaped chips produced when using uncoated carbide, CVD diamond coated and PCD drills respectively. Additionally, analysis of swarf thickness confirmed that thinner chips were obtained as drilling speed was increased, in line with the lower thrust force and torque observed in Tests 2, 6 and 8.





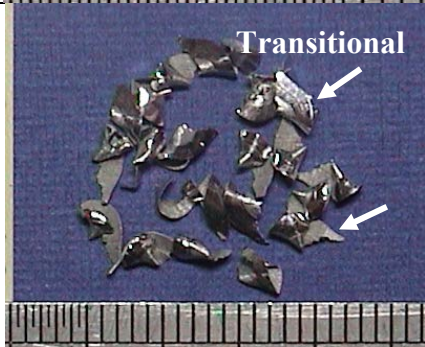



Drill type	130m/min cutting speed	260m/min cutting speed
Uncoated tungsten carbide		
CVD diamond		
Brazed PCD CTB010		
Brazed PCD CTM302		

Figure 156: Phase 4A – Various chip forms/shapes produced when drilling C355 aluminium at different cutting speeds and tool materials

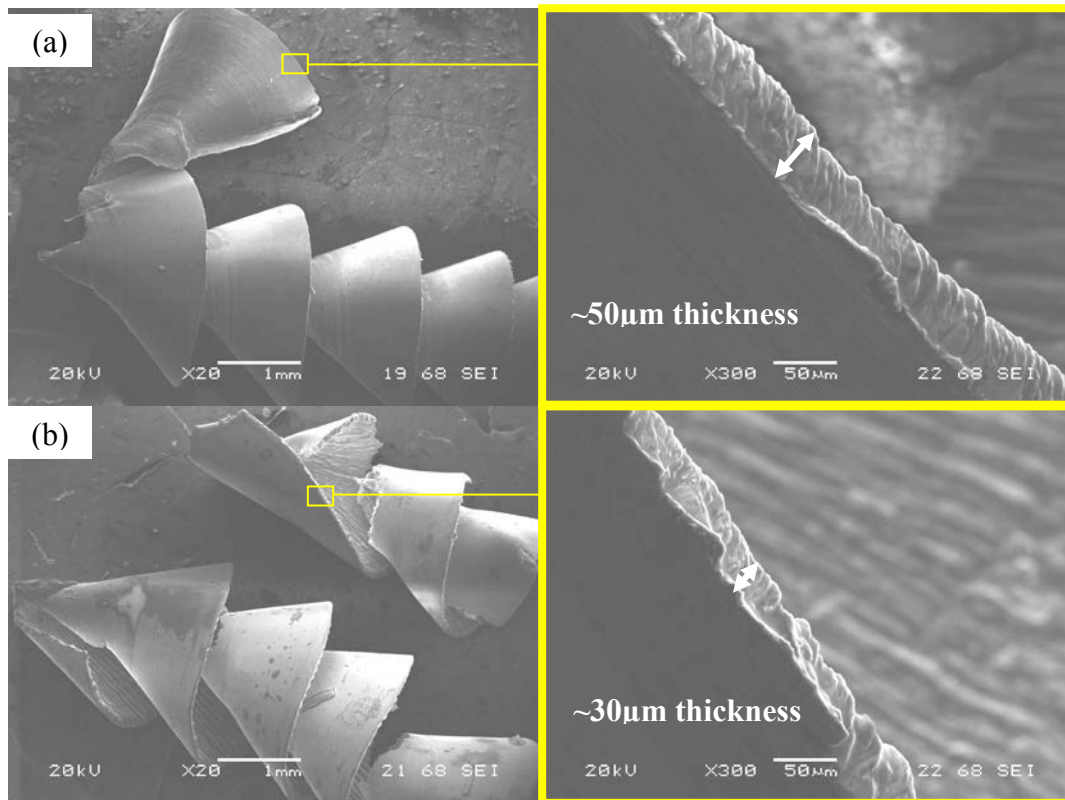


Figure 157: Chip formation produced by uncoated tungsten carbide drills under different cutting speeds in (a) Test 1 (130m/min) and (b) Test 2 (260m/min)

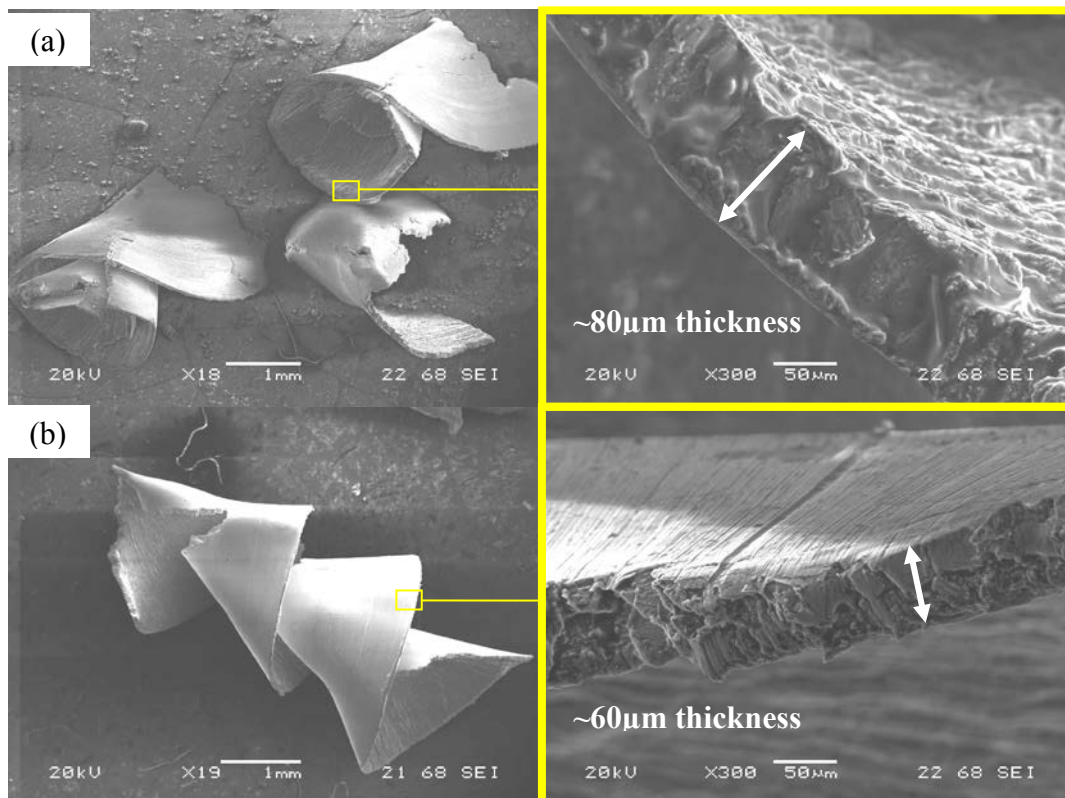


Figure 158: Chip formation produced by CVD diamond coated drills under different cutting speeds in (a) Test 3 (130m/min) and (b) Test 4 (260m/min)

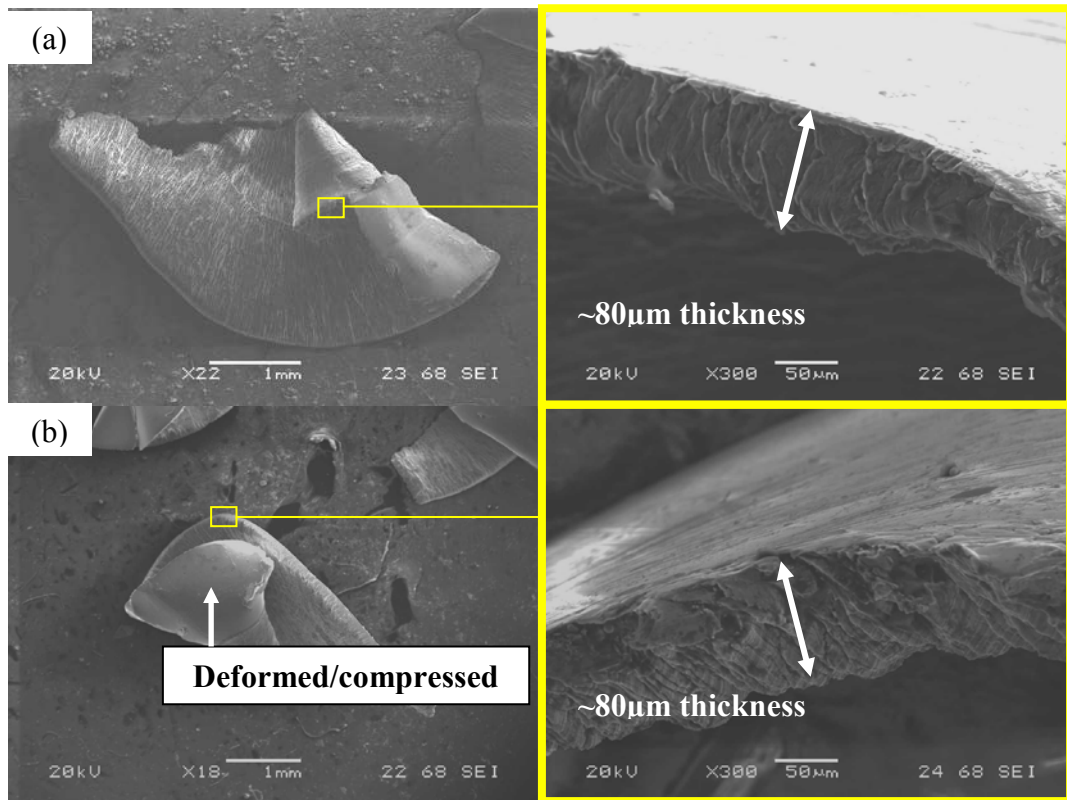


Figure 159: Chip formation produced by PCD CTB010 drills under different cutting speeds in (a) Test 5 (130m/min) and (b) Test 6 (260m/min)

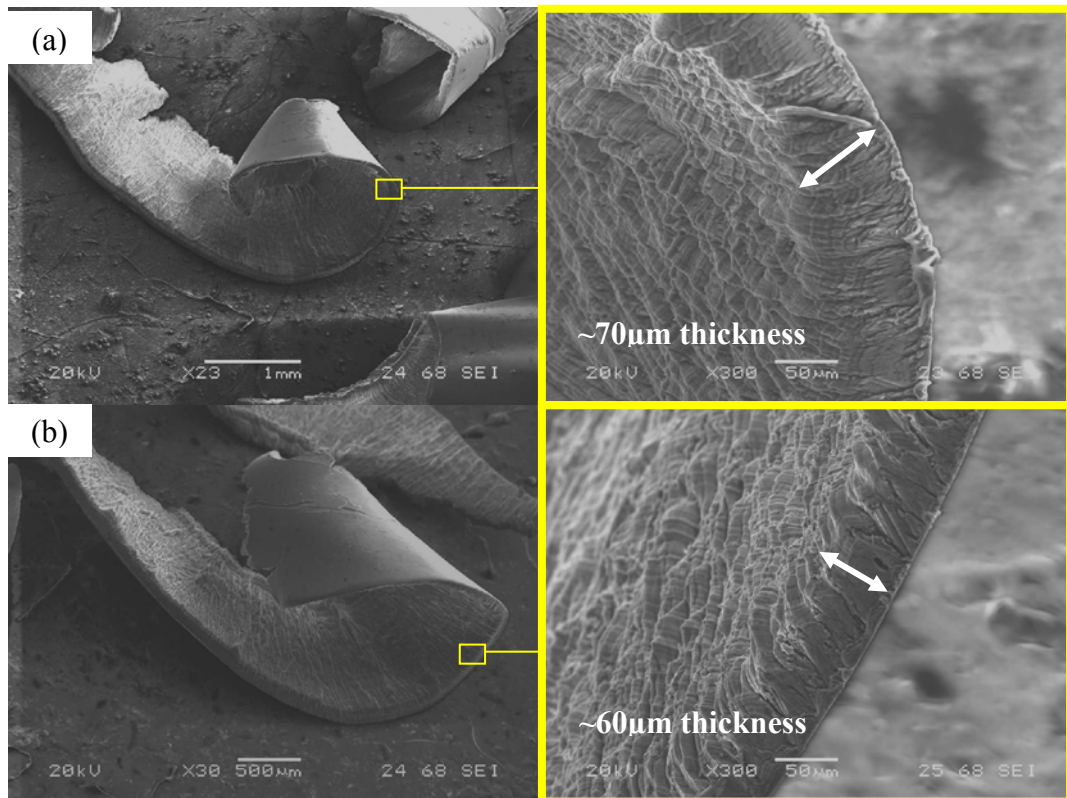


Figure 160: Chip formation produced by PCD CTM302 drills under different cutting speeds in (a) Test 7 (130m/min) and (b) Test 8 (260m/min)

5.2.3.3 Workpiece quality

Hole diameter in general decreased as cutting progressed due to tool wear. Figure 161 shows the evolution of average values of hole diameter versus number of drilled holes. All holes produced with the CVD diamond tools (Tests 3 and 4) were above the nominal drill size ($\varnothing 4.8\text{mm}$), which was a result of the coating thickness ($8\mu\text{m}$). The uncoated carbide tools in Tests 1 and 2 also experienced a similar trend initially (oversized by $4\text{--}10\mu\text{m}$) but this decreased steadily below the nominal size after hole 280, with the average diameter measuring 4.790mm and 4.795mm respectively at the end of the trial. While all of the holes drilled using the PCD tools (Tests 5 to 8) were undersized, there was minimal diametral variation over the entire experiment, which indicated a stable process.

Hole quality results in terms of roundness, cylindricity and parallelism are presented in Figure 162. The average roundness did not exceed $7\mu\text{m}$ and was comparable for each of the different tool materials evaluated. These were good results for a roughing operation considering that the hole roundness tolerance/requirement is $5\mu\text{m}$. In terms of hole cylindricity, the mean deviation was marginally higher when using the PCD drills, although this did not exceed $22\mu\text{m}$. This was most likely due to the difficulty in chip/swarf evacuation as a result of the straight fluted tool geometry. In addition, the cylindricity tended to improve when operating at lower cutting speed. The majority of the drilled holes had positive parallelism values, which suggested that the hole diameter was larger/tapered at the hole entry. Three dimensional form measurement of holes further confirmed this conclusion, see Figure 163. Hole parallelism also tended to improve when employing lower cutting speed.

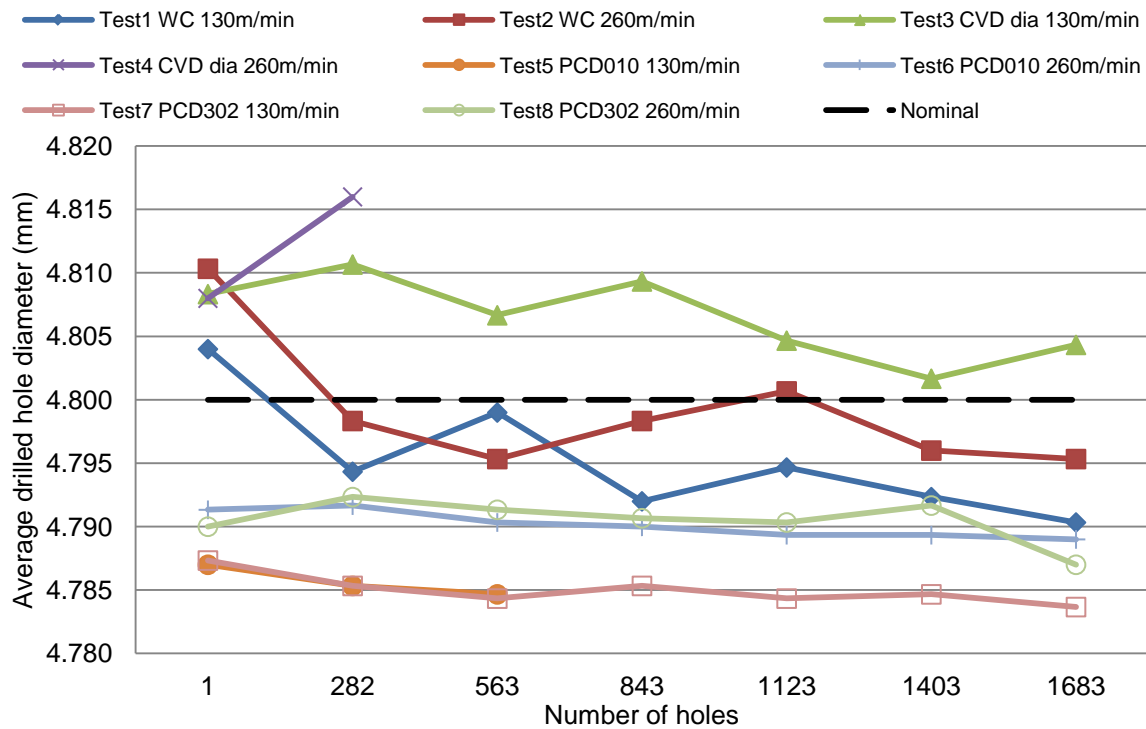


Figure 161: Phase 4A – Drilled hole diameter

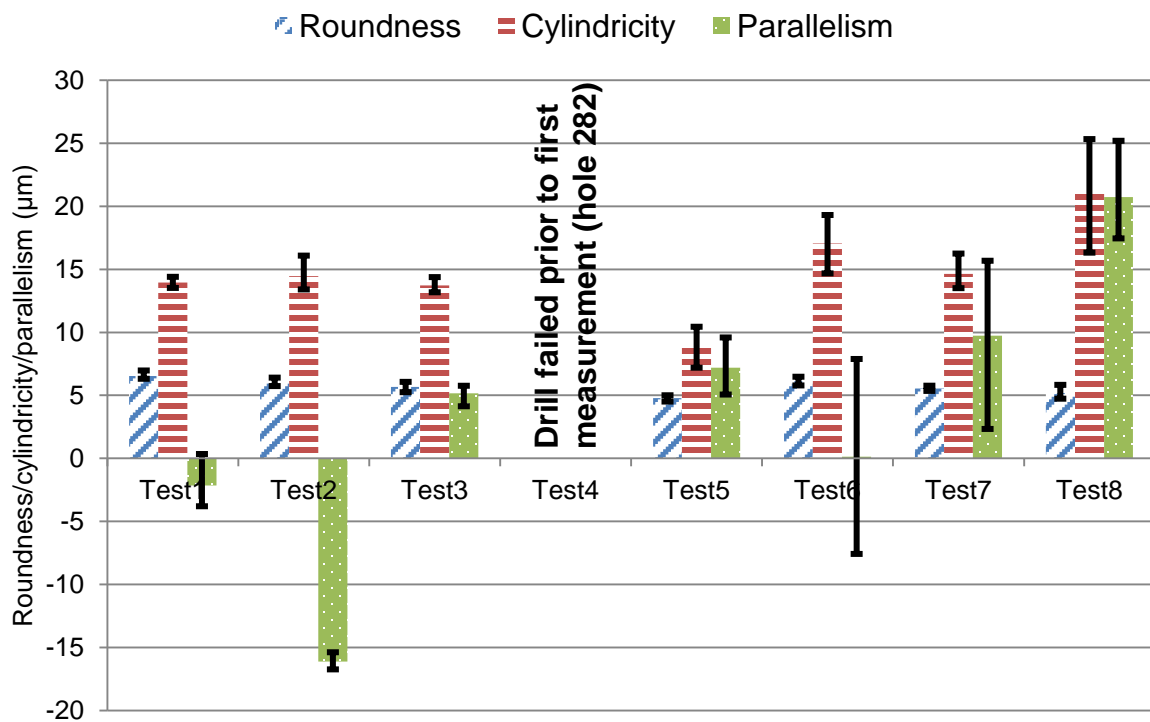


Figure 162: Phase 4A – Drilled hole quality

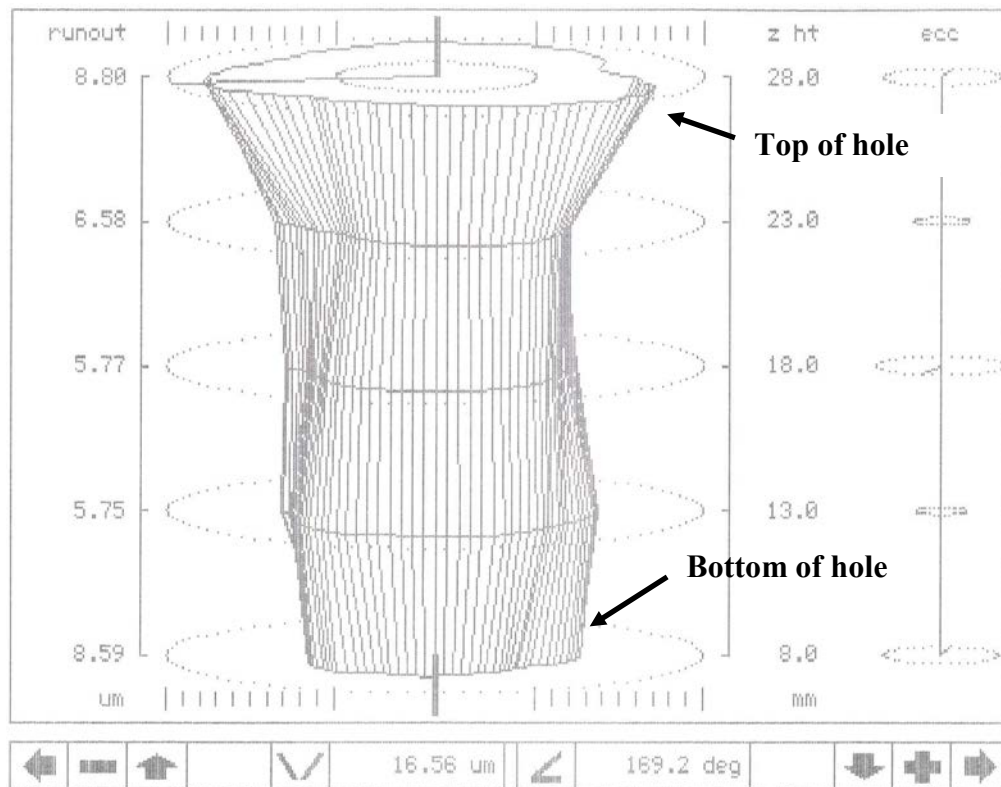


Figure 163: Typical form cylindricity with positive parallelism observed in Test 6 using CTB010 PCD at a cutting speed of 260m/min

5.2.3.4 Workpiece surface roughness and integrity

Hole surface roughness results measured at the entry and exit locations are detailed in Figure 164 and Figure 165 respectively. Surface roughness near the hole entry was generally lower compared to that observed towards the bottom location. This was most likely due to the increased difficulty of swarf evacuation and possible tool vibration as drilling depth increased [229]. In most cases, the uncoated carbide drills produced holes with the poorest surface finish particularly towards the exit position, reflecting greater tool wear and high levels of BUE as evident from the tool micrographs detailed in Figure 147. The PCD drills generated the lowest surface roughness irrespective of cutting speed, which was below $0.3\mu\text{m}$ Ra even after 1683 holes and consistent over the entire hole length.

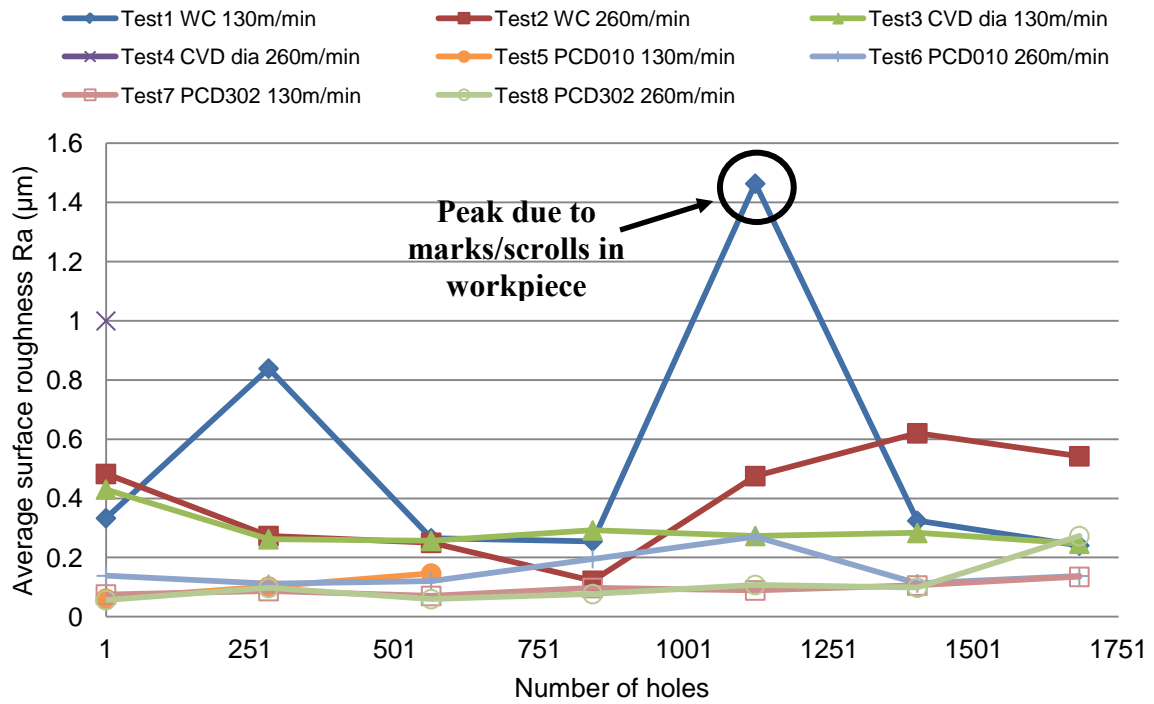


Figure 164: Phase 4A – Drilled hole surface roughness (2mm from entry)

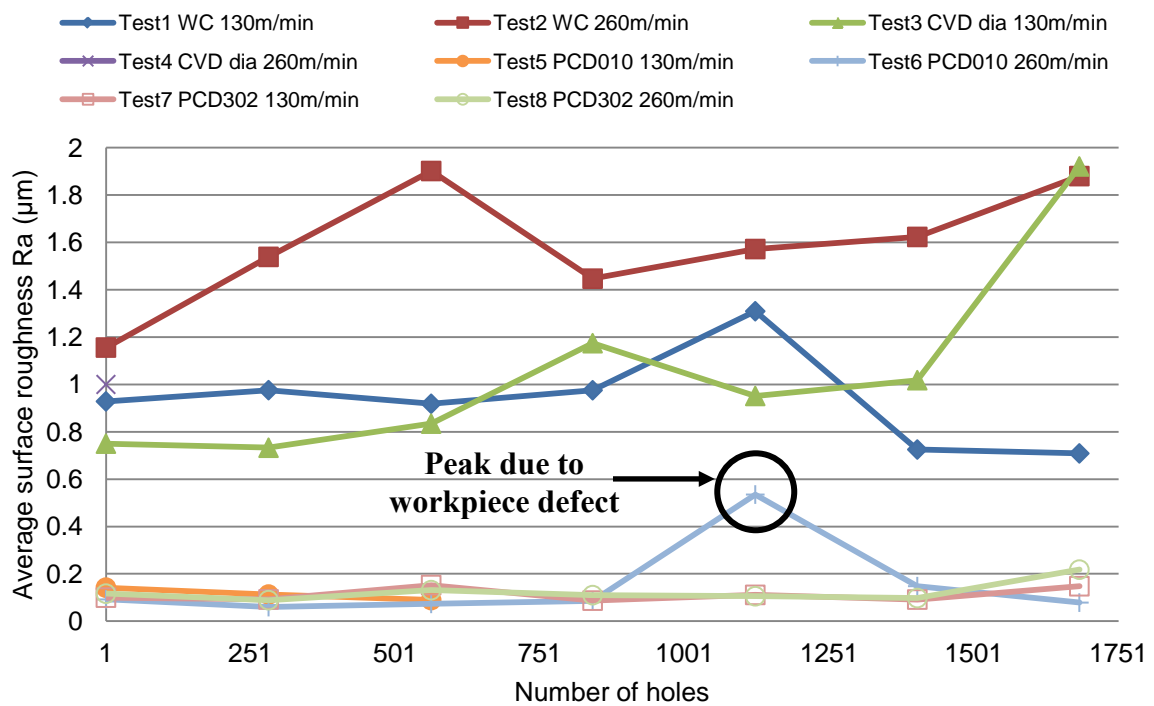


Figure 165: Phase 4A – Drilled hole surface roughness (25mm from entry)

A number of unusual peaks/spikes however were observed on the roundness profiles which compromised hole quality. One of the factors contributing to this was the formation of ‘scuff’/feed marks such as those illustrated in Figure 166 (a) from Test 1, which were caused by ploughing/re-deposited material. The occasional presence of workpiece defects (inclusions, voids, etc.) similar to that shown in Figure 166 (b) was also detected, which led to the Ra deviation seen in Test 6 (Figure 165).

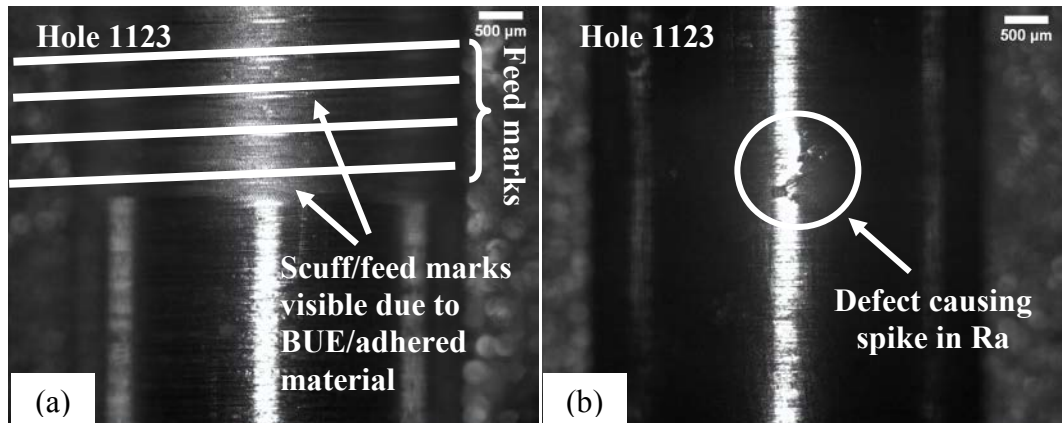


Figure 166: Cross-sections of holes from (a) Test 1 – entry and (b) Test 6 – exit

Microhardness depth profiles for Phase 4A drilling tests (Tests 1-3, 6-8) at 130m/min and 260m/min cutting speed are shown in Figure 167 and Figure 168 respectively. Results from Tests 4 and 5 (CVD diamond at 260m/min and PCD CTB010 grade at 130m/min) were not included due to premature cessation of the respective trials. A hardened region up to a maximum of 169.7HK_{0.025} (~10% above bulk hardness) and extending to a depth of 75μm from the hole surface was observed in the majority of specimens produced with a worn tool. In contrast, there was either no variation or only a marginal rise in hardness (<9%) for holes drilled with new tools (hole 1). Additionally, there was no significant effect on workpiece hardness detected due to changes in drill speed.

Assessment of cross-sectional micrographs of the drilled hole surface/subsurface (in Tests 1, 2, 3, 6, 7 and 8) showed no obvious evidence of microcracks, surface damage or microstructural alterations, irrespective of tool condition, see Figure 169 to Figure 174. Minor pitting was however seen in the last and first holes from Tests 1 and 2 (uncoated WC tools) respectively. Such defects however would be removed by the subsequent finishing/reaming operation.

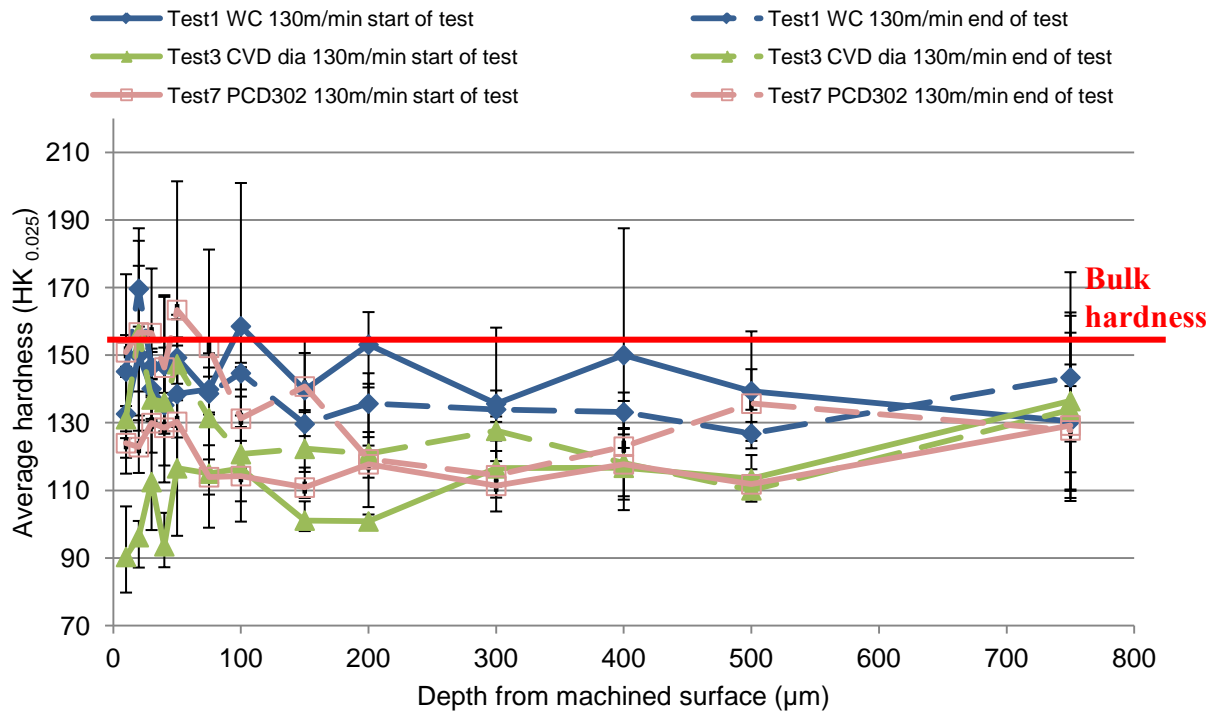


Figure 167: Phase 4A –Microhardness of cross-sections of drilled hole (12mm from entry, drilling speed 130m/min)

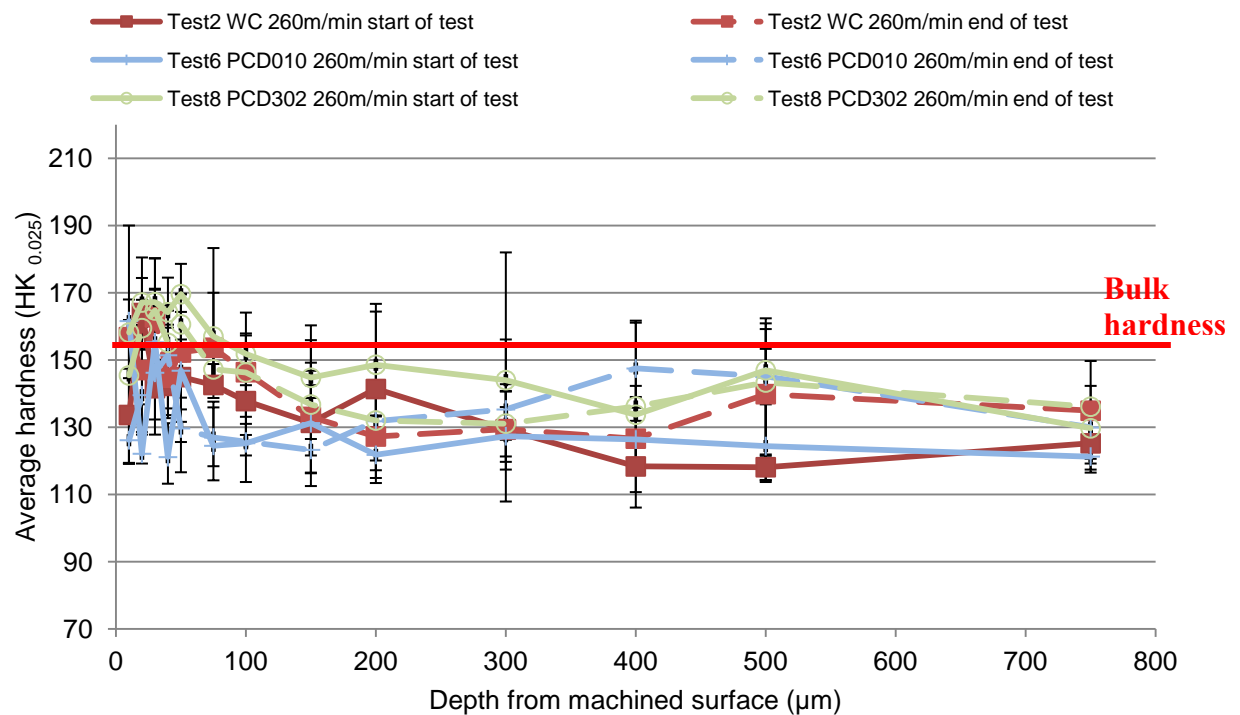


Figure 168: Phase 4A –Microhardness of cross-sections of drilled hole (12mm from entry, drilling speed 260m/min)

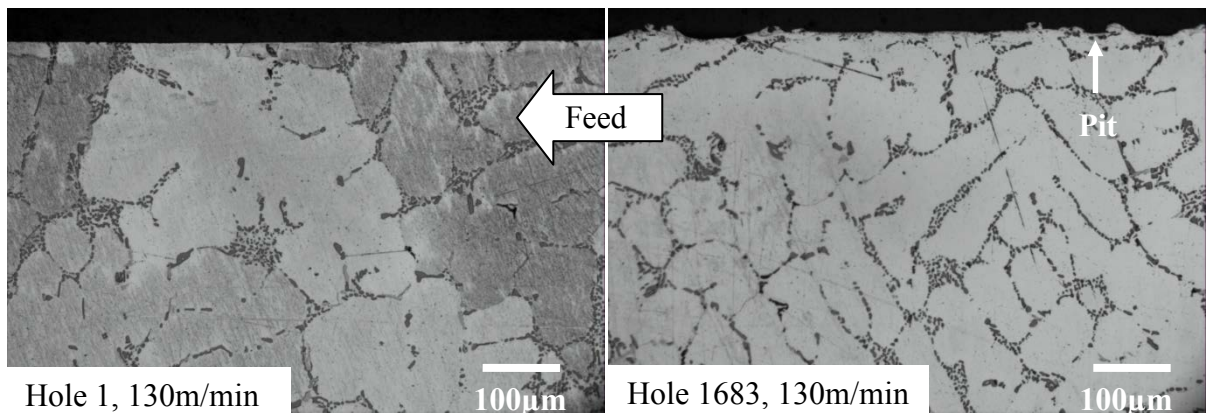


Figure 169: Phase 4A – Subsurface microstructure of drilled hole produced with uncoated carbide tool – Test 1 (12mm from entry)

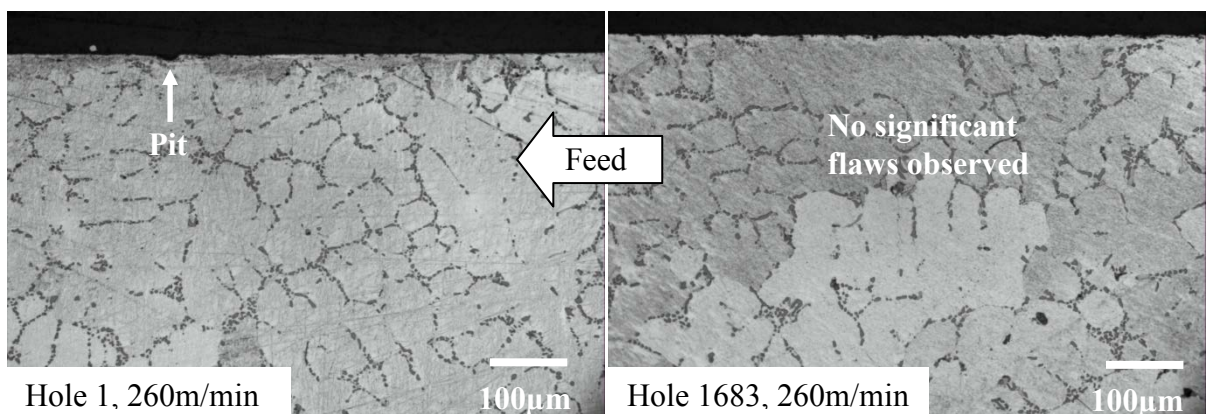


Figure 170: Phase 4A – Subsurface microstructure of drilled hole produced with uncoated carbide tool – Test 2 (12mm from entry)

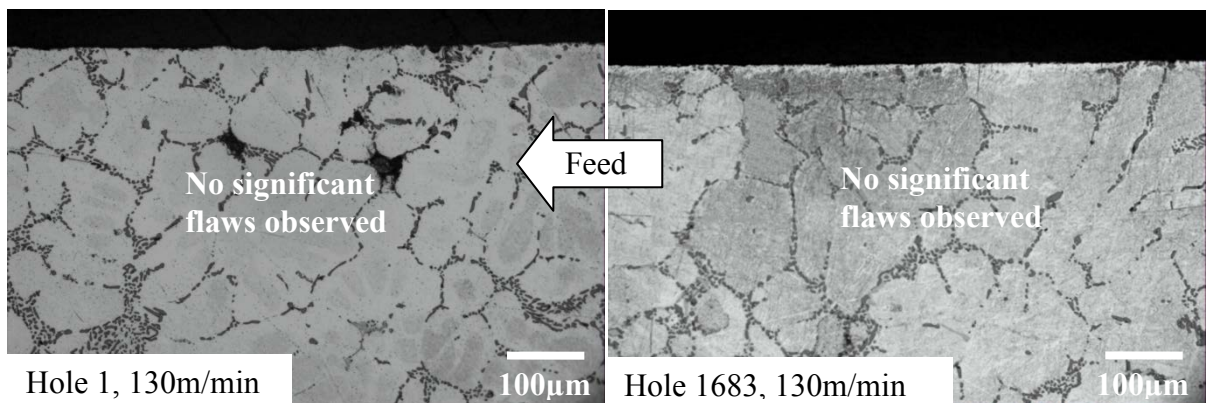


Figure 171: Phase 4A – Subsurface microstructure of drilled hole produced with CVD diamond coated tool – Test 3 (12mm from entry)

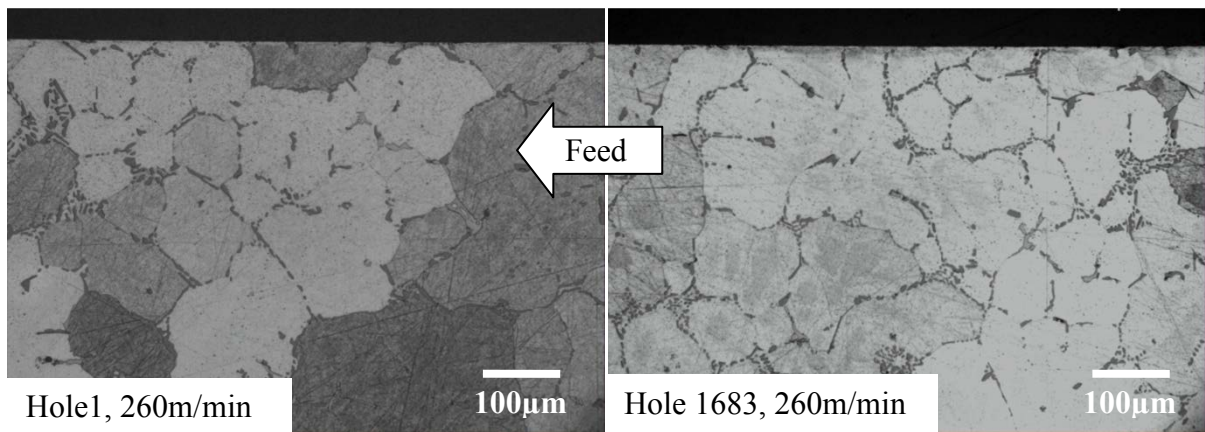


Figure 172: Phase 4A – Subsurface microstructure of drilled hole produced with PCD CTB010 tool – Test 6 (12mm from entry)

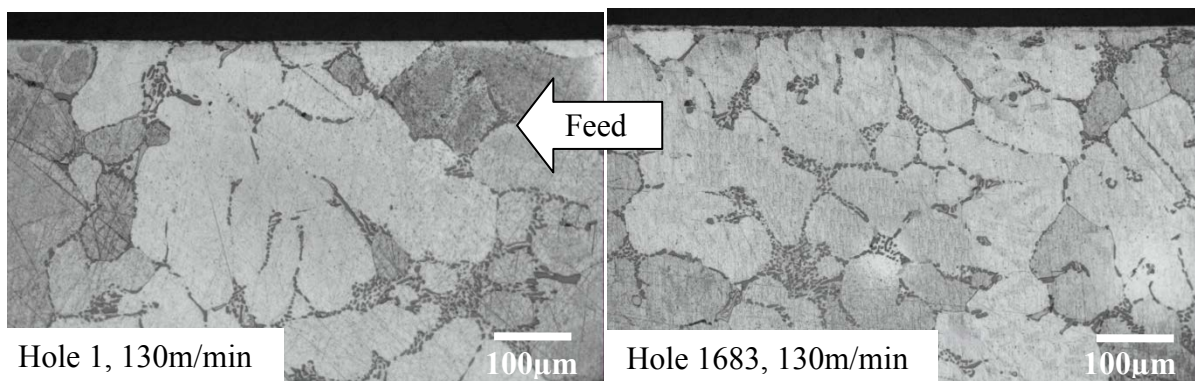


Figure 173: Phase 4A – Subsurface microstructure of drilled hole produced with PCD CTM302 tool – Test 7 (12mm from entry)

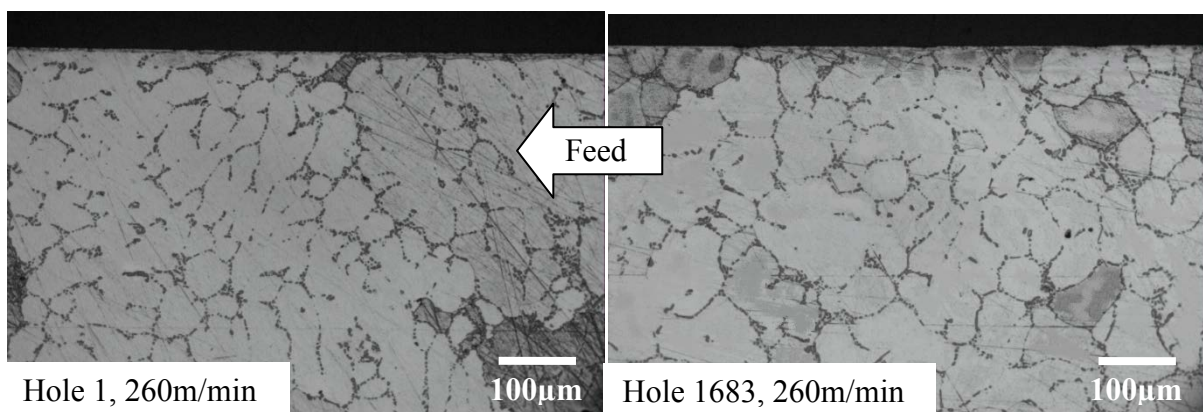


Figure 174: Phase 4A – Subsurface microstructure of drilled hole produced with PCD CTM302 tool – Test 8 (12mm from entry)

5.2.4 Phase 4B: Evaluation of diamond coated and PCD tools when reaming cast C355 aluminium alloy

This phase of experimental work involved reaming of C355 aluminium alloy at two different cutting speeds (32m/min and 96m/min) at a constant feed rate of 0.12mm/rev under high pressure cutting fluid application (70bar).

5.2.4.1 Tool conditions and cutting force

Evidence of aluminium smearing and BUE formation was observed from optical micrographs showing the tool flank face of uncoated carbide reamers used in Tests 1 and 2 (32 and 96m/min), see Figure 175. In contrast, no signs of workpiece material deposition/adhesion were visible on either the CVD diamond coated (Tests 3 and 4) or brazed PCD reamers (Tests 5 to 8) even after machining 1683 holes, see Figure 176 to Figure 178. Appendix F further shows tool wear/condition of the reamers used in Phase 4B. Indications of any wear scars on the diamond based reamers however were not apparent under the magnification of the optical microscope. Whereas, flank wear (VB_{Bmax}) of up to 32.5 μ m and 38.5 μ m were found on tools used in Tests 1 and 2 respectively. The wear levels on the carbide tools were comparable with the results presented by Lugscheider et al. [83] when cutting AlSi12 with hard coated reamers.

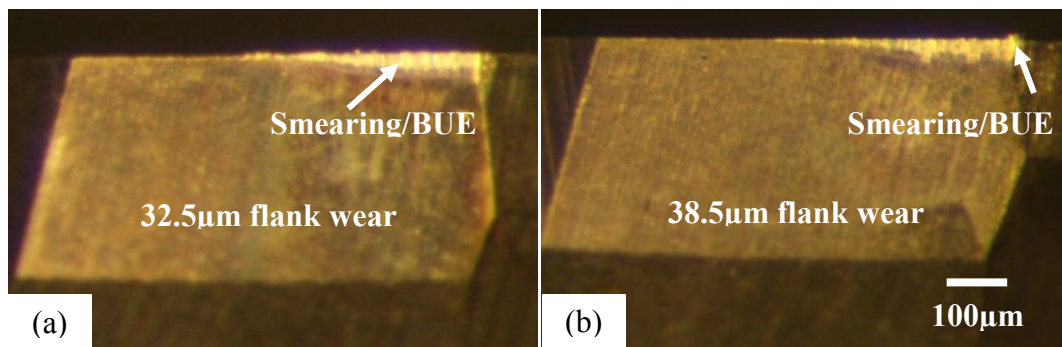


Figure 175: Phase 4B – End of test micrographs for uncoated carbide reamers in (a) Test 1 and (b) Test 2

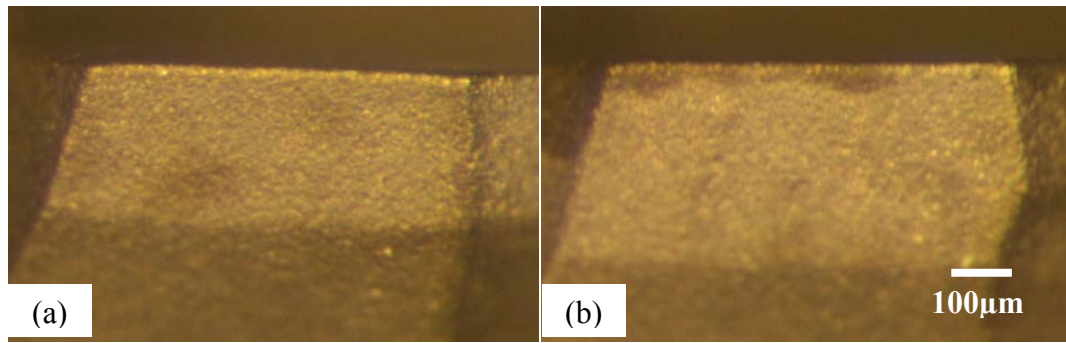


Figure 176: Phase 4B – End of test micrographs for CVD diamond reamers in (a) Test 3 and (b) Test 4

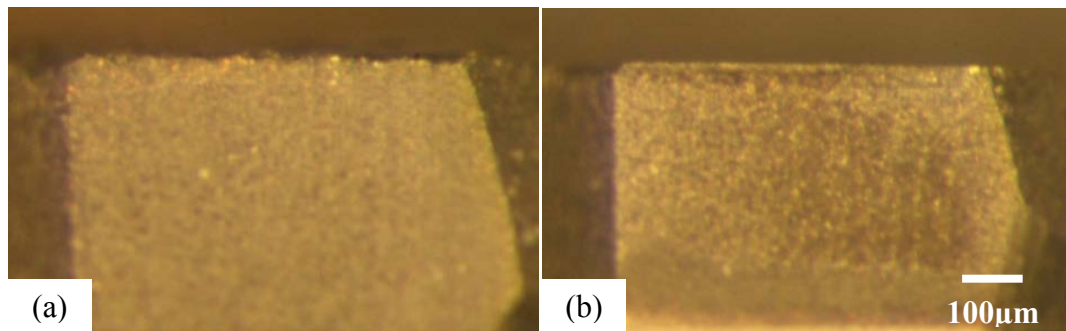


Figure 177: Phase 4B – End of test micrographs for PCD CTB002 reamers in (a) Test 5 and (b) Test 6

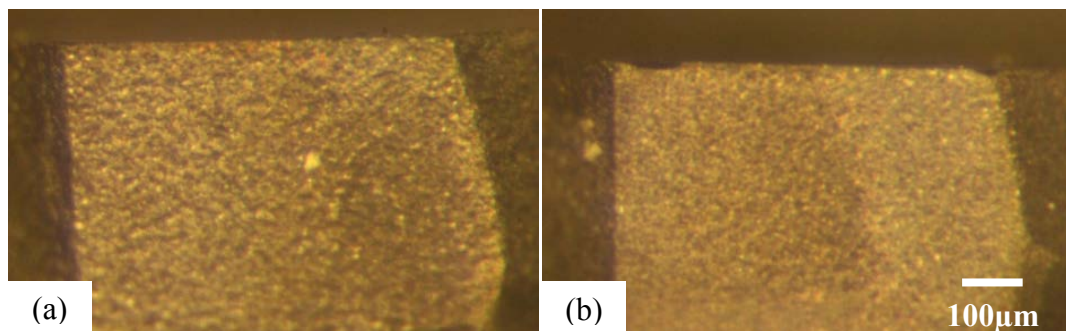


Figure 178: Phase 4B – End of test micrographs for PCD CTM302 reamers in (a) Test 7 and (b) Test 8

The progression of thrust force and torque during the reaming trials is detailed in Figure 179 and Figure 180 respectively. The CVD diamond coated reamers employed in Tests 3 and 4 were found to produce ~50% higher thrust force (ranging between 36N and 84N) and 125% higher torque (ranging between 31Ncm and 67Ncm) compared to the standard uncoated carbide tools in Tests 1 and 2 at equivalent operating conditions. This was most likely due to the duller/larger cutting edge radius of the former as a result of the thickness of the diamond coating (3 μ m) shown in Figure 181. Minimum thrust force (17-21N) was achieved with both

the fine (CTB002) and mixed (CTM302) graded PCD grades when operating at 96m/min cutting speed. Force values did not exceed ~85N in any of the trials.

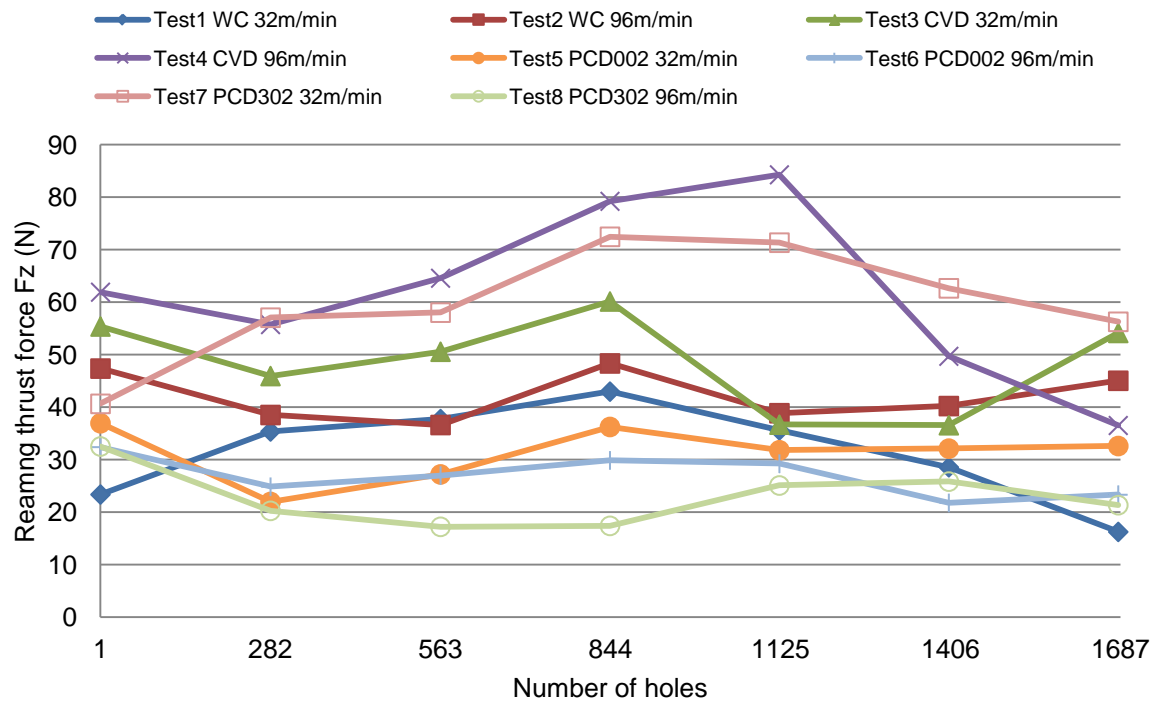


Figure 179: Phase 4B – Maximum reaming thrust force

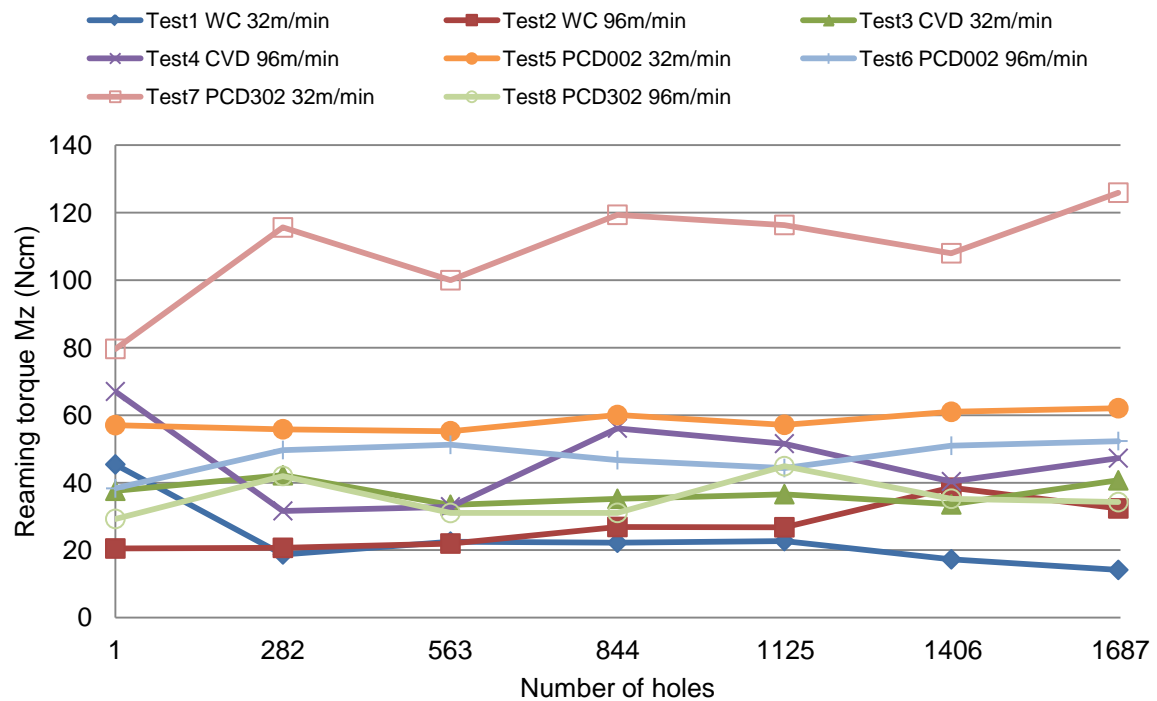


Figure 180: Phase 4B – Maximum reaming torque

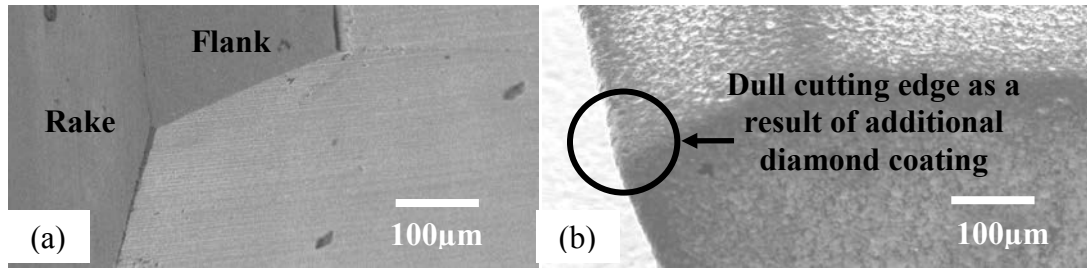


Figure 181: SEM images of new (a) uncoated and (b) CVD diamond coated reamers

Torque levels, except for Test 4 and 7, after hole 1 were stable throughout the test duration with the maximum value of 60Ncm when reaming with the PCD002 at 32m/min (Test 5). The CVD coated reamer operating at higher cutting speed (Test 4) generated fluctuating torque (32-67Ncm). Test 7 involving the PCD302 produced the highest torque at up to 125Ncm, although after hole 282 the rise was only ~26Ncm to test cessation. The uncharacteristically high torque levels measured in both tests were possibly due to tool vibration during the trial. Figure 182 shows the typical unstable force signals observed during the reaming trials using the CVD diamond and PCD302 reamers.

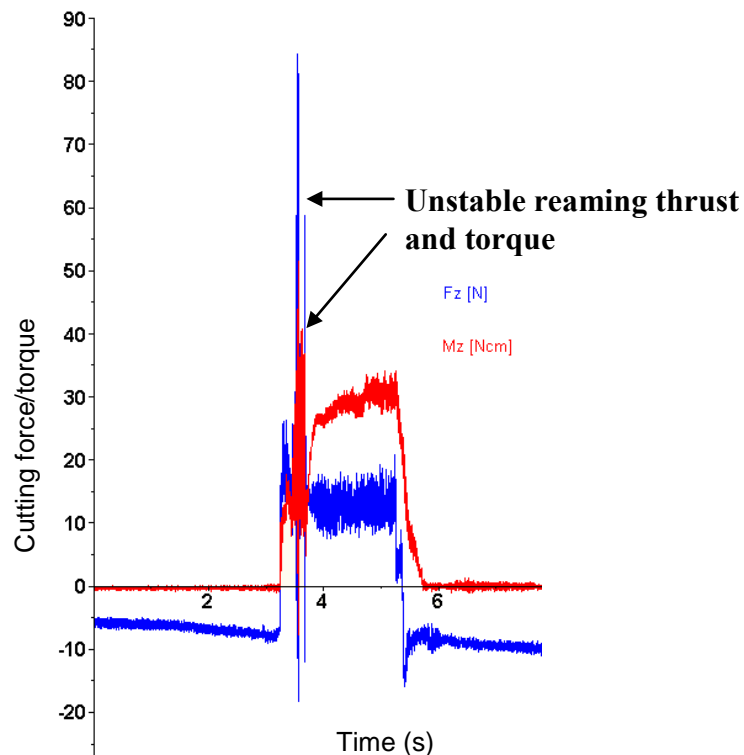


Figure 182: Typical unstable thrust force and torque signal recorded in Test 4 and 7

5.2.4.2 Workpiece quality

Final hole diameter and associated geometric quality measures following the finish reaming operation are presented in Figure 183 and Figure 184 respectively. All the holes machined with the uncoated and CVD diamond coated reamers were oversize by between $2\mu\text{m}$ and $11\mu\text{m}$. While the PCD tools used in Test 6 (CTB002) and Test 8 (CTM302) resulted in holes with the lowest deviation, which was consistently within $\pm 2\mu\text{m}$ of the nominal value (5.08mm) over the duration of the experiment. The holes in Test 7 however showed a decreasing trend in size from 5.077mm at the first hole to 5.073mm at the last hole.

The average hole roundness was less than $5\mu\text{m}$ in all of the experiments performed, with the best performance seen in Test 6 involving the CTB002 grade reamer. Hole cylindricity values did not exceed $14\mu\text{m}$ following reaming, with the lowest deviation of $5.28\mu\text{m}$ corresponding to the CVD diamond coated tool in Test 3. In terms of parallelism, positive values were prevalent in almost all of the tests undertaken, suggesting that the reamed holes were tapered towards the hole entry. Generally, Test 4 (CVD diamond) and Test 7 (PCD CTM302) produced poor reamed hole quality due to tool vibration during the experiments. The high reaming thrust force (Figure 179) and torque (Figure 180) further supports this observation.

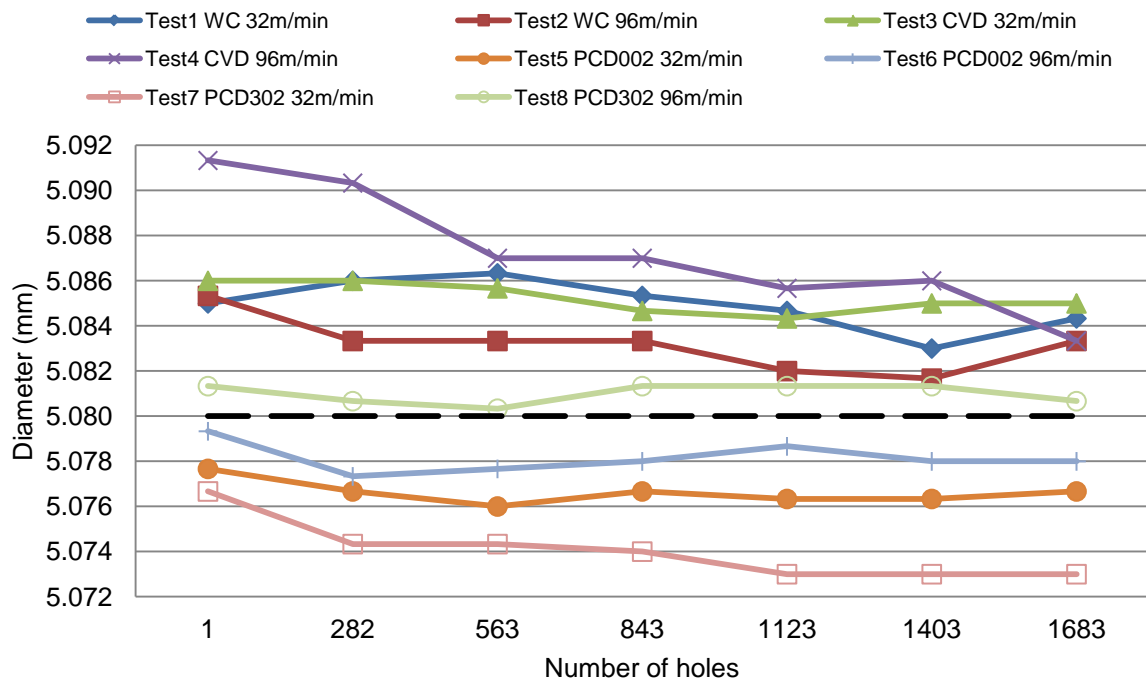


Figure 183: Phase 4B – Reamed hole diameter

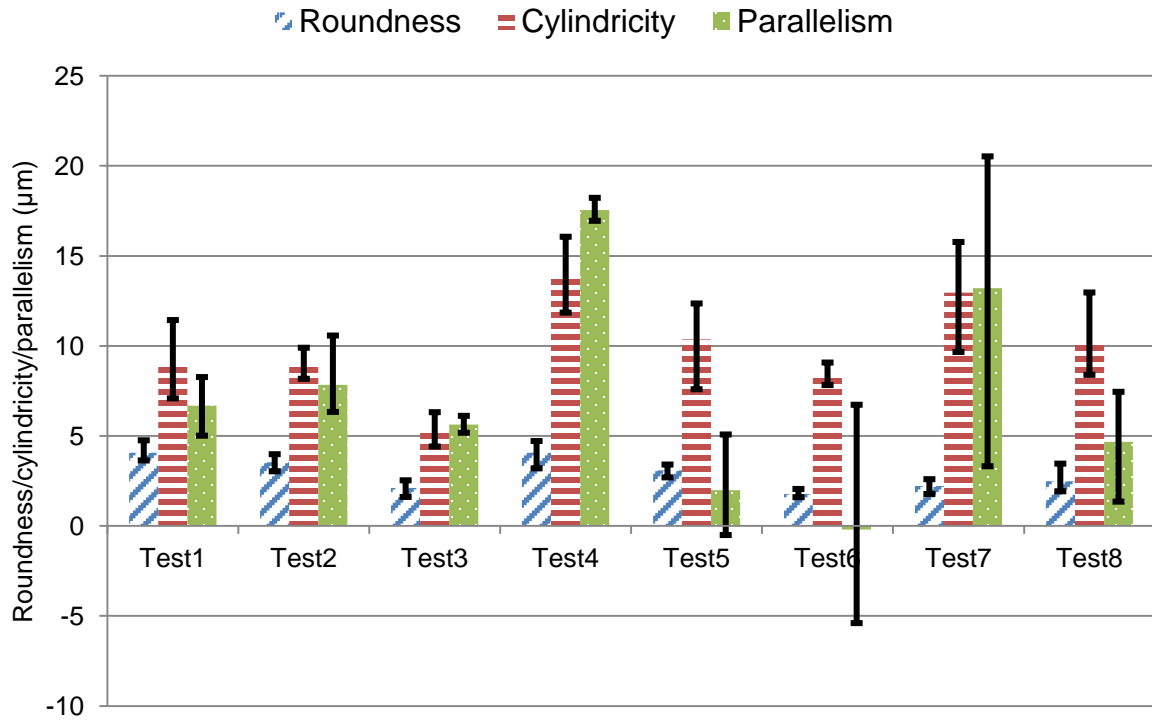


Figure 184: Phase 4B – Reamed hole geometric quality

5.2.4.3 Workpiece surface roughness and integrity

Figure 185 and Figure 186 show the progression in reamed hole surface roughness (R_a) measured at the entry and exit locations respectively. Aside from a number of uncharacteristic peaks/spikes in R_a recorded in Test 3 (hole 282) and Test 5 (hole 563), the workpiece surface quality was found to be generally better at the top of the reamed holes compared with that obtained towards the bottom. The unusual peaks were possibly due to flaws in hole surfaces within the region of the evaluation length, similarly discussed in Section 5.2.1.4. The general trend also suggests that surface finish improved as the cutting speed was increased to 96m/min. Previously published work relating to the machining of non-ferrous materials [198, 237] suggested that an increase in cutting speed raised the temperature within the machining zone that led to thermal softening of the workpiece, thus resulting in a considerable reduction in surface damage and roughness. Typically, the CTM302 grade PCD reamers produced the lowest and most consistent overall surface roughness ($\sim 0.05\mu\text{m } R_a$) regardless of the cutting speed, followed by the finer grained CTB002. The PCD reamers also generated superior workpiece surface roughness compared to the CVD diamond coated and uncoated tools, due to their greater wear resistance and lower affinity to BUE formation/material adhesion.

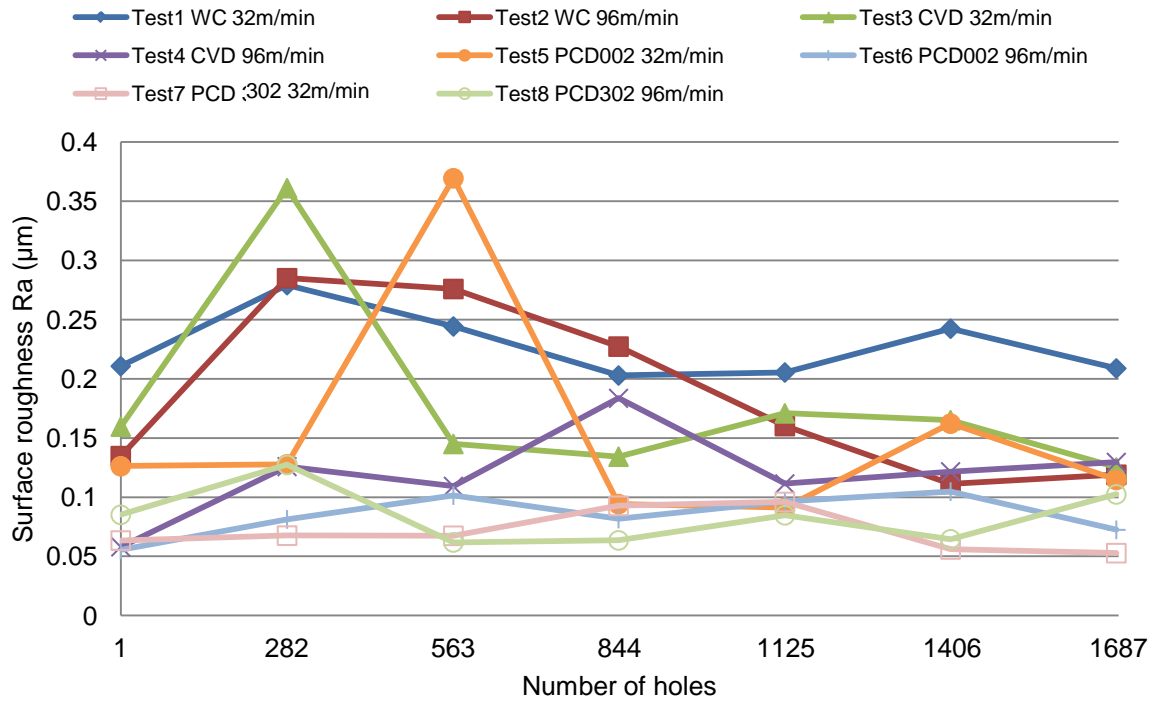


Figure 185: Phase 4B – Reamed hole surface roughness (2mm from entry)

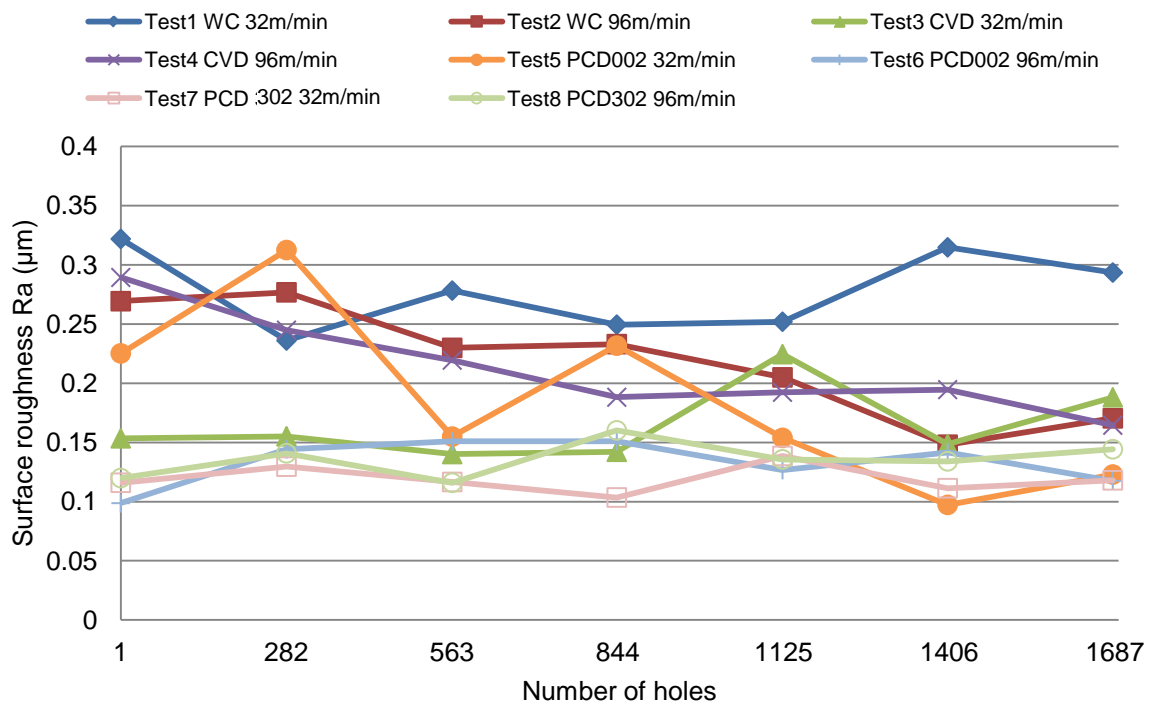


Figure 186: Phase 4B – Reamed hole surface roughness (23mm from entry)

Microhardness profiles measured perpendicular to the feed direction for 32m/min and 96m/min cutting speed are shown in Figure 187 and Figure 188 respectively. Minimal changes in surface/subsurface microhardness levels were observed in the majority of tests, although a hardened layer of up to $24.6\text{HK}_{0.025}$ (~17%) above the bulk hardness and up to a depth of $75\mu\text{m}$ was found in Test 4 involving the CVD diamond tool at the start and end of tests. High silicon dispersion within the indentation area could have been the reason for the deviated microhardness values. However, examination of the etched cross-sectional microstructure samples from each trial shown in Figure 189 to Figure 196 revealed no major surface/subsurface damage or microstructural deformation either with new or worn reamers regardless of the operating parameters. This also equated with hole roughness observations in all tests, surfaces being extremely consistent from the start to the end of the experiments.

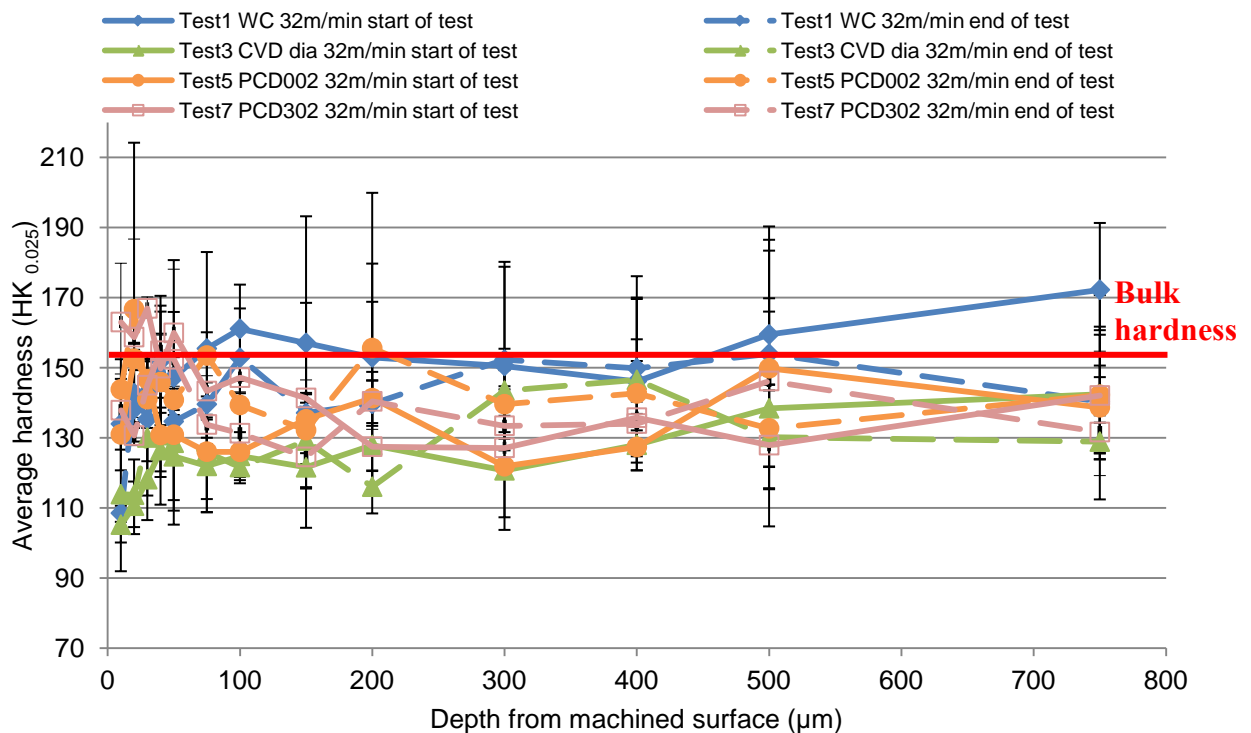


Figure 187: Phase 4B – Microhardness of cross-sections of reamed hole (12mm from entry, reaming speed 32m/min)

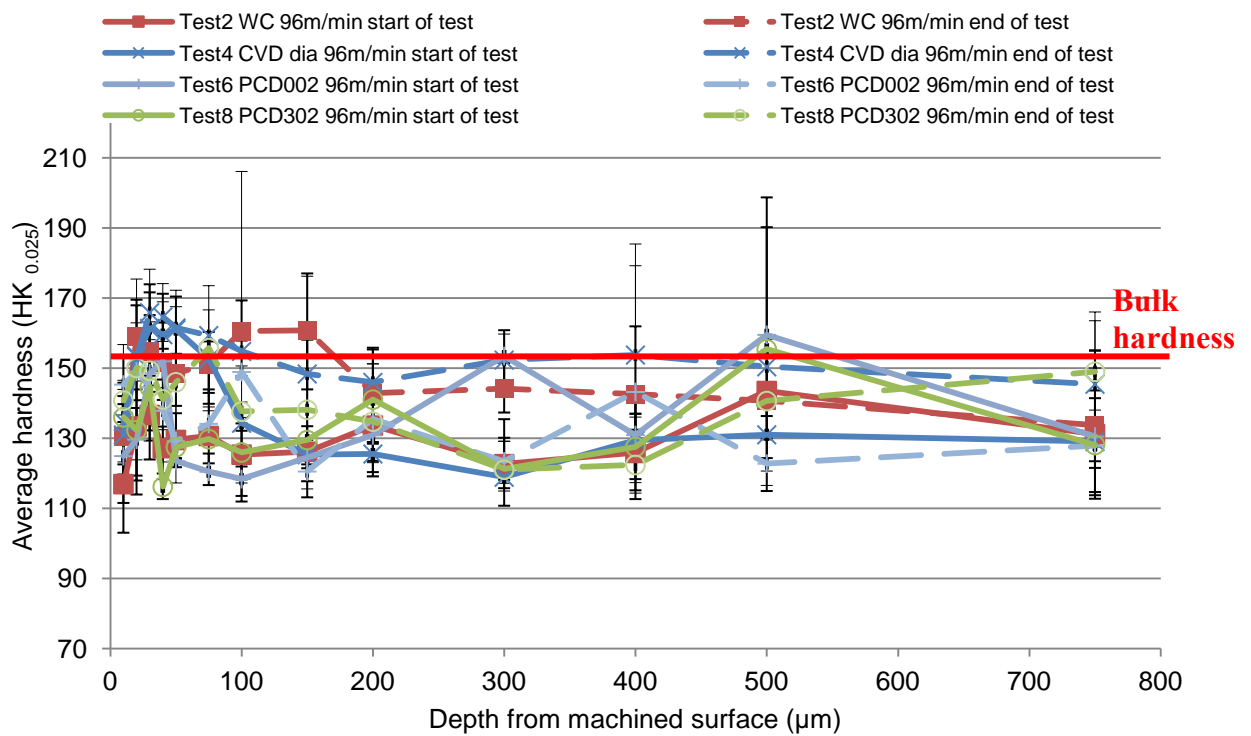


Figure 188: Phase 4B – Microhardness of cross-sections of reamed hole (12mm from entry, reaming speed 96m/min)

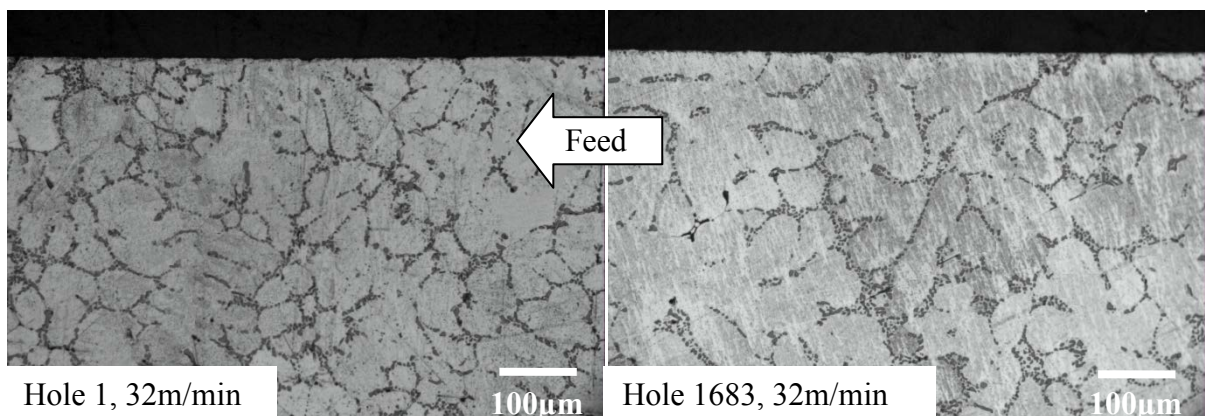


Figure 189: Phase 4B – Subsurface microstructure of reamed hole produced with uncoated carbide tool – Test 1 (12mm from entry)

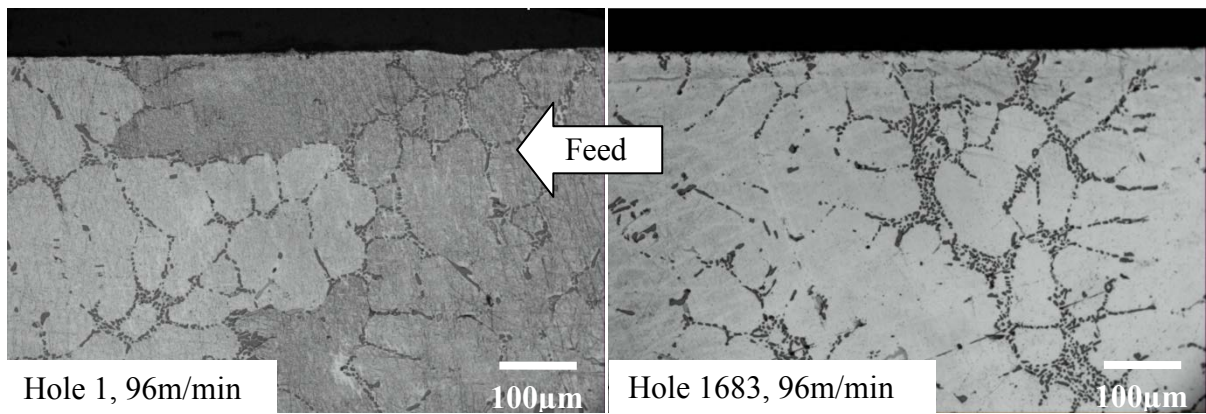


Figure 190: Phase 4B – Subsurface microstructure of reamed hole produced with uncoated carbide tool – Test 2 (12mm from entry)

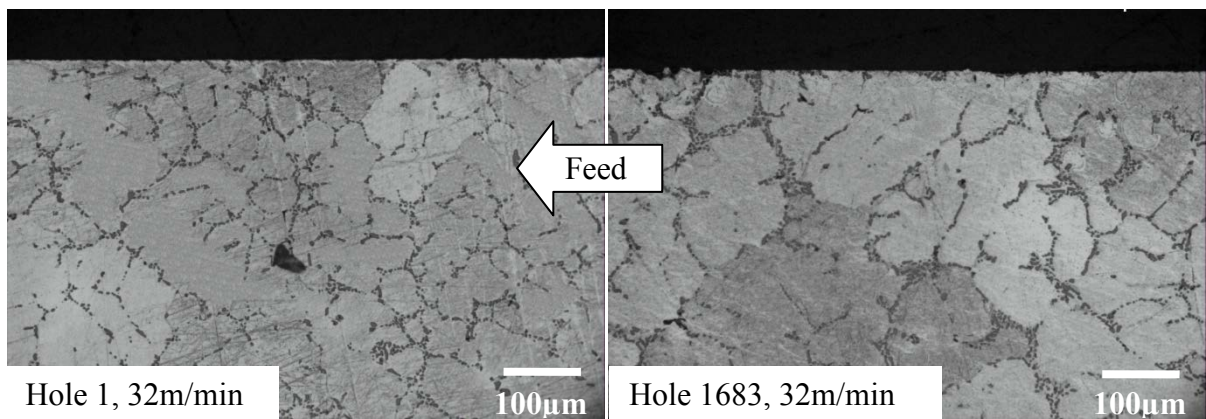


Figure 191: Phase 4B – Subsurface microstructure of reamed hole produced with CVD diamond carbide tool – Test 3 (12mm from entry)

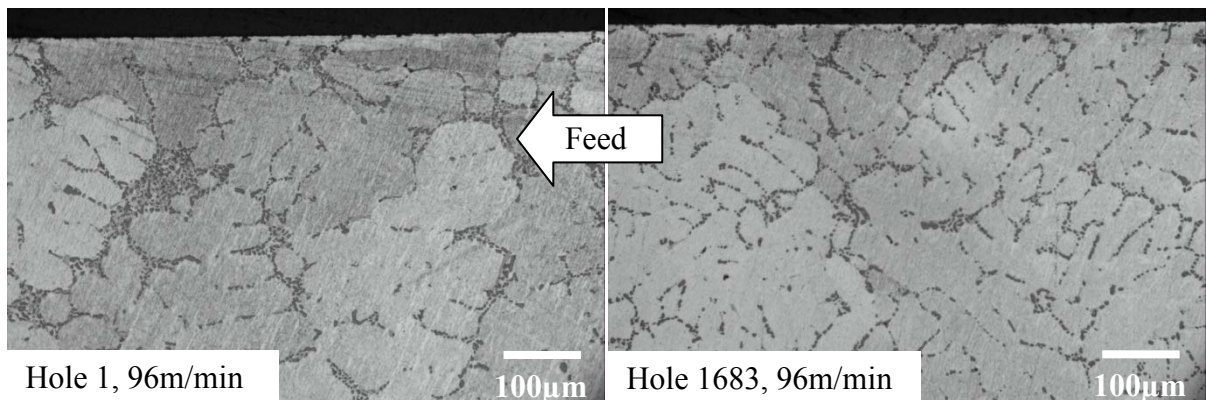


Figure 192: Phase 4B – Subsurface microstructure of reamed hole produced with CVD diamond carbide tool – Test 4 (12mm from entry)

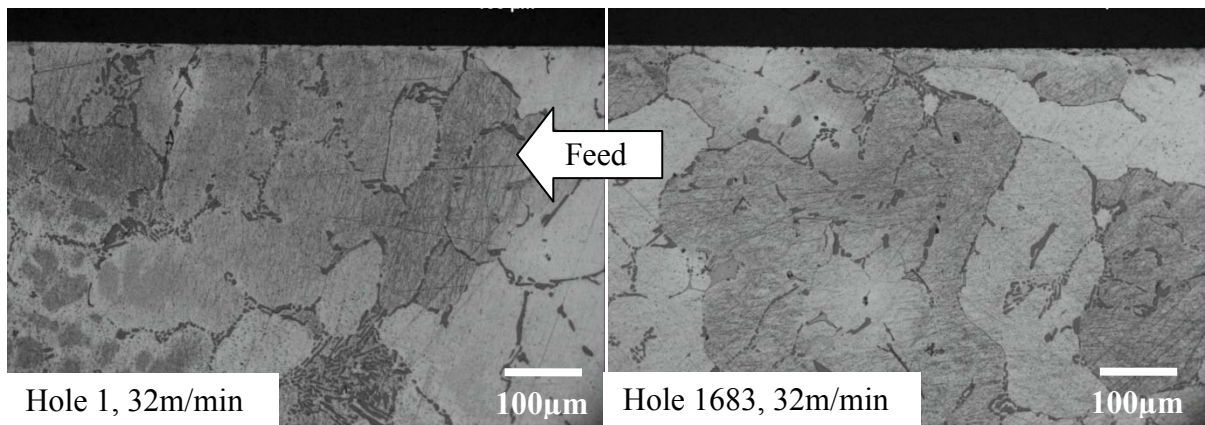


Figure 193: Phase 4B – Subsurface microstructure of reamed hole produced with PCD CTB002 tool – Test 5 (12mm from entry)

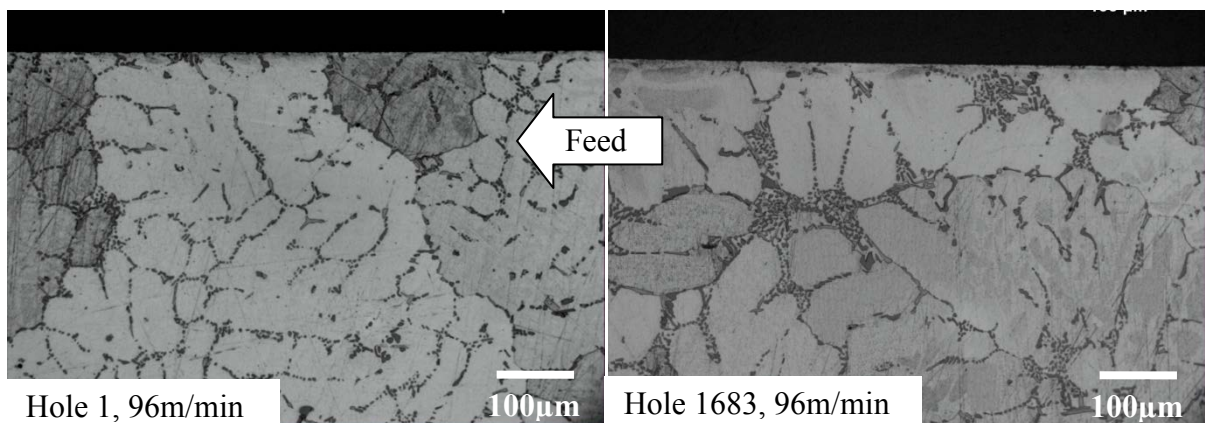


Figure 194: Phase 4B – Subsurface microstructure of reamed hole produced with PCD CTB002 tool – Test 6 (12mm from entry)

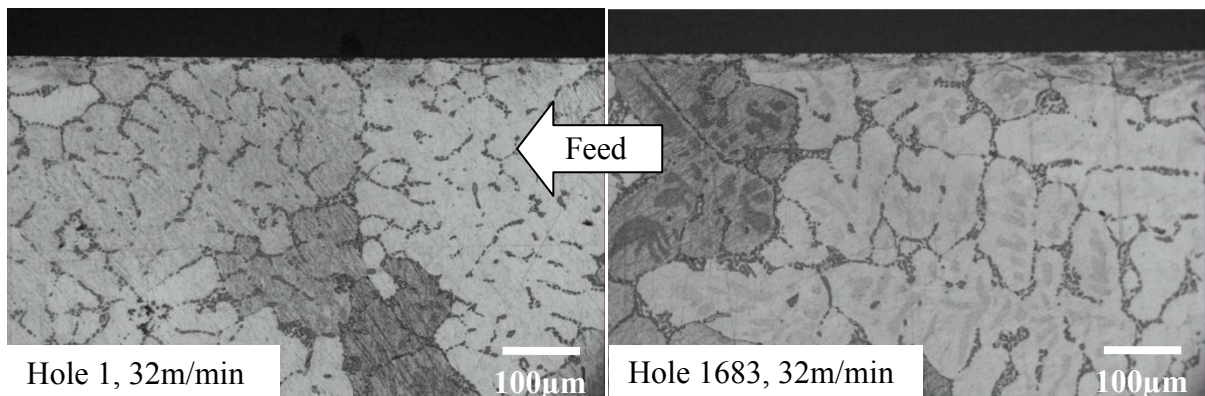


Figure 195: Phase 4B – Subsurface microstructure of reamed hole produced with PCD CTM302 tool – Test 7 (12mm from entry)

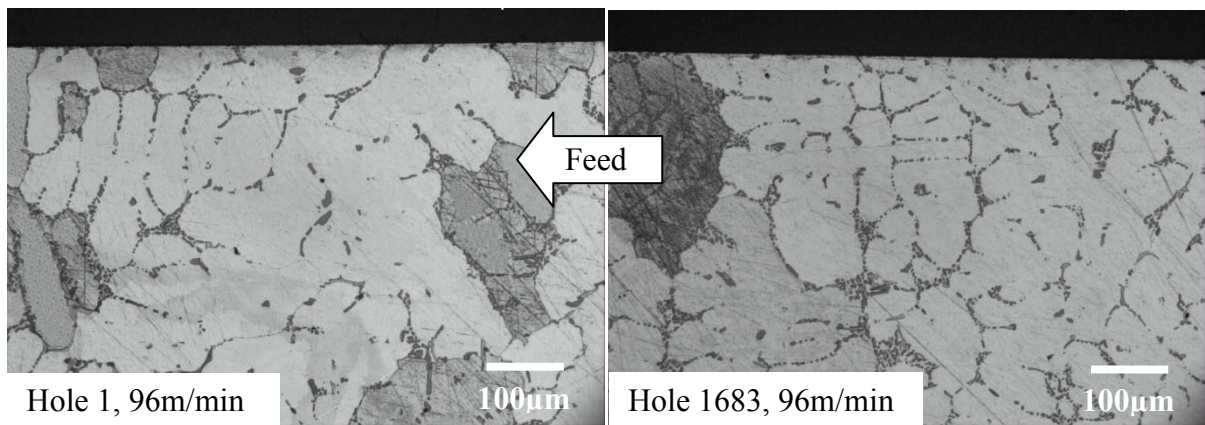


Figure 196: Phase 4B – Subsurface microstructure of reamed hole produced with PCD CTM302 tool – Test 8 (12mm from entry)

CHAPTER 6: CONCLUSIONS

6.1 Literature review

- Literature relating to the machining of aluminium alloys is extensive, with the majority of studies focusing on abrasive hypereutectic alloys $>13\%Si$ over the last 60 years. Cutting tool materials for aluminium encompass high speed steels, uncoated tungsten carbides (WC) and advanced diamond tooling (chemical vapour deposited diamond and polycrystalline diamond). Use of PCD tools is especially prevalent in high volume production allowing extended tool life and the possibility of enabling higher cutting speeds in order to improve productivity without diminishing workpiece quality.
- Commonly observed issues with machining aluminium include adhered workpiece material, built-up layer and built-up edge on tools, which subsequently compromises surface finish and repeatability/consistency of component geometry. Increasing levels of silicon content causes higher tool abrasion and subsequent rises in machining costs.
- To date, only limited information has been reported on the reaming of aluminium alloys. Recent research has focused primarily on the drilling process with assessment parameters predominantly relating to geometrical accuracy and workpiece surface roughness. Data relating to workpiece surface/subsurface integrity following drilling of aluminium alloys however is scarce.
- Dry machining has been a major topic of research over the past ~15years particularly for the drilling/reaming of aluminium in response to the need for reducing costs as well as for issues relating to environmental and health and safety aspects. However, workpiece material packing/clogging in the tool flute path is still a major problem for mechanical hole making operations and cutting fluid application, even under minimum quantity conditions, has proven to be essential for achieving high geometrical accuracy and prolonging tool life when drilling/reaming aluminium. In addition to reducing drilling thrust force and torque, the use of fluid/lubricants helps lower temperatures at the tool-workpiece interface during high speed cutting and aids swarf evacuation under low speed operation.

- Since its introduction in the mid 1970's, polycrystalline diamond (PCD) has become the cutting tool material of choice for machining abrasive silicon aluminium alloys. It has an established track record of being able to produce excellent surface finish at the most economical operational cost. More recently, CVD diamond (thin film) has emerged as an alternative with hardness and coefficient of friction levels similar to single crystal diamond. However, galling/chipping of coating layers is still a major problem which makes it unsuitable for intermittent and/or high depth of cut machining.

6.2 Experimental work

6.2.1 Industry based work

6.2.1.1 Phase 1: Assessment and capability study of current compressor impeller machining processes

- Typically, the level of overall equipment effectiveness (OEE) in Doncasters Sterling's machine shop was approximately 80%. The relatively low OEE was largely due to the unscheduled downtime/breakdown of the machine tools and the number of cutting tool changes required. It was established that there was an opportunity for improvement in the OEE through regular maintenance of equipment as well as utilising/implementing alternative types of cutting tools from different suppliers.
- Component scrap level directly relating to machining was approximately 6% with bore defects, including scores/scuff marks and over/undersizing of the drilled/reamed holes, being the dominant cause.
- Process capability studies showed that the Index G200 machine tool was capable of providing a stable and consistent process in producing compressor impellers when employing the WC Walter Titex drill, Beck WC reamer, TiB₂ coated WC roughing and Exactaform PCD finishing cutting inserts.
- Capability indices, Cp and Cpk, of the critical component features, including hole diameter, hole surface roughness, squareness of nose and back of the component, either met or exceeded the minimum automotive industry requirement of 1.66.
- Cylindricity of the drilled/reamed holes however had a Cp value of 1.24, which was below the standard level (1.66). This was subsequently improved (Cp of 1.79)

following a calibration of the necessary metrology equipment (Taylor Hobson Talyrond series 131). Lower than normal Cpk values (~45%) however were acceptable for critical features that only had a single sided/upper tolerance, such as squareness of the nose (CR2) and back (CR3) of the component, hole surface roughness (CR4) and hole cylindricity (CR5).

- Hourly-recorded control charts were introduced in the machine shop to allow operators to monitor the behaviour of the drilling/reaming process. The observations showed that interrupting the machining operation, i.e. stop/start, staff lunch break, etc., which caused the machine spindles and/or tool holders to cool down, contributed to the unstable hole machining process.

6.2.1.2 Phase 2: Production tooling trials and comparative work of Sterling standard tools against alternative cutting tool materials

- Burr formation on the compressor impeller blades and outside diameter was found to be the principal factor in determining the tool life of roughing inserts rather than component geometrical size.
- Production tooling trials with brazed PCD cutters supplied by Mapal demonstrated that the tools (Type 3 and 4) were capable of producing acceptable workpiece quality to specifications required by Doncasters Sterling with tool life greatly exceeding (~16 times) that of standard carbide tools (Type 1).
- The relatively weak geometrical feature (7° clearance and 12° rake angle) of the Exactaform cutting insert (Type 2) was found to be unsuitable for the interrupted, heavy rough turning/facing operation.
- The standard Mapal (Type 4) PCD roughing insert showed the best performance in terms of tool life, lasting ~1.8 times longer than the Mapal Type 3 (with chip breaker) cutting insert for operation 1 under the same machining conditions. The PCD insert also proved to be the most economical tool for the rough turning/facing of the aluminium impellers with a typical cost per cutting edge of 0.57p/unit. It is anticipated that the longer tool life of the Mapal product would minimise the machine downtime/setup time leading to higher productivity in production. Furthermore, the insert can potentially be reground and reused up to three times, leading to further operational/tooling cost reduction.

- Comparative work involving uncoated WC Titex and TiN coated Guhring drills showed that the hardmetal coating (2400HV) of the latter prolonged the tool life by 10% compared with the former. High amounts of workpiece material clogging in the drill flutes of the Guhring tool however contributed to appreciably higher drilling forces (~30% thrust and ~18% torque) over the standard uncoated WC drill.
- Overall, the Walter Titex uncoated WC drill was found to be the cheaper option (~27% less operational cost) for blind-hole/ drilling (Op3) of aluminium compressor impellers.
- Over the course of 2 machining runs (following a regrind) the PCD reamer demonstrated 62% and 110% longer tool life respectively compared with its carbide counterpart (Beck RV3188).
- Due to high capital cost, the PCD reamer was found to be ~10% more expensive compared to the uncoated WC Beck reamer (based on an estimated total of 24,800 components machined for the PCD reamer). However, it was found that the Mapal PCD reamer offered significantly reduced machine downtime (67%) compared with the standard carbide reamers.

6.2.2 Laboratory based work

6.2.2.1 Phase 3A: Evaluation of diamond-like carbon coated tools when drilling cast C355 aluminium alloy

- Graphit-iC™ had the lowest wear rate (0.03µm/hole) which was 25% and 40% lower compared with the Dymon-iC™ coated and uncoated WC drills when evaluated using Doncasters Sterling's current production parameters (flood cutting fluid at cutting speed of 130m/min).
- The application of external high pressure (70bar) cutting fluid, regardless of the cutting speed, was found to reduce tool wear levels by ~13% as well as the incidence of BUE formation/material adhesion, as a result of improved cutting fluid access to the cutting zone.
- Higher pressure cutting fluid was also found to contribute to consistent hole diameter, but at the expense of tool instability/chatter. This led to poorer overall results with respect to cutting forces and workpiece geometrical accuracy.

- The Graphit-iC™ and Dymon-iC™ improved the hole cylindricity by 7% and 30% when operating under a flood cutting fluid at 130m/min and 260m/min respectively.
- Increasing cutting speed produced poorer overall hole geometrical accuracy, particularly in relation to the roundness (84% poorer) and cylindricity (27% poorer) of the drilled holes.
- Drilling thrust force and torque fluctuated during experiments, which was partially caused by inconsistencies in the cast workpiece material properties as well as inclusions and silicon particles. Drilling thrust force was observed to be lower as cutting speed increased in all tests, although the resulting geometrical tolerance of the holes was compromised.
- Drilled hole surface roughness did not exceed 2.3µm Ra in any of the tests evaluated. Surface integrity evaluation showed that the Graphit-iC™ coated drill produced the least amount of workpiece surface/subsurface damage due to microstructural change. As a result, the Graphit-iC™ was selected for production tooling trials at Doncasters Sterling for blind-hole drilling of compressor impellers. The drill was capable of producing parts required by the customer with cylindricity less than 5µm on the hole cylindricity.
- Analysis suggested that a Graphit-iC™ coated drill would potentially machine ~5000 components, using Doncasters Sterling's production parameters, at 0.35p/unit as opposed to 0.53p/unit when utilising the Walter Titex uncoated WC drill.

6.2.2.2 Phase 3B: Evaluation of diamond-like carbon coated tools when reaming 6082-T6 aluminium alloy

- BUE on tools was evident during the reaming of 6082-T6 (1%Si) aluminium alloy. Swarf deposited on the tool holder was also observed during the trial, which required remedial action. The swarf/BUE problem was minimised when the reaming speed was increased.
- Graphit-iC™ and Dymon-iC™ were subject to significantly lower wear rates by 150% and 57% respectively compared with uncoated WC.
- The majority of reaming thrust force and torque levels generated were generally high at the start of the trials, but remained stable until test cessation.
- The reaming thrust force values generally dropped with an increase in reaming speed, due partially to minimal BUE/material adhesion. In any case, the reaming thrust force and torque values were considered insignificant.
- Workpiece quality in terms of hole diameter, roundness, cylindricity and parallelism, was best achieved with Doncasters Sterling's cutting parameter of 32m/min cutting speed, 0.12mm/rev and 2000rev/min compared with the 96m/min cutting speed.
- The uncoated tungsten carbide reamer produced the lowest overall hole surface roughness, with average Ra values of 0.16µm and 0.28µm towards the hole entry and bottom position respectively. It was expected that the average reamed hole surface roughness result obtained from the experiment would not satisfy Sterling's requirement of 0.2µm Ra max. However, this result may improve when the cutting tool is employed in production in conjunction with a floating-feature reamer holder.
- With regard to surface/subsurface integrity, no pits or tears were observed.
- Graphit-iC™ coated tools produced minimal hardness alteration.

6.2.2.3 Phase 4A: Evaluation of diamond coated and PCD tools when drilling cast C355 aluminium alloy

- Substantial amounts of aluminium adhesion and built-up edge was experienced with the uncoated carbide drills in all tests. In contrast, there was minimal adhesion on the brazed PCD and CVD diamond coated tool.

- Although the CVD diamond coating generally increased the life of the drills compared with the uncoated tools, the poor bonding of the diamond coating to the substrate led to peeling/delamination at high cutting speed.
- A combination of flank wear on the uncoated WC drills together with BUE/material adhesion was considered responsible for the comparatively high thrust forces obtained.
- Drilling thrust force was observed to drop with an increase in drilling cutting speed. Uncoated WC, CVD diamond coated, brazed PCD (CTB010 and CTM302) drills produced steady levels of thrust force and torque throughout the experiment. Brazed PCD CTB010 generated the most stable response, of around $\pm 10\text{N}$, and the lowest average maximum thrust force even at high cutting speed compared with the uncoated WC and CVD diamond coated drills.
- Short-continuous conical and fan shaped chips were produced with helical flute uncoated WC and CVD diamond coated drills, whilst transitional chips were produced with the straight flute brazed PCD drills during the machining of cast C355 aluminium alloy. The brazed PCD products, (CTB010 and CTM302) had through-hole geometry and were expected to perform much better when used with high pressure cutting fluid.
- Generally, smaller and broken chips were produced at higher cutting speed during the drilling of aluminium C355, which contributed to lower thrust force and torque.
- Tests involving the uncoated WC and PCD tools produced undersized holes, whilst the CVD diamond coated tools produced holes $\sim 10\mu\text{m}$ larger than the nominal diameter due to the additional coating.
- Drilled hole quality in terms of cylindricity and parallelism was more consistent and improved at low cutting speed. The hole surface roughness produced using PCD products (CTB010 and CTM302 grades), gave the best result and did not exceed $0.3\mu\text{m Ra}$ even after 1683 holes.
- Hardened layers which measured $\sim 10\%$ above the material bulk hardness to a depth of $\sim 75\mu\text{m}$ from the drilled surface were recorded for the last hole drilled for all tests. Hole cross-sectional assessment revealed no microcracks or microstructural alteration in any of the specimens evaluated.

6.2.2.4 Phase 4B: Evaluation of diamond coated and PCD tools when reaming cast C355 aluminium alloy

- Evidence of aluminium smearing and BUE was observed on the flank of the uncoated tungsten carbide tools under low (32m/min) and high (96m/min) reaming speeds. However, this was not experienced with the PCD or the CVD diamond coated reamers.
- Wear scars were only visible on the uncoated carbide tools for trials at cutting speeds of 32m/min and 96m/min. Here the wear measured 32.5µm and 38.5µm respectively.
- Generally, the diameter of holes produced using the uncoated tungsten carbide and the CVD diamond coated reamers were oversize and exceeded the +3µm tolerance required by Doncasters Sterling. In contrast, hole diameter was within ±2µm even after 1683 holes when employing the PCD tools, both CTB002 and CTM302 grades, at a cutting speed of 96m/min.
- Roundness values of the reamed holes was <5µm for all specimens assessed. The lowest surface roughness achieved was 0.05µm Ra when using the brazed PCD CTM302 reamers.
- There was minimal change to hole surface/subsurface microhardness following reaming, with the exception of Test 4 (CVD diamond tool) which showed a hardened layer with a maximum of ~25HK_{0.025} above the bulk material to a depth of 75µm.
- Microstructure evaluation revealed no surface/subsurface damage in all tests involving the standard carbide, the CVD diamond coated carbide or the brazed PCD reamers.

6.3 Summary and recommendations for machining operations of aluminium compressor impellers

6.3.1 Process capability study on Index G200 machining centre

The process capability study (Cp and Cpk) performed when machining various impeller features on the Index G200 cell indicated that the majority of the features met/exceeded the required process capability requirement (minimum Cp and Cpk value of 1.66 is standard for the automotive industry). See Table 40 in Section 5.1.1.2. Low Cpk

(<1.66) was not uncommon and was acceptable for the features with a one-sided set tolerance (squareness of back-face and nose, surface roughness and cylindricity).

6.3.2 Roughing turning/facing, Op1, of aluminium compressor impellers

The rough turning/facing operation of the compressor impellers removes a minimum of 1mm of material per pass/cut per component, (~3 passes leaving 0.2mm for the finishing operation) and Mapal CCGW09T308 F01N0AA PCD insert (Type 4) showed reduced tool setup times/machine downtime per cutting insert, whilst able to meet the specified requirement. The operational cost per component was proved to be cheaper when employing the Mapal PCD insert than the carbide with a further tool cost saving of 58% following a tool regrind, which is expected to be up to 3 times.

Table 44: Summary of Operation 1/rough turning/facing

Recommended tool material	Mapal CCGW09T308 F01N0AA PCD, Syndite CTB010 10µm grain, 0° rake and 7° relief angle
Cutting speed, feed rate	850m/min, 0.15mm/rev
Operational cost per edge [after 1st tool regrind @£15]	0.57p/unit [0.23p/unit, 60% cheaper than WC]
Production tool life	6000 components (650% higher than WC) for 1mm depth of cut , typical ø45mm impeller

6.3.3 Blind-hole drilling, Op3, of aluminium compressor impellers

CVD diamond would have been an excellent cutting tool material of choice for the drilling operation due to its excellent abrasive resistance, less tendency to material build up, ability to produce acceptable workpiece geometry accuracy and relatively cheaper compared with the brazed PCD tools. However, the poor bond of the diamond coating was a limiting factor. In contrast, Mapal PCD CTB010 and Mapal PCD CTM302 are good substitutes with regard to tool robustness. Both PCD tools have extensive tool life compared with the current tungsten carbide drill. Production tool life observation (though not included in Section 5.12) showed that the PCD CTB010 produced 6300 components (110% higher than the uncoated WC). The overall operational cost (based on £212 capital cost, £30 regrind cost), provided the production tool life is not compromised and that a total of three tool regrinds was possible, would be 0.84p/unit. The PCD product would equate to ~58% more expensive compared to

the WC drill. A reduction of overall tool changeovers/downtime is however a benefit offered by the PCD drill, but only in high volume production. Graphit-iC™ coating, however, is an alternative tool material that is capable of providing exceptional workpiece quality and potentially higher tool life compared with the WC drill. With the current persisting casting defects contributing to the breakage, a Graphit-iC™ coated drill would be a cheaper option than both the PCD and uncoated carbide drills.

Table 45: Summary of Operation 3/drilling

Recommended tool material	Walter Titex A1167B , K10 WC, with Graphit-iC™ coating, twist, 15° helix, 150° point angle
Cutting speed, feed rate	130m/min, 0.1mm/rev
Operational cost per tool	0.35p/unit @ £18 (34% cheaper than WC)
Expected tool life	~5000 holes (66% higher than WC) for 28mm depth, ø4.8mm

6.3.4 Blind-hole reaming, Op4, of aluminium compressor impellers

A Mapal brazed PCD reamer may be employed to reduce the extensive time, 30min, taken for the reamer setup. The PCD tool, once set, is expected to last for at least fifteen 8hr-shifts, which will increase the productivity considerably especially when the machine tool is operating for 24hr per day.

Amongst the hole machining operations, currently reaming takes the longest time, 6.3 seconds per hole at 2000rev/min and 0.12mm/rev. The reaming time could potentially be reduced to 2.1 seconds per hole by utilising 6000rev/min maximum spindle speed without compromising the quality of the component.

On the economical side, CVD diamond coated reamer is expected to be the cheaper option for the reaming operation compared with the standard carbide and PCD (CTB010 and CTM302 grades) tools. However, dimensional accuracy of the reamed hole is imperative and the evidence suggested that the CVD diamond tool may not be able to satisfy the stringent tolerance requirement.

Mapal brazed PCD with CTM302 grade has the capability to meet the requirement and is a cheaper option compared with WC and PCD CTB002 reamers. Therefore, Mapal PCD

CTM302 is recommended, either in a low/current or high cutting speeds, for the reaming operation. However, the governing limit that needs to be taken into account is the work-holding unit (WHU) which loads and unloads the workpiece to and from the spindles. This needs to be modified to accommodate a faster reaming operation. The tool will help save the machining cost compared with the standard carbide Beck reamer currently in use at Sterling, only if the tool regrind is possible, i.e. no tool breakage.

Table 46: Summary of Operation 4/reaming

Tool material	Mapal brazed PCD, Syndite CTM302 mixed grades of 2µm to 30µm, 2 cutting edges, straight fluted with through holes for high pressure cutting fluid, 0° rake angle and 45° chamfer
Cutting speed, feed rate	32m/min or 96m/min, 0.12mm/rev
Operational cost per tool [after 1st regrind @ £30]	5.92p/unit @ £355 [0.5p/unit 70% cheaper than WC]
Expected tool life	6000 holes (100% higher than WC) for 25mm depth, 0.28mm depth of cut, at lower cutting speed

CHAPTER 7: RECOMMENDATIONS FOR FUTURE WORK

A number of areas were highlighted during the research which merits further investigation. These include;

- Establishment and evaluation of capability indices (C_p and C_{pk}) for the aluminium impeller machining processes, including turning/facing, drilling and reaming, on the Index G200 machining centre using the recommended cutting tools (Mapal CCGW09T308 F01N0AA PCD roughing insert, Walter Titex A1167B with Graphit-iC™ coating and Mapal brazed PCD reamer with Syndite CTM302 grade).
- Production tooling trial investigation of a single-pass/combined rough (Op1) and finish (Op5) turning/facing operations using Mapal CCGW09T308 F01N0AA (Type 4) PCD roughing insert to further increase the material removal rate and productivity.
- Further study of production tool life of the Mapal PCD products, including rough turning/facing (Op1), drilling (Op3) and reaming (Op4) operations, in order to establish limitation of the total number of tool regrinds and operational cost.
- Investigation of cutting forces (thrust force and torque) when blind-hole drilling of defective impellers/castings containing blowhole/porosity.
- Use of through-hole high pressure cutting fluid (70bar) application when drilling cast C355 aluminium using brazed PCD tool and to investigate workpiece quality and BUE/material adhesion on the tool substrate.
- Further investigation of tool life, cutting forces (thrust and torque), workpiece quality (surface roughness and integrity) when reaming cast C355 aluminium using a floating tool holder.
- Investigations of increasing cutting speed for PCD tooling.

REFERENCES

1. Anon, *Doncasters Group Ltd.* 2010,
2. Wallace, G., Jackson, A. P., Midson, S. P. and Zhu, Q., *High-quality aluminum turbocharger impellers produced by thixocasting*. Transactions of Nonferrous Metals Society of China, 2010. 20(9): p. 1786-1791, 1003-6326.
3. Kane, J., *Turbochargers: Technology and Developments*. Race Engine Technology, 2012(58),
4. Anon, *INDEX-Werke GmbH & Co. KG Hahn & Tessky*. 2010,
5. Anon, *Aluminium and aluminium alloys - Chemical composition and form of wrought products*. BS EN 573:2009, 978 0 580 63982 1.
6. Polmear, I., *Light alloys: From traditional alloys to nanocrystals*. 2006: Butterworth Heinemann. 205-235, 0750663715.
7. Mondolfo, L. F., *Aluminium alloys: structure and properties*. 1976: Butter Worth. 759-775, 0408706805.
8. Bauccio, M., *ASM metals reference book*. 1993: ASM International. 152-421, 0871704781.
9. Davis, J. R., *ASM Specialty Handbook: Aluminum and aluminum alloys*. 1993: ASM International Handbook Committee, 087170496x.
10. Anon, *Machining data handbook*. 3 ed. Vol. 2. 1980, Ohio: Machinability Data Center, 0936974028.
11. Carrilero, M. S., Bienvenido, R., Sánchez, J. M., Álvarez, M., González, A. and Marcos, M., *A SEM and EDS insight into the BUL and BUE differences in the turning processes of AA2024 Al-Cu alloy*. International Journal of Machine Tools and Manufacture, 2002. 42(2): p. 215-220, 0890-6955.
12. Shen, C. H., *The importance of diamond coated tools for agile manufacturing and dry machining*. Surface and Coatings Technology, 1996. 86-87(Part 2): p. 672-677, 0257-8972.
13. List, G., Nouari, M., Géhin, D., Gomez, S., Manaud, J. P., Le Petitcorps, Y. and Girot, F., *Wear behaviour of cemented carbide tools in dry machining of aluminium alloy*. Wear, 2005. 259(7-12): p. 1177-1189, 0043-1648.
14. Sánchez, J. M., Rubio, E., Álvarez, M., Sebastián, M. A. and Marcos, M., *Microstructural characterisation of material adhered over cutting tool in the dry machining of aerospace aluminium alloys*. Journal of Materials Processing Technology, 2005. 164-165: p. 911-918, 0924-0136.
15. Nouari, M., List, G., Girot, F. and Coupard, D., *Experimental analysis and optimisation of tool wear in dry machining of aluminium alloys*. Wear, 2003. 255(7-12): p. 1359-1368, 0043-1648.
16. Durante, S., Rutelli, G. and Rabezzana, F., *Aluminum-based MMC machining with diamond-coated cutting tools*. 24th International Conference on Metallurgical Coatings and Thin Films, 1997. 94-95: p. 632-640, 0257-8972.
17. Rubio, E. M., Camacho, A. M., Sánchez-Sola, J. M. and Marcos, M., *Surface roughness of AA7050 alloy turned bars: Analysis of the influence of the length of machining*. Journal of Materials Processing Technology, 2005. 162-163: p. 682-689, 0924-0136.
18. Farid, A. A., Sharif, S. and Idris, M. H., *Surface integrity study of high-speed drilling of Al-Si alloy using HSS drill*. Proceedings of the Institution of Mechanical Engineers, Part B: Journal of Engineering Manufacture, 2011. 225(5): p. 1-7,
19. Basavakumar, K. G., Mukunda, P. G. and Chakraborty, M., *Influence of melt treatments and turning inserts on cutting force and surface integrity in turning of Al-*

- 12Si and Al-12Si-3Cu cast alloys*. Surface and Coatings Technology, 2007. 201(8): p. 4757-4766, 0257-8972.
20. Yousefi, R. and Ichida, Y., *A study on ultra-high-speed cutting of aluminium alloy: Formation of welded metal on the secondary cutting edge of the tool and its effects on the quality of finished surface*. Precision Engineering, 2000. 24(4): p. 371-376, 0141-6359.
21. Smith, G. T., *Advanced machining: The handbook of cutting technology*. 1989: IFS Publications Ltd, 1854230220.
22. Haan, D. M., Batzer, S. A., Olson, W. W. and Sutherland, J. W., *An experimental study of cutting fluid effects in drilling*. Journal of Materials Processing Technology, 1997. 71(2): p. 305-313, 0924-0136.
23. Jayal, A. D., Balaji, A. K., Sesek, R., Gaul, A. and Lillquist, D. R., *Machining Performance and Health Effects of Cutting Fluid Application in Drilling of A390.0 Cast Aluminum Alloy*. Journal of Manufacturing Processes, 2007. 9(2): p. 137-146, 1526-6125.
24. Bhowmick, S. and Alpas, A. T., *Minimum quantity lubrication drilling of aluminium-silicon alloys in water using diamond-like carbon coated drills*. International Journal of Machine Tools and Manufacture, 2008. 48(12-13): p. 1429-1443, 0890-6955.
25. Gangopadhyay, S., Acharya, R., Chattopadhyay, A. K. and Sargade, V. G., *Effect of cutting speed and surface chemistry of cutting tools on the formation of BUL or BUE and surface quality of the generated surface in dry turning of AA6005 aluminium alloy*. Machining Science and Technology, 2010. 14(2): p. 208-223, 10910344.
26. Davim, J. P., *Machining : fundamentals and recent advances*. 2008, New York ; London: Springer. 361-361, 9781848002128.
27. Manna, A. and Bhattacharayya, B., *A study on machinability of Al/SiC-MMC*. Journal of Materials Processing Technology, 2003. 140(1-3): p. 711-716, 0924-0136.
28. Cooper, J., Pretorius, N., Bowler, J. and Perkins, N., *Machining of metal matrix composites using PCD, natural diamond, single crystal CVD and polycrystalline CVD diamond*. Industrial Diamond Review, 2007(3): p. 34-38,
29. Ozben, T., Kilickap, E. and Çakir, O., *Investigation of mechanical and machinability properties of SiC particle reinforced Al-MMC*. Journal of Materials Processing Technology, 2008. 198(1-3): p. 220-225, 0924-0136.
30. Ding, X., Liew, W. Y. H. and Liu, X. D., *Evaluation of machining performance of MMC with PCBN and PCD tools*. 15th International Conference on Wear of Materials, 2005. 259(7-12): p. 1225-1234, 0043-1648.
31. Monaghan, J. and O'reilly, P., *The drilling of an Al/SiC metal-matrix composite*. Journal of Materials Processing Technology, 1992. 33(4): p. 469-480, 0924-0136.
32. Tosun, G. and Muratoglu, M., *The drilling of Al/SiCp metal-matrix composites. Part II: workpiece surface integrity*. Composites Science and Technology, 2004. 64(10-11): p. 1413-1418, 0266-3538.
33. El-Gallab, M. and Sklad, M., *Machining of Al/SiC particulate metal matrix composites: Part II: Workpiece surface integrity*. Journal of Materials Processing Technology, 1998. 83(1-3): p. 277-285, 0924-0136.
34. Sarkar, A. D. and Clarke, J., *Friction and wear of aluminium-silicon alloys*. Wear, 1980. 61(1): p. 157-167, 0043-1648.
35. Wang, L., Makhoulouf, M. and Apelian, D., *Aluminium die casting alloys: alloy composition, microstructure, and properties-performance relationships*. International Materials Reviews, 1995. 40(6): p. 221-238,

36. Dwivedi, D. K., Sharma, R. and Kumar, A., *Influence of silicon content and heat treatment parameters on mechanical properties of cast Al-Si-Mg alloys*. International Journal of Cast Metals Research, 2006. 19(5): p. 275-282,
37. Ng, E. G., Szablewski, D., Dumitrescu, M., Elbestawi, M. A. and Sokolowski, J. H., *High Speed Face Milling of a Aluminium Silicon Alloy Casting*. CIRP Annals - Manufacturing Technology, 2004. 53(1): p. 69-72, 0007-8506.
38. Bezerra, A. A., Machado, A. R., Souza, A. M. and Ezugwu, E. O., *Effects of machining parameters when reaming aluminium-silicon (SAE 322) alloy*. Journal of Materials Processing Technology, 2001. 112(2-3): p. 185-198, 0924-0136.
39. Keen, D., *An investigation into the possible advantages of using polycrystalline diamond tools instead of single crystal diamond tools for turning Al/Si alloy pistons*. Wear, 1974. 28(3): p. 319-330, 0043-1648.
40. Roy, P., Sarangi, S. K., Ghosh, A. and Chattopadhyay, A. K., *Machinability study of pure aluminium and Al-12% Si alloys against uncoated and coated carbide inserts*. International Journal of Refractory Metals and Hard Materials, 2009. 27(3): p. 535-544, 0263-4368.
41. Dwivedi, D. K., Sharma, A. and Rajan, T. V., *Machining of LM13 and LM28 cast aluminium alloys: Part I*. Journal of Materials Processing Technology, 2008. 196(1-3): p. 197-204, 0924-0136.
42. Uhlmann, E., Reimers, F., Byrne, F. and Klaus, M., *Analysis of tool wear and residual stress of CVD diamond coated cemented carbide tools in the machining of aluminium silicon alloys*. Prod. Eng. Res. Devel., 2010. 4(2-3): p. 203-209,
43. Grum, J. and Kisin, M., *Influence of microstructure on surface integrity in turning--part I: the influence of the size of the soft phase in a microstructure on surface-roughness formation*. International Journal of Machine Tools and Manufacture, 2003. 43(15): p. 1535-1543, 0890-6955.
44. Anon, *Tool-life testing with single-point turning tools, ISO 3685:1993*. 1993,
45. Sreejith, P. S., *Machining of 6061 aluminium alloy with MQL, dry and flooded lubricant conditions*. Materials Letters, 2008. 62(2): p. 276-278, 0167-577X.
46. Vernaza-Pena, K. M., Mason, J. J. and Li, M., *Experimental study of the temperature field generated during orthogonal machining of an aluminium alloy*. Experimental Mechanics, 2001. 42(2): p. 221-229,
47. Kazban, R. V., Vernaza-Pena, K. M. and Mason, J. J., *Measurements of forces and temperature fields in high-speed machining of 6061-T6 aluminium alloy*. Experimental Mechanics, 2008. 48(3): p. 307-317,
48. Deng, W. J., Xia, W., Zhao, X. L., Tang, Y., Yan, X.-T., Jiang, C. and Eynard, B., *Modelling of Temperature History During Machining of Cast Aluminium Alloy Advanced Design and Manufacture to Gain a Competitive Edge*. 2008, Springer London. p. 231-240, 978-1-84800-241-8.
49. Astakhov, V. P., *The assessment of cutting tool wear*. International Journal of Machine Tools and Manufacture, 2004. 44(6): p. 637-647, 0890-6955.
50. Leep, H. R. and Eldridge, T. W., *Effects of cutting conditions on drilling of aluminium 380*. Materials Engineering and Performance, 1992. 1(6): p. 797-800,
51. Heath, P. J., *Developments in applications of PCD tooling*. Journal of Materials Processing Technology, 2001. 116(1): p. 31-38, 0924-0136.
52. Batzer, S. A., Haan, D. M., Rao, P. D., Olson, W. W. and Sutherland, J. W., *Chip morphology and hole surface texture in the drilling of cast Aluminum alloys*. Journal of Materials Processing Technology, 1998. 79(1-3): p. 72-78, 0924-0136.
53. Liu, Q. and Matsuda, N., *Study of drilling temperature and performance on drilling of Al-17 mass % alloy*. 1998: International Academic Publishers, 7800034291.

54. Klocke, F. and Eisenblätter, G., *Dry Cutting*. CIRP Annals - Manufacturing Technology, 1997. 46(2): p. 519-526, 0007-8506.
55. Bono, M. and Ni, J., *The effects of thermal distortions on the diameter and cylindricity of dry drilled holes*. International Journal of Machine Tools and Manufacture, 2001. 41(15): p. 2261-2270, 0890-6955.
56. Dasch, J. M., Ang, C. C., Wong, C. A., Cheng, Y. T., Weiner, A. M., Lev, L. C. and Konca, E., *A comparison of five categories of carbon-based tool coatings for dry drilling of aluminum*. Surface and Coatings Technology, 2006. 200(9): p. 2970-2977, 0257-8972.
57. Dasch, J. M., Ang, C. C., Wong, C. A., Waldo, R. A., Chester, D., Cheng, Y. T., Powell, B. R., Weiner, A. M. and Konca, E., *The effect of free-machining elements on dry machining of B319 aluminum alloy*. Journal of Materials Processing Technology, 2009. 209(10): p. 4638-4644, 0924-0136.
58. Wain, N., Thomas, N. R., Hickman, S., Wallbank, J. and Teer, D. G., *Performance of low-friction coatings in the dry drilling of automotive Al-Si alloys*. Surface and Coatings Technology, 2005. 200(5-6): p. 1885-1892, 0257-8972.
59. Christoffel, J., *Development trends in the machining of bores*. 2000, IDR. p. 138-140.
60. Nouari, M., List, G., Girot, F. and Géhin, D., *Effect of machining parameters and coating on wear mechanisms in dry drilling of aluminium alloys*. International Journal of Machine Tools and Manufacture, 2005. 45(12-13): p. 1436-1442, 0890-6955.
61. Thangaraj, A. and Wright, P. K., *Drill wear sensing and failure prediction for untended machining*. Robotics and Computer-Integrated Manufacturing, 1988. 4(3-4): p. 429-435, 0736-5845.
62. Jantunen, E., *A summary of methods applied to tool condition monitoring in drilling*. International Journal of Machine Tools and Manufacture, 2002. 42(9): p. 997-1010, 0890-6955.
63. Kanai, M., Iwata, K., Fiujii, S. and Kanda, Y., *Statistical characteristics of drill wear and drill life for the standardised performance tests*. CIRP Annals - Manufacturing Technology, 1978. 27(1): p. 61-66,
64. Lenz, E., Mayer, J. E. and Lee, D. G., *Investigation in drilling*. CIRP Annals - Manufacturing Technology, 1978. 27(1): p. 49-53,
65. Chou, Y. K., Thompson, R. G. and Kumar, A., *CVD-diamond technologies for dry drilling applications*. Thin Solid Films, 2010. 518(24): p. 7487-7491, 0040-6090.
66. Braga, D. U., Diniz, A. E., Miranda, G. W. A. and Coppini, N. L., *Using a minimum quantity of lubricant (MQL) and a diamond coated tool in the drilling of aluminum-silicon alloys*. Journal of Materials Processing Technology, 2002. 122(1): p. 127-138, 0924-0136.
67. Lin, W. S., *The reliability analysis of cutting tools in the HSM processes*. International Scientific, 2008. 30(2): p. 97-100,
68. Lin, S. C. and Ting, C. J., *Tool wear monitoring in drilling using force signals*. Wear, 1995. 180(1-2): p. 53-60, 0043-1648.
69. Miller, S. F., Tao, J. and Shih, A. J., *Friction drilling of cast metals*. International Journal of Machine Tools and Manufacture, 2006. 46(12-13): p. 1526-1535, 0890-6955.
70. Kelly, J. F. and Cotterell, M. G., *Minimal lubrication machining of aluminium alloys*. Journal of Materials Processing Technology, 2002. 120(1-3): p. 327-334, 0924-0136.
71. Kim, H. Y., Ahn, J. H., Kim, S. H. and Takata, S., *Real-time drill wear estimation based on spindle motor power*. Journal of Materials Processing Technology, 2002. 124(3): p. 267-273, 0924-0136.

72. Rincon, D. M., Ulsoy, A. G. and Kaftanoglu, B., *Effects of Drill Vibrations on Cutting Forces and Torque*. CIRP Annals - Manufacturing Technology, 1994. 43(1): p. 59-62, 0007-8506.
73. Trent, E. M. and Wright, P. K., *Metal cutting*. 2000, Boston ; Oxford: Butterworth-Heinemann. 9-242, 075067069X.
74. Anon, *Aluminium and aluminium alloy ingots and castings for general engineering purposes*. BS 1490:1988, 0 580 16575 2.
75. Coelho, R. T., Yamada, S., Aspinwall, D. K. and Wise, M. L. H., *The application of polycrystalline diamond (PCD) tool materials when drilling and reaming aluminium based alloys including MMC*. International Journal of Machine Tools and Manufacture, 1995. 35(5): p. 761-774, 0890-6955.
76. Hamade, R. F., Seif, C. Y. and Ismail, F., *Extracting cutting force coefficients from drilling experiments*. International Journal of Machine Tools and Manufacture, 2006. 46(3-4): p. 387-396, 0890-6955.
77. Williams, J. A. and Tabor, D., *The role of lubricants in machining*. Wear, 1977. 43(3): p. 275-292, 0043-1648.
78. Lugscheider, E., Knotek, O., Barimani, C., Leyendecker, T., Lemmer, O. and Wenke, R., *PVD hard coated reamers in lubricant-free cutting*. Surface and Coatings Technology, 1999. 112(1-3): p. 146-151, 0257-8972.
79. Arunachalam, S., Gunasekaran, A. and O'sullivan, J. M., *Analysing the process behaviour of abrasive reaming using an experimental approach*. International Journal of Machine Tools and Manufacture, 1999. 39(8): p. 1311-1325, 0890-6955.
80. Zeng, Z., *The influence of cutting depth on resolving power of cutting fluid efficiency in reaming test*. ICPCG, 1996: p. 296-300,
81. Belluco, W. and De Chiffre, L., *Surface integrity and part accuracy in reaming and tapping stainless steel with new vegetable based cutting oils*. Tribology International, 2002. 35(12): p. 865-870, 0301-679X.
82. Schlogl, H. and Schwarz, R., *Machining oil pumps with PCD-tipped reamers*. 1995, IDR. p. 109-111.
83. Lugscheider, E., Knotek, O., Barimani, C., Leyendecker, T., Lemmer, O. and Wenke, R., *Investigations on hard coated reamers in different lubricant free cutting operations*. Surface and Coatings Technology, 1997. 90(1-2): p. 172-177, 0257-8972.
84. Ohgo, K., Satoh, A., Mizuno, T. and Itoh, T., *Relation between cutting conditions and precision in the reaming of gray iron castings*. Wear, 1979. 52(1): p. 79-88, 0043-1648.
85. Mills, B., *Recent developments in cutting tool materials*. Journal of Materials Processing Technology, 1996. 56(1-4): p. 16-23, 0924-0136.
86. Almond, E. A., *Towards improved tests based on fundamental properties*, in *Proceedings of the International Conference on Improved Performance of tool materials*. 1981, The National Laboratory and the Metals Society: Teddington, Middlesex. p. 161-169.
87. Brookes, K. J. A., *World directory and handbook of hardmetals*. 1996, United Kingdom: International carbide data, 0950899542.
88. Anon, *Application of hard cutting materials for machining by chip removal - Designation of the main groups of chip removal and groups of application*. BS 7662:1993, 0 580 21790 6.
89. Smith, G. T., *Cutting Tool Technology*. Cutting Tool Technology. 2008: Springer London, 978-1-84800-205-0.

90. Yang, Q., Senda, T. and Ohmori, A., *Effect of carbide grain size on microstructure and sliding wear behavior of HVOF-sprayed WC-12% Co coatings*. Wear, 2003. 254(1-2): p. 23-34, 0043-1648.
91. Saito, H., Iwabuchi, A. and Shimizu, T., *Effects of Co content and WC grain size on wear of WC cemented carbide*. Wear, 2006. 261(2): p. 126-132, 0043-1648.
92. Shi, X., Yang, H., Shao, G., Duan, X. and Wang, S., *Oxidation of ultrafine-cemented carbide prepared from nanocrystalline WC-10Co composite powder*. Ceramics International, 2008. 34(8): p. 2043-2049, 0272-8842.
93. Yang, Q., Senda, T. and Hirose, A., *Sliding wear behavior of WC-12% Co coatings at elevated temperatures*. Surface and Coatings Technology, 2006. 200(14-15): p. 4208-4212, 0257-8972.
94. Ferreira, J. A. M., Amaral, M. A. P., Antunes, F. V. and Costa, J. D. M., *A study on the mechanical behaviour of WC/Co hardmetals*. International Journal of Refractory Metals and Hard Materials, 2009. 27(1): p. 1-8, 0263-4368.
95. Abdel-Aal, H. A., Nouari, M. and Mansori, M. E., *The effect of thermal property degradation on wear of WC-CO inserts in dry cutting*. Wear, 2008. 265(11-12): p. 1670-1679, 0043-1648.
96. Klocke, F. and Krieg, T., *Coated Tools for Metal Cutting – Features and Applications*. CIRP Annals - Manufacturing Technology, 1999. 48(2): p. 515-525, 0007-8506.
97. Aramcharoen, A., Mativenga, P. T., Yang, S., Cooke, K. E. and Teer, D. G., *Evaluation and selection of hard coatings for micro milling of hardened tool steel*. International Journal of Machine Tools and Manufacture, 2008. 48(14): p. 1578-1584, 0890-6955.
98. Critchlow, G. W., Hampshire, J., Kingdon, R., Naeem, Z., Smith, A. B. and Teer, D. G., *Adhesion of wear resistant hard coatings to steel substrates*. Tribology International, 1997. 30(7): p. 499-506, 0301-679X.
99. Hintermann, H. E., *Tribological and protective coatings by chemical vapour deposition*. Thin Solid Films, 1981. 84(3): p. 215-243, 0040-6090.
100. Grzesik, W., *Experimental investigation of the cutting temperature when turning with coated indexable inserts*. International Journal of Machine Tools and Manufacture, 1999. 39(3): p. 355-369, 0890-6955.
101. Grzesik, W. and Nieslony, P., *Thermal Characterization of the Chip-Tool Interface When Using Coated Turning Inserts*. Journal of Manufacturing Processes, 2000. 2(2): p. 79-87, 1526-6125.
102. Grzesik, W. and Wanat, T., *Surface finish generated in hard turning of quenched alloy steel parts using conventional and wiper ceramic inserts*. International Journal of Machine Tools and Manufacture, 2006. 46(15): p. 1988-1995, 0890-6955.
103. Fox, V., Jones, A., Renevier, N. M. and Teer, D. G., *Hard lubricating coatings for cutting and forming tools and mechanical components*. Surface and Coatings Technology, 2000. 125(1-3): p. 347-353, 0257-8972.
104. Field, S. K., Jarratt, M. and Teer, D. G., *Tribological properties of graphite-like and diamond-like carbon coatings*. Tribology International, 2004. 37(11-12): p. 949-956, 0301-679X.
105. Jones, B. L., *Prospects for new applications of diamond*. IDR, 1992(4): p. 175-179,
106. Inspektor, A., Bauer, C. E. and Oles, E. J., *Superhard coatings for metal cutting applications*. Surface and Coatings Technology, 1994. 68-69: p. 359-368, 0257-8972.
107. Coe, S. E. and Sussmann, R. S., *Optical, thermal and mechanical properties of CVD diamond*. Diamond and Related Materials, 2000. 9(9-10): p. 1726-1729, 0925-9635.
108. Anon, *Syndite as a wear resistant material - An assessment*. Industrial Diamond Review, 1998. 58(4): p. 179-182,

109. Hayes, D., *PCD for a gloss finish*. Industrial Diamond Review, 1994. 54(4): p. 181-184,
110. Jennings, M., *All round success for Syndite*. Industrial Diamond Review, 1991. 51(4): p. 184-185,
111. Jennings, M., *Twin peaks for PCD tooling*. Industrial Diamond Review, 1991. 51(3): p. 129-130,
112. Jennings, M. and Clark, I., *PCD in the automotive industry*. Industrial Diamond Review, 1995. 55(2): p. 51-53,
113. Li, X. S., Boland, J. N. and Guo, H., *A comparison of wear and cutting performance between diamond composite and tungsten carbide tools*. Industrial Diamond Review, 2008. 68(1): p. 51-54,
114. Mikhail, P., *Efficient precision machining of the smallest bores 0.015 to 4mm in diameter*. Industrial Diamond Review, 2008. 68(2): p. 51-55,
115. Uhlmann, E., Friemel, J. and Brucher, M., *Machining of a hypereutectic aluminium silicon alloy*. Industrial Diamond Review, 2001. 61(4): p. 260-265,
116. Uhlmann, E., Koenig, J., Durst, G., Hilty, B. and Sueess, B., *Performance of diamond coated cutting tools as a function of material properties*. Industrial Diamond Review, 2008. 68(2): p. 51-55,
117. Wiemann, E., Koenig, M., Keunecke, M. and Richter, V., *Superhard coatings for cutting tools*. Industrial Diamond Review, 2007. 67(1): p. 19-22,
118. Anon, *PCD & PCBN usage in Japanese industry*. Industrial Diamond Review, 1990. 50(4): p. 194-196,
119. Spain, I. L. and Paauwe, J., *High pressure technology : applications and processes*. Vol. 2. 1977, New York: M. Dekker, 0824765915.
120. Walmsley, J. C., *The microstructure of ultrahard material compacts studied by transmission electron microscopy*. Materials Science and Engineering: A, 1988. 105-106(Part 2): p. 549-553, 0921-5093.
121. Anon, *Element Six Ltd*. 2010,
122. Karagöz, S. and Zeren, M., *The microstructural design of diamond cutting tools*. Materials Characterization, 2001. 47(2): p. 89-91, 1044-5803.
123. Karagöz, S. and Zeren, M., *The property optimization of diamond-cutting tools with the help of micro-structural characterization*. International Journal of Refractory Metals and Hard Materials, 2001. 19(1): p. 23-26, 0263-4368.
124. Zeren, M. and Karagöz, S., *Defect characterization in the diamond cutting tools*. Materials Characterization, 2006. 57(2): p. 111-114, 1044-5803.
125. Zeren, M. and Karagöz, S., *Sintering of polycrystalline diamond cutting tools*. Materials & Design, 2007. 28(3): p. 1055-1058, 0261-3069.
126. Werner, G. and Renter, M., *Grindability of PCD*. Industrial Diamond Review, 1989. 49(1): p. 15-19,
127. Konstanty, J., *Powder metallurgy diamond tools*. Metal powders technology series. 2005, Amsterdam ; London: Elsevier. 152-152, 1856174409.
128. Clark, I. E. and Sen, P. K., *Advances in the development of ultrahard cutting tool materials*. Industrial Diamond Review, 1998(2),
129. Reis, D. D. and Abrao, A. M., *The machining of aluminium alloy 6351*. Proceedings of the Institution of Mechanical Engineers, Part B: Journal of Engineering Manufacture, 2005. 219(1): p. 27-33, 0954-4054.
130. Wilks, J., *Performance of diamonds as cutting tools for precision machining*. Precision Engineering, 1980. 2(2): p. 57-72, 0141-6359.

131. Xiao, X., Lev, L. C. and Lukitsch, M. J., *Material transfer during machining of aluminum alloys with polycrystalline diamond cutting tools*. Journal of Materials Processing Technology, 2009. 209(17): p. 5760-5765, 0924-0136.
132. Anon, *US auto industry to expand PCD tool use*. Industrial Diamond Review, 1988. 48(3): p. 99-100,
133. Jennings, M., *Syndite - The great Dinish success*. 1992. 52(6): p. 308-310,
134. Okuzumi, F., Matsuda, J. and O'oka, K., *Gaseous phase synthesis of diamond and its practical application*. Science and Technology of New Diamond, 1990: p. 149-153,
135. Huang, T. H., Kuo, C. T., Chang, C. S., Kao, C. T. and Wen, H. Y., *Tribological behaviours of the diamond-coated cemented carbide tools with various cobalt contents*. Diamond and Related Materials, 1992. 1(5-6): p. 594-599, 0925-9635.
136. May, P. W., *CVD diamond: a new technology for the future?* Endeavour, 1995. 19(3): p. 101-106, 0160-9327.
137. Kamo, M. and Sato, Y., *Diamond synthesis form the gas phase*. Progress in Crystal Growth and Characterization of Materials, 1992. 23: p. 1-22, 0960-8974.
138. Gäbler, J. and Pleger, S., *Precision and micro CVD diamond-coated grinding tools*. International Journal of Machine Tools and Manufacture, 2010. 50(4): p. 420-424, 0890-6955.
139. Novikov, N. V. and Dub, S. N., *Hardness and fracture toughness of CVD diamond film*. Diamond and Related Materials, 1996. 5(9): p. 1026-1030, 0925-9635.
140. Karner, J., Pedrazzini, M., Reineck, I., Sjöstrand, M. E. and Bergmann, E., *CVD diamond coated cemented carbide cutting tools*. Proceedings of the 5th International Conference on the Science of Hard Materials, 1996. 209(1-2): p. 405-413, 0921-5093.
141. Uhlmann, E. and Koenig, J., *CVD diamond coatings on geometrically complex cutting tools*. CIRP Annals - Manufacturing Technology, 2009. 58(1): p. 65-68, 0007-8506.
142. Deuerler, F., Peterseim, J., Gruner, H., Wang, Q. and Buck, V., *Process control during diamond coating of tools*. International Journal of Refractory Metals and Hard Materials, 1998. 16(3): p. 191-199, 0263-4368.
143. Heaney, P. J., Sumant, A. V., Torres, C. D., Carpick, R. W. and Pfefferkorn, F. E., *Diamond coatings for micro end mills: Enabling the dry machining of aluminum at the micro-scale*. Diamond and Related Materials, 2008. 17(3): p. 223-233, 0925-9635.
144. Yashiki, T., Nakamura, T., Fujimori, N. and Nakai, T., *Practical properties of chemical vapour deposition diamond tools*. Surface and Coatings Technology, 1992. 52(1): p. 81-85, 0257-8972.
145. Lux, B., Haubner, R. and Renard, P., *Diamond for tooling and abrasives*. Diamond and Related Materials, 1992. 1(10-11): p. 1035-1047, 0925-9635.
146. Oles, E. J., Inspektor, A. and Bauer, C. E., *The new diamond-coated carbide cutting tools*. Proceedings of the 6th European Conference on Diamond, Diamond-like and Related Materials Part 2, 1996. 5(6-8): p. 617-624, 0925-9635.
147. Hu, J., Chou, Y. K. and Thompson, R. G., *Nanocrystalline diamond coating tools for machining high-strength Al alloys*. International Journal of Refractory Metals and Hard Materials, 2008. 26(3): p. 135-144, 0263-4368.
148. Yoshikawa, H. and Nishiyama, A., *CVD diamond coated insert for machining high silicon aluminum alloys*. Diamond and Related Materials, 1999. 8(8-9): p. 1527-1530, 0925-9635.
149. Yoshimura, H., Nakahara, K., Yamashita, H. and Kikuchi, N., *Characteristics of CVD diamond coated inserts*. Science and Technology of New Diamond, 1990: p. 111-118,
150. Kikuchi, N., Komatsu, T. and Yoshimura, H., *Characteristics of thin film growth in the synthesis of diamond by chemical vapour deposition and application of the thin*

- film synthesis technology for tools*. Materials Science and Engineering: A, 1988. 105-106(Part 2): p. 525-534, 0921-5093.
151. Kim, J.-D. and Kang, Y.-H., *High-speed machining of aluminium using diamond endmills*. International Journal of Machine Tools and Manufacture, 1997. 37(8): p. 1155-1165, 0890-6955.
 152. Polini, R., *Chemically vapour deposited diamond coatings on cemented tungsten carbides: Substrate pretreatments, adhesion and cutting performance*. Thin Solid Films, 2006. 515(1): p. 4-13, 0040-6090.
 153. Polini, R., Bravi, F., Casadei, F., D'antonio, P. and Traversa, E., *Effect of substrate grain size and surface treatments on the cutting properties of diamond coated Co-cemented tungsten carbide tools*. Diamond and Related Materials, 2002. 11(3-6): p. 726-730, 0925-9635.
 154. Raghuveer, M. S., Yoganand, S. N., Jagannadham, K., Lemaster, R. L. and Bailey, J., *Improved CVD diamond coatings on WC-Co tool substrates*. Wear, 2002. 253(11-12): p. 1194-1206, 0043-1648.
 155. Hanyu, H., Kamiya, S., Odagi, H., Murakami, Y. and Saka, M., *Development of high performance diamond-coated drills for cutting high silicon aluminum alloy*. Thin Solid Films, 2002. 413(1-2): p. 139-146, 0040-6090.
 156. Stephan, P. M., Hay, R. A. and Dean, C. D., *The new diamond technology and its application in cutting tools*. Diamond and Related Materials, 1992. 1(5-6): p. 710-716, 0925-9635.
 157. Olsen, R. H., Dewes, R. C. and Aspinwall, D. K., *Machining of electrically conductive CVD diamond tool blanks using EDM*. 14th International Symposium on Electromachining (ISEM XIV), 2004. 149(1-3): p. 627-632, 0924-0136.
 158. Kanda, K., Takehana, S., Yoshida, S., Watanabe, R., Takano, S., Ando, H. and Shimakura, F., *Application of diamond-coated cutting tools*. Surface and Coatings Technology, 1995. 73(1-2): p. 115-120, 0257-8972.
 159. Hu, J., Chou, Y. K., Thompson, R. G., Burgess, J. and Street, S., *Characterizations of nano-crystalline diamond coating cutting tools*. Surface and Coatings Technology, 2007. 202(4-7): p. 1113-1117, 0257-8972.
 160. Meng, X. M., Tang, W. Z., Hei, L. F., Li, C. M., Askari, S. J., Chen, G. C. and Lu, F. X., *Application of CVD nanocrystalline diamond films to cemented carbide drills*. International Journal of Refractory Metals and Hard Materials, 2008. 26(5): p. 485-490, 0263-4368.
 161. Hanyu, H., Kamiya, S., Murakami, Y. and Saka, M., *Dry and semi-dry machining using finely crystallized diamond coating cutting tools*. Surface and Coatings Technology, 2003. 174-175: p. 992-995, 0257-8972.
 162. Sreejith, P. S. and Ngoi, B. K. A., *Dry machining: Machining of the future*. Journal of Materials Processing Technology, 2000. 101(1-3): p. 287-291, 0924-0136.
 163. Davim, J. P., Sreejith, P. S., Gomes, R. and Peixoto, C., *Experimental studies on drilling of aluminium (AA1050) under dry, minimum quantity of lubricant, and flood-lubricated conditions* oceedings of the Institution of Mechanical Engineers, Part B: Journal of Engineering Manufacture, 2006. 220(10): p. 1605-1611,
 164. Enke, K., Dimigen, H. and Hubsch, H., *Frictional properties of diamondlike carbon layers*. Applied Physics Letters, 1979. 36(4): p. 291 - 292, 0003-6951
 165. Paulmier, D., Zaidi, H., Nery, H., Huu, T. L. and Mathia, T., *Tribological behaviour of diamond-like coatings: effect of active gases in atomic and molecular states*. Surface and Coatings Technology, 1993. 62(1-3): p. 570-576, 0257-8972.

166. Le Huu, T., Nery, H., Zaidi, H. and Paulmier, D., *Tribological behaviour of hard carbon coatings deposited on steel substrates by plasma-assisted chemical vapour deposition*. Diamond and Related Materials, 1994. 3(7): p. 1028-1033, 0925-9635.
167. Yang, S. and Teer, D. G., *Investigation of sputtered carbon and carbon/chromium multi-layered coatings*. Surface and Coatings Technology, 2000. 131(1-3): p. 412-416, 0257-8972.
168. Robertson, J., *Diamond-like amorphous carbon*. Materials Science and Engineering: R: Reports, 2002. 37(4-6): p. 129-281, 0927-796X.
169. Grill, A., *Diamond-like carbon: state of the art*. Diamond and Related Materials, 1999. 8(2-5): p. 428-434, 0925-9635.
170. Ronkainen, H., Varjus, S., Koskinen, J. and Holmberg, K., *Differentiating the tribological performance of hydrogenated and hydrogen-free DLC coatings*. Wear, 2001. 249(3-4): p. 260-266, 0043-1648.
171. Fukui, H., Okida, J., Omori, N., Moriguchi, H. and Tsuda, K., *Cutting performance of DLC coated tools in dry machining aluminum alloys*. Surface and Coatings Technology, 2004. 187(1): p. 70-76, 0257-8972.
172. Teer, D. G., *New solid lubricant coatings*. Wear, 2001. 251(1-12): p. 1068-1074, 0043-1648.
173. Monaghan, D. P., Teer, D. G., Logan, P. A., Efeoglu, I. and Arnell, R. D., *Deposition of wear resistant coatings based on diamond like carbon by unbalanced magnetron sputtering*. Surface and Coatings Technology, 1993. 60(1-3): p. 525-530, 0257-8972.
174. Stallard, J., Mercs, D., Jarratt, M., Teer, D. G. and Shipway, P. H., *A study of the tribological behaviour of three carbon-based coatings, tested in air, water and oil environments at high loads*. Surface and Coatings Technology, 2004. 177-178: p. 545-551, 0257-8972.
175. Stallard, J. and Teer, D. G., *A study of the tribological behaviour of CrN, Graphit-iC and Dymon-iC coatings under oil lubrication*. Surface and Coatings Technology, 2004. 188-189: p. 525-529, 0257-8972.
176. Bhowmick, S. and Alpas, A. T., *The performance of hydrogenated and non-hydrogenated diamond-like carbon tool coatings during the dry drilling of 319 Al*. International Journal of Machine Tools and Manufacture, 2008. 48(7-8): p. 802-814, 0890-6955.
177. Coldwell, H. L., Dewes, R. C., Aspinwall, D. K., Renevier, N. M. and Teer, D. G., *The use of soft/lubricating coatings when dry drilling BS L168 aluminium alloy*. Surface and Coatings Technology, 2004. 177-178: p. 716-726, 0257-8972.
178. Yang, S., Camino, D., Jones, A. H. S. and Teer, D. G., *Deposition and tribological behaviour of sputtered carbon hard coatings*. Surface and Coatings Technology, 2000. 124(2-3): p. 110-116, 0257-8972.
179. Kalidas, S., Devor, R. E. and Kapoor, S. G., *Experimental investigation of the effect of drill coatings on hole quality under dry and wet drilling conditions*. Surface and Coatings Technology, 2001. 148(2-3): p. 117-128, 0257-8972.
180. Kurt, M., Kaynak, Y. and Bagci, E., *Evaluation of drilled hole quality in Al 2024 alloy*. Advanced Manufacturing Technology, 2008. 37(11-12): p. 1051-1060,
181. Whitehouse, D., *Roundness and related subjects*, in *Surfaces and Their Measurement*. 2002, Kogan Page Science: Oxford. p. 235-289, 978-1-90-399601-0.
182. Anon, *Geometrical product specifications (GPS) - Roundness*. DD CEN 12181:2007, 978 0 580 57989 9.
183. Dawson, D. J. W., *Cylindricity and its measurement*. International Journal of Machine Tools and Manufacture, 1992. 32(1-2): p. 247-253, 0890-6955.

184. Chajda, J., Grzelka, M., Gapinski, B., Pawlowski, M., Szelewski, M. and Rucki, M., *Coordinate measurement of complicated parameters like roundness, cylindricity, gear teeth or free-form surface*, in *Advanced manufacturing operations*. 2008, Advanced materials and operations society. p. 225-231.
185. Ramaswami, R., Kanagaraj, S. and Anand, S., *An inspection advisor for form error in cylindrical features*. *Advanced Manufacturing Technology*, 2009. 40(1-2): p. 128-143,
186. Jawahir, I. S., Brinksmeier, E., M'saoubi, R., Aspinwall, D. K., Outeiro, J. C., Meyer, D., Umbrello, D. and Jayal, A. D., *Surface integrity in material removal processes: Recent advances*. *CIRP Annals - Manufacturing Technology*, 2011. 60(2): p. 603-626, 0007-8506.
187. Field, M. and Kahles, J. F., *The surface integrity of machined and ground high strength steels*. DMIC Report, 1964. 210: p. 54-77,
188. Field, M. and Kahles, J. F., *Review of surface integrity of machined components*. *CIRP Annals - The international institution for production engineering research*, 1971. 20(2): p. 153-163,
189. Griffiths, B., *Manufacturing surface technology: Surface integrity & functional performance*. *Manufacturing Surface Technology*. 2001, Oxford: Kogan Page Science, 1-85-718029-1.
190. Kahles, J. F. and Field, M., *Surface integrity - A new requirement for surfaces generated by material removal methods* *Proceedings of the Institution of Mechanical Engineers*, 1967. 182(3K): p. 31-45, 0367-8849.
191. Field, M., Kahles, J. F. and Cammett, J. T., *A review of measuring methods for surface integrity*. *CIRP Annals - The international institution for production engineering research*, 1972. 21(2): p. 219-238,
192. Kahles, J. F. and Field, M., *Surface integrity guidelines for machining*. *Society of Manufacturing Engineers*, 1971. SEM Paper IQ-72-206,
193. Zhang, X. P., Liu, C. R. and Yao, Z. Q., *Experimental study and evaluation methodology on hard surface integrity*. *The International Journal of Advanced Manufacturing Technology*, 2007. 34(1-2): p. 141-148,
194. Ulutan, D. and Ozel, T., *Machining induced surface integrity in titanium and nickel alloys: A review*. *International Journal of Machine Tools and Manufacture*, 2011. 51(3): p. 250-280, 0890-6955.
195. Byrne, G., Barry, J. and Young, P., *Surface Integrity of AISi9 Machined with PCD Cutting Tools*. *CIRP Annals - Manufacturing Technology*, 1997. 46(1): p. 489-491, 0007-8506.
196. Jasinevicius, R. G., Duduch, J. G., Porto, A. J. V. and Purquã©Rio, B. M., *Critical aspects on the behavior of material from the mechanical tool-workpiece interaction in single point diamond turning*. *Journal of the Brazilian Society of Mechanical Sciences*, 1999. 21: p. 509-518, 0100-7386.
197. Yuan, Z. J., Zhou, M. and Dong, S., *Effect of diamond tool sharpness on minimum cutting thickness and cutting surface integrity in ultraprecision machining*. *Journal of Materials Processing Technology*, 1996. 62(4): p. 327-330, 0924-0136.
198. Jeelani, S. and Musial, M., *Effect of cutting speed and tool rake angle on the fatigue life of 2024-T351 aluminium alloy*. *International Journal of Fatigue*, 1984. 6(3): p. 169-172, 0142-1123.
199. Suresh Kumar Reddy, N., Kwang-Sup, S. and Yang, M., *Experimental study of surface integrity during end milling of Al/SiC particulate metal-matrix composites*. *Journal of Materials Processing Technology*, 2008. 201(1â€“3): p. 574-579, 0924-0136.

200. Ge, Y. F., Xu, J. H., Yang, H., Luo, S. B. and Fu, Y. C., *Workpiece surface quality when ultra-precision turning of SiCp/Al composites*. Journal of Materials Processing Technology, 2008. 203(1&2): p. 166-175, 0924-0136.
201. Schubert, A. and Nestler, A., *Enhancement of Surface Integrity in Turning of Particle74 Reinforced Aluminium Matrix Composites by Tool Design*. Procedia Engineering, 2011. 19(0): p. 300-305, 1877-7058.
202. Kannan, S. and Kishawy, H. A., *Surface characteristics of machined aluminium metal matrix composites*. International Journal of Machine Tools and Manufacture, 2006. 46(15): p. 2017-2025, 0890-6955.
203. Whitehouse, D. J., *Surface metrology instrumentation*. Phys. E: Sci. Instrum, 1987. 20(10): p. 1145-1155,
204. Anon, *Surface texture: Surface roughness, Waviness, and Lay*. 1978: ANSI B46.1,
205. Whitehouse, D. J., *Surface metrology*. Journal of Meas. Sci. Technol., 1997. 8(9): p. 955-972,
206. Ormandy, P. G., *An introduction to metallurgical laboratory techniques*. 1968: Pergamon Press, 080034144.
207. Basavakumar, K. G., Mukunda, P. G. and Chakraborty, M., *Impact toughness in Al-12Si and Al-12Si-3Cu cast alloys--Part 1: Effect of process variables and microstructure*. International Journal of Impact Engineering, 2008. 35(4): p. 199-205, 0734-743X.
208. Grum, J. and Kisin, M., *The influence of the microstructure of three Al-Si alloys on the cutting-force amplitude during fine turning*. International Journal of Machine Tools and Manufacture, 2006. 46(7-8): p. 769-781, 0890-6955.
209. Hashimoto, F., Guo, Y. B. and Warren, A. W., *Surface Integrity Difference between Hard Turned and Ground Surfaces and Its Impact on Fatigue Life*. CIRP Annals - Manufacturing Technology, 2006. 55(1): p. 81-84, 0007-8506.
210. Xie, M. and Goh, T. N., *Statistical techniques for quality*. The TQM Magazine, 1999. 11(4): p. 238-241, 0954-478X.
211. Montgomery, D. C., *Introduction to statistical quality control*. 2nd ed. 1991: John Wiley & Sons, 0471529931.
212. Anon, *Statistical process control (SPC) reference manual*. 2 ed. 2005,
213. Dale, B. G. and Shaw, P., *Statistical process control: An examination of some common queries*. International Journal of Production Economics, 1991. 22(1): p. 33-41, 0925-5273.
214. Xie, M., Lu, X. S., Goh, T. N. and Chan, L. Y., *A quality monitoring and decision-making scheme for automated production processes*. Quality & Reliability Management, 1999. 16(2): p. 148-157, 0265-671X.
215. Oakland, J. S., *Statistical process control*. 5 ed. 2003: Butterworth-Heinemann, 0750657669.
216. Dudek-Burlikowska, M., *Quality estimation of process with usage control charts type X-R and quality capability of process Cp, Cpk*. Journal of Materials Processing Technology, 2005. 162-163: p. 736-743, 0924-0136.
217. Motorcu, A. R. and Güllü, A., *Statistical process control in machining, a case study for machine tool capability and process capability*. Materials & Design, 2006. 27(5): p. 364-372, 0261-3069.
218. Anon, *Statistical methods in process management - Capability and performance*. ISO 22514: 2007, 978 0 580 53056 2.
219. Anon, *Titex Plus Precision Cutting: The Complete 2002 Catalogue*. 2002,
220. Anon, *Mapal Ltd*. 2010,
221. Anon, *Kennametal Catalog 2010*. 2010,

222. Anon, *Exactaform Ltd.* 2010,
223. Anon, *Guhring: The Tool Company Catalogue*. 9 ed. 2006,
224. Anon, *Teer Coatings Ltd.* 2011,
225. Anon, *CemeCon AG.* 2011,
226. Anon, *Control charts*. BS ISO 7870: 2007, 978 0 580 56466 6.
227. Anon, *Geometric product specification (GPS) - Surface texture - Profile method: Rules and procedures for the assessment of surface texture*. BS EN ISO 4288:1998, 0 580 27033 5.
228. Shaw, M. C., *Metal cutting principles*. Oxford series on advanced manufacturing. 2005, New York ; Oxford: Oxford University Press. 651-651, 0195142063 : '62.00.
229. El-Khabeery, M. M., Saleh, S. M. and Ramadan, M. R., *Some observations of surface integrity of deep drilling holes*. Wear, 1991. 142(2): p. 331-349, 0043-1648.
230. Sun, J. and Guo, Y. B., *A comprehensive experimental study on surface integrity by end milling Ti-6Al-4V*. Journal of Materials Processing Technology, 2009. 209(8): p. 4036-4042, 0924-0136.
231. Sharman, A. R. C., Hughes, J. I. and Ridgway, K., *An analysis of the residual stresses generated in Inconel 718(TM) when turning*. Journal of Materials Processing Technology, 2006. 173(3): p. 359-367, 0924-0136.
232. Sharman, A. R. C., Amarasinghe, A. and Ridgway, K., *Tool life and surface integrity aspects when drilling and hole making in Inconel 718*. Journal of Materials Processing Technology, 2008. 200(1-3): p. 424-432, 0924-0136.
233. Davim, J. P., *Surface Integrity in Machining*. 2010, New York: Springer, 978-1-84882-873-5.
234. Moufki, A., Molinari, A. and Dudzinski, D., *Modelling of orthogonal cutting with a temperature dependent friction law*. Journal of the Mechanics and Physics of Solids, 1998. 46(10): p. 2103-2138, 0022-5096.
235. Nayebi, A., Mauvoisin, G. and Vaghefpoor, H., *Modeling of twist drills wear by a temperature-dependent friction law*. Journal of Materials Processing Technology, 2008. 207(1-3): p. 98-106, 0924-0136.
236. Zitoune, R., Krishnaraj, V. and Collombet, F., *Study of drilling of composite material and aluminium stack*. Composite Structures. 92(5): p. 1246-1255, 0263-8223.
237. Moneim, M. E. A., *Effect of drilling speed on the required torque and thrust force for non-ferrous materials*. Wear, 1981. 66(1): p. 65-75, 0043-1648.

APPENDIX A

Collaborators' contact details

This project was conducted in collaboration with Doncasters Sterling, Mapal Ltd, Element Six Ltd and University of Birmingham. Contacts of these companies and academic at the time of the research are included in Table A1 and A2 respectively.

APPENDIX B





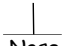
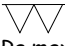

Machine capacity study

Table B1: OEE of Index G200 machine tool

	Wk41	Wk42	Wk43	Wk44	Wk45	Wk46	Wk47	Wk48	Wk49	Wk50	Wk51
OVERALL OEE (EQUIPMENT AVAILABILITY x PERFORMANCE x %SCRAP)	73.82%	67.68%	89.74%	74.83%	82.43%	82.60%	92.14%	86.52%	81.31%	89.00%	80.10%
TARGET	85.00%	85.00%	85.00%	85.00%	85.00%	85.00%	85.00%	85.00%	85.00%	85.00%	85.00%
OVERALL CHANGE OVERS	6	6	6	4	7	2	6	2	3	7	6
AVAILABILITY (M1 & M2)	92.29%	83.51%	99.41%	83.70%	92.24%	90.33%	95.43%	84.95%	77.54%	91.69%	80.98%
AVAILABLE TIME MINUTES PER WEEK	20160	20160	20160	20160	20160	20160	20160	20160	20160	20160	20160
SCHEDULED DOWNTIME MINUTES PER WEEK	1030	840	625	310	960	410	990	390	415	1005	1375
UNSCHEDULED DOWNTIME MINUTES PER WEEK (MC BREAKDOWN)	2265	3065	740	3305	1790	2320	1386	3366	4849	2597	4708
NO OPERATOR MINUTES PER WEEK	240	960	0	240	660	0	480	0	0	0	240
ACTUAL MACHINE TIME MINUTES	17655	16135	19420	16615	17710	17840	18294	16794	15311	17563	15212
AVAILABLE MACHINE TIME MINUTES	19130	19320	19535	19850	19200	19750	19170	19770	19745	19155	18785
PERFORMANCE (M1 & M2)	83.24%	84.87%	91.87%	90.89%	92.05%	94.13%	98.71%	103.39%	106.50%	99.01%	100.83%
AVE MACHINE CYCLE TIME MINUTES	1.25	1.25	1.25	1.25	1.25	1.25	1.25	1.25	1.25	1.25	1.25
TOTAL GOOD PARTS MADE	11298	10460	14024	11883	12662	13051	14131	13684	12844	13638	12037
TOTAL SCRAP	459	495	249	198	379	383	315	207	201	274	234
TOTAL PARTS MADE	11757	10955	14273	12081	13041	13434	14446	13891	13045	13912	12271
POTENTIAL OUTPUT	14124	12908	15536	13292	14168	14272	14635.2	13435.2	12248.8	14050.4	12169.6
QUALITY	96.10%	95.48%	98.26%	98.36%	97.09%	97.15%	97.82%	98.51%	98.46%	98.03%	98.09%
TOTAL GOOD PARTS MADE	11298	10460	14024	11883	12662	13051	14131	13684	12844	13638	12037
TOTAL PARTS MADE	11757	10955	14273	12081	13041	13434	14446	13891	13045	13912	12271

Process capability study on Index G200

Table B2: Measurements of critical features on compressor impeller

	 Backface	 Middle	 Nose	 Backface	 Nose	 Ra max	 Cylindricity
Component No.	5.087 5.093	5.087 5.093	5.087 5.093	0.005	0.01	0.2	0.005
1	5.0907	5.0911	5.0916	0.0020	0.0010	0.05	0.00327
2	5.0907	5.0910	5.0911	0.0020	0.0010	0.05	0.00249
3	5.0906	5.0911	5.0916	0.0020	0.0010	0.06	0.00207
4	5.0908	5.0910	5.0917	0.0020	0.0010	0.05	0.00139
5	5.0905	5.0910	5.0914	0.0015	0.0015	0.05	0.00170
6	5.0905	5.0910	5.0916	0.0025	0.0020	0.05	0.00170
7	5.0908	5.0910	5.0914	0.0020	0.0005	0.05	0.00224
8	5.0910	5.0908	5.0910	0.0025	0.0010	0.05	0.00362
9	5.0906	5.0909	5.0918	0.0020	0.0015	0.05	0.00138
10	5.0910	5.0909	5.0920	0.0015	0.0020	0.05	0.00240
11	5.0908	5.0909	5.0914	0.0020	0.0015	0.05	0.00239
12	5.0907	5.0909	5.0917	0.0025	0.0015	0.06	0.00211
13	5.0908	5.0909	5.0908	0.0020	0.0015	0.05	0.00190
14	5.0904	5.0908	5.0914	0.0015	0.0015	0.05	0.00291
15	5.0908	5.0908	5.0916	0.0025	0.0005	0.06	0.00296
16	5.0910	5.0907	5.0913	0.0015	0.0010	0.05	0.00250
17	5.0909	5.0909	5.0913	0.0015	0.0005	0.06	0.00443
18	5.0907	5.0908	5.0916	0.0015	0.0010	0.05	0.00205
19	5.0907	5.0911	5.0911	0.0020	0.0020	0.07	0.00280
20	5.0907	5.0911	5.0915	0.0020	0.0010	0.05	0.00223
21	5.0907	5.0909	5.0914	0.0020	0.0010	0.06	0.00207
22	5.0907	5.0911	5.0911	0.0020	0.0010	0.05	0.00257
23	5.0907	5.0908	5.0911	0.0020	0.0005	0.06	0.00207
24	5.0906	5.0909	5.0909	0.0025	0.0010	0.05	0.00238
25	5.0905	5.0910	5.0915	0.0015	0.0015	0.05	0.00223
26	5.0906	5.0910	5.0916	0.0015	0.0010	0.06	0.00213
27	5.0905	5.0910	5.0913	0.0020	0.0010	0.05	0.00163
28	5.0907	5.0910	5.0911	0.0020	0.0010	0.05	0.00233
29	5.0905	5.0910	5.0910	0.0015	0.0015	0.05	0.00264
30	5.0906	5.0910	5.0912	0.0015	0.0010	0.05	0.00245
31	5.0907	5.0908	5.0914	0.0020	0.0010	0.05	0.00392
32	5.0905	5.0908	5.0911	0.0020	0.0010	0.05	0.00272
33	5.0907	5.0910	5.0911	0.0025	0.0010	0.06	0.00292
34	5.0907	5.0910	5.0909	0.0020	0.0005	0.06	0.00258
35	5.0910	5.0909	5.0912	0.0020	0.0010	0.05	0.00324
36	5.0905	5.0908	5.0913	0.0020	0.0010	0.05	0.00218
37	5.0906	5.0909	5.0915	0.0015	0.0015	0.05	0.00242
38	5.0906	5.0909	5.0908	0.0015	0.0010	0.07	0.00295
39	5.0903	5.0909	5.0911	0.0025	0.0015	0.07	0.00262
40	5.0904	5.0910	5.0911	0.0020	0.0010	0.05	0.00225
41	5.0904	5.0910	5.0915	0.0015	0.0005	0.06	0.00200
42	5.0904	5.0910	5.0911	0.0015	0.0010	0.06	0.00270
43	5.0905	5.0910	5.0909	0.0020	0.0010	0.06	0.00223
44	5.0905	5.0909	5.0911	0.0015	0.0015	0.06	0.00296
45	5.0906	5.0910	5.0914	0.0020	0.0010	0.06	0.00272
46	5.0907	5.0911	5.0911	0.0020	0.0015	0.06	0.00228
47	5.0905	5.0909	5.0914	0.0025	0.0010	0.06	0.00336
48	5.0905	5.0910	5.0915	0.0025	0.0020	0.06	0.00213
49	5.0907	5.0910	5.0915	0.0025	0.0020	0.06	0.00498
50	5.0908	5.0908	5.0915	0.0025	0.0005	0.06	0.00284

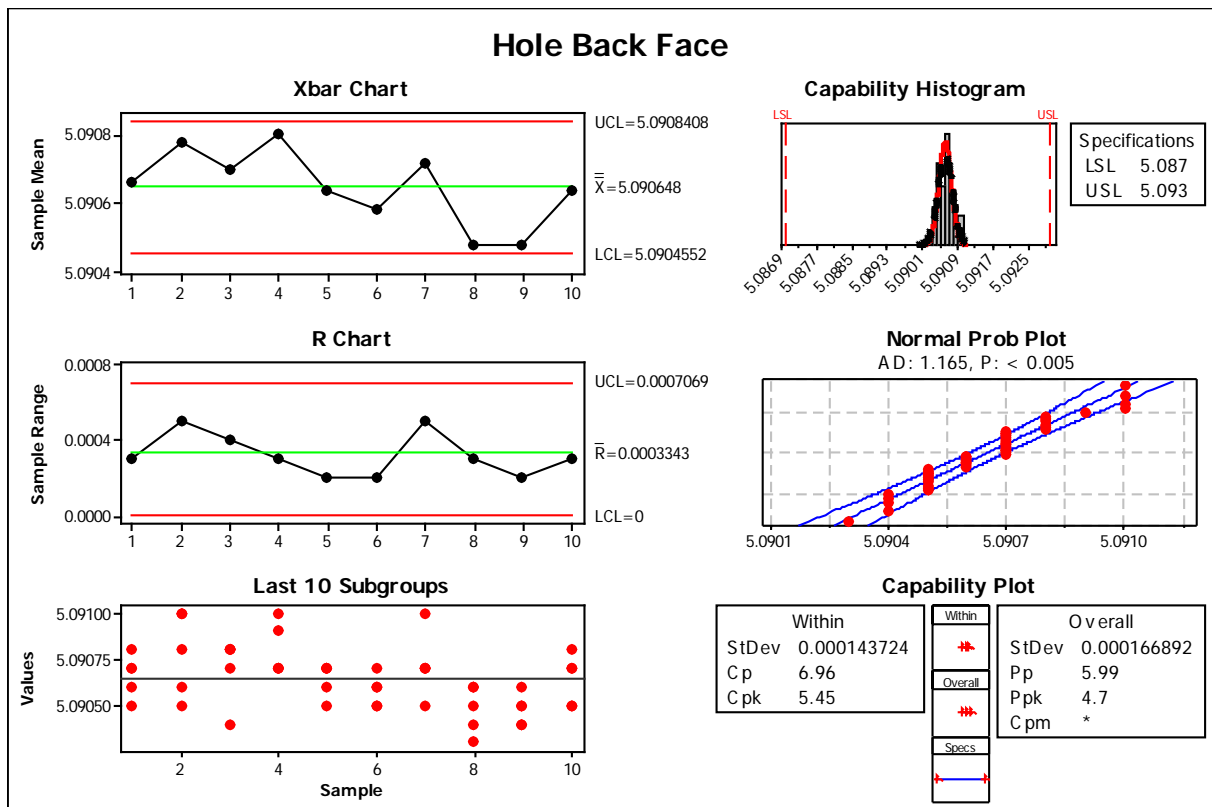


Figure B1: Detailed analysis of impeller hole process capability with Minitab (5mm from back-face)

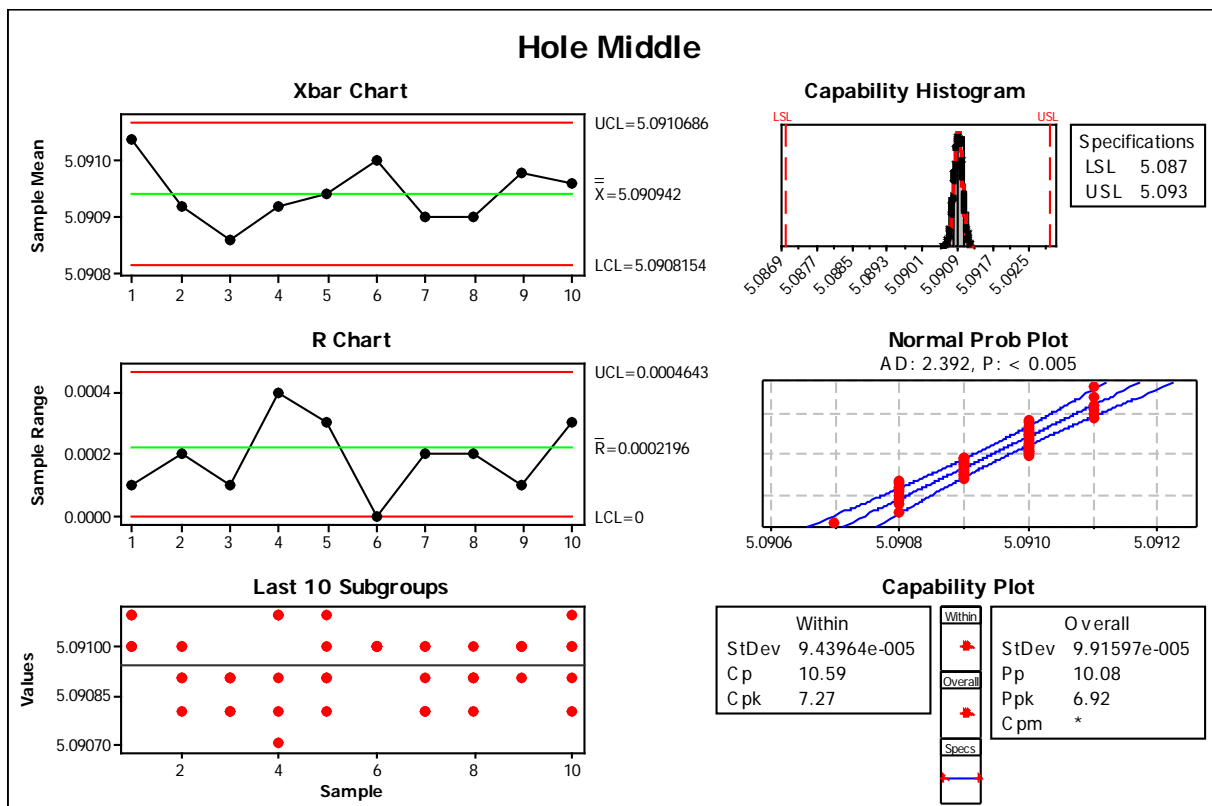


Figure B2: Detailed analysis of impeller hole process capability with Minitab (middle of hole)

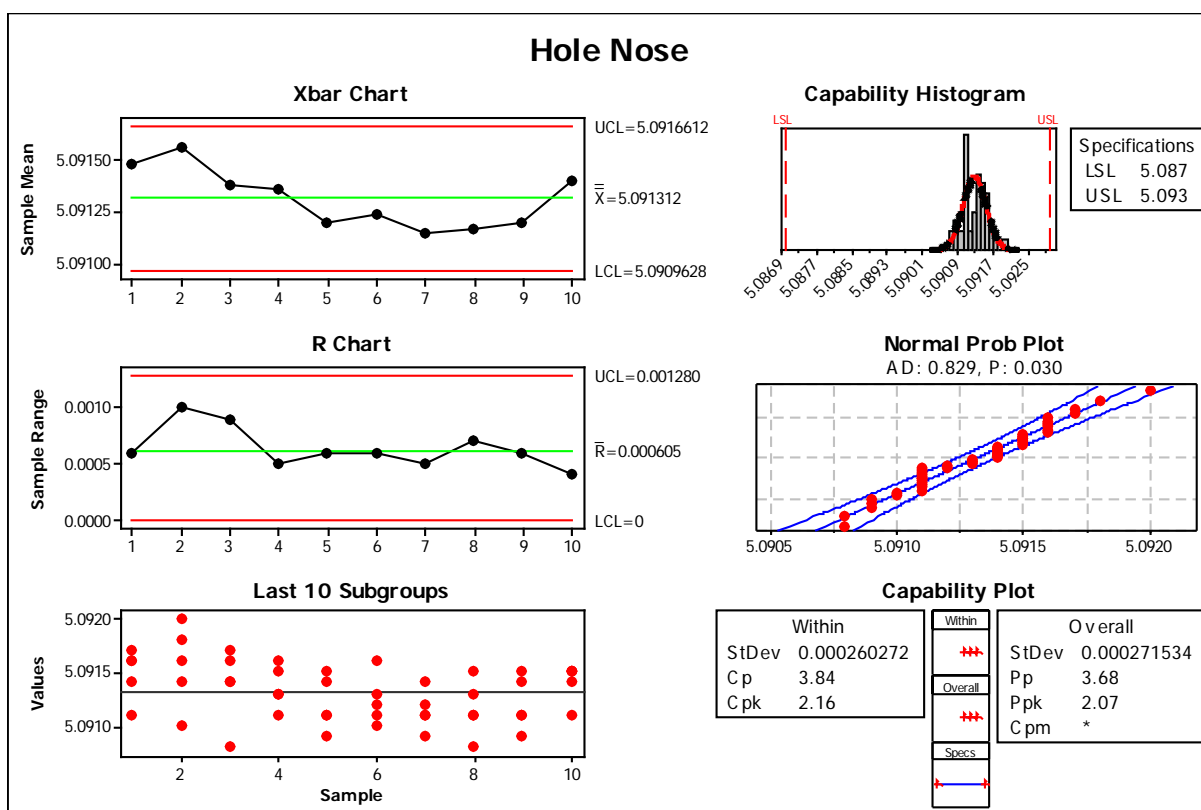


Figure B3: Detailed analysis of impeller hole process capability with Minitab (5mm from nose face)

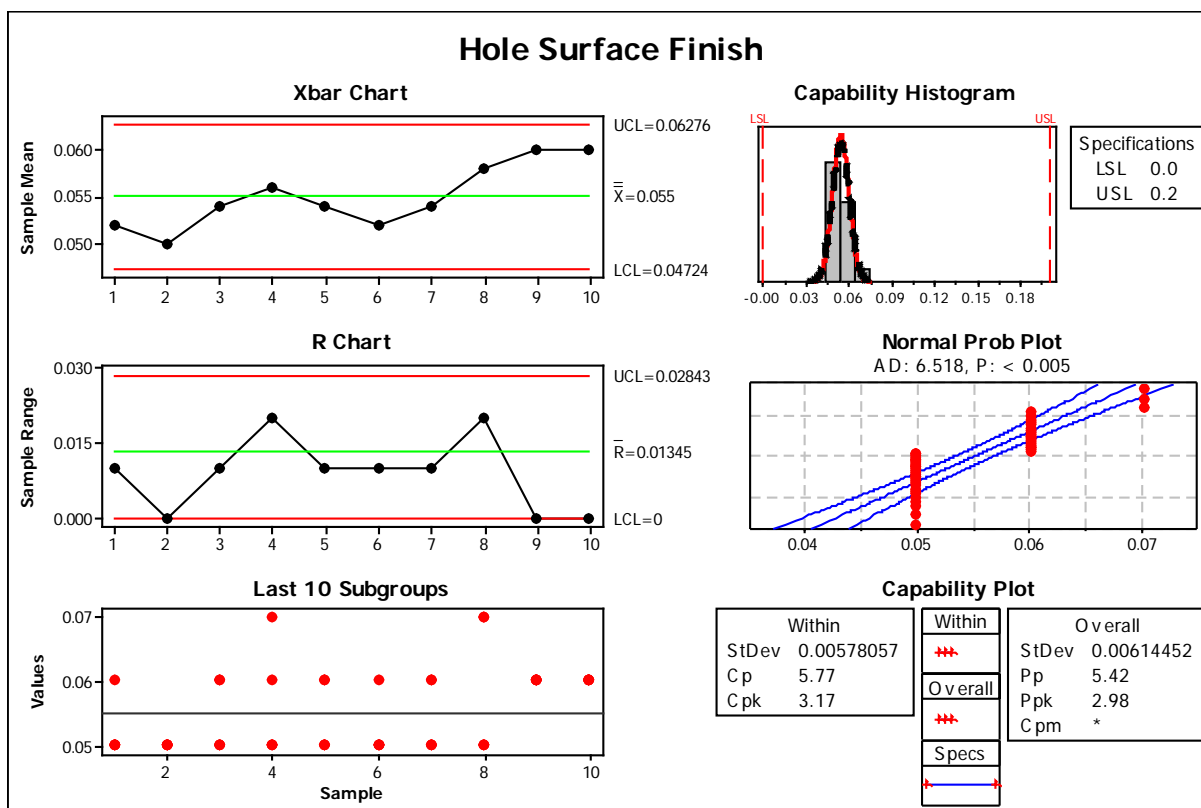


Figure B4: Detailed analysis of impeller hole surface finish process capability with Minitab

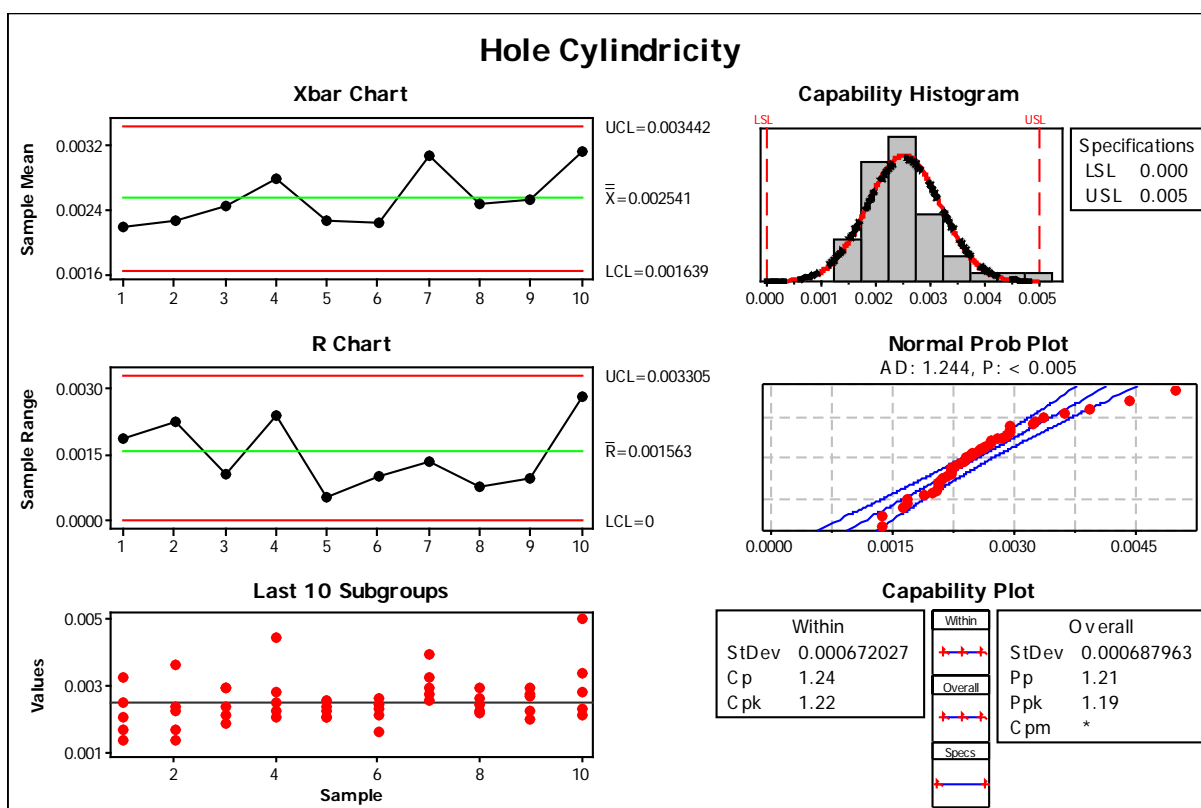


Figure B5: Detailed analysis of impeller hole cylindricity process capability with Minitab

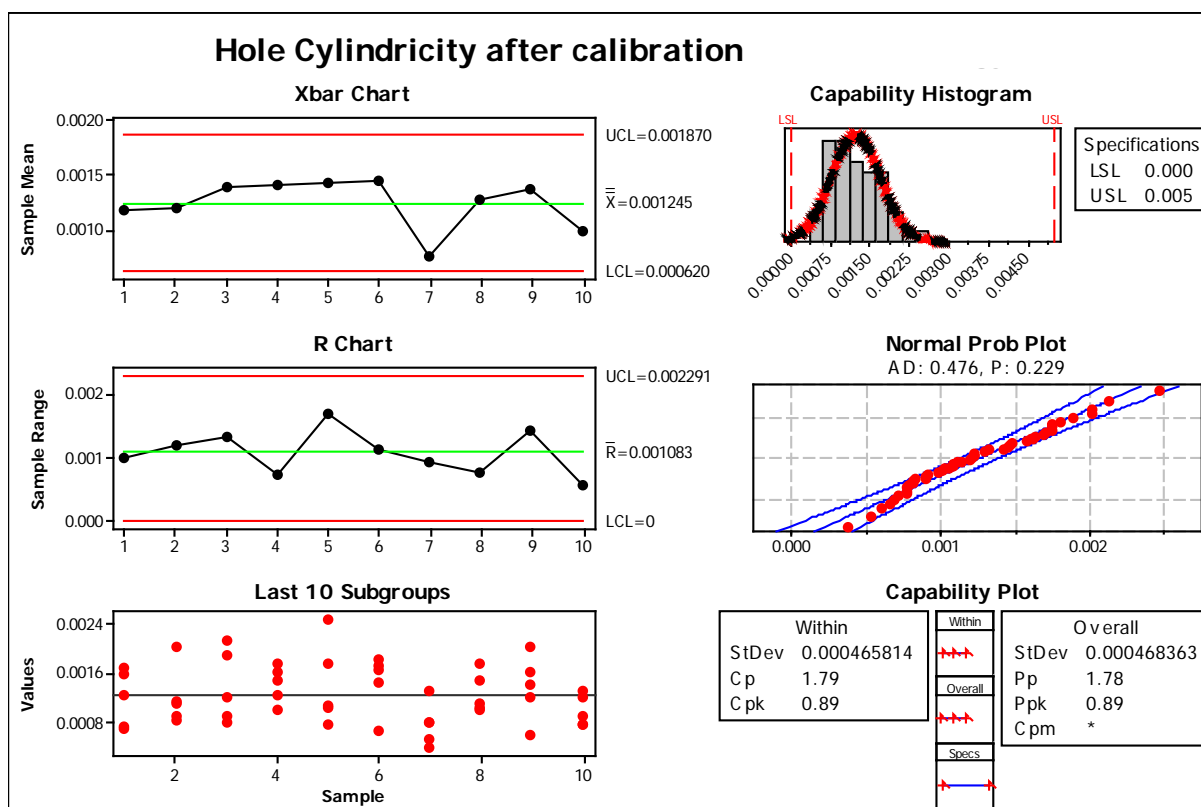


Figure B6: Improved results of hole cylindricity following the calibration of Talyrond 131

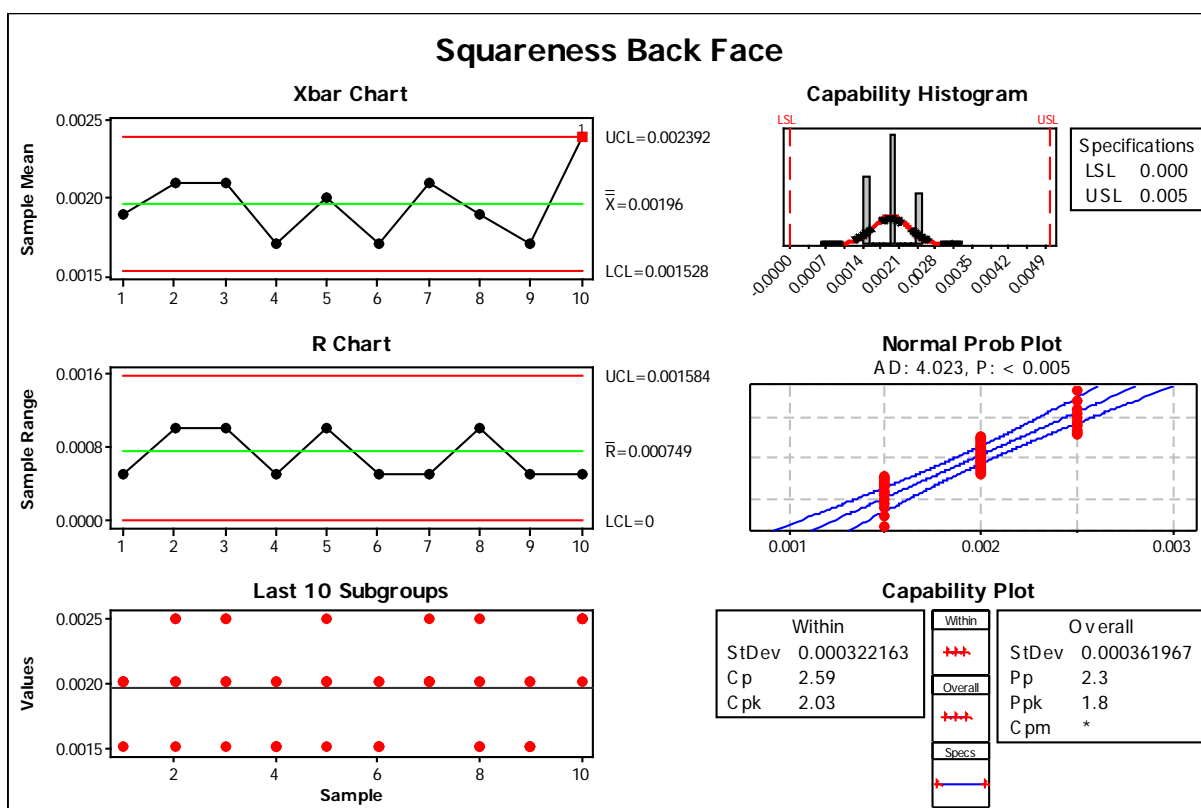


Figure B7: Detailed analysis of impeller squareness process capability with Minitab (back-face)

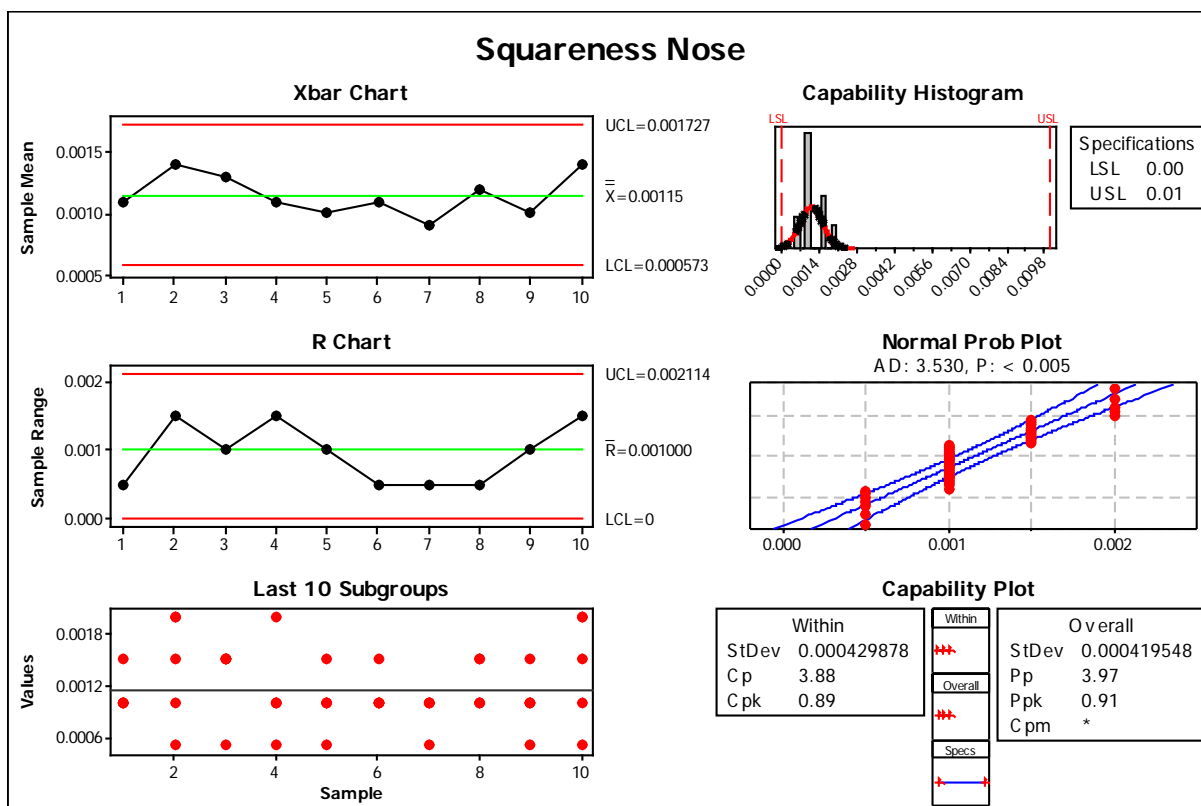


Figure B8: Detailed analysis of impeller squareness process capability with Minitab (Nose)

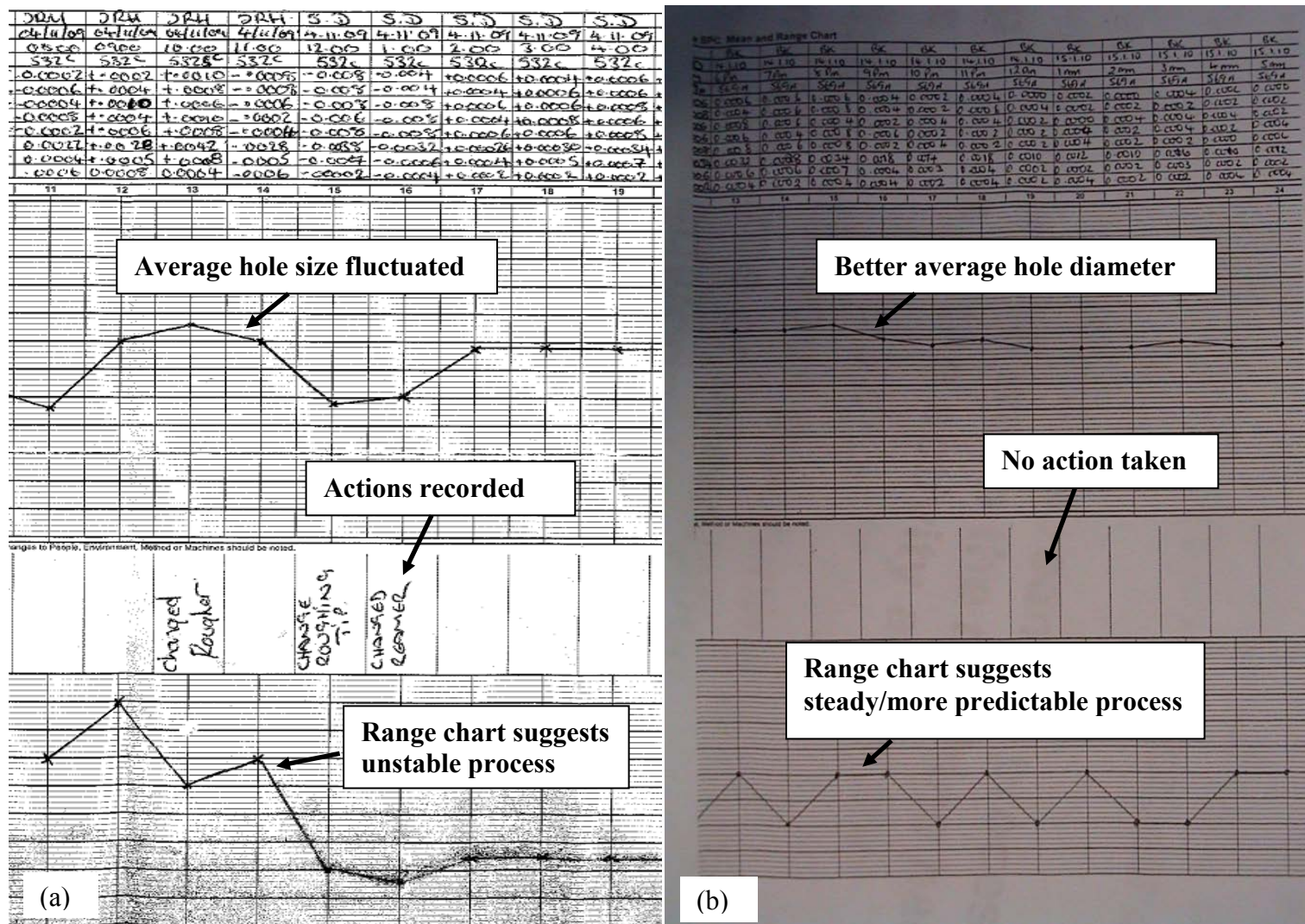


Figure B9: Copy of scanned drilling and reaming process control charts showing (a) fluctuated and (b) stable processes

APPENDIX C

Phase 3A: Evaluation of diamond-like carbon coated tools when drilling cast C355 aluminium alloy

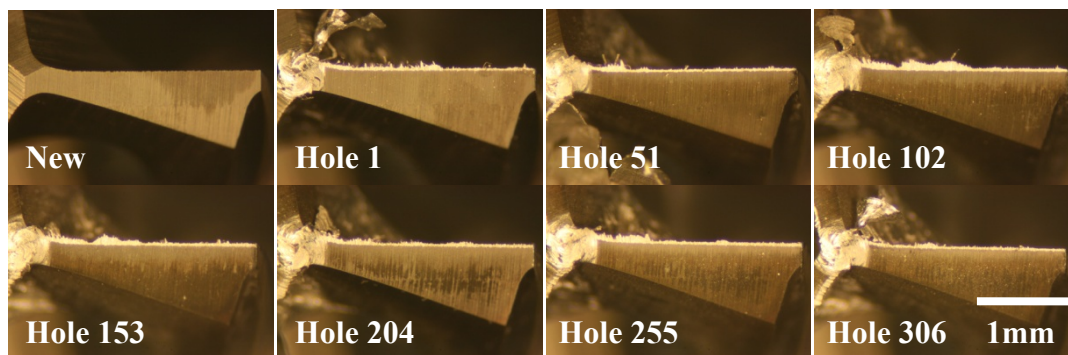


Figure C1: Tool wear micrographs of uncoated carbide drill under 3bar cutting fluid, 130m/min cutting speed (Test 1)

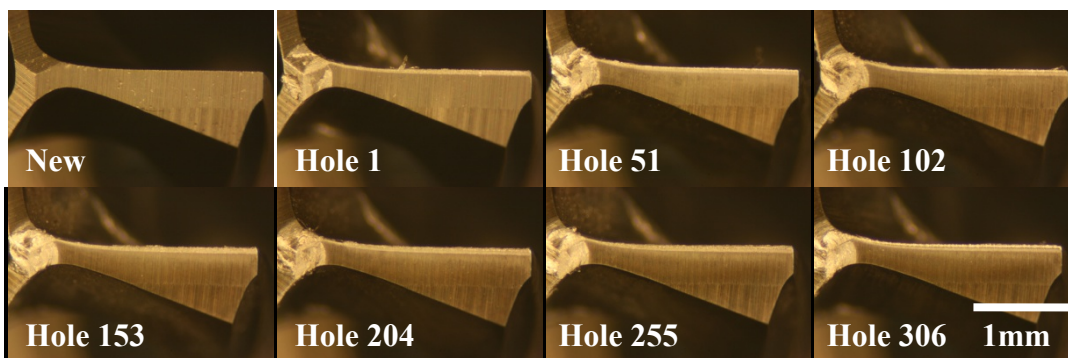


Figure C2: Tool wear micrographs of uncoated carbide drill under 3bar cutting fluid, 260m/min cutting speed (Test 2)

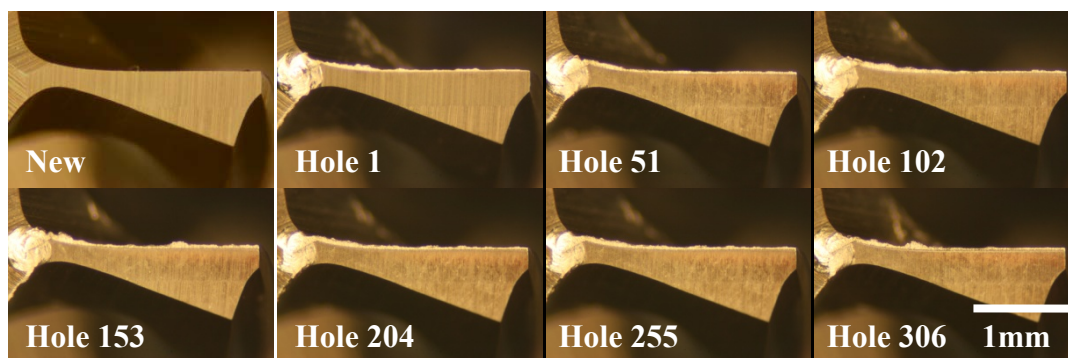


Figure C3: Tool wear micrographs of uncoated carbide drill under 70bar cutting fluid, 130m/min cutting speed (Test 7)

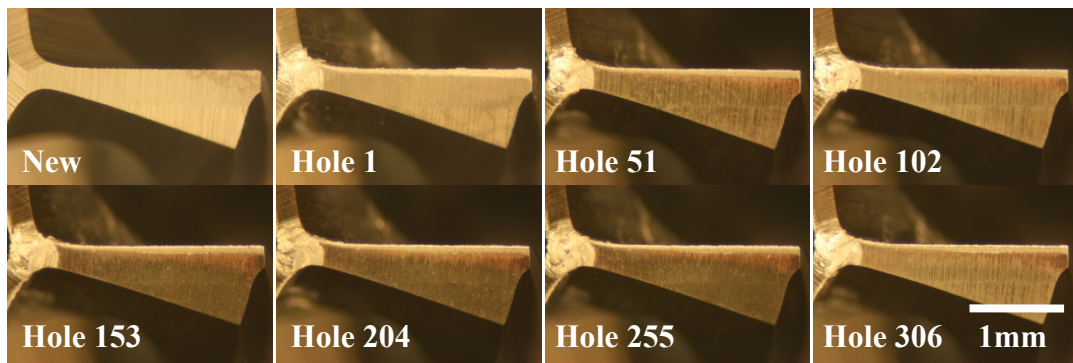


Figure C4: Tool wear micrographs of uncoated carbide drill under 70bar cutting fluid, 260m/min cutting speed (Test 8)

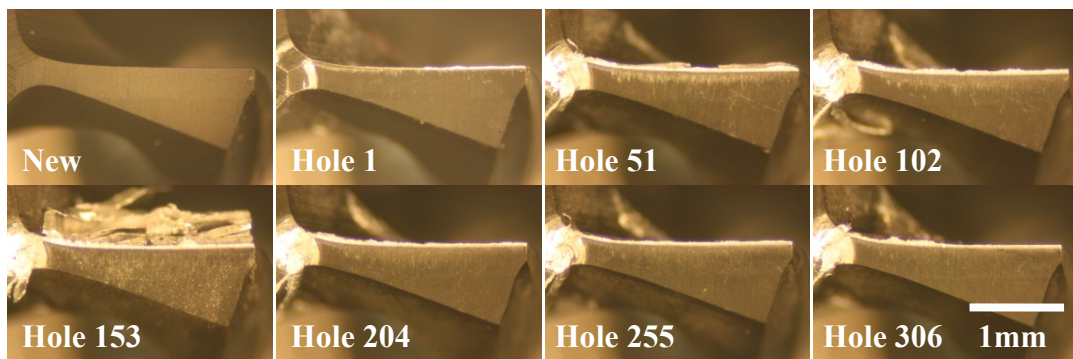


Figure C5: Tool wear micrographs of Graphit-iC™ drill under 3bar cutting fluid, 130m/min cutting speed (Test 3)

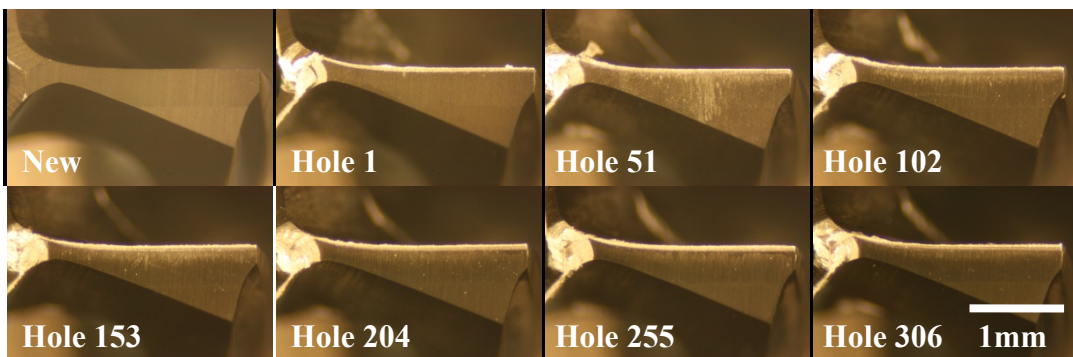


Figure C6: Tool wear micrographs of Graphit-iC™ drill under 3bar cutting fluid, 260m/min cutting speed (Test 4)

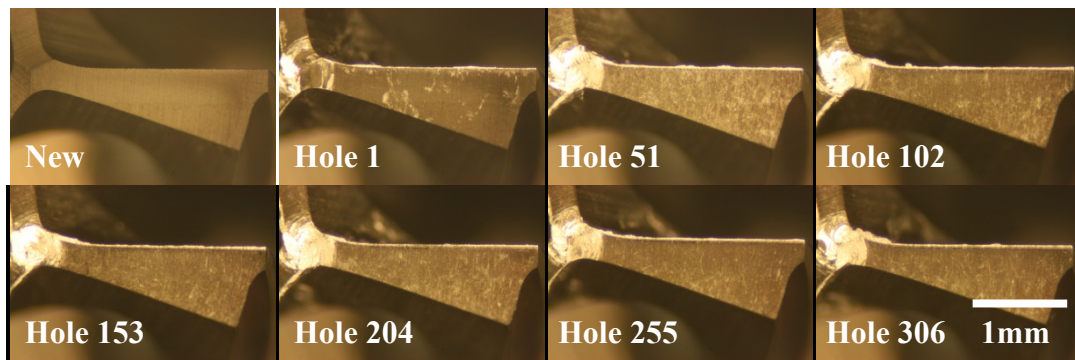


Figure C7: Tool wear micrographs of Graphit-iC™ drill under 70bar cutting fluid, 130m/min cutting speed (Test 9)

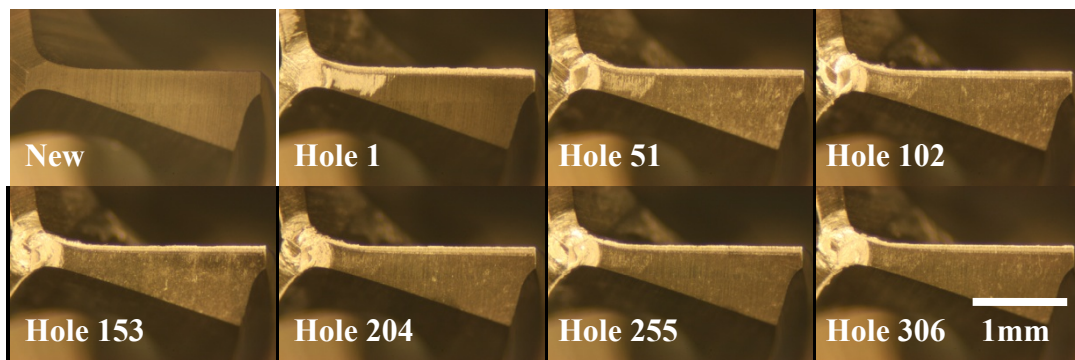


Figure C8: Tool wear micrographs of Graphit-iC™ drill under 70bar cutting fluid, 260m/min cutting speed (Test 10)

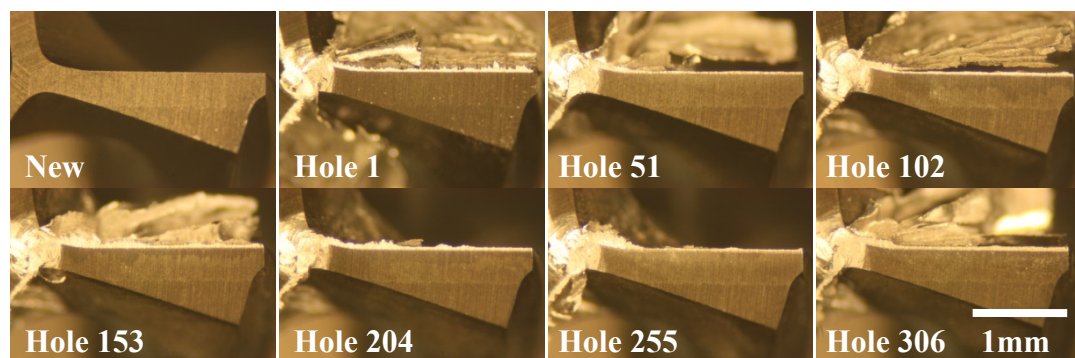


Figure C9: Tool wear micrographs of Dymon-iC™ drill under 3bar cutting fluid, 130m/min cutting speed (Test 5)

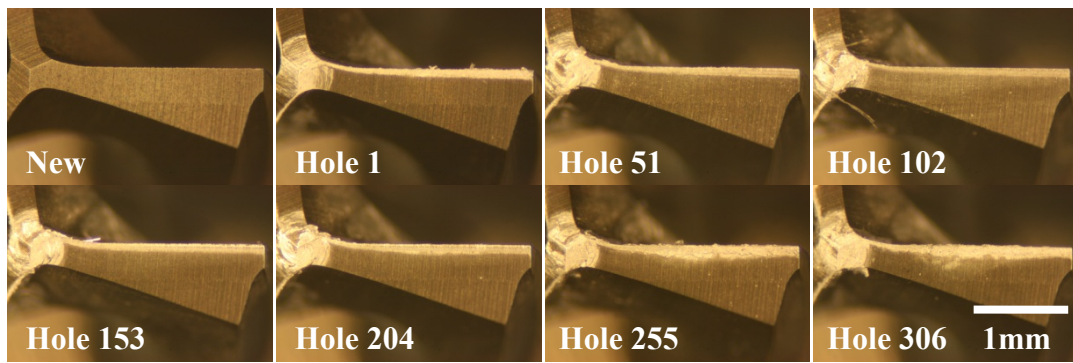


Figure C10: Tool wear micrographs of Dymon-iC™ drill under 3bar cutting fluid, 260m/min cutting speed (Test 6)

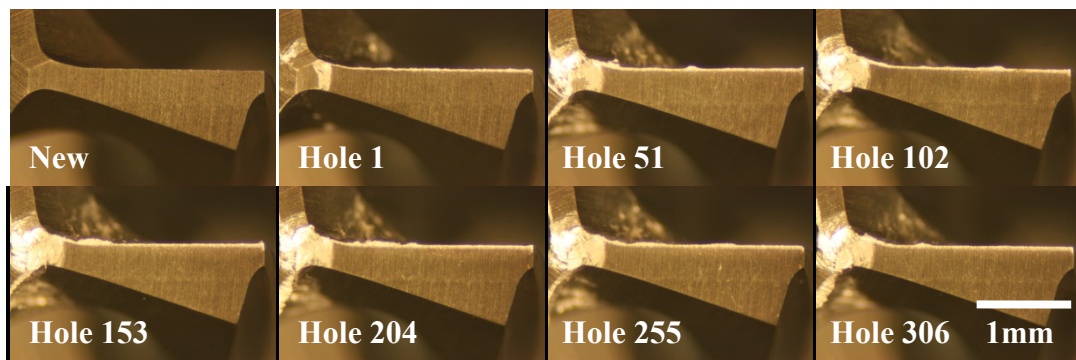


Figure C11: Tool wear micrographs of Dymon-iC™ drill under 70bar cutting fluid, 130m/min cutting speed (Test 11)

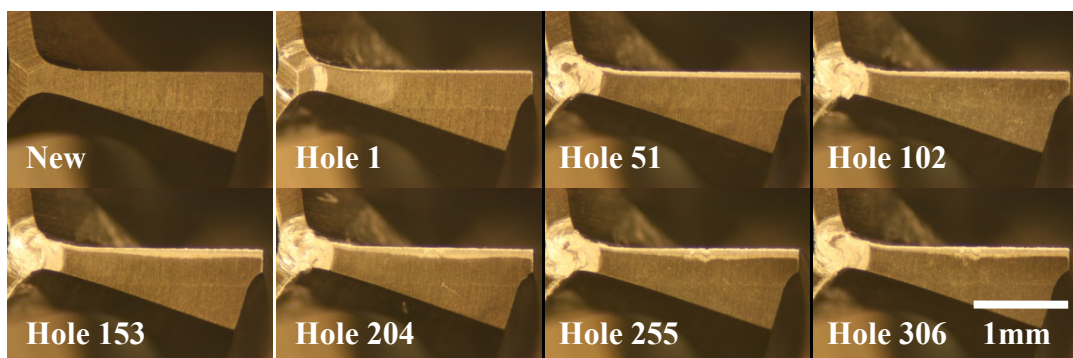


Figure C12: Tool wear micrographs of Dymon-iC™ drill under 70bar cutting fluid, 260m/min cutting speed (Test 12)

APPENDIX D

Phase 3B: Evaluation of diamond-like carbon coated tools when reaming 6082-T6 aluminium alloy

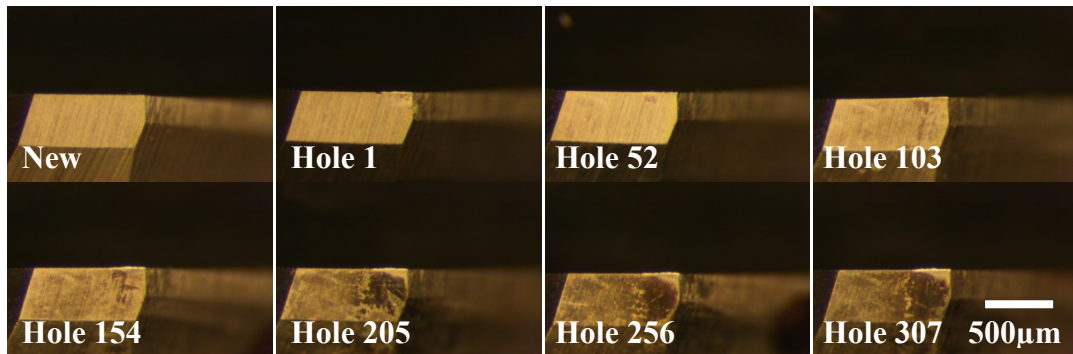


Figure D1: Tool wear micrographs of uncoated carbide reamer under 70bar through-hole cutting fluid, 32m/min cutting speed (Test 1)

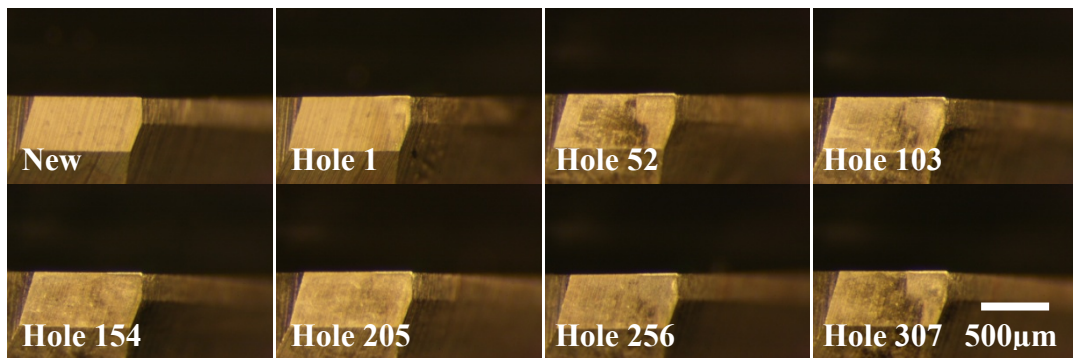


Figure D2: Tool wear micrographs of uncoated carbide reamer under 70bar through-hole cutting fluid, 96m/min cutting speed (Test 2)

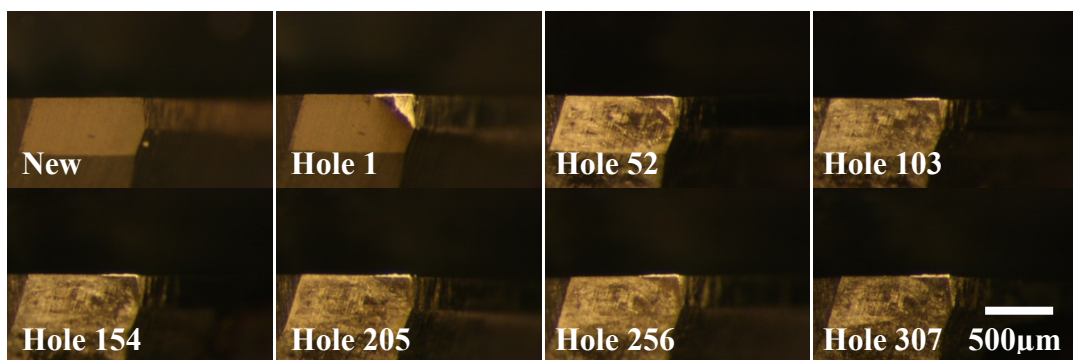


Figure D3: Tool wear micrographs of Graphit-iC™ reamer under 70bar through-hole cutting fluid, 32m/min cutting speed (Test 3)

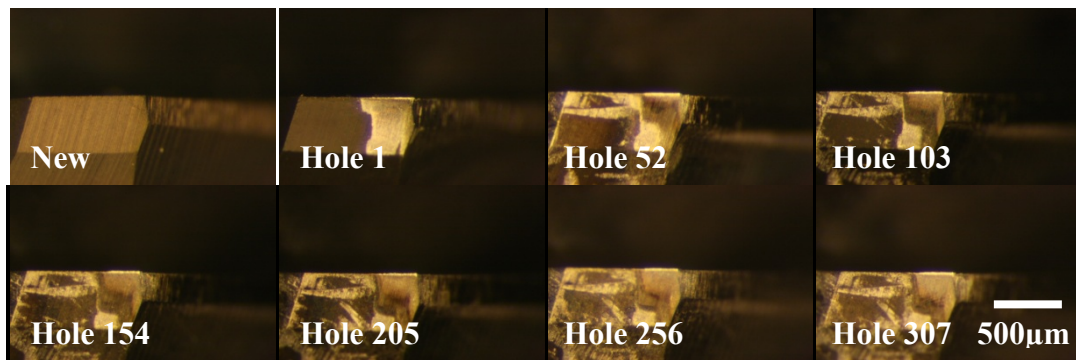


Figure D4: Tool wear micrographs of Graphit-iC™ reamer under 70bar through-hole cutting fluid, 96m/min cutting speed (Test 4)

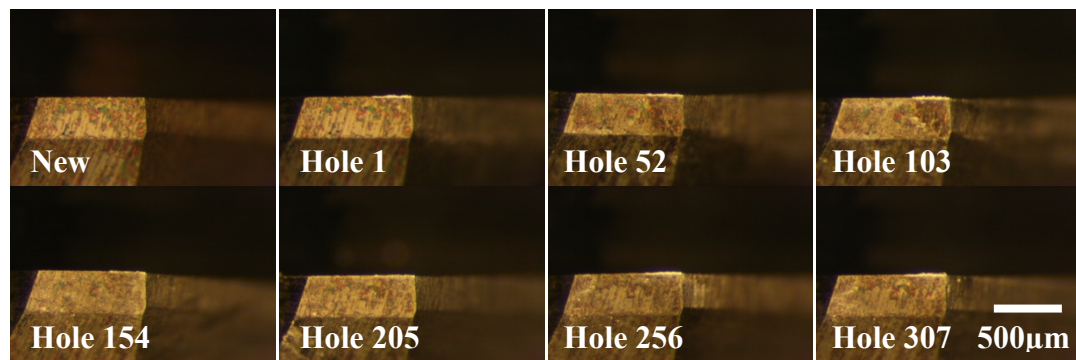


Figure D5: Tool wear micrographs of Dymon-iC reamer under 70bar through-hole cutting fluid, 32m/min cutting speed (Test 5)

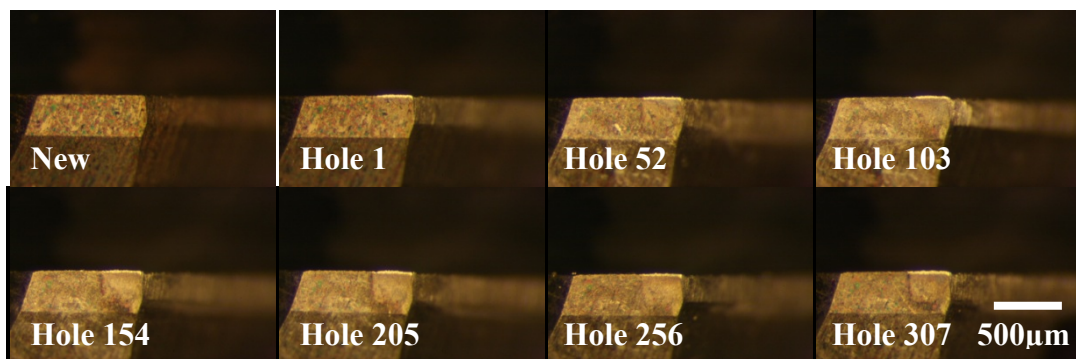


Figure D6: Tool wear micrographs of Dymon-iC™ reamer under 70bar through-hole cutting fluid, 96m/min cutting speed (Test 6)

APPENDIX E

Phase 4A: Evaluation of diamond coated and PCD tools when drilling cast C355 aluminium alloy

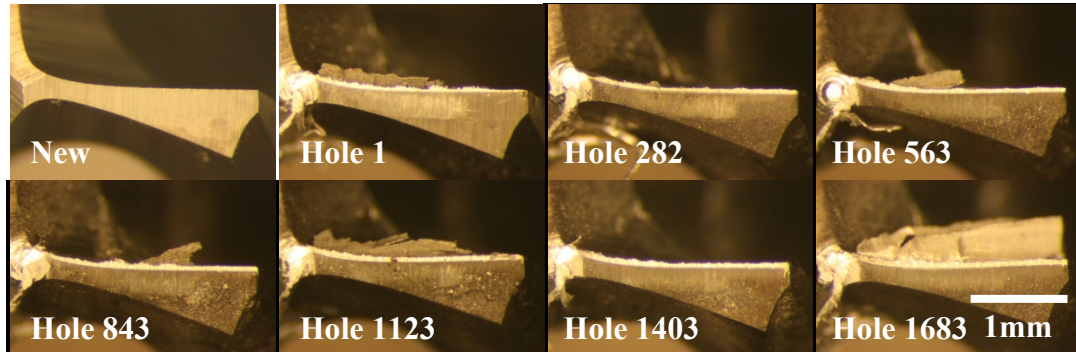


Figure E1: Tool wear micrographs of uncoated carbide drill under 3bar cutting fluid, 130m/min cutting speed (Test 1)

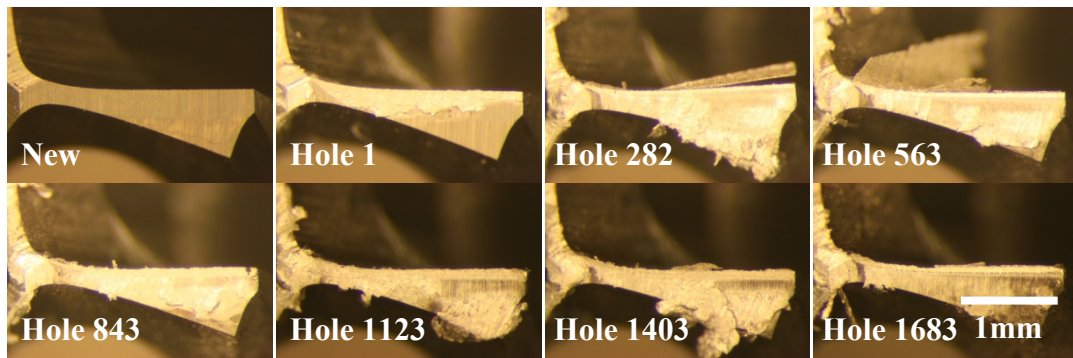


Figure E2: Tool wear micrographs of uncoated carbide drill under 3bar cutting fluid, 260m/min cutting speed (Test 2)

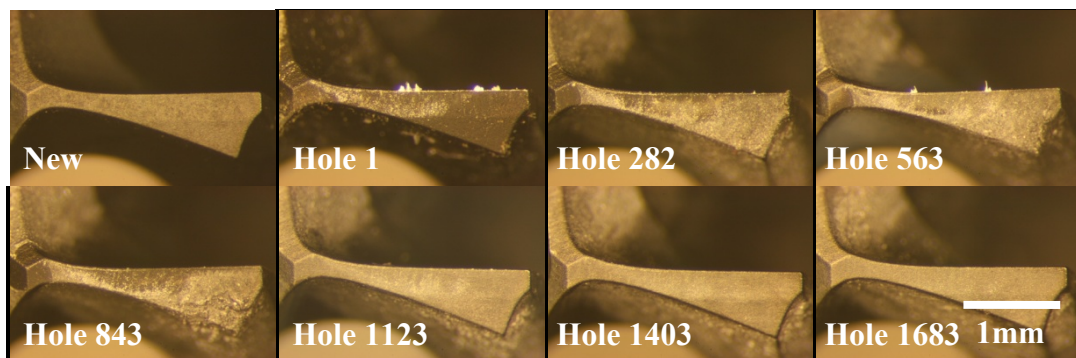


Figure E3: Tool wear micrographs of CVD diamond coated drill under 3bar cutting fluid, 130m/min cutting speed (Test 3)

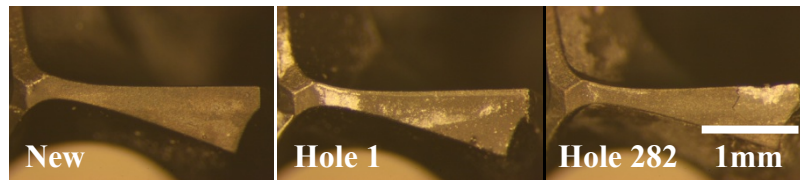


Figure E4: Tool wear micrographs of CVD diamond coated drill under 3bar cutting fluid, 260m/min cutting speed (Test 4)

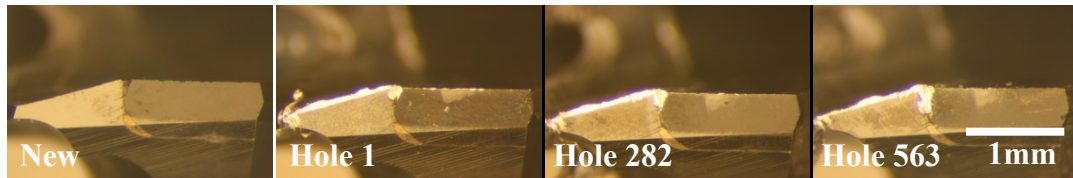


Figure E5: Tool wear micrographs of brazed PCD CTB010 drill under 3bar cutting fluid, 130m/min cutting speed (Test 5)

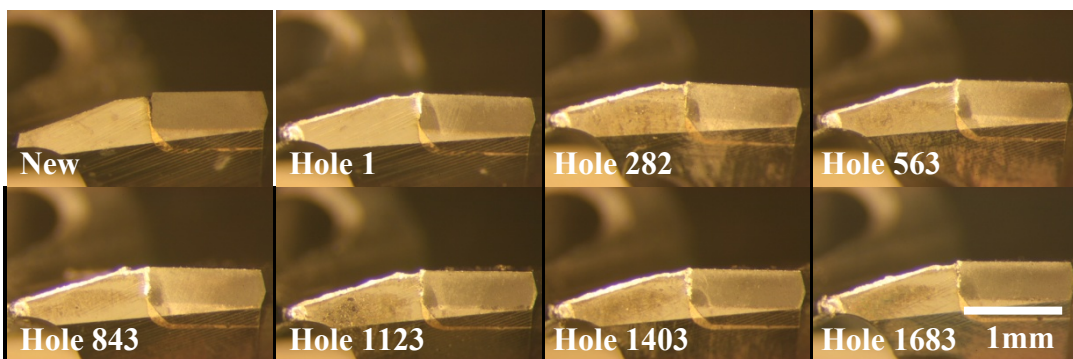


Figure E6: Tool wear micrographs of brazed PCD CTB010 drill under 3bar cutting fluid, 260m/min cutting speed (Test 6)

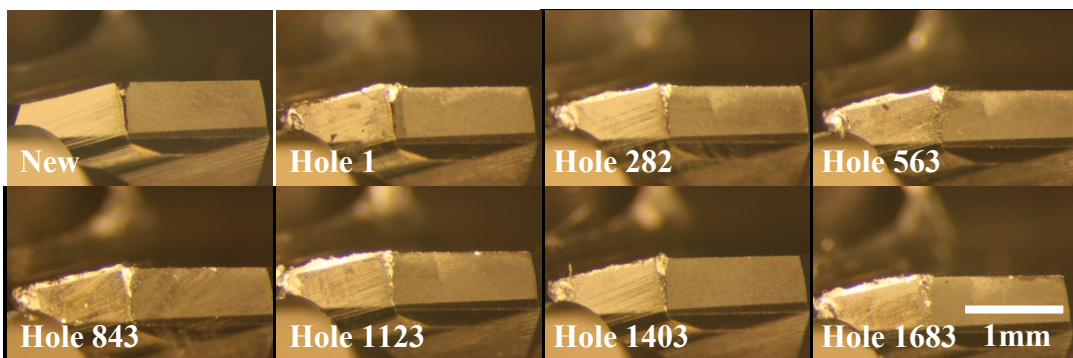


Figure E7: Tool wear micrographs of brazed PCD CTM302 drill under 3bar cutting fluid, 130m/min cutting speed (Test 7)

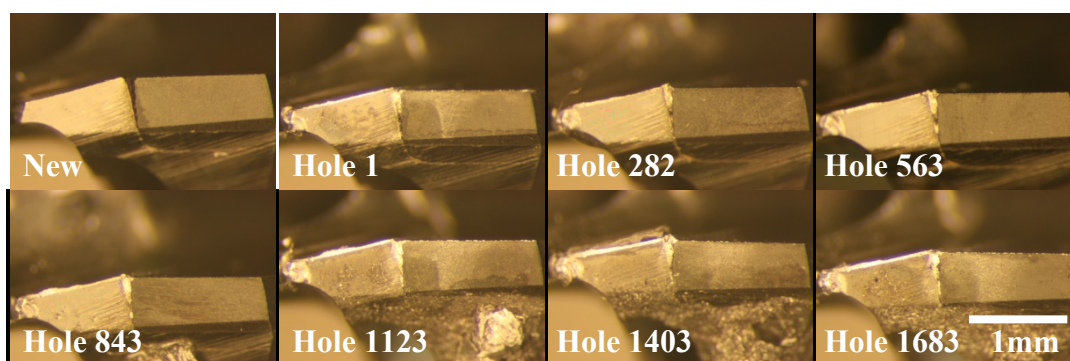


Figure E8: Tool wear micrographs of brazed PCD CTM302 drill under 3bar cutting fluid, 260m/min cutting speed (Test 8)

APPENDIX F

Phase 4B: Evaluation of diamond coated and PCD tools when reaming cast C355 aluminium alloy

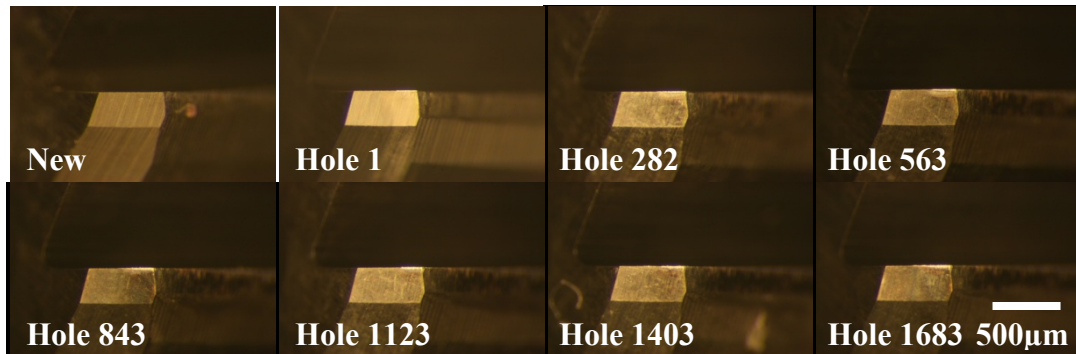


Figure F1: Tool wear micrographs of uncoated carbide reamer under 70bar through-hole cutting fluid, 32m/min cutting speed (Test 1)



Figure F2: Tool wear micrographs of uncoated carbide reamer under 70bar through-hole cutting fluid, 96m/min cutting speed (Test 2)

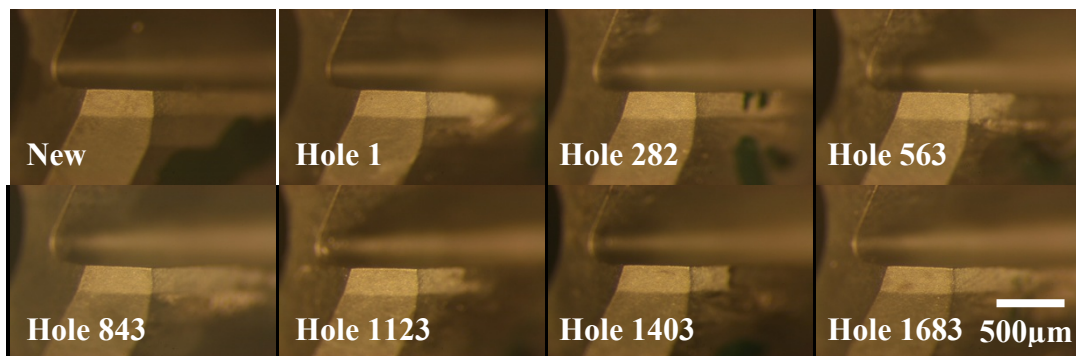


Figure F3: Tool wear micrographs of CVD diamond coated reamer under 70bar through-hole cutting fluid, 32m/min cutting speed (Test 3)

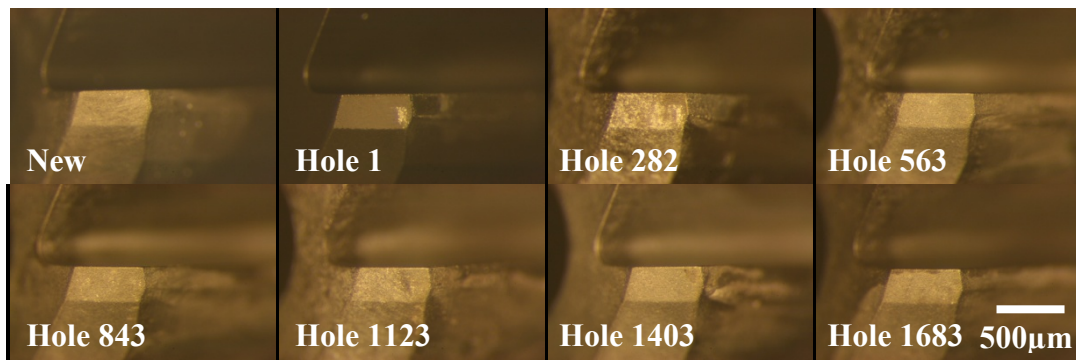


Figure F4: Tool wear micrographs of CVD diamond coated reamer under 70bar through-hole cutting fluid, 96m/min cutting speed (Test 4)

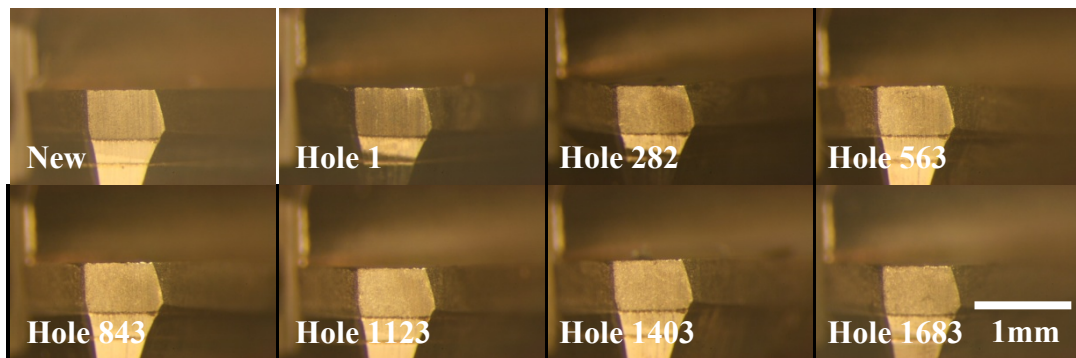


Figure F5: Tool wear micrographs of brazed PCD CTB002 reamer under 70bar through-hole cutting fluid, 32m/min cutting speed (Test 5)

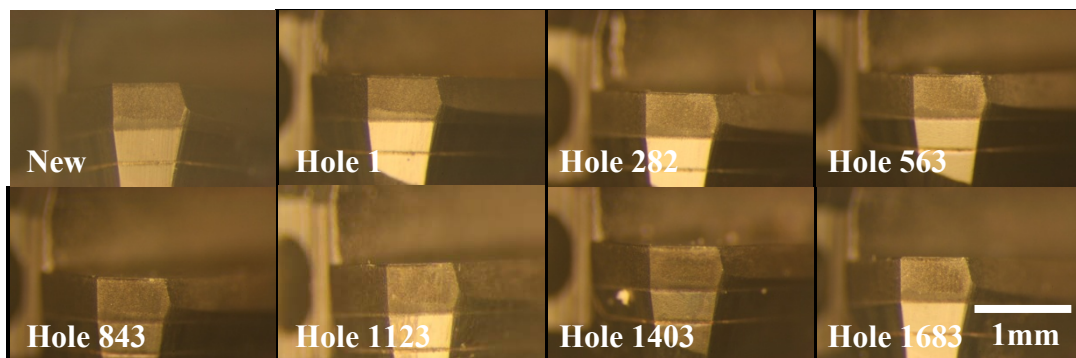


Figure F6: Tool wear micrographs of brazed PCD CTB002 reamer under 70bar through-hole cutting fluid, 96m/min cutting speed (Test 6)

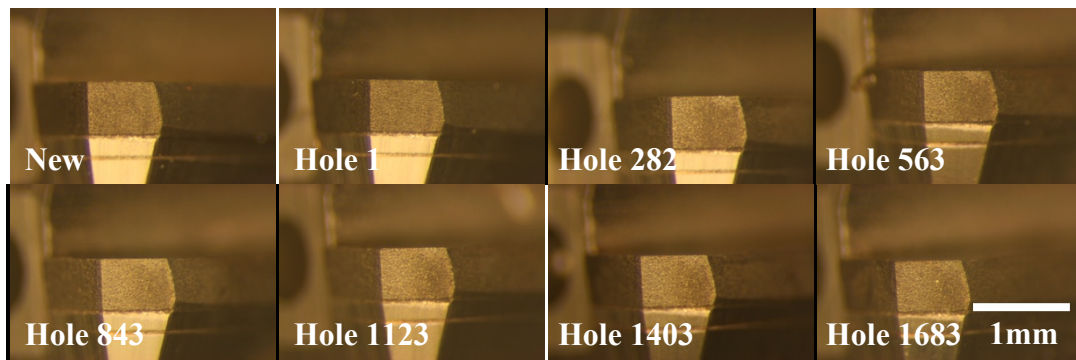


Figure F7: Tool wear micrographs of brazed PCD CTM302 reamer under 70bar through-hole cutting fluid, 32m/min cutting speed (Test 7)

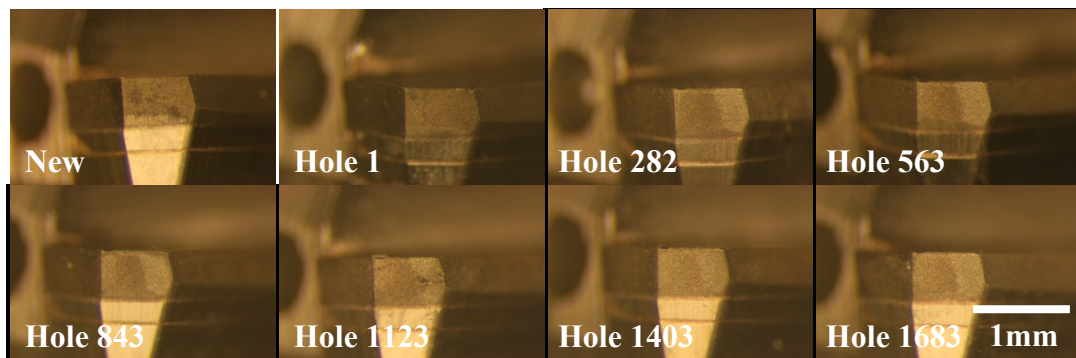


Figure F8: Tool wear micrographs of brazed PCD CTM302 reamer under 70bar through-hole cutting fluid, 96m/min cutting speed (Test 8)

APPENDIX G

List of publications:

Paper published

R. Rattanakit, S.L. Soo, D.K. Aspinwall, B. Haffner, Z. Zhang, D. Arnold, P. Harden
Evaluation of tool performance and hole quality when drilling C355 aluminium alloy using
diamond coated and PCD drills
Proceedings of the 37th International MATADOR Conference, Manchester, United Kingdom,
25 -27 July 2012, pp.173-176.

Paper under preparation

R. Rattanakit, R.J. Beck, S.L. Soo, D.K. Aspinwall, B. Haffner, Z. Zhang, D. Arnold,
P. Harden, K. Cooke
Influence of low friction, diamond like carbon (DLC) coatings on the drilling of cast
automotive aluminium alloy
To be submitted to Surface and Coatings Technology.